

AD-A063 876

AIR FORCE AERO PROPULSION LAB WRIGHT-PATTERSON AFB OHIO  
COLLISION INDUCED DISSOCIATION OF DIATOMIC MOLECULES.(U)

F/G 7/4

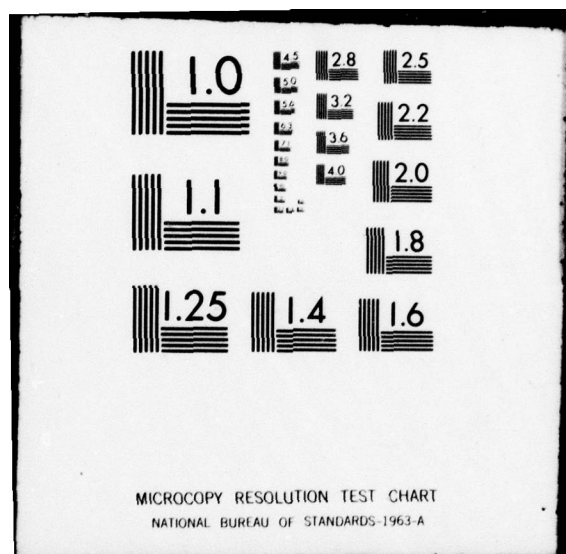
UNCLASSIFIED

NOV 78 W F BAILEY  
AFAPL-TR-78-105

NL

1 of 3  
AD  
A063 876  
1 of 3





AFAPL-TR-78-105

**LEVEL**

(2)

AD A063876

DDC FILE COPY

## **COLLISION INDUCED DISSOCIATION OF DIATOMIC MOLECULES**

*HIGH POWER BRANCH  
AEROSPACE POWER DIVISION*

NOVEMBER 1978

TECHNICAL REPORT AFAPL-TR-78-105  
Final Report for Period January 1976 through June 1978



Approved for public release; distribution unlimited.

AIR FORCE AERO PROPULSION LABORATORY  
AIR FORCE WRIGHT AERONAUTICAL LABORATORY  
AIR FORCE SYSTEMS COMMAND  
WRIGHT-PATTERSON AIR FORCE BASE, OHIO 45433

79 01 26 080

NOTICE

When Government drawings, specifications, or other data are used for any purpose other than in connection with a definitely related Government procurement operation, the United States Government thereby incurs no responsibility nor any obligation whatsoever; and the fact that the government may have formulated, furnished, or in any way supplied the said drawings, specifications, or other data, is not to be regarded by implication or otherwise as in any manner licensing the holder or any other person or corporation, or conveying any rights or permission to manufacture, use, or sell any patented invention that may in any way be related thereto.

This report has been reviewed by the Information Office (OI) and is releasable to the National Technical Information Service (NTIS). At NTIS, it will be available to the general public, including foreign nations.

This technical report has been reviewed and is approved for publication.

*William F. Bailey*

WILLIAM F. BAILEY, Major, USAF  
Research Physicist/AFAPL

FOR THE COMMANDER

*Philip E. Stover*

PHILIP E. STOVER  
Chief, High Power Branch  
Aerospace Power Division

"If your address has changed, if you wish to be removed from our mailing list, or if the addressee is no longer employed by your organization please notify AFAPL/POP, W-PAFB, OH 45433 to help us maintain a current mailing list".

Copies of this report should not be returned unless return is required by security considerations, contractual obligations, or notice on a specific document.

UNCLASSIFIED

SECURITY CLASSIFICATION OF THIS PAGE (When Data Entered)

REPORT DOCUMENTATION PAGE		READ INSTRUCTIONS BEFORE COMPLETING FORM
1. REPORT NUMBER AFAPL-TR-78-105	2. GOVT ACCESSION NO.	3. RECIPIENT'S CATALOG NUMBER
4. TITLE (and Subtitle) COLLISION INDUCED DISSOCIATION OF DIATOMIC MOLECULES	5. TYPE OF REPORT & PERIOD COVERED Final Report. Jan 76 - Jun 78	6. PERFORMING ORG. REPORT NUMBER
7. AUTHOR(s) William F. Bailey	8. CONTRACT OR GRANT NUMBER(s)	
9. PERFORMING ORGANIZATION NAME AND ADDRESS Air Force Aero Propulsion Laboratory Wright Patterson AFB OH 45433	10. PROGRAM ELEMENT, PROJECT, TASK AREA & WORK UNIT NUMBERS Program Element 61102F Project 2301-S2-04	
11. CONTROLLING OFFICE NAME AND ADDRESS AFAPL/POD Air Force Aero Propulsion Laboratory Wright Patterson AFB OH 45433	12. REPORT DATE Nov 78	13. NUMBER OF PAGES 278
14. MONITORING AGENCY NAME & ADDRESS (if different from Controlling Office) Same	15. SECURITY CLASS. (of this report) Unclassified	15a. DECLASSIFICATION/DOWNGRADING SCHEDULE
16. DISTRIBUTION STATEMENT (of this Report) Approved for public release; distribution unlimited.		
17. DISTRIBUTION STATEMENT (of the abstract entered in Block 20, if different from Report) Same		
18. SUPPLEMENTARY NOTES		
19. KEY WORDS (Continue on reverse side if necessary and identify by block number) Dissociation Molecular Kinetics Electron Kinetics Energy Transfer		
20. ABSTRACT (Continue on reverse side if necessary and identify by block number) A discrete collisional theory of dissociation under equilibrium and nonequilibrium conditions using a quantum kinetic approach to molecular energy transfer was investigated. The kinetic equations for molecular dissociation in a pure diatomic gas and diatomic gases in the presence of an inert diluent were formulated and solved. The incubation time was calculated and exhibited good agreement with experimental measurements. An analytic steady state form for the vibrational population and dissociation rate was developed which agreed with the time-dependent calculations. It was determined that rotational states play a		

DD FORM 1 JAN 73 1473

EDITION OF 1 NOV 65 IS OBSOLETE

UNCLASSIFIED

011 570

SECURITY CLASSIFICATION OF THIS PAGE (When Data Entered)

79 01 26 080

UNCLASSIFIED

SECURITY CLASSIFICATION OF THIS PAGE(When Data Entered)

Cont. from Block 20.

significant role in the dissociation process and that the standard ladder model is inadequate. When rotational effects are properly included in the analysis, good agreement with experimental data is obtained. The kinetics developed to address thermal dissociation under equilibrium conditions were extended to treat the highly nonequilibrium conditions achieved through intense optical pumping or electron impact excitation. The nonequilibrium treatment included a detailed investigation of electron impact dissociation. A parametric study of heavy particle and electron impact dissociation rates revealed that under conditions typically encountered in electric discharges, electron impact dissociation dominates the heavy particle rate.

UNCLASSIFIED

SECURITY CLASSIFICATION OF THIS PAGE(When Data Entered)

# FOREWORD

The material reported herein is based on the author's dissertation submitted in partial fulfillment of the requirements for the Doctor of Philosophy degree at the Air Force Institute of Technology, Wright Patterson Air Force Base, Ohio. The research effort was performed in the High Power Branch of the Aerospace Power Division of the Air Force Aero Propulsion Laboratory, Air Force Systems Command, Wright Patterson AFB, Ohio, under Project 2301, Task S2, and Work Unit 04. This effort was conducted by William F. Bailey during the period January 1976 to June 1978. A discrete collisional theory of dissociation under equilibrium and nonequilibrium conditions was investigated.

ACCESSION for	
NTIS	White Section <input checked="" type="checkbox"/>
DDC	Blue Section <input type="checkbox"/>
UNANNOUNCED	<input type="checkbox"/>
JUSTICE DIV	
DISTRIBUTION/AVAILABILITY CODES	
SPECIAL	
A	

## Table of Contents

	Page
I. Introduction . . . . .	1
Purpose and Objective of This Study . . . . .	1
Overview of Contents and Results . . . . .	4
Energy Transfer Mechanisms . . . . .	6
Theory of Vibrational Energy Exchange . . . . .	7
The Dissociation Process . . . . .	11
II. Dissociation Theories: Approaches to the Problem .	
Classical Theory . . . . .	17
Phase Space Theories . . . . .	20
Collisional Approach . . . . .	22
Contradictions and Inconsistencies . . . . .	32
III. Development of the Master Equation . . . . .	36
Introduction . . . . .	36
System and Assumptions . . . . .	36
Transition Rates . . . . .	40
Master Equation Formalism . . . . .	43
Numerical Method . . . . .	46
Steady State Solutions of the	
Master Equation . . . . .	47
Conclusion . . . . .	59
IV. Dissociation Models . . . . .	60
General . . . . .	60
Standard Ladder Model . . . . .	60
Rotational Structure . . . . .	62
Rotational Models . . . . .	67
Dissociating States . . . . .	68
An Alternate Path to Dissociation . . . . .	84

	Page
V. Calculated Dissociation and Recombination Rates	92
General	92
Matrix of Computational Capabilities	92
Time Dependent Results	96
Dissociation of Diatomics	
Diluted in an Argon Heat Bath	109
Hydrogen	111
Oxygen and Nitrogen	113
Bromine and Iodine	116
Carbon Monoxide	120
Dissociation in Pure Gases	122
Hydrogen	123
Oxygen	126
Bromine	128
Recombination Coefficients	130
Hydrogen	134
Oxygen	134
Nitrogen	137
Bromine	137
Iodine	140
Summary	140
VI. Dissociation Under Highly Non-Equilibrium Conditions	143
Introduction to Non-Equilibrium Processes	143
Electron Kinetics	145
Background	145
Boltzmann Equation Theory	146
Electron Collision Processes	156
Calculated Electron Energy Distributions	163
Summary	168
Molecular Kinetics	170
Background	170
Characteristic Regions of the VED	172
Analytic Approach to VED's	182
V-V and V-T Rates at Low Temperatures	190
Comparison with Optically Pumped VED's	195
Parameterization of Dissociation	198
Electron Impact Dissociation	200
Dissociation Due to Heavy Particle Collisions: Electric Discharge Conditions	205
Dissociation Due to Heavy Particle Collisions: Optical Pumping	210

	Page
Evaluation and Comparison of Heavy Particle Dissociation Rates . . . .	215
Alternative Processes and Reaction Mechanisms . . . . .	220
VII. A Review and Some Considerations for Future Study . . . . .	229
General Review . . . . .	229
New Aspects of Dissociation for Near- Equilibrium Conditions . . . . .	230
Non-equilibrium Dissociation--Heavy Particle Vs. Electron Impact . . . . .	233
Consideration for Future Study . . . . .	235
Bibliography . . . . .	238
Appendix A: The Influence of Anharmonicity on Vibrational Energy Transfer . . . .	252
Appendix B: Number of Bound Vibrational States . . . .	263

## List of Illustrations

Figure	Page
4-1 Standard Ladder Model . . . . .	61
4-2 Effective Potential Curves for a Diatomic Molecule . . . . .	63
4-3 Bound and Dissociated States of a Diatomic Molecule . . . . .	65
4-4 Coupled Rotational Model . . . . .	69
4-5 Effective Potential Energy Curves for the Hydrogen Molecule . . . . .	71
4-6 Effective Potential Energy Curves for the Oxygen Molecule . . . . .	72
4-7 Effective Potential Energy Curves for the Nitrogen Molecule . . . . .	73
4-8 Effective Potential Energy Curves for the Carbon Monoxide Molecule . . . . .	74
4-9 Effective Potential Energy Curves for the Bromine Molecule . . . . .	75
4-10 Effective Potential Energy Curves for the Iodine Molecule . . . . .	76
4-11 Temperature Dependence of Dissociating State Population . . . . .	79
4-12 Alternate Paths for Dissociation . . . . .	86
4-13 CDS for Mechanism A, Over-the-Top . . . . .	88
4-14 CDS for Mechanism C, Equal Energy Transition . . . . .	89
5-1 Time Profiles and Uni-Directional Flux . . . . .	98
5-2 Time Dependent Results for $O_2$ -Ar . . . . .	.102
5-3 Time dependent Results for $H_2$ -Ar . . . . .	.103

Figure	Page
5-4 Time Dependence of Unidirectional Dissociation Flux . . . . .	.106
5-5 Induction Times in $O_2$ -Ar . . . . .	.107
5-6 Dissociation of Hydrogen Diluted in Argon . . . . .	.112
5-7 Dissociation of Oxygen Diluted in Argon . . . . .	.114
5-8 Arrhenius Plot of $O_2$ Dissociation . . . . .	.115
5-9 Arrhenius Plot of Nitrogen Dissociation . . . . .	.117
5-10 Dissociation of Bromine Diluted in Argon . . . . .	.118
5-11 Dissociation of Iodine Diluted in Argon . . . . .	.119
5-12 Arrhenius Plot of CO Dissociation . . . . .	.121
5-13 Rate Enhancement in $H_2$ . . . . .	.124
5-14 Rate Enhancement in $O_2$ . . . . .	.127
5-15 Rate Enhancement in $Br_2$ . . . . .	.129
5-16 $H_2$ Recombination Coefficient . . . . .	.135
5-17 $O_2$ Recombination Coefficient . . . . .	.136
5-18 $N_2$ Recombination Coefficient . . . . .	.138
5-19 $Br_2$ Recombination Coefficient . . . . .	.139
5-20 $I_2$ Recombination Coefficient . . . . .	.141
6-1 Collision Geometry . . . . .	.150
6-2 Effective Vibrational Cross Section . . . . .	.159
6-3 CO Vibrational Cross Sections . . . . .	.160
6-4 CO Dissociative Ionization Cross Section . . . . .	.162
6-5 CO Dissociative Attachment Cross Section . . . . .	.164
6-6 Electron Energy Distributions, eed's . . . . .	.165
6-7 Fractional Electron Power Transferred . . . . .	.167
6-8 Influence of Superelastic Collisions on the eed . . . . .	.169

Figure	Page
6-9 Representative Exchange Probabilities . . . . .	.174
6-10 Treanor Distribution Parameterized in $T_1$ . . . . .	.177
6-11 Treanor Distribution Parameterized in $T$ . . . . .	.178
6-12 Numerical Solutions of VED Parameterized in $T_1$ . . . . .	.180
6-13 Numerical Solutions of VED Parameterized in $T$ . . . . .	.181
6-14 Comparison of Numerical and Analytic VED's . . . . .	.186
6-15 V-T Deactivation of CO . . . . .	.189
6-16 Rate Constants for CO-CO V-V Exchange . . . . .	.194
6-17 Optically Pumped VED's . . . . .	.196
6-18 Dissociative Ionization Coefficients ( $k_d^e$ ) . . . . .	.203
6-19 Electron Impact Dissociation Coefficients ( $k_d^e$ ) . . . . .	.206
6-20 Equilibrium Comparison of Electron Impact and Heavy Particle Dissociation . . . . .	.208
6-21 Non-Equilibrium Heavy Particle Dissociation Constant . . . . .	.209
6-22 Optical Pumping, Time Dependent Calculation . . . . .	.212
6-23 Optical Pumping, Heavy Particle Dissociation Constant . . . . .	.214
6-24 Saturation of Heavy Particle Dissociation . . . . .	.216
6-25 Isotope Separation Coefficient for Laser Induced CO Dissociation . . . . .	.225
A-1 Collinear Collision Geometry . . . . .	.253
A-2 Transition Probabilities, V-T . . . . .	.261

## List of Tables

Table	Page
I    Experimental Data on Activation Energies for the Dissociation of Homonuclear Diatomic Molecules . . . . .	15
II   Status Table of Dissociation Theories . . . . .	33
IV   Comparison of Dissociating States . . . . .	82
V-I   Matrix of Computational Capabilities . . . . .	94
V-II   Spectroscopic Data for the Molecules . . . . .	131

## Chapter I. Introduction

### Purpose and Objective of This Study

Dissociation and energy transfer in diatomic gases is a topic embracing a broad class of physical phenomena and has direct application to a wide variety of technical fields. Gas temperatures of a few thousand degrees Kelvin are encountered in the operating environment of re-entry vehicles, rocket engines, and hypersonic aircraft. The need for a detailed understanding of the processes and phenomena associated with this environment has spurred interest in the chemical kinetics of the dissociation and the recombination of molecules. The development of chemical, electric discharge and gas-dynamic lasers has accelerated interest in the allied field of intermolecular energy transfer and identified the dissociation or recombination processes as fundamental to the development of new and reliable laser systems. Our interest in the dissociation process grew out of studies (ref 1) of the characteristics of closed cycle, electric discharge lasers. Within these studies, we established that plasma chemistry has a critical influence on discharge stability and laser performance. The dissociation reaction initiates the chemical evolution of the gas discharge, and is therefore fundamental to an understanding of the kinetics of closed cycle lasers.

While the modern literature and texts contain numerous studies of energy transfer and dissociation in diatomic molecules, recent measurements of dissociation (refs 2, 3, 4) and relaxation rates (refs 5, 6, 7, 8) indicate substantial deviations from previous theories. Most previous theories of dissociation (refs 9, 10) are based upon a steady state, "ladder climbing" analysis with the vibrational energy of the dissociating molecule making the dominant contribution to the reaction energy. Recent detailed calculations utilizing this theory (refs 11, 12) have shown that this model fails to characterize the process consistently, and yields dissociation rates an order of magnitude lower than observed experimentally. On the other hand, several recent publications (refs 11, 12, 13, 14, 15) based on a modified "ladder" analysis have met with varying degrees of success. These analyses have been inconsistent with regard to relaxation rates, and yielded contradictory results. These recent works have included a variety of additional processes viz: anharmonic effects, multiple quantum transitions, complex exchanges and rotational effects. However, these processes have been treated individually and for specific conditions so that detailed comparisons are difficult.

The apparent anomalies and inconsistencies in the theories of thermal dissociation have not tempered the very recent extension of the standard "ladder" model to highly non-equilibrium conditions (refs 16, 17, 18). These

non-equilibrium studies have been confined to an analytical steady state analysis and have examined the dissociation reaction rate under conditions of intense optical or collisional pumping. Rotational effects and the influence of electron impact dissociation have not been included in the analysis.

This study is addressed to establishing a consistent, discrete collisional theory of dissociation under equilibrium and non-equilibrium conditions and to five corresponding objectives.

The first objective is to examine the standard ladder model of dissociation and evaluate its predictive utility when realistic transfer rates are incorporated into the analysis. A variety of gases are analyzed over a broad range of temperatures. Anticipating the failure of the standard "ladder" model, the second objective is to evaluate the role of rotational effects in modifying the collisional activation process and hence to determine to what extent rotation does alter the calculated dissociation rates. While rotational effects have long been invoked as leading to enhanced dissociation, few serious and extensive analyses have been performed. Within the evaluation of the standard and rotational models, the third objective will be to examine the time dependent characteristics of the dissociation process and assess the influence of the models on the observed incubation times. The fourth objective is to analyze the effect of V-V exchanges and of changes in

collisional efficiencies due to mass variations. This objective will address the resolution of the inconsistencies that have arisen in the literature regarding rate enhancement in pure gas. The fifth objective is then to extend the analysis to the highly non-equilibrium situation of intense optical or electron impact pumping and to parameterize the dissociation process in this regime.

### Overview of Contents and Results

In this chapter we begin with a review of collisional energy exchange mechanisms in molecules, an examination of the theories of vibrational energy transfer, and an introduction to the dissociation process.

In Chapter II, a historical review of the theories of dissociation is presented which provides a guide to a number of more complete review papers. The physical concepts and critical assumptions of previous theories are then discussed. Here the dissociation terminology of vibrational depletion, incubation time and vibrational bias is introduced. Previous calculations are reviewed and results cited. The contradictions and inconsistencies present in previous works are then highlighted and attention is pointed towards the need for the present analysis.

Chapter III is devoted to the development of the Master Equation formalism for diatomic gases diluted in inert gases and pure diatomic gases. The numerical technique

used for the time-dependent solution is discussed and a steady state solution derived.

Building on the formalism developed in Chapter III, three simplified models of dissociation are presented and examined in Chapter IV. Results of detailed numerical calculations of dissociation rates based on these models are presented in Chapter V and compared with experimental data. The time-dependent behavior of the dissociation process is also examined. In addition, the extent of rate enhancement due to changes in collisional efficiencies, complex energy exchanges and coupling to excited electronic states are also discussed.

Chapter VI deals with the highly non-equilibrium conditions achieved through electron impact excitation or intense optical pumping. In order to address electron impact dissociation, a solution of the collisional Boltzmann transport equation is developed and the electron impact rates are examined for parameters characteristic of electrical discharges. Next, the characteristics of the vibrational energy distribution are discussed within the framework of an analytical steady-state solution of the Master Equation for strongly pumped conditions. Time dependent and steady state results are then presented in a parametric study of the heavy particle and electron impact dissociation processes. A comparison is made of the efficiencies of electron impact dissociation and heavy particle dissociation. Finally, Chapter VII summarizes the new aspects

of the results of this study and presents some considerations and recommendations for additional theoretical and experimental study.

#### Energy Transfer Mechanisms

In considering the dissociation of diatomic molecules in pure gases or in highly diluted mixtures with an inert gas, five distinct energy transfer mechanisms resulting from the collisional interaction of heavy particles can be identified. These are:

1. Vibration-Translation exchange (V-T)
2. Rotation-Translation exchange (R-T)
3. Electronic-Translation exchange (e-T)
4. Vibration-Vibration exchange (V-V)
5. Electronic-Vibration exchange (e-V)

A V-T exchange is characterized by a collision of a molecule with another atom/molecule in which the molecule gains or loses vibrational energy from/to the translation mode. The R-T and e-T processes represent a similar exchange except they involve the transfer of rotational and electronic energy respectively. V-V and e-V exchanges are classified as complex exchanges. AV-V exchange may occur when two molecules collide. One molecule gains vibrational energy, the other molecule loses vibrational energy, and any energy mismatch is compensated by the translational mode. An e-V exchange parallels a V-V exchange except that electronic and vibrational energies are exchanged.

In the present work, it will be assumed that the rotational mode is in equilibrium with the translational mode; and we will therefore omit an explicit treatment of rotational energy exchanges during collisions. The assumption of rotational equilibrium is easily justified for low lying rotational states, being consistent with the experimental observation of rapid rotational energy relaxation during collisions (ref 24). However, when very large values of the rotational quantum number,  $J$ , are considered, the assumption is questionable. We retain this assumption, however, based on the simplification it introduces and the lack of any experimental or theoretical exchange rate data for very high  $J$  levels. e-T exchanges will also be neglected. Their omission is justified by the adiabatic nature of such an exchange in the temperature range considered. The explicit evaluation of e-V exchanges is also omitted in the present analysis. However, the possible role played by e-V exchange in the dissociation process will be discussed when we examine dissociation under non-equilibrium conditions in Chapter VI. Thus in this work, we will concentrate on the V-T and V-V mechanisms as we proceed with the development of a collisional theory of dissociation.

#### Theory of Vibrational Energy Exchange

Having identified the critical energy transfer mechanisms as V-V and V-T exchange, we proceed by outlining the development of the theory of vibrational energy exchange.

Landau and Teller (ref 19) first examined the theory of vibrational relaxation in 1936 using a classical mechanical approach. Schwartz, Slawsky, and Herzfeld (ref 20) published an analogous quantum mechanical theory in 1952. This "SSH" theory has received widespread use and represents the standard with which most relaxation data are compared. The SSH analysis is based upon an adiabatic "distorted wave" quantum mechanical theory of scattering developed by Jackson and Mott (ref 21). Since the appearance of the "SSH" theory, an extensive amount of theoretical work on collisional energy exchange has been accomplished. This includes both rotational and vibrational energy exchange. This work has been reviewed in the landmark work of Herzfeld and Litovitz (ref 22), and by Takayanagi (ref 23), Cottrell and McCoubrey (ref 24), Rapp (ref 25), and Nikitin (ref 26).

Subsequent improvements in the basic SSH theory centered around the anharmonic features of the molecular potential. Rich (ref 14) improved the SSH approach by using an "exact" form of the Morse transition probabilities. Mies (ref 27) identified the critical dependence of the transition probability upon the ratio of the diagonal matrix elements. In 1965 Keck and Carrier (ref 28) were able to extend the SSH formalism through a numerical calculation and curve fitting procedure to provide a smooth transition from the adiabatic to non-adiabatic limits of the V-T exchange. In 1970, Rich and Treanor (ref 29) presented a comprehensive review of vibrational relaxation in

gasdynamic flows. The early seventies brought in widespread efforts to deal with new laser requirements for the analysis of vibrational energy transfer in CO and CO<sub>2</sub> laser systems. At this time detailed numerical calculations of V-V and V-T rates started to surface. These calculations have been described by Secrest (ref 30) who also reviewed their application to rotational and vibrational energy transfer. Numerical calculations have been a useful gauge of the validity of the various approximations in the analytic theories. These assumptions include those of an exponential interaction potential and the applicability of first order perturbation theory. The recent fully quantum calculations of Rabitz (ref 31) and the semi-classical calculations of McKenzie (ref 32) represent the state of the art. These calculations themselves, however, have been quite limited in number of gases and temperature ranges considered. This is easily understood since these analyses are quite lengthy from a computational standpoint and are limited by the accuracy of the interaction potential surface used.

When applying collisional energy exchange theory to the problem of molecular dissociation, three aspects of the exchange rates must be considered.

1. Temperature dependence
2. Magnitude
3. Variation with vibrational state

The vibrational level scaling of the rates reflects the influence of the anharmonic nature of the vibrational energy levels on the calculated transition probabilities. When we consider highly excited states the consequent limitations on the validity of perturbation and simple harmonic oscillator theories must be realized and can be accounted for by using Morse transition probabilities and the Mies (ref 27) asymmetrical correction factor. For a more detailed discussion see Appendix A. In addition to the influence of molecular anharmonicity on the transition elements, the variation in the spacing of the vibrational energy levels also changes the nature of the collisional interaction. Due to this variation in energy level spacing, collisions involving low lying vibrational levels are adiabatic in character while collisions involving vibrational states near the dissociation limit are non-adiabatic or impulsive. Experimental data on excited state V-T measurements are limited, but comparison with the available data of Hancock and Smith (ref 33) show favorable agreement with the SSH theory as modified by Keck and Carrier. Based on this comparison with experiment and numerical calculations of McKenzie (ref 32), the SSH theory as modified by Keck and Carrier (ref 28) will be utilized throughout the present analysis and fitted to experimental data where available.

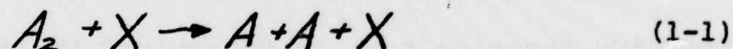
### The Dissociation Process

The previous sections have dealt with the physics of collisional energy transfer and vibrational energy exchange. The energy transfer mechanisms of V-V and V-T exchange have been defined and discussed. As the vibrational excitation, relaxation, and excitation sequence proceeds, excitation to higher and higher vibrational levels occurs. If this excitation proceeds sufficiently far, molecular bonding is overcome and two free atoms are formed; the molecule dissociates. Thus if the energy of a diatomic molecule exceeds the dissociation energy, the molecule will decompose at a frequency on the order of vibrational frequency. This frequency is much greater than the gas kinetic collision frequency and therefore this phase of the reaction may be considered as instantaneous. As a result, the effective reaction rate is determined by the rate of excitation to the dissociating state. Thus in order to investigate the dissociation process and thermal activation, it is essential to know the behavior of the collision induced transition probabilities.

Experimental evidence from resonance emission spectroscopy (refs 34, 35, 36) and theoretical calculations (refs 31, 32) indicate that energy transfers involving the exchange of more than one or two vibrational quanta are extremely improbable. Whereas, the probability of populating the vibrational states from those immediately below has a relatively high value. This restriction on the

number of quanta exchanged in a collision leads one to view the excitation of the vibrational states during relaxation as a stepwise process. The activation of excited vibrational states therefore occurs primarily through single quantum exchanges and the overall energization of the vibrational manifold can be characterized as a stepwise process in which excitation proceeds up the "ladder" of vibrational energy levels to high lying states from which dissociation occurs. This concept of stepwise excitation to a dissociating state is the essence of the "ladder model" of dissociation and relaxation.

The collisionally induced dissociation of diatomic molecule,  $A_2$ , can be represented as a simple chemical process



The rate equation for the reaction (1) takes the form

$$\frac{dA_2}{dt} = -\frac{1}{2} \frac{dA}{dt} = \{-k_d[A_2] + k_r[A]^2\}[X] \quad (1-2)$$

where the number densities of the particles have been denoted by their symbols. The reaction rates depend on the type of molecule or atom, and gas temperature. In predicting the dissociation reaction rates from the properties of the reacting molecules and/or atoms, one is concerned

with the evaluation of the dissociation rate coefficient  $k_d$ . The recombination rate coefficient  $k_r$  is related to  $k_d$  through the law of mass action or rate quotient law:

$$\frac{k_d}{k_r} = K_c(T) \quad (1-3)$$

where  $K_c(T)$  is the equilibrium constant. Due to the development of the shock tube as a reliable tool for high temperature kinetic studies, extensive data exist on the dissociation coefficients of  $H_2$ ,  $O_2$ ,  $N_2$ ,  $Br_2$ ,  $I_2$  and CO gases diluted in an argon mixture. Data are also available for pure diatomic gases, although these data are not quite as extensive. The dissociation rate in pure gases is generally enhanced over that value obtained when the diatomic gas is diluted in an inert gas. The magnitude and temperature dependence of the enhancement varies from gas to gas. We will consider the possible sources of this enhancement in Chapter V.

The results of experimental measurements of the dissociation coefficient are often fitted to the form

$$k_d = C \beta^{-m} \exp(-\beta D_0) \quad (1-4)$$

where  $\beta = 1/(kT)$ ,  $T$  is the translational temperature,  $D_0$  the dissociation energy, and  $C$  a constant. The Arrhenius activation energy,  $E_{act.}$ , is given by

$$E_{act.} = -\frac{d}{d\beta} [\ln(k_d)] \quad (1-5)$$

Thus for the form given in (1-4), the activation energy is

$$\begin{aligned} E_{act.} &= D_o + m/\beta \\ &= D_o + m k T \end{aligned} \quad (1-6)$$

Table I, extracted from Johnston and Birks (ref 9), presents experimental data on the observed activation energies,  $E_{obs}$ , and the power of the temperature,  $m$ , for a given reactant (A), gas diluent (X), and temperature range. Note that the observed activation energies are less than the dissociation energies so that the empirical parameter  $m$  is always negative. This fact serves as a guide in evaluating the various models of dissociation that we will introduce in Chapter IV.

TABLE 1

EXPERIMENTAL DATA ON ACTIVATION ENERGIES FOR THE  
DISSOCIATION OF HOMONUCLEAR DIATOMIC MOLECULES

A	X	T, K	D <sub>0</sub> , kcal	E <sub>obs.</sub> , kcal	m
F <sub>2</sub>	Ar	1300-1600	37.1	30 ± 4	-2.5
	Ne	1650-2700		24 ± 5	-3.0
	Ar	1300-1600		27.3 ± 2.5	-3.4
	Xe	1300-1600		31.1	-2.1
Cl <sub>2</sub>	Ar	1700-2500	57.0	48.3	-2.1
		1600-2600		50	-1.7
		1700-2600		41 ± 5	-4.0
		1600-2600		45 ± 2	-2.9
		1700-2600		48.3	-2.0
Br <sub>2</sub>	Ar	1300-1900	45.5	41.4	-1.3
		1400-2700		41.4	-1.0
		1200-2200		32.4	-3.8
I <sub>2</sub>	Ar	1000-1600	35.6	29.7	-2.3
		850-1650		30.4	-2.1
O <sub>2</sub>	Ar	5000-18000	118.0	110	-0.4
		3800-5000		106 ± 5	-1.4
		4000-6000		108	-1.0
		3400-7500		108	-1.2
		3000-5000		114	-0.5
	O <sub>2</sub>	3000-5000		98	-2.5
		4000-7000		91	-2.5

TABLE 1--Continued

A	X	T,K	D <sub>O</sub> ,kcal	E <sub>obs.</sub> ,kcal	m
		2500-4000		108	-1.5
		3000-6000		100 $\pm$ 5	-1.0
		2600-7000		85	-3.7
			11		
H <sub>2</sub>	Ar	2800-4500	103.3	97	-0.9
		3000-5300		97	-0.8
		2800-5000		97	-0.8
		2900-3790		97	-1.0
	Xe	3000-4500		100	-0.4
	H <sub>2</sub>	3000-4500		92	-1.5
	H	3000-4500		100	-0.4
D <sub>2</sub>	Ar	3000-4800	105	97	-1.0
	Ar	3000-4900		97	-1.0
N <sub>2</sub>	Ar	6000-9000	225	218	-0.5
		6000-10000		204	-1.3
	N <sub>2</sub>	6000-9000		218	-0.5
		6000-10000		198	-1.7
	N	6000-9000		203	-1.5

## NOTES:

D<sub>O</sub>--Dissociation EnergyE<sub>obs.</sub>--Observed activation energy

m--Non-exponential temperature dependence

(Data taken from Ref 9)

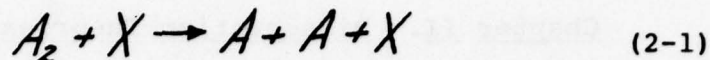
## Chapter II. Dissociation Theories;

### Approaches to the Problem

Having discussed vibrational energy transfer and introduced the dissociation process, let us turn to previous work on dissociation theories and review the approaches, assumptions, and results. It is convenient to divide these approaches into three groups: the classical approach, which treats the molecular energy levels as a continuum and gives no reference to the quantum nature of the activation or reaction processes; the statistical approach, where reactions are considered as systems crossing boundaries in a multi-dimensional phase space; and finally, the collisional approach, involving a discrete kinetic analysis of molecular activation and reaction. We will consider these approaches in turn.

#### Classical Theory

The early theories of the dissociation of diatomic molecules used classical mechanics and kinetic theory. Within this framework, it was assumed that in order for a molecule to dissociate as a result of a binary encounter, the relative kinetic energy of the collision partners must only be in excess of some activation energy. Under this "Available Energy Theory" the specific rate of the reaction



at a temperature T, is given by (ref 37)

$$k_d = PZ \exp(-\beta D_0) \quad (2-2)$$

where Z is the collision rate, P a steric factor,  $\beta=1/kT$  and  $D_0$  is the dissociation energy. This approach has been extended to include the influence of internal energy in all participating modes. At dissociation temperatures, molecules will have significant rotational and vibrational energy. Assuming equipartition of this energy over  $2s$  classical dynamical variables and classical excitation of these modes, the rate constant is given by (ref 37):

$$k_d = \frac{PZ}{s!} (\beta D_0)^s \exp(-\beta D_0) \quad (2-3)$$

This form is similar to that discussed previously in Chapter I and is frequently used to correlate experimental data as presented in Table I. Rice (refs 38-39) attempted to refine this theory by assuming that on the average a molecule that is about to dissociate upon a collision will have an energy within  $kT$  of the dissociation energy. This assumption coupled with a correction for electronic state

multiplicity resulted in a significant increase in the effective Z in (2.3). Careri (refs 40-41), however, cited Rice's omission of rotation and upon including rotational effects he obtained

$$k_d = PZ [1 - \exp(-\beta h\nu)] \exp(-\beta D_0) \left[ \frac{\beta h\nu}{2} - \beta D_0 \left( \frac{2}{\beta h\nu} - \frac{1}{2} \right) + (\beta D_0)^2 \left( \frac{2}{3\beta h\nu} \right) \right] \quad (2-4)$$

where  $\nu$  is the vibrational frequency of the ground state. Rice (ref 39) criticized this result. Although agreeing that rotation should be included, he pointed out that adding the rotational term to the potential energy curve would produce a weak maximum at some inter-nuclear separation greater than the equilibrium separation. This maximum is known as the rotational barrier. Rice stated that the barrier would result in a reduction in the dissociation rate. No quantitative evaluation of this effect was made in the paper.

In addition to raising the question of rotational effects, the theories of Rice and Careri have resulted in the formation of two different theoretical "camps" regarding vibrational bias or how dissociation is distributed over the vibrational levels. Rice calculated the dissociation rate by assuming a strong bias of the dissociation reaction toward high vibrational states. He assumed that dissociation

proceeded dominantly from vibrational states within  $kT$  of the continuum and that it was necessary for molecules to climb the "ladder" of vibrational states from the lower states to these upper levels prior to undergoing a collision resulting in dissociation. Conversely, Careri felt that the dissociation process was more evenly distributed over the various vibrational states (that is, had a weaker vibrational bias). In his view, dissociation was likely to occur by direct transitions from low vibrational levels as well. We'll return to this point when we review the collisional approach, but at this time state that this question of bias has yet to be resolved and the two "camps" remain separated.

It is easy to cite the limitations of the classical approach especially if we are considering highly non-equilibrium circumstances. The assumptions of equilibrium and of every collision possessing sufficient energy resulting in reaction are questionable. The rate of collisionally induced dissociation should be amenable to a calculation based on the detailed mechanics of the collision without invoking such strong and limiting assumptions. The task of establishing a more detailed analytic theory is certainly worthwhile and has been pursued utilizing both the statistical and the collisional approaches.

### Phase Space Theories

The statistical theories approach the problem of dissociation and recombination by reasoning that near the

dissociation limit, transitions between states are very rapid and a classical approximation is valid. Keck (refs 42, 43, 44) states that because of the high density of levels near the dissociation limit, the classical Master Equation is appropriate for treating dissociation and recombination. In the limit of small energy transfers this integro-differential equation may be reduced to an equivalent diffusion equation. Reactions are then considered as systems crossing boundaries and described as the motion of a representative point in an 18 dimensional phase space. Wigner (refs 45, 46, 47) pioneered research in this area by considering the phase space volume accessible to the three recombining atoms. The phase space is divided into a recombined region, where two atoms have recombined in the presence of a third body, and a free region. The division into two regions is based on the fact that in the recombined region the relative kinetic energy is negative and in the free region it is positive. The trajectories of the atoms represent lines in phase space and the reaction rate is represented by the number of such trajectories entering the recombined region. This analysis only yields an upper bound to the recombination rate since it neglects recrossing of the phase boundary surface. Some ambiguity may exist in definition of the recombined region. In order to remove the ambiguity, the recombined region of phase space is taken as a "trial surface," which is then varied subject to the condition that the rate constant obtained is a minimum and a

least upper bound is obtained. Refinements of the theory over the past 10 years have included the evaluation of a recrossing parameter and a correction for departures from equilibrium. Suitable choice of adjustable parameters in the theory has yielded rate constants of the correct order of magnitude and temperature dependence for a variety of diatomic molecules (ref 109).

### Collisional Approach

A collisional approach to dissociation is undertaken in the present work. Adoption of this approach is encouraged by the rapid advances in vibrational kinetic studies relating to laser technology and the new availability of experimental data on non-equilibrium vibrational distributions and kinetic rates. Moreover, the collisional approach offers the unique prospect of treating the highly non-equilibrium situations of intense optical pumping and analyzing the new generation of excimer laser systems.

Several detailed collisional theories of molecular dissociation have surfaced over the past twenty years. As brought out in Chapter I, since the decomposition of the molecule can be assumed to be instantaneous, the observed dissociation rate is governed by the rates of thermal activation and energy exchange of the molecule. We can investigate this thermal activation providing we know the transition rates, V-V and V-T, of the various vibrational states of the molecule. The calculation of the dissociation rate is then based on the solution of the Master Equation, a system

of coupled kinetic equations describing transitions between all the bound and free states of the diatomic molecule. The Master Equation formalism will be developed in the next chapter. Here we review previous collisional approaches to the dissociation problem. The main differences in the various calculations relate to the internal modes considered, the mechanisms of energy exchange, and the vibrational bias of the dissociation reaction. These differences lead to variations in the magnitude and temperature dependence of the calculated rates.

First let us consider those works concerned with a single quantum stepwise excitation. The early work of Nikitin (refs 48, 49, 50) treated the dissociation of diatomic molecules in the presence of an inert diluent. The molecule was represented as non-rotating Morse oscillator and each molecular vibrational state was treated as a distinct species. Within this analysis he established the importance of changes in adiabaticity with respect to vibrational transitions and demonstrated that most of the steps in the vibrational excitation process are near adiabatic, occurring with small probability for large exchanges in vibrational energy. In the temperature range of interest for most studies of dissociation, it was determined that only those levels within  $kT$  of the dissociation energy were definitely non-adiabatic. In this region, collisions are impulsive and transitions occur with a probability

approaching unity. The following expression for the dissociation rate was obtained

$$k_d = Z \left[ \sum_{j=0}^d \exp(-\beta E_j) \sum_{K=j}^{d+1} \exp(\beta E_K) / P_{K,K-1} \right] \quad (2-5)$$

where  $E_j$  denotes the vibrational energy of levels  $v=0$  to  $d$ , and  $P_{K,K-1}$  the V-T probability. Upon replacing the summations with an integration he obtained

$$k_d = Z \hbar \omega / (D_0 / \beta)^{1/2} \exp(-\beta D_0) [1 - \exp(-\beta \hbar \omega)] \quad (2-6)$$

revealing an activation energy,  $E_{act}$ , less than the dissociation energy,  $D_0$ . The dissociation rate was then averaged over all rotational states assuming rotational equilibrium and making allowance for the fact that the depth of the radial potential will decrease with increasing angular momentum. Application of this analysis was limited to  $\text{Br}_2$  at one temperature.

In a subsequent paper by Stupochenko (ref 51), the Master Equation was solved under the assumption of the existence of a steady state in all vibrational states. He concluded, as Nikitin had, that a strong vibrational bias existed for the dissociation reaction. In addition, the existence of vibrational depletion was discussed. Vibrational depletion results from the coupling of vibrational and dissociative kinetics and is manifested in a reduction

in the population of the vibrational states from their equilibrium value. This depletion is most significant for highly excited vibrational states. Stupochenko provided no detailed calculation of transfer rates or quantitative calculations of the dissociation rate.

These previous works favor the "ladder" model concept and conclude that the rate determining step in the dissociation reaction is the activation of lower states. Concurrent with these publications were the works of Montroll and Shuler (refs 52, 53, 54, 55, 56) in which they considered the vibrational relaxation of molecular systems. They considered a system of simple harmonic and later anharmonic oscillators. In the latter investigation (ref 54), the solution was achieved through a numerical solution of the Master Equation. In all circumstances, they concluded that single quantum transitions are most likely and that relaxation and dissociation processes are "ladder-like." Calculated dissociation rates (ref 55), however, were several orders of magnitude lower than experimental values. Pritchard (ref 57) performed a quantitative investigation of the kinetics of dissociation of a diatomic gas in which he numerically calculated Morse matrix elements for use in the Jackson-Mott (ref 21) transition probabilities for hydrogen. Bound-bound and bound-free transitions were evaluated. He showed that single step transitions dominate and that a depopulation or depletion of high vibrational levels would occur.

Benson and Fueno (ref 58) modeled the recombination process assuming a cascaded, stepwise process. Landau-Teller (ref 19) transition probabilities based on simple harmonic oscillator matrix elements were used. Rotational effects were accounted for by introducing a long-range, polarization term, to the potential. A steady-state solution was obtained and the recombination coefficient calculated for a variety of gases. Order of magnitude agreement was obtained.

Treanor and Marrone (refs 59, 60) analyzed the effect of vibrational-dissociation coupling using a modified form of the Landau-Teller relaxation equation. They exercised great care in incorporating experimentally determined relaxation times and equilibrium rate constants. Various empirical biases for the dissociation reaction were investigated ranging from an Available Energy approach to a more strongly biased dissociation probability. The results of this analysis supported the ladder model to a degree, but suggested a range of participating vibrational levels rather than a single transition occurring from the last bound vibrational level.

At this point in the historical development of collisional rate theories, the "ladder" model had obtained a strong vote. Most analyses, however, were quite limited and qualitative. Vibrational structure of the ground electronic state was the by-word with little critical attention being devoted to incorporating a detailed experimentally consistent set of V-T rates, examining the role of rotation

and electronically excited states, or examining the effect of complex collisions. Time dependent solutions of the Master Equation were in the wings awaiting better numerical methods and faster computers. We will now discuss the "New Era" of collisional theories during which significant strides were taken to address the areas cited above.

Although published in 1959, Herzfeld's (ref 61) work on molecular dissociation revealed an excellent perspective. The paper, although marred by several errors which obviate his quantitative results, attempted to utilize a realistic set of kinetic rates based on the SSH theory using Morse oscillator wave functions and an exponential interaction potential. In addition, he specifically considered the effect of V-V transfer on the dissociation of a pure gas.

The influence of rotational states on the dissociation process was discussed by Bauer and Tsang (ref 62) in a thought-provoking article. Here they called attention to several mechanisms which effectively couple translational and vibrational states through the intermediary of chemical reactions. They proposed that the transfer of energy involving both rotation and vibration at approximately constant total energy can be induced by distant collisions. Consideration of such collisions gave new importance to the rotational structure and provided alternative paths for rapid vibrational relaxation. Bauer and Tsang hypothesized that this may account for the fact that the observed dissociation rates are considerably higher than those calculated

under the assumptions of the standard ladder model. The fact that detailed calculations of dissociation rate for a variety of gases using the "ladder" were not completed at this time left this hypothesis unproved.

Snider (ref 63) considered the effect of angular momentum on the dissociation rate in diatomic molecules, assuming rotational equilibrium. Using a classical approach, he analyzed the influence of rotation on the mechanics of the collision. His results did not differ substantially from those of Nikitin (ref 50).

A comprehensive study of the "ladder" model, vibrational depletion, and V-V exchange was presented by Rich (ref 64). Following the work of Herzfeld (ref 61), he used the Jackson and Mott (ref 21) near-adiabatic distorted wave treatment with an exponentially repulsive interaction potential in an approximate form that enabled him to obtain a simple analytic form for the matrix elements. Under the approximation used, a single quantum selection rule emerged, while still retaining the effects of anharmonicity in the matrix elements. This form was used in an SSH calculation of the transition probabilities. A time dependent solution of the coupled rate equations was obtained in addition to an analytical expression for the quasi-steady state dissociation rate. Good agreement was obtained with experimental data; however the Mies asymmetrical correction factor (Appendix A), was not properly accounted for, resulting in

a serious overestimation of the transition probabilities.\* Rich proposed that V-V exchange accounted for the observed rate enhancement in pure gases and calculated the cross-section for resonant V-V exchange. Based on the magnitude of the calculated resonant exchange cross-section, he concluded that it was sufficient to account for the rate enhancement.

Dove (ref 65) investigated the vibrational relaxation and dissociation of hydrogen diluted in an argon heat bath by performing a numerical integration of the coupled rate equations. Collisional transition probabilities, for V-T exchange, were calculated by the SSH method modified for a Morse oscillator. The time-dependent Master Equation was numerically integrated and vibrational depletion discussed. After correcting his transition probabilities to agree with experimentally determined relaxation data, the calculated dissociation rates were a factor of 30 too low. Multiple quantum transitions were later included in the analysis and resulted in an increase in the dissociation rate of less than 15%. Moreover, the computed activation energy was too large. In a subsequent paper by Dove (ref 66), the ladder approach was modified to take explicit account of rotational effects using the matrix elements of Roberts (ref 67). This distributed the dissociation among the vibrational levels and resulted in an increase in the dissociation rate and a

---

\*The correction factor was assumed to be independent of vibrational state.

reduction in the activation energy. This calculation yielded good agreement with experimental data both in rate magnitude and temperature dependence.

The relationship of the observed activation energy to vibrational bias was examined by Johnston (ref 68). Noting that the experimentally observed activation energy is always less than the dissociation energy, and decreases with increasing temperature, he analyzed the consistency of various models of dissociation with respect to these criteria in a steady state analysis. He concluded that a ladder-climbing model for the reaction process with dissociation occurring only from the top vibrational level was unacceptable and that diatomic molecules dissociate from all levels.

The influence of V-V transfer on the dissociation rate was investigated by Kiefer (ref 69). He used a steady-state approximation for a single-quantum step Master Equation, and concluded that the rate was only slightly enhanced when V-V transitions were included. Using the "ladder" model he achieved "quite satisfactory agreement" for dissociation and recombination rates in  $O_2$ ,  $H_2$  and  $HCl$  and provided "qualitative explanations for nearly all the unusual features" of the measured rate. No rotational effects were included.

(As you can now see, contradictions and inconsistencies have arisen in the literature cited regarding the applicability of the ladder model, the role of rotation, and the influence of V-V effects. We will continue with this review

of the collisional theories, however, and later evaluate the status of collisional dissociation theories.)

Pritchard examined the rotational contribution to dissociation and recombination in a series of papers (refs 70, 71, 72) and found it to be significant. In addition, he addressed the relation of rotational transitions to observed activation energies and their temperature dependence. He concluded that inclusion of rotation adequately accounted for these variations.

Recently Kiefer (ref 73) has taken a new and refreshing look at the problem of dissociation. He concludes, in light of recent measurements of dissociation and relaxation rates, that there can be at most a very weak vibrational bias for dissociation from vibrational states. The ladder model is out. His analytic approach demanded consistency in the magnitude and temperature dependence of the dissociation rate and induction or incubation time (the time to establish steady state dissociation). He also investigated the effect of vibrational depletion. He points out that depletion is so severe that any theory which assumes that dissociation proceeds only from highly excited vibrational states is unacceptable. This is an extremely interesting comment, since only three years ago (ref 69) the same author used a ladder model and achieved "quite satisfactory agreement." He concludes at this time, however, that dissociation must take place to an appreciable extent from low lying vibrational states in accordance with the early ideas

of Careri (ref 41) and the recent theory of Johnston (ref 68).

Time-dependent solutions of the vibrational Master Equation for hydrogen, including dissociation, have recently been obtained by Kewley (ref 74) using the standard ladder model without rotation. The rates used were of the SSH form (ref 20) as modified by Keck and Carrier (ref 28) and fitted to the experimental relaxation data. The calculated dissociation rate showed fair agreement in magnitude and temperature dependence with experimental data. When V-V exchanges changes were included in the analysis, it was noted that they resulted in only a small enhancement of the dissociation rate.

#### Contradictions and Inconsistencies

Through this review of the collisional theories of dissociation, it has become apparent that despite the introduction of new computational techniques and the existence of reasonable transfer rate data, inconsistencies and contradictions exist. In order to highlight this fact and capsule the historical review of collisional rate theories, a status table of dissociation theories is presented in Table II. In this table we list the author and year of the work cited, evaluate the success of the theory, classify the approach and vibrational bias, and list the gases considered. In addition, we point out in those works considering the effects of V-V transfer, whether or not this

TABLE II

## STATUS TABLE OF DISSOCIATION THEORIES

Agreement with Experiment	Approach					Vibrational Bias			V-V Enhancement	Cases Considered
	A	N	SS	TD		L	R	O		
Good - G										
Fair - F										
Poor - P										
See Text - ST										
Montroll & Shuler (57-59) P	X	X	X	X		X			-	H <sub>2</sub>
Pritchard (61) ST		X	X			X			-	H <sub>2</sub>
Rich (65) G	X	X	X	X		X			Yes	H <sub>2</sub> O <sub>2</sub> , Br <sub>2</sub>
Dove (71) P		X		X		X			Yes	H <sub>2</sub>
Johnston (72) P		X	X			X			-	H <sub>2</sub> N <sub>2</sub> , I <sub>2</sub> , O <sub>2</sub> F <sub>2</sub>
Kiefer (72) G		X	X			X			No	H <sub>2</sub> O <sub>2</sub> , HCl
Kiefer (75) P	X		X			X			No	H <sub>2</sub> O <sub>2</sub> , N <sub>2</sub> CO, F <sub>2</sub> , HCl
Kewley (75) F		X		X		X			No	H <sub>2</sub>
Nikitin (57, 59) G	X		X				X		No	Br <sub>2</sub> (lTemp.)
Dove (72) G		X		X			X		-	H <sub>2</sub>
Johnston (72) G		X	X					X	-	H <sub>2</sub> N <sub>2</sub> , I <sub>2</sub> , O <sub>2</sub> , F <sub>2</sub>
Pritchard (73, 76) G(H <sub>2</sub> ), F		X	EQ				X		-	H <sub>2</sub> O <sub>2</sub> , N <sub>2</sub> CO, Br <sub>2</sub> , I <sub>2</sub>
Present Study	X	X	X	X		X	X	X	X	H <sub>2</sub> O <sub>2</sub> , N <sub>2</sub> CO, Br <sub>2</sub> , I <sub>2</sub>

exchange mechanism led to an enhancement of the dissociation rate. Observe that calculations utilizing the ladder model have extended over the past twenty years and have yielded agreement ranging from good to poor. Fully time dependent calculations have been limited in scope and yielded contradictory results. Steady state analyses based on the ladder model, while having treated a wider variety of gases, also have yielded contradictory results. Investigations of rotational effects and empirical biases have been limited to steady state and equilibrium analyses, with time dependent calculations concentrating on  $H_2$ .

In the present study, we shall address many of the inconsistencies which have arisen. We will attempt to develop a collisional model of dissociation that provides reasonably accurate values for dissociation and recombination coefficients, exhibits an acceptable temperature dependence, and permits an evaluation of rate enhancement effects in pure gases. We will utilize both a detailed time dependent and steady state analysis in a thorough and consistent evaluation of the kinetics of the dissociation process and study the following questions which have been raised by previous works:

1. Can a standard "ladder" model of dissociation accurately predict dissociation rate magnitude and temperature dependence for a variety of gases over broad temperature ranges?

2. What role is played by rotational structure and must it be included for accurate rate determination?

3. Is it possible to select a particular model based on the observed incubation times?

4. Can the observed rate enhancement in pure gases be attributed to complex exchange phenomena?

These questions will be addressed by considering a variety of gases, not limiting ourselves to hydrogen as have others, and utilizing a fully coupled time-dependent solution of the Master Equation, to validate any steady-state assumption or analysis.

### Chapter III. Development of the Master Equation

#### Introduction

In this chapter we will develop the Master Equation formalism which will be applied to a collisional investigation of the dissociation reaction. The Master Equation approach to the dissociation problem is attractive because it maintains the discrete nature of the individual states of the molecule, is exact in principle, and provides a better understanding of the course of internal relaxation and its coupling to the dissociation reaction. In addition, this approach may be easily transferred to the related problem areas of kinetic modeling of lasers.

#### System and Assumptions

The physical system under consideration is a pure gas consisting of diatomic molecules or a gas mixture of a diatomic gas diluted in an inert gas, such as argon. We will model the dissociation of diatomic gases as observed under experimental conditions typical in shock tube studies. Under these conditions the shocked gas is suddenly raised to a high temperature and maintained at constant volume. The experimental dissociation rates are inferred by using a light absorption (ref 102) or interferometric technique (ref 97) to measure the density profiles behind the shock. In our analysis, chemical reactions, other than dissociation

and recombination, will be excluded. The energy of the system is contained in the translational, rotational, vibrational, and electronic modes of the molecules. Energy is exchanged or transferred through the various modes by means of collisions. Translational and rotational energy are exchanged readily, and therefore these modes rapidly equilibrate only requiring of the order of 100 collisions (ref 24). In this analysis, we will be concerned primarily with the exchange of vibrational energy resulting from V-V and V-T exchanges and with the development of a formalism for treating the vibrational and dissociative relaxation of diatomic gas.

The overall dissociation process, although representing one of the simplest of all collisionally induced gas phase reactions, is extremely complex. The process is governed by a set of coupled non-linear differential equations for each of the internal molecular states as well as the continuum. Formally each state population will be governed by an equation

$$\frac{dN_l}{dt} = \sum_{j,k} \tilde{R}_{jil}^{ki} N_j N_k - \sum_{j,k} \tilde{R}_{lij}^{kj} N_l N_i$$

where  $N_l$  is the concentration of molecules in state  $l$ , and the  $\tilde{R}$ 's represent generalized rate coefficients for the population or depopulation of state  $l$ . This set of equations is commonly referred to as the Master Equation and

is generally applicable (refs 75, 76, 77) for determining the rate law for the dissociation reaction.

In principle, the rate of molecular dissociation could be calculated by incorporating the detailed mechanics of the molecular collisions into the generalized rate coefficients and solving the resulting set of equations for each and every state. Speaking realistically, though, this is not possible and probably not desirable. Hydrogen, simple  $H_2$ , would require close to 350 states to be tracked while Iodine would require over 50,000 states to treat the ground electronic state alone. The attempt in this analysis will be to obtain a simplified Master Equation while retaining only those physically important mechanisms required to describe and understand the process of dissociation. To that end, the following assumptions are introduced.

- i. The translational and rotational degrees of freedom are in complete Boltzmann equilibrium.
- ii. The molecules in each vibrational state are treated as separate species.
- iii. Only single quantum vibrational exchanges occur.
- iv. The molecule is represented as a Morse oscillator rigid rotator system.

Given the experience of previous works, the results of experimental relaxation studies, and the state-of-the-art of collision theory, the above assumptions are reasonable

for the scope of this research. As justification for (i), one may offer the standard response of the extremely rapid relaxation of the translational and rotational degrees of freedom. Since rotation is involved in the dissociation process, it is possible that this equilibrium may be perturbed. However, to effectively analyze the extent of any departure from equilibrium would require rate data that is simply not available. Assumption (iii) may be viewed as quite severe; however the restriction to single quantum transitions has been examined previously and has been shown to have little effect on the dissociation rate (refs 65, 90). This fact is consistent with the adiabatic nature of the multiple quantum, V-T exchanges. In addition, it points out that the interplay of the dissociation and vibrational relaxation processes results in an increased vibrational depletion and a resultant saturation of the dissociation rate. A Morse potential was selected because of its simplicity and ease of application to theoretical heavy particle collision probabilities. The Morse potential is able to match very well the spectroscopically observed vibrational energies and retains the important anharmonic features of the molecular potential. Here, vibrational energies are measured from the dissociation limit and within the Morse representation are given by (ref 77)

$$\begin{aligned}
 E_v &= -D_e + \frac{\hbar^2}{2Mr_e^2} \left\{ 2\alpha\gamma(v+\frac{1}{2}) - \alpha^2(v+\frac{1}{2})^2 \right\} \\
 &= -D_e + \hbar\omega(v+\frac{1}{2}) \left\{ 1 - \delta(v+\frac{1}{2}) \right\}
 \end{aligned}
 \tag{3-2a}$$

where  $\hbar\omega = \frac{\hbar^2\alpha^2\gamma}{Mr_e^2}$  and  $\alpha^2 = \frac{\omega^2 Mr_e^2}{2D_e}$

for the Morse potential

$$V(r) = D_e \left\{ 1 - \exp[\alpha(r-r_e)] \right\}^2 \tag{3-2b}$$

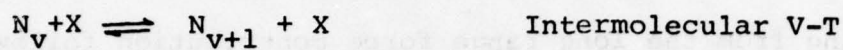
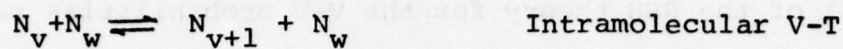
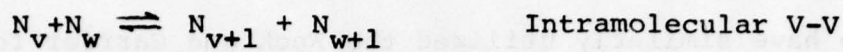
$D_e$  is the well depth,  $M$  the reduced mass,  $r_e$  the equilibrium separation,  $\omega$  the oscillator frequency. Values of the required constants were obtained from Herzberg (ref 78).

### Transition Rates

Let's now discuss the rates that are to be incorporated into the Master Equation. The pumping and relaxation process controlling the state populations can be separated into two collisional classes: collisions between heavy particles and electron impact collisions.

The heavy particle transfer rates, V-V and V-T were discussed in Chapter I. In summary, these processes can

be represented by the following reactions under the single quantum assumption:



It is conventional to express the heavy particle kinetic rates as the product of the collisions frequency,  $Z$ , the applicable two populations, and the transition probability. For the V-T processes we utilize the SSH form (ref 22) as modified by Keck and Carrier (ref 28) and fit this form to the data of Millikan and White (ref 79) and Miller and Millikan (ref 80). The transition probability for  $v+1 \rightarrow v$  is then written

$$P_{v+1,v} = P_0(\tau) \frac{v}{(1-\delta v)} F_{v+1,v}(\lambda_{v+1,v}) \quad (3-3)$$

where

$$F_{v+1,v} = \frac{1}{2} \{ 3 - \exp(-\frac{2}{3} \lambda_{v+1,v}) \} \exp(-\frac{2}{3} \lambda_{v+1,v})$$

$$\lambda_{v+1,v} = (2)^{-\frac{1}{2}} \sqrt{\frac{\theta}{T}} (1-2\delta v) \hbar \omega$$

and  $\Theta$  is the SSH group of molecular constants (ref 22), while  $P_0$  is obtained from the experimental vibrational relaxation times.

We have similarly utilized the Keck and Carrier form (ref 28) of the SSH theory for the V-V probabilities resulting from short range forces and augmented this with a term resulting from the long range force contribution following Sharma and Brau (ref 81) where appropriate. The resulting probability expression for  $v+1 \rightarrow v$  and  $w \rightarrow w+1$  is

$$P_{v+1,v}^{w,w+1} = [S_{v+1,v}^{w,w+1} + L_{v+1,v}^{w,w+1}] \exp\left[\frac{\beta(E_{v+1} - E_v - E_{w+1} + E_w)}{2}\right] \quad (3-4)$$

where the short and long range contribution are designated by S and L. The short range contribution is functionally similar to the SSH V-T model while the long range terms are complex and are matched by a simple algebraic form. The details of both terms are given by Herzfeld and Litovitz (ref 22), Sharma (ref 81), and Fisher (ref 82).

The electron impact collision rates are utilized only in the non-equilibrium portion of the present work and are obtained from a steady state solution of the collisional Boltzmann equation for the electron energy distribution. We will discuss this treatment in Chapter VI and for the moment merely include the effective electron impact rates in the development of the Master Equation for completeness.

### Master Equation Formalism

Having discussed the physical system and the rates, let us proceed to write the rate equations for the instantaneous population of the  $v$ th vibrational state,  $N_v$ .

$$\begin{aligned}
 \dot{N}_v = n_e \sum_k (R_{vk} N_v + R_{kv} N_k) + N_{v+1} (VT_{v+1,v} + \sum_{k=0}^{v-1} W_{k,v}^{k,k+1} N_k) \\
 - N_v (VT_{kv-1} + VT_{v,v+1} + \sum_{k=0}^{v-1} VV_{k,v-1}^{k,k+1} N_k + \sum_{k=1}^v VV_{k,v+1}^{v,v+1} N_k) \\
 + N_{v-1} (VT_{v-1,v} + \sum_{k=1}^{v-1} W_{k,v-1}^{v-1,v} N_k) \\
 - N_v d_v + r_v A^2 \quad v=0,1,\dots,v^*
 \end{aligned} \tag{3-5}$$

Here the first term accounts for electron impact collisions and the last five terms account for heavy particle collisions with

$n_e (\text{cm}^{-3})$  = electron number density

$R_{vk} (\text{cm}^3/\text{sec})$  = electron excitation rate from vibrational state  $v$  to  $k$

$VV_{k,v}^{k,k+1} (\text{cm}^3/\text{sec}) = Z P_{v+1,v}^{k,k+1}$  = V-V transfer rate for  $v+1 \rightarrow v$  and  $k \rightarrow k+1$

$VT_{v+1,v} (\text{1/sec}) = Z M P_{v+1,v}$  = V-T transfer rate for  $v+1 \rightarrow v$

$VT_{v,v+1} (\text{1/sec}) = Z M P_{v,v+1}$  = V-T transfer rate for  $v \rightarrow v+1$

$d_v$  (1/sec) = dissociation rate out of level  $v$

$N_v$  ( $\text{cm}^{-3}$ ) = vibrational population of level  $v$

$r_v$  ( $\text{cm}^3/\text{sec}$ ) = recombination rate into level  $v$

$A$  ( $\text{cm}^{-3}$ ) = atom number density

For rare gas mixtures, the VT rates are summed over all species  $M_s$ . In addition, it should be pointed out that microscopic reversibility or detailed balance requires that

$$VT_{v+1,v} = VT_{v,v+1} \exp[\beta(E_{v+1} - E_v)]$$

$$VV_{v+1,v}^{w,w+1} = VV_{v,v+1}^{w,w+1} \exp[\beta(E_{v+1} - E_v + E_w - E_{w+1})]$$

$$d_v = K_v^c r_v$$

where  $K_v^c = \frac{g_A g_A}{g_{A_2}} \left( \frac{Q_{\text{trans}}^2(A)}{Q_{\text{trans}}(A_2)} \right) \left( \frac{\exp(-\beta(D_e - E_v))}{Q_{\text{rot},v}(A_2)} \right)$

is the specific vibrational equilibrium constant and with the  $g$ 's representing the electronic degeneracy and the  $Q$ 's the single particle partition functions. It should be noted that

$$[K_c]^{-1} = \sum_v [K_v^c]^{-1}$$

For further computations and manipulations it is helpful to introduce the following "lumped" form of the Master Equation

$$\begin{aligned} \dot{N}_v = & N_{v+1} \rho_{v+1,v} + N_{v-1} \rho_{v-1,v} - N_v (\rho_{v,v+1} + \rho_{v,v-1}) \\ & - d_v N_v + \epsilon_v - n_v A^2 \end{aligned} \quad (3-6)$$

where  $\epsilon_v$  = electronic pumping term for level  $v$

$$\rho_{v+1,v} = VT_{v+1,v} + \sum_{k=0}^{v*1} W_{v+1,v}^{k,k+1} N_k$$

$$\rho_{v-1,v} = VT_{v-1,v} + \sum_{k=0}^{v*} W_{v-1,v}^{v-1,v} N_k$$

Analytical solutions of these  $(v^*+1)$  coupled non-linear rate equations for an anharmonic oscillator have not been obtained. However, if we consider a highly diluted gas mixture, and consequently obtain a linear set, the formal solution is well known, in terms of a series of exponentials in the eigenvalues (ref 83). Numerical procedures could be utilized to determine the roots of the  $(v^*+1)$ th order polynomial. Rather than taking this approach, we will attach the general problem with a numerical integration of the rate equations.

### Numerical Method

Given an initial state population distribution and a set of suitably defined rates, we wish to perform a time-dependent integration of the rate equations. Since the relaxation rate is governed by the transition probabilities, V-V and V-T, which range over many orders of magnitude, the resulting time constants for the coupled set differ substantially in magnitude. Simply stated the system of equations is stiff.

Gear (ref 84) has summarized the general philosophy of stiffness. Let us here discuss stiffness in the context of vibrational relaxation. Vibrational relaxation kinetics include fast and slow reactions. The decay times  $\tau$  can be related to the eigenvalues  $\mu$  of the Master Equation Jacobian. The fast reactions control numerical stability and step size, while the slow reactions determine the truncation error. In this study the "multistep implicit stiffly stable scheme" proposed by Gear (ref 85) was utilized. The Gear scheme utilizes a predictor-corrector technique to perform the stiff integration. The predicting technique, that insures stiff stability, is coupled to a correcting scheme that utilizes the Jacobian to accomplish time step adjustment. The "Gear package" is an extremely user oriented, flexible code, and efficiently handles the integration of the Master Equation.

### Steady State Solutions of the Master Equation

A complete time dependent solution of the Master Equation is complex and computationally, fairly time consuming. In addition, a direct integration while providing results, often fails to provide the insight that can be obtained from an analytic approach. For this reason, we will also investigate steady state solutions to the coupled rate equations.

Any steady state analysis is based on differences in characteristic times. The relevant times here are those of vibrational relaxation and dissociation. If the processes of vibrational relaxation and dissociation are separable with the rate of vibrational relaxation being greater than the rate of dissociation, a quasi-steady state may be assumed to exist in the vibrational populations. A more general existence of this steady state has been documented (refs 64, 86, 87) and numerous analyses based on the assumption have evolved (refs 48, 49, 63, 64, 69).

We shall assume, and later numerically validate, the existence of a steady state in the following development of the vibrational distribution and dissociation rate. The steady state form to be derived will then be applied to the situation of thermal dissociation and the highly non-equilibrium situations obtained under electric discharge or optical pumping conditions. Let us proceed by writing the generalized rate equations, where we will omit

recombination terms since we are far from equilibrium. It will be assumed that the steady state achieved is characterized by the vibrational distribution assuming a self-similar form, that is

$$\frac{\dot{N}_v}{N_v} = -\alpha = \text{constant} \quad v=0,1,\dots,v^* \quad (3-7)$$

From (3-6)

$$\dot{N}_0 = N_1 \rho_{1,0} - N_0 \rho_{0,1} - N_0 d_0 + E_0$$

$$\dot{N}_1 = N_2 \rho_{2,1} + N_0 \rho_{0,1} - N_1 \rho_{1,2} - N_1 \rho_{1,0} - N_1 d_1 + E_1$$

$$= N_2 \rho_{2,1} - N_1 \rho_{1,2} - \dot{N}_0 - N_0 d_0 + E_0 - N_1 d_1 + E_1$$

$$\dot{N}_j = N_{j+1} \rho_{j+1,j} - N_j \rho_{j,j+1} - \sum_{i=0}^{j-1} (\dot{N}_i + N_i d_i - E_i) + E_j - N_j d_j$$

$$\dot{N}_{v^*} = N_{v^*+1} \rho_{v^*+1,v^*} - N_{v^*} \rho_{v^*,v^*+1} - N_{v^*} d_{v^*} + E_{v^*}$$

$$= - \sum_{k=0}^{v^*-1} (\dot{N}_k + N_k d_k - E_k) - d_{v^*} N_{v^*} + E_{v^*} \quad (3-8)$$

Defining  $G_j \equiv \sum_{i=0}^j \{ \dot{N}_i + N_i d_i - E_i \}$  (3-9)

and substituting in (3-8) yields

$$G_j = N_{j+1} \rho_{j+1,j} - N_j \rho_{j,j+1} \quad (3-10)$$

and

$$N_j = \frac{\rho_{j-1,j} N_{j-1} + G_{j-1}}{\rho_{j,j-1}} \quad (3-11)$$

in view of (3-7)

$$N_j = \frac{\rho_{j-1,j} N_{j-1}}{\rho_{j,j-1}} + \sum_{i=0}^{j-1} \frac{\{[d_i - \alpha_i] N_i - \epsilon_i\}}{\rho_{j,j-1}} \quad (3-12)$$

upon noting  $G_j = 0$ , we obtain

$$N_{j-1} = \frac{\rho_{j,j-1} N_j}{\rho_{j-1,j}} + \sum_{i=j}^{v^*} \frac{\{[d_i - \alpha_i] N_i - \epsilon_i\}}{\rho_{j-1,j}} \quad (3-13)$$

Explicitly relating the V-V and V-T rates to the  $\rho$ 's after invoking detailed balance we obtain the simplified identification

$$\begin{aligned} \rho_{j-1,j} &= e^{-\delta_j} \left[ \sum_{w=1}^{v^*} W_{j,j-1}^{w,w} N_w e^{\delta_w} + VT_j \right] \\ \rho_{j,j-1} &= \sum_{w=1}^{v^*} V_{j,j-1}^{w,w} N_{w-1} + VT_j \end{aligned} \quad (3-14)$$

where  $\delta_w \equiv \beta (E_w - E_{w-1})$ .

Equation (3-13) is an extremely simple steady state solution and will provide insight as to limiting forms of the vibrational distribution and the sensitivity and extent of vibrational depletion. For a specified set of V-V and V-T rates, and any distribution of dissociation rates we can use the steady state form of (3-13) to calculate both the vibrational distribution and the steady state dissociation rate. In addition, it is a stable representation of the distributions amenable to rapid solution using iterative techniques. These results will be presented in Chapter V.

Here, let us first establish the various limiting forms for the distribution. With no dissociation or pumping,  $G_j=0$ . Then  $N_j=N_{j-1}e^{-\delta_j}$ ; the distribution is Boltzmann as anticipated. The Treanor distribution (ref 29)

$$N_j = N_0 \exp(\phi j - \beta E_j)$$

or

$$\frac{N_j}{N_{j-1}} = \exp(\phi - \delta_j) \quad (3-15)$$

where  $\phi$  is the vibrational temperature parameter, must also be obtained when only V-V terms are retained. Substituting into (3-13) we obtain

$$\frac{N_j}{N_{j-1}} = e^{-\delta_j} \frac{\sum_{w=1}^{v^*} \{ V_{j,j-1}^{w-1,w} N_w e^{\delta_w} \}}{\sum_{w=1}^{v^*} \{ V_{j,j-1}^{w-1,w} N_w \frac{N_{w-1}}{N_w} \}}$$

which reduces to

$$\frac{N_j}{N_{j-1}} = \frac{e^{\delta_j} \sum_{w=1}^{v^*} \{V_{j,j-1}^{w,w} N_w e^{\delta_w}\}}{\sum_{w=1}^{v^*} \{V_{j,j-1}^{w,w} N_w e^{-\phi} e^{\delta_w}\}} = e^{\phi} e^{-\delta_j}$$

Thus again a consistent form is yielded.

Next let's look at a situation typical of many shock tube experiments where a diatomic gas is highly diluted in an inert gas. Under these circumstances we may neglect the V-V and  $\epsilon$  terms and obtain from (3-13)

$$N_{j-1} = \left\{ N_j + \sum_{i=j}^{v^*} \frac{[d_i - \alpha_i] N_i}{VT_j} \right\} e^{\delta_j} \quad (3-16)$$

From (3-16) we observe that the dissociation process causes the vibrational populations to deviate from the equilibrium distribution. This deviation results in a reduction in the dissociation rate below the value that would be obtained if no deviation occurred. The extent and character of this departure from equilibrium is dictated by the behavior of the summation term in (4-8). This term is controlled by the transfer rate, V-T, and the magnitude and bias of the dissociation rates,  $d_v$ . Note that for the special case, where  $d_v$  is a constant, there is no depletion. For the V-T rates and all biases considered in this study,

dissociation monotonically decreases the population of the vibrational states below their equilibrium value.

Let us now develop an alternate steady state solution, based on the analysis of Nikitin (ref 50). This solution yields an analytic form for the dissociation rate and does not require iteration. However, no information regarding the vibrational distribution is obtained. Consider a diatomic gas diluted in an inert gas such as argon, with dissociation proceeding only from the last bound level to an unbound pseudo-level. From (3-5), upon neglecting V-V terms, we obtain

$$\dot{N}_V = N_{V+1} VT_{V+1,V} - N_V (VT_{V,V-1} + VT_{V,V+1}) + N_{V-1} VT_{V-1,V} \quad (3-17)$$

with

$$VT_{V+1,V} = P_{V+1,V} Z$$

$$VT_{V,V+1} = VT_{V,V-1} = VT_{V+1,V} e^{-\delta_{V+1}}$$

Writing out this first few rate equations explicitly we obtain

$$\begin{aligned} \dot{N}_0 &= N_1 P_{1,0} Z - N_0 (e^{-\delta_1} P_{1,0} Z) \\ \dot{N}_1 &= N_2 P_{2,1} Z - N_1 (Z P_{1,0} + Z P_{2,1} e^{-\delta_2}) + N_0 P_{1,0} Z e^{-\delta_1} \\ \dot{N}_2 &= N_3 P_{3,2} Z - N_2 (Z P_{2,1} + Z P_{3,2} e^{-\delta_3}) + N_1 P_{2,1} Z e^{-\delta_2} \\ \dot{N}_k &= Z \{ P_{k,k-1} e^{-\delta_k} N_{k-1} - (P_{k,k-1} + P_{k+1,k} e^{-\delta_{k+1}}) N_k + P_{k+1,k} N_{k+1} \} \end{aligned}$$

for  $k=0,1,\dots,v^*$  and with

$$N_{v^*+1} = 0 \quad \text{and} \quad N_1 = 0 \quad (3-18)$$

As mentioned earlier, the general solution can be represented\* in terms of the eigenvalues,  $\mu_m$ , of the resulting matrix B

$$[\dot{N}] = [B][N]$$

resulting in a general solution of the form

$$N_k(t) = \sum_{m=0}^{v^*} A_k(\mu_m) \exp(-\mu_m t) \quad (3-19)$$

where the eigenvalues are ordered in increasing order of  $\mu_m$ .

Within the framework of the standard ladder model, dissociation will proceed from the last bound level to an unbound pseudo-level, with a rate given by  $P_{v^*+1, v^*} e^{-\delta_{v^*+1}} \equiv P_{\infty} e^{-\delta_{v^*+1}}$ . If  $P_{\infty} = 0$  which implies no dissociation, the matrix B yields the eigenvalues,  $\mu_m^0$ , corresponding to the thermal relaxation of the system with  $\mu_0^0 = 0$ . If  $P_{\infty} \neq 0$ , all values of  $\mu_m$  will be displayed in the same direction relative to  $\mu_m^0$ . Therefore  $\mu_m > \mu_m^0$  when dissociation is present. If  $\mu_0 < \mu_1$ , the distribution will reach a pseudo-steady-state and exponentially decay, reflecting the thermal dissociation

---

\*Provided B is non-defective, which we assume.

or decomposition of the molecule. Assuming that this inequality holds, the smallest eigenvalue,  $\mu_0$ , corresponding to the dissociation constant, can be found by expanding the determinant in the power series of  $\mu$  while retaining only first order terms. For a two level system the rate equations are:

$$\begin{aligned}\dot{N}_0 &= Z \left\{ -N_0 P_{1,0} e^{-\epsilon_1} + N_1 P_{1,0} \right\} = -\tilde{\mu}_0 Z N_0 \\ \dot{N}_1 &= Z \left\{ N_0 P_{1,0} e^{-\epsilon_1} - N_1 (P_{1,0} + P_{2,1} e^{-\epsilon_2}) \right\} = -\tilde{\mu}_0 Z N_1\end{aligned}\quad (3-20)$$

where  $\tilde{\mu}_0 \equiv \mu_0 / Z$

The determinant is given by,

$$\begin{bmatrix} -(P_{1,0} \alpha_1 - \tilde{\mu}_0) & P_{1,0} \\ P_{1,0} \alpha_1 & -(P_{1,0} + P_{2,1} \alpha_2 - \tilde{\mu}_0) \end{bmatrix} = 0 \quad (3-21)$$

where  $\alpha_n = \exp(-\beta[E_n - E_{n-1}])$

Setting the determinant equal to zero, we obtain

$$P_{1,0} \alpha_1 [P_{1,0} + P_{2,1} \alpha_2] - \alpha_1 P_{1,0} \tilde{\mu}_0 - \tilde{\mu}_0 (P_{1,0} + P_{2,1} \alpha_2) - \alpha_1 P_{1,0}^2 = 0$$

$$\text{Thus } \tilde{\mu}_0 = \frac{\alpha_1 \alpha_2 P_{2,1} P_{1,0}}{P_{1,0}(1 + \alpha_1) + P_{2,1} \alpha_2} = \left[ \frac{1}{\alpha_1 \alpha_2 P_{2,1}} + \frac{1}{\alpha_2 P_{2,1}} + \frac{1}{\alpha_1 P_{1,0}} \right]^{-1} \quad (3-22)$$

Similarly for a three level system,

$$\tilde{\mu}_{III}^{-1} = \left\{ \frac{1}{P_{3,2}} \left( \frac{1}{\alpha_1 \alpha_2 \alpha_3} + \frac{1}{\alpha_2 \alpha_3} + \frac{1}{\alpha_3} \right) + \frac{1}{P_{2,1}} \left( \frac{1}{\alpha_1 \alpha_2} + \frac{1}{\alpha_2} \right) + \frac{1}{P_{1,0} \alpha_1} \right\} \quad (3-23)$$

Since  $\alpha_n \alpha_{n-1} \dots \alpha_{n-k} = \exp [-\beta(E_n - E_{n-k-1})]$  this form can

be simplified to yield,

$$\begin{aligned} \tilde{\mu}_{III}^{-1} &= \frac{1}{P_{3,2}} \left[ e^{\beta(E_3 - E_0)} + e^{\beta(E_3 - E_1)} + e^{\beta(E_3 - E_2)} \right] \\ &\quad + \frac{1}{P_{2,1}} \left[ e^{\beta(E_2 - E_0)} + e^{\beta(E_2 - E_1)} \right] + \frac{e^{\beta(E_1 - E_0)}}{P_{1,0}} \quad (3-24) \\ &= \sum_{i=1}^3 \left\{ \frac{e^{\beta E_i}}{P_{i,i-1}} \left[ \sum_{s=0}^{i-1} e^{-\beta E_s} \right] \right\} \end{aligned}$$

We can now generalize to a system with  $(v^*+1)$  levels to obtain,

$$\tilde{\mu}_0^{-1} = \sum_{i=1}^{v^*+1} \left\{ \frac{e^{\beta E_i}}{P_{i,i-1}} \left[ \sum_{s=0}^{i-1} e^{-\beta E_s} \right] \right\} = \frac{Z}{k_d} \quad (3-25)$$

This differs from the form obtained by Nikitin (ref 50).

He obtains

$$\tilde{\mu}_0^{-1} = \sum_{j=0}^{v^*} \left\{ e^{-\beta E_j} \left[ \sum_{K=j}^{v^*+1} e^{\beta E_K} / P_{K,K-1} \right] \right\} \quad (3-26)$$

Equation (3-25) is a general form which will be utilized later in a steady-state analysis. As pointed out earlier, in contrast to (3-13), it yields no information on the vibrational distribution and is limited to the case where dissociation occurs only from the last bound state. However, for a given set of V-T rates and a specified dissociation rate, it does provide the dissociation constant and does not require iteration. For the moment, in order to attempt to establish an upper bound on the dissociation constant and examine depletion effects, we will assume all  $P_{i,i-1}=1$ . This can later be refined by replacing the  $P_{i,i-1}$  by effective average,  $\langle P_{i,i-1} \rangle$ . Let us now assume that terms with large  $i$  dominate the summation due to the term  $\exp(\beta E_i)$ . Then the summation over  $s$  rapidly approaches the standard vibrational partition function and can be removed from the summation. Thus

$$\tilde{\mu}_0^{-1} = e^{\beta D_0} Q_{vib.} \sum_{i=1}^{v_{*}+1} \left\{ e^{\beta E_i} / P_{i,i-1} \right\} \quad (3-27)$$

Recalling that for a Morse potential with

$$\omega^2 = 2D_e \alpha^2 / M$$

and

$$d \equiv \left( \frac{8\pi^2 M D_e}{\alpha^2 \hbar^2} \right) = \frac{2D_e}{\hbar \omega}$$

$E_i$  can be represented as (Ref 61),

$$E_i = - \frac{D_e}{d^2} \left[ d - (i + 1/2) \right]^2 \quad (3-28)$$

with the highest bound level,  $v^*$ , given by

$$v^* = d - 1/2 - \delta \quad (3-29)$$

with  $\delta$  a positive number less than 1. Defining the  $q$ th vibrational level below  $v^*$  and relating it to  $i$ , we obtain

$$i = v^* - q = d - \delta - 1/2 - q$$

or

$$i + 1/2 = d - \delta - q$$

then

$$E_q = - \frac{\hbar \omega}{2d} (q + \delta)^2 \approx - \frac{\hbar \omega}{2d} q^2 \quad (3-30)$$

Substituting in (3-27) we obtain

$$\mu = \frac{Z}{Q_{vib} e^{\beta D_0} \sum_{q=0}^{v^*+1} \exp(-\beta \hbar \omega / (2d) q^2)} \quad (3-31)$$

Where upon approximating the summation by an integral we obtain

$$\mu = \frac{Z}{Q_{vib.} e^{\beta D_0} \left[ \frac{\pi v^*}{2\beta \hbar \omega} \right]^{1/2}} = \frac{Z e^{-\beta D_0}}{Q_{vib.} \left[ \frac{\pi v^* k T}{2 \hbar \omega} \right]^{1/2}}$$

$$= \frac{Z \hbar \omega e^{-\beta D_0}}{Q_{vib.} [\pi D_0 k T]^{1/2}}$$

So that

$$k_d = \frac{Z \hbar \omega e^{-\beta D_0}}{Q_{vib.} [\pi D_0 k T]^{1/2}} \quad (3-32)$$

At this point we should note that, under the assumption of  $P_{i,i-1}=1$ , the rate of dissociation from the last bound level, assuming a Boltzmann distribution for the vibrational levels is given by

$$k_d = \frac{Z e^{-\beta D_0}}{Q_{vib.}} \quad (3-33)$$

Thus we may identify the term,  $[\pi D_0 k T]^{1/2} / (\hbar \omega)$ , as a depletion factor resulting from the coupling of vibrational transfer and dissociation. This term reduces the dissociation rate below its equilibrium value and introduces a stronger negative temperature dependence to the rate which results in a lowering of the activation energy.

## Conclusion

In this chapter, we have developed the formalism, theory, and numerical approaches required for time-dependent and steady state solutions of the Master Equation. Recognizing the stiff nature of the set of simultaneous differential equations, we have selected the Gear (ref 85) integration technique for their solution. This time-dependent solution will be used to examine the temporal behavior of the dissociation process, assess the degree of vibrational-dissociative coupling, and validate the subsequent use of both steady state analyses.

## Chapter IV. Dissociation Models

### General

Having established the Master Equation formalism, and developed the computational approaches to be used in this study, we are now prepared to address the dissociation process itself. Within the framework of the four assumptions given in Chapter III, Morse oscillator, single quantum transitions, rotational equilibrium, and distinct vibrational states, we will now present three models of the dissociation reaction. All three are based upon the ladder climbing model, the differences lying in how rotational effects are treated. Through a consistent examination of these models, we will attempt to resolve the inconsistencies and contradictions that have arisen regarding the vibrational bias of the dissociation reaction, the role of rotation, and the source of rate enhancement in pure gases.

### Standard Ladder Model

The first model is designated as the standard ladder model. It has been used extensively and recently (refs 65, 88) in time dependent and steady state analyses of dissociation. Application of this model has yielded inconsistent results, as was brought out in the review of collisional theories of dissociation. The model can be understood by referring to Fig. 4-1 which displays a typical potential

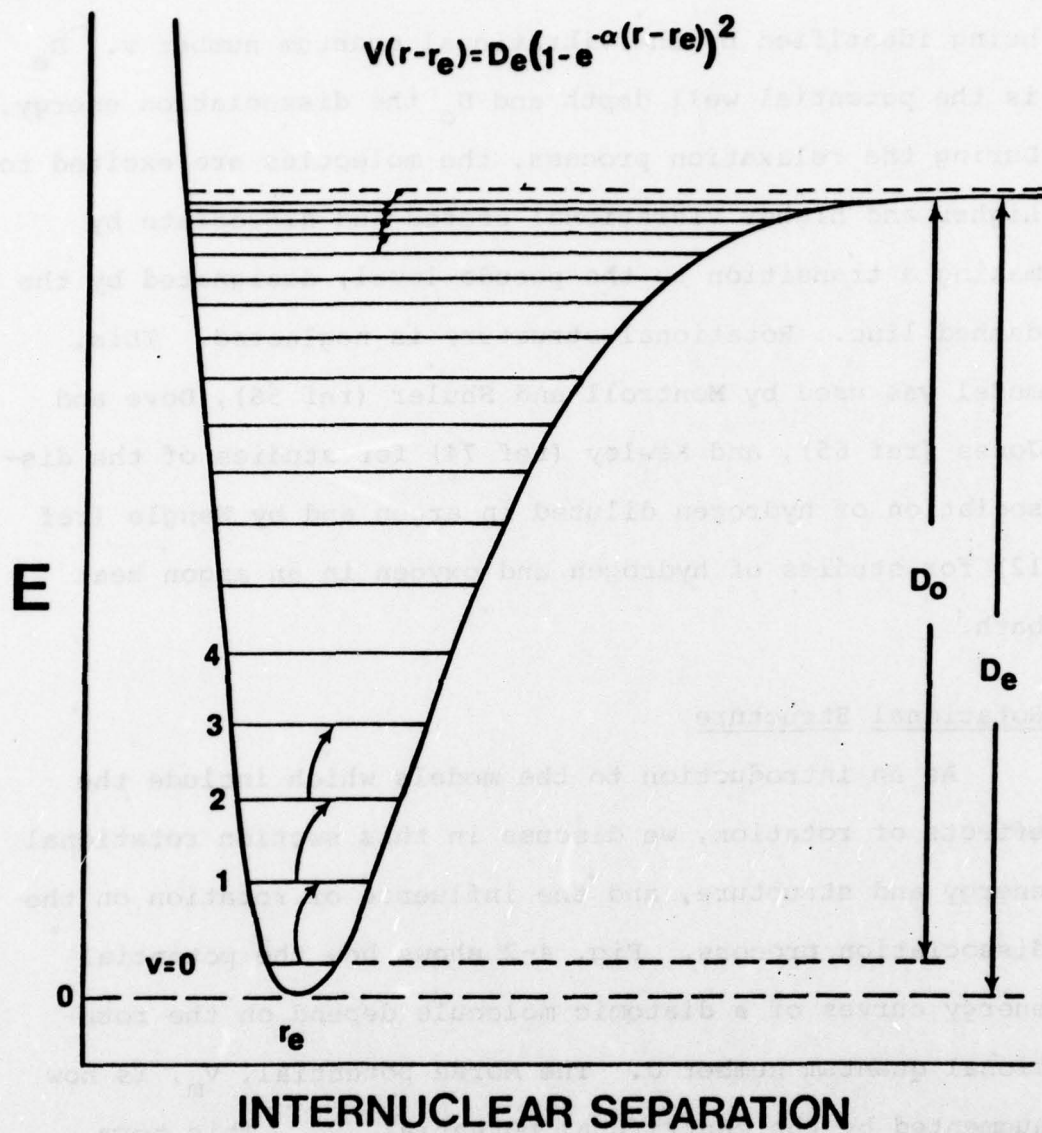
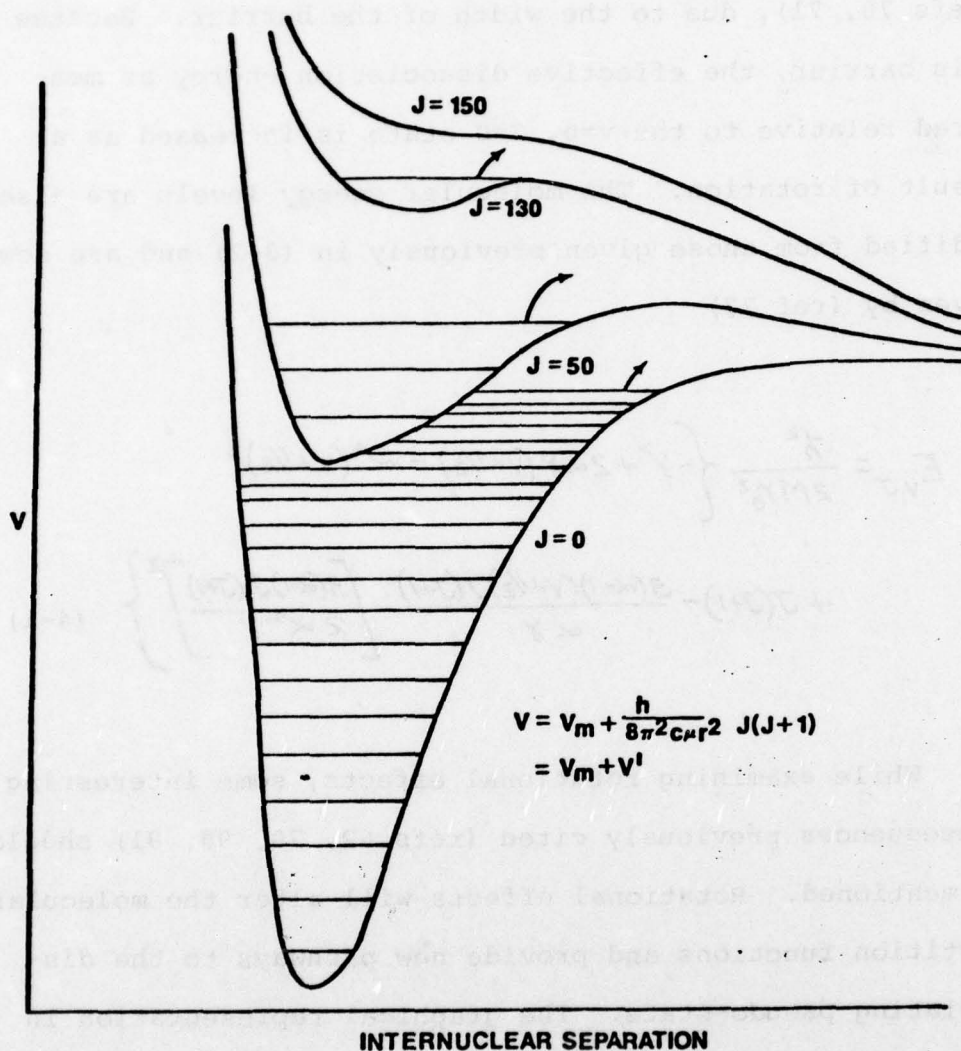


Fig 4-1 Standard Ladder Model

energy diagram using the Morse representation. Superimposed is the vibrational energy structure with the states being identified by the vibrational quantum number  $v$ .  $D_e$  is the potential well depth and  $D_0$  the dissociation energy. During the relaxation process, the molecules are excited to higher and higher vibrational states and dissociate by making a transition to the pseudo-level, designated by the dashed line. Rotational structure is neglected. This model was used by Montroll and Shuler (ref 56), Dove and Jones (ref 65), and Kewley (ref 74) for studies of the dissociation of hydrogen diluted in argon and by Wengle (ref 12) for studies of hydrogen and oxygen in an argon heat bath.

#### Rotational Structure

As an introduction to the models which include the effects of rotation, we discuss in this section rotational energy and structure, and the influence of rotation on the dissociation process. Fig. 4-2 shows how the potential energy curves of a diatomic molecule depend on the rotational quantum number  $J$ . The Morse potential,  $V_m$ , is now augmented by the centrifugal potential,  $V'$ . This term results in a reduction in the potential well depth and shift in the potential minimum to a larger internuclear separation. A rotational or centrifugal barrier arises and is usually of sufficient height to result in the formation of one or more quasi-bound states which are metastable with



**Fig. 4-2 Effective Potential Curves  
for a Diatomic Molecule**

respect to the normal dissociation limit for  $J=0$ . These states can predissociate via a penetration of the barrier, but in most cases this is of only secondary importance (refs 70, 71), due to the width of the barrier. Because of this barrier, the effective dissociation energy as measured relative to the  $v=0, J=0$  state is increased as a result of rotation. The molecular energy levels are also modified from those given previously in (3-2) and are now given by (ref 77)

$$E_{v,J} = \frac{\hbar^2}{2Mr_e^2} \left\{ -Y^2 + 2\alpha Y (v+1/2) - \alpha^2 (v+1/2)^2 + J(J+1) - \frac{3(\alpha-1)(v+1/2)J(J+1)}{\alpha Y} - \left[ \frac{3(\alpha-1)J(J+1)}{2\alpha^2 Y} \right]^2 \right\} \quad (4-1)$$

While examining rotational effects, some interesting consequences previously cited (refs 62, 70, 90, 91) should be mentioned. Rotational effects will alter the molecular partition functions and provide new pathways to the dissociating pseudo-state. The graphical representation in Fig. 4-3, proposed by Bauer and Widom (ref 62), gives a schematic representation of these new possible vibrational-rotational energy transfer processes. At each point in the plot the total energy is given by the sum of the abscissa, (rotation), and ordinate, (vibration) values. The heavy curve denotes the dissociation limit, and the dashed lines

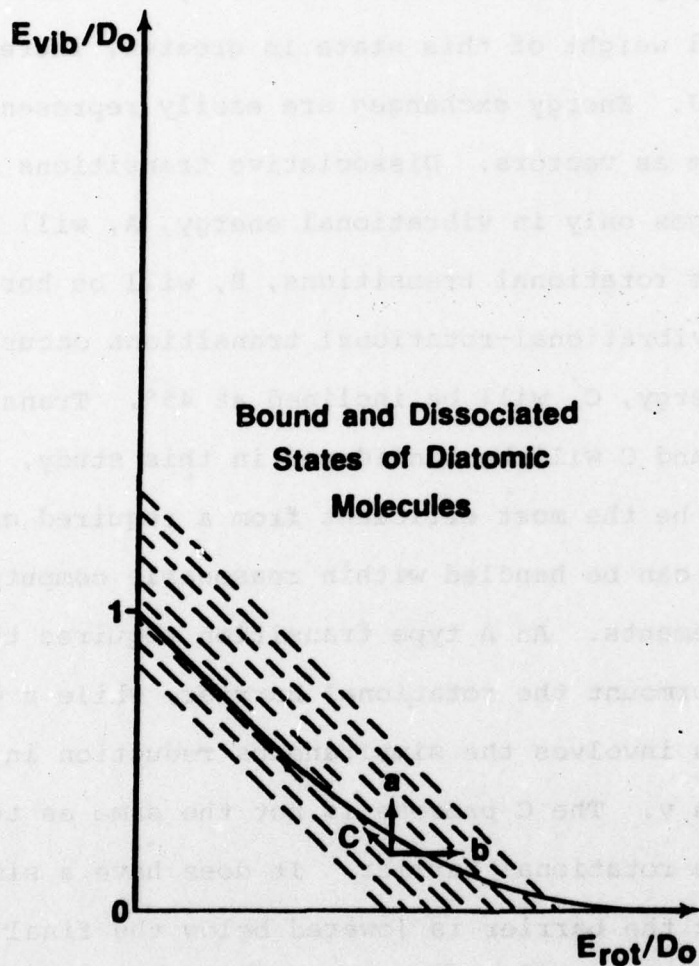


**Fig. 4-3 Bound and Dissociated States  
of a Diatomic Molecule**

represent constant total energy. Note again that a molecule must accumulate more total energy if it is to dissociate from a high J state, which would imply a reduction in the dissociation rate relative to the J=0 state. This reduction is tempered, on the other hand, by the fact that the statistical weight of this state is greater, increasing linearly with J. Energy exchanges are easily represented on this diagram as vectors. Dissociative transitions involving changes only in vibrational energy, A, will be vertical. Pure rotational transitions, B, will be horizontal, while vibrational-rotational transitions occurring at constant energy, C, will be inclined at 45°. Transitions of the type A and C will be considered in this study, as they appear to be the most efficient from a required energy standpoint and can be handled within reasonable computer storage requirements. An A type transition requires that the molecule surmount the rotational barrier, while a C type transition involves the simultaneous reduction in J and increase in v. The C process is not the same as tunneling through the rotational barrier. It does have a similar effect, in that the barrier is lowered below the final vibrational state and dissociation occurs. The importance of such collisions, especially for heavy molecules, has been intuitively-argued (refs 62, 90) and recent trajectory calculations (ref 92) have confirmed their importance. We will discuss equal energy transitions in greater deal in a following section.

Let's recap the implications of rotational effects before proceeding to introduce the two rotational-vibrational dissociation models. As a result of the variation of the rotational barrier with  $J$  and the variation of the rotational population with gas temperature, the effective molecular potential is temperature dependent. In addition, including rotational structure introduces new dissociative states and transitions which will be found to enhance the dissociation process and distribute the reaction among the vibrational states.

#### Rotational Models

In this section, two rotational-vibrational models of the dissociation process will be introduced. Both models will include the rotational effects discussed in the previous section, but will differ with respect to the form of the assumed vibrational-rotational coupling. The form of the assumed coupling is directly related to the question of vibrational bias and consequently vibrational depletion. By considering these models, in addition to the standard ladder model, we can evaluate the sensitivity of the dissociation process to the distribution of the dissociation rates among the vibrational levels. As in the standard ladder model, dissociation will be assumed to occur upon making a transition to an unbound pseudo-level.

Referring to Fig. 4-2, we introduce the first rotational model which will be designated the uncoupled model.

In this model, each  $J$  value will represent a distinct molecular species and vibrational ladder. This model will be analyzed under the standard ladder model procedures using a time-dependent, steady-state or analytic approach.

In contrast to the uncoupled model, the second rotational model assumes that rotational states are closely linked or strongly coupled to a given vibrational state. This model is called the coupled model and is represented in Fig. 4-4. Here we plot the  $J=0$  vibrational potential and superimpose the  $J=0$  vibrational energy level structure. To the right, the rotational energy level structure,  $E(v,J)$  for  $v=0$  and  $v=6$  is also presented. Under the strongly coupled assumption, dissociation now proceeds from the last bound rotational state of every vibrational level.

#### Dissociating States

The first step in the analysis of collisionally induced dissociation is the identification of the dissociating states. These are the last bound or quasi-bound vibrational states,  $v^*(J)$ , from which a dissociative transition (to the unbound pseudo-level), takes place. The states were identified, within the adopted Morse formalism, by a numerical calculation of the bound vibrational states using (4-1).<sup>\*</sup> The standard ladder model omits rotation and

---

<sup>\*</sup>There exists some uncertainty associated with the exact specification of the dissociating states. This uncertainty does not critically affect the present analysis, but is discussed further in Appendix B.

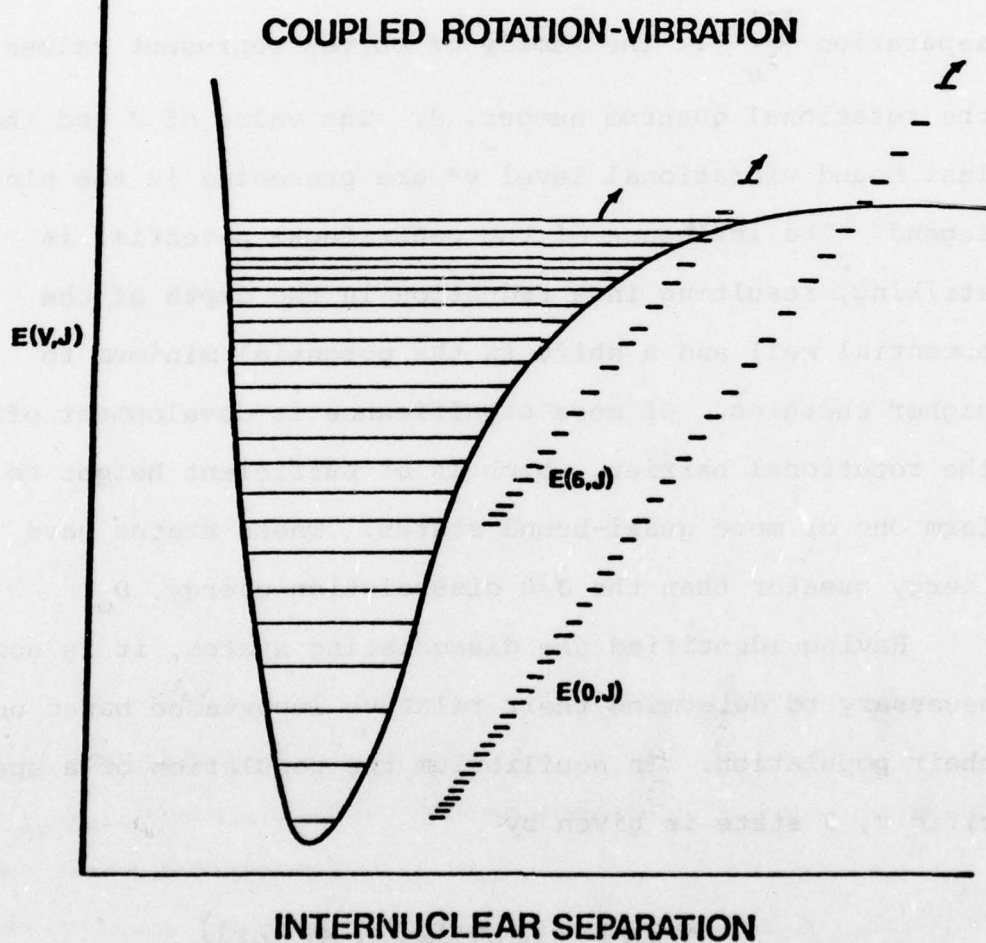


**Fig. 4-4 Coupled Rotational Model**

is analyzed as the  $J=0$  case. The rotational models, however, consider all values of  $J$  for which there exists a bound or quasi-bound vibrational state.

Figs. 4-5 to 4-10 show the calculated potential curves for  $H_2$ ,  $N_2$ ,  $O_2$ ,  $CO$ ,  $Br_2$ , and  $I_2$  parameterized in  $J$ . The plots are linear with the ordinate given by the normalized energy,  $E/D_0$ . The abscissa is the normalized internuclear separation  $\frac{r-r_e}{r_e}$ . The family of curves represent values of the rotational quantum number,  $J$ . The value of  $J$  and the last bound vibrational level  $v^*$  are presented in the plot legend. The influence of the centrifugal potential is striking, resulting in a reduction in the depth of the potential well and a shift in the potential minimum to higher energies. Of more significance is development of the rotational barrier, which is of sufficient height to form one or more quasi-bound states. These states have energy greater than the  $J=0$  dissociation energy,  $D_0$ .

Having identified the dissociating states, it is now necessary to determine their relative importance based on their population. In equilibrium the population of a specific  $v, J$  state is given by

$$\frac{N(v,J)}{N_{tot}} = \frac{(2J+1)\exp(-\beta E(v,J))}{Q_{tot}}$$

where  $N_{tot}$  is the total number of molecules and  $Q_{tot}$  the total partition function. The population of the last bound

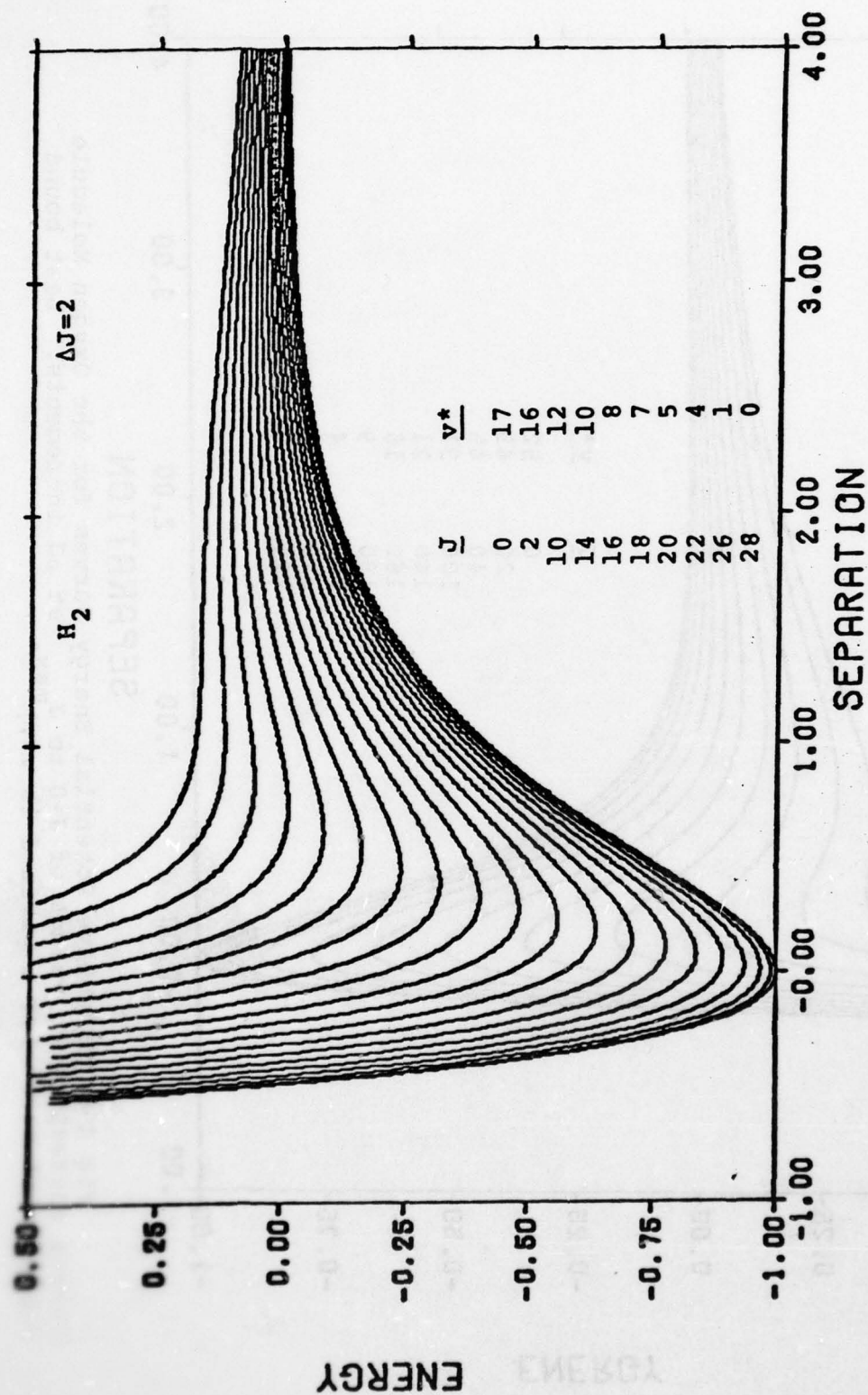


Fig 4-5 Effective Potential Energy Curves for the Hydrogen Molecule (Curves correspond to values of  $J=0$  to  $J_{max}$ . at  $\Delta J$  increments. Last bound vibrational state for a given  $J$  is  $v^*$ .)

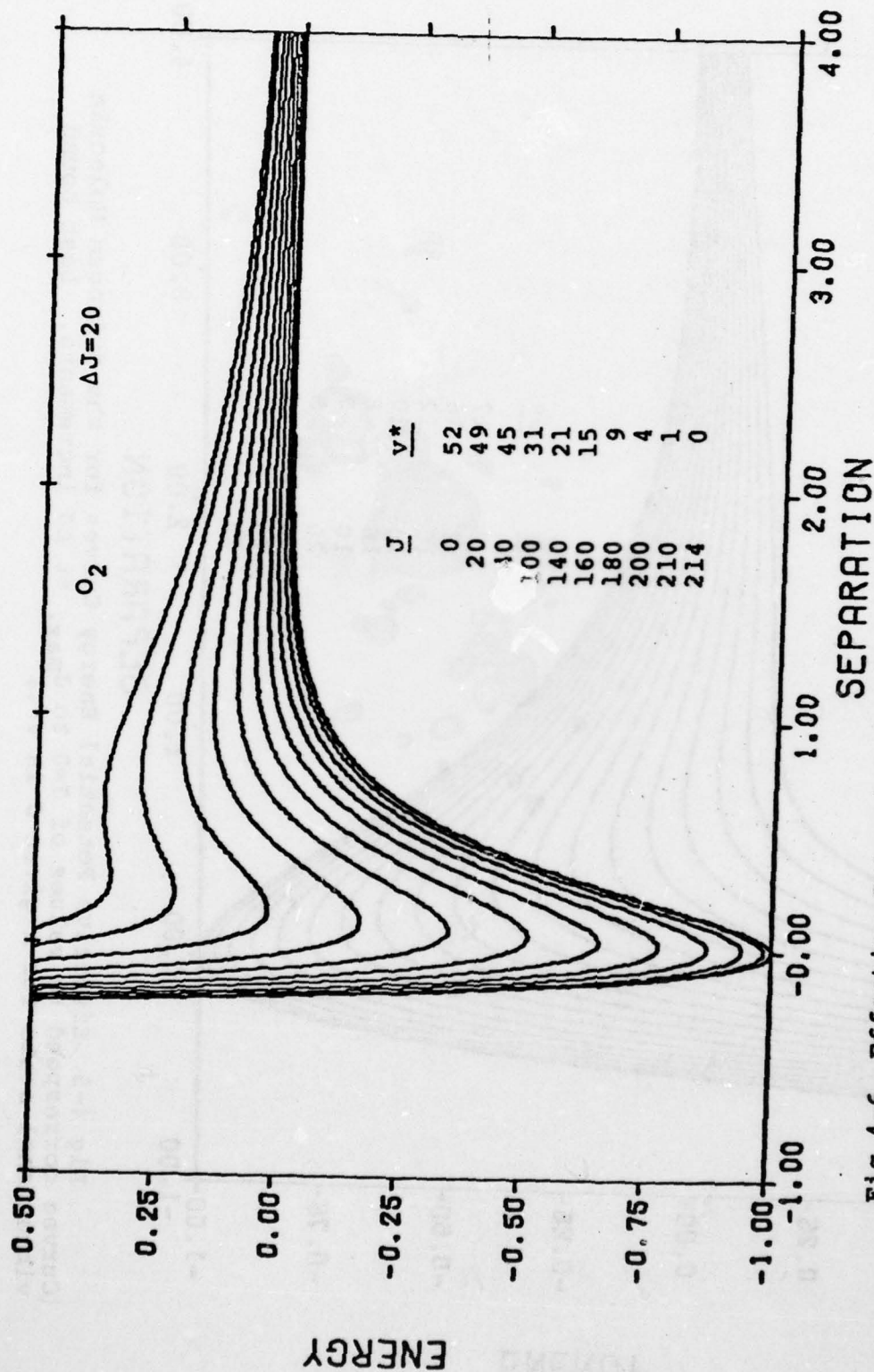


Fig 4-6 Effective Potential Energy Curves for the Oxygen Molecule (Curves correspond to values of  $J=0$  to  $J_{max}$  at  $\Delta J$  increments. Last bound vibrational state for a given  $J$  is  $v^*_{max}$ .)

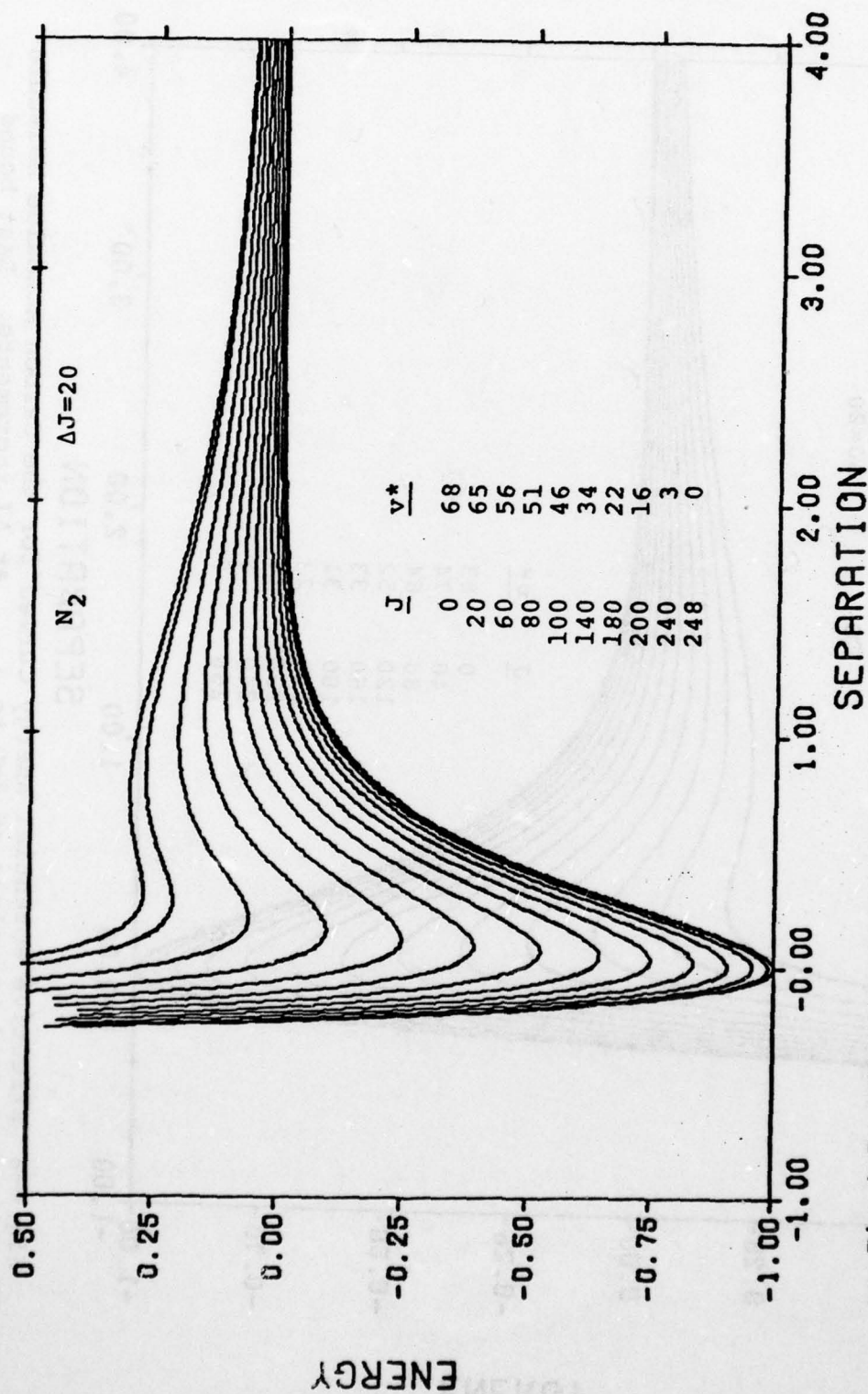


Fig 4-7 Effective Potential Energy Curves for the Nitrogen Molecule (Curves correspond to values of  $J=0$  to  $J_{\text{max}}$  at  $\Delta J$  increments. Last bound vibrational state for a given  $J$  is  $v^*_{\text{max}}$ .)

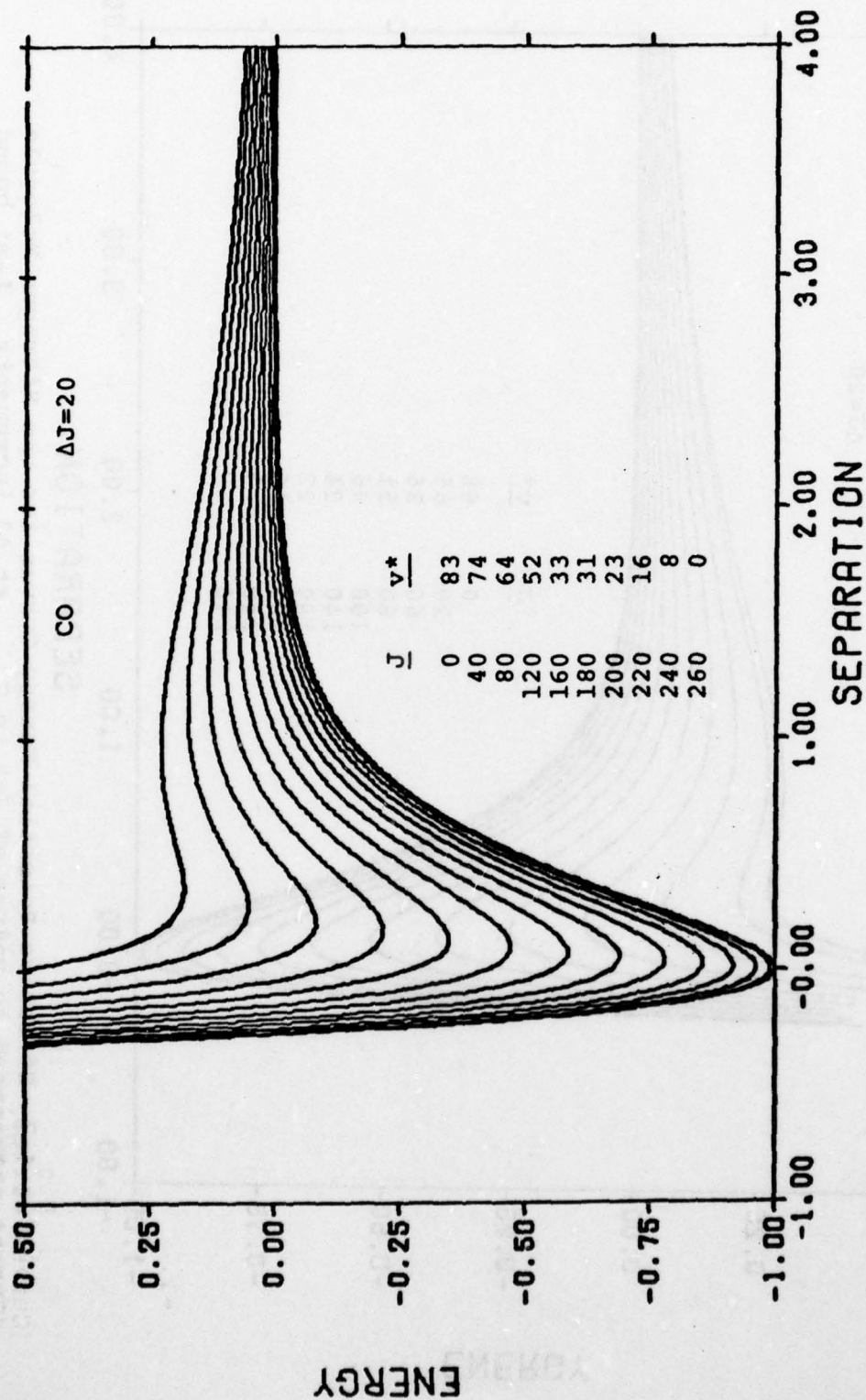


Fig 4-8 Effective Potential Energy Curves for the Carbon Monoxide Molecule (Curves correspond to values of  $J=0$  to  $J_{\text{max}}$  at  $\Delta J$  increments. Last bound vibrational state for a given  $J$  is  $v^*_{\text{max}}$ .)

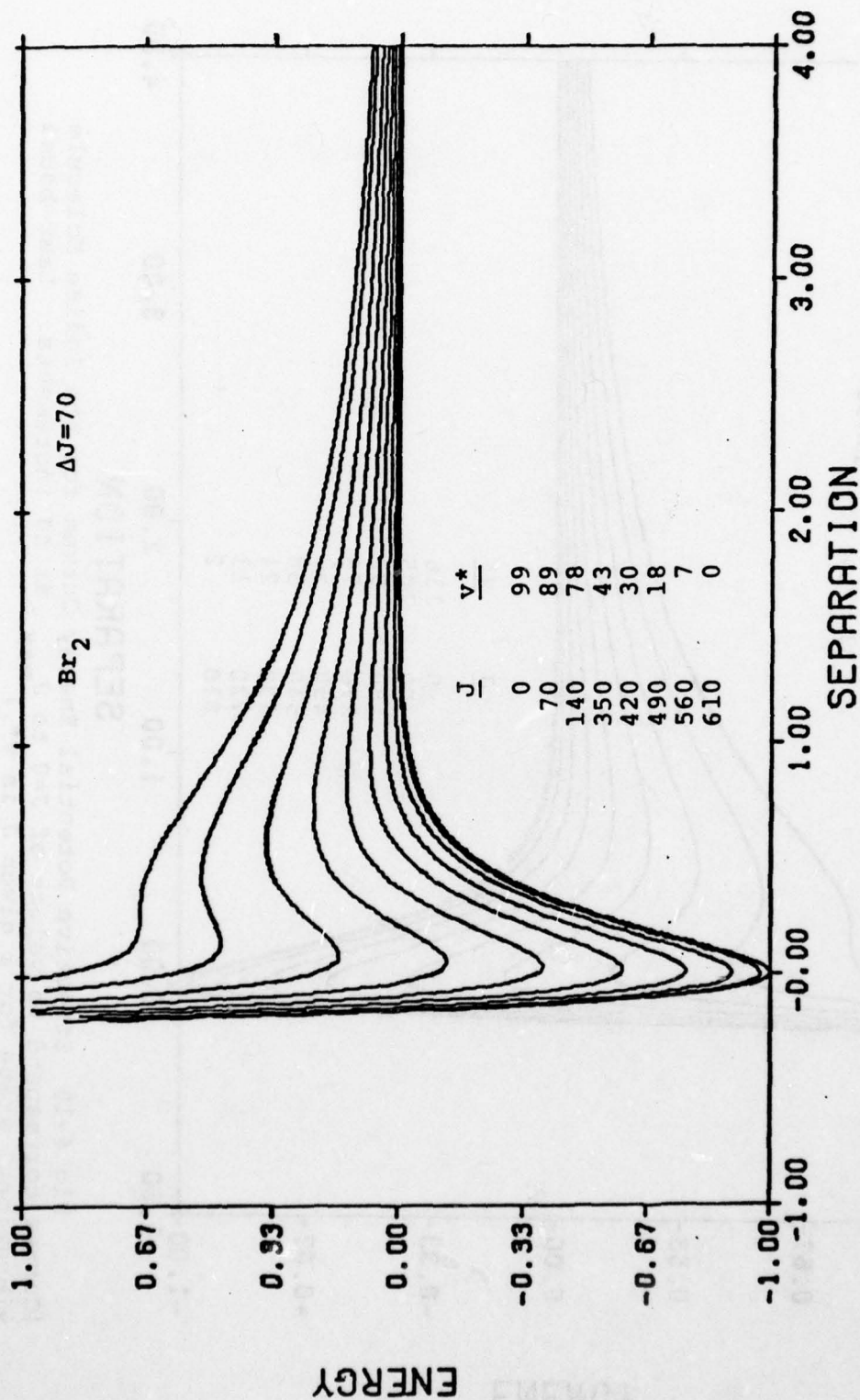


Fig 4-9 Effective Potential Energy Curves for the Bromine Molecule (Curves correspond to values of  $J=0$  to  $J_{\text{max}}$  at  $\Delta J$  increments. Last bound vibrational state for a given  $J$  is  $v^*_{\text{max}}$ .)

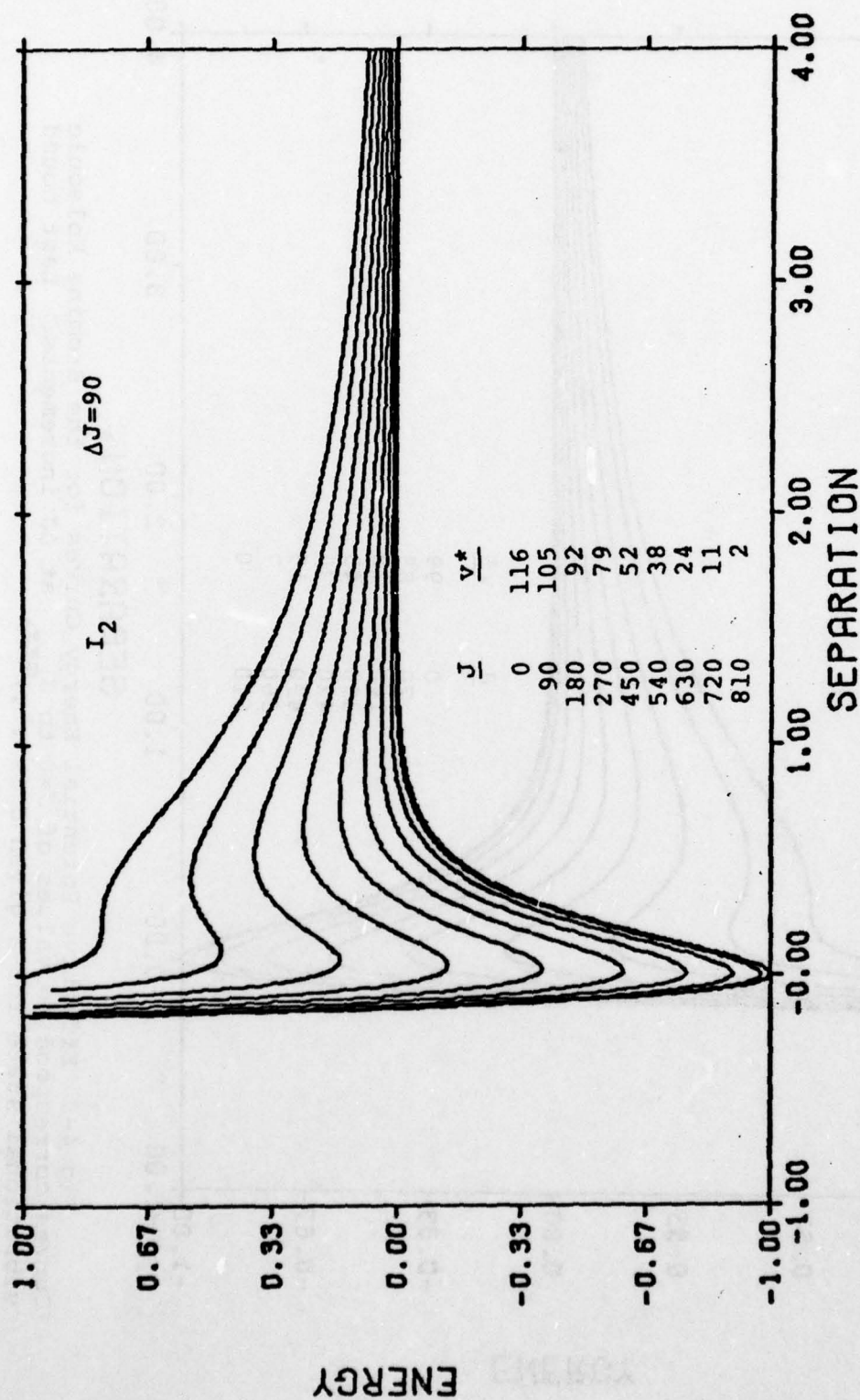


Fig 4-10 Effective Potential Energy Curves for the Iodine Molecule  
(Curves correspond to values of  $J=0$  to  $J_{max}$  at  $\Delta J$  increments. Last bound vibrational state for a given  $J$  is  $v^*$ .)

vibrational state,  $v^*(J)$ , for a given value of  $J$  will be given by

$$\frac{N(v^*(J), J)}{N_{tot}} = \frac{(2J+1) \exp(-\beta E(v^*(J)))}{Q_{tot}} \quad (4-3)$$

Assuming that

$$E(v^*(J), J) = D_0 (1 + \delta(J))$$

where  $\delta$  represents the variation in the rotational barrier height, then

$$\frac{N(v^*(J), J)}{N_{tot}} = \frac{(2J+1) \exp(-\beta D_0) \exp(-\beta \delta D_0)}{Q_{tot}} \quad (4-4)$$

For all gases examined

$$\delta \approx a_1 J^{2.5}$$

where  $a_1$  is a constant depending on the gas considered.

Incorporating this dependence into (4-4) yields

$$\frac{N(v^*(J), J)}{N_{tot}} = \frac{(2J+1) \exp(-\beta D_0) \exp(-\beta a_1 D_0 J^{2.5})}{Q_{tot}} \quad (4-5)$$

which gives the population of the last bound vibrational state as a function of  $J$  and temperature. It should be noted at this point that  $N(v^*(J), J)$  is distributed in a manner similar to the normal rotational distribution (ref 78)

$$\frac{N(J)}{N_{tot}} = \frac{(2J+1) \exp(-\beta h c B J(J+1))}{Q_{rot}} \quad (4-6)$$

The peak value of the  $N(v^*, J)$  distribution varies approximately as  $(T)^{\frac{1}{2}}$  as does the peak of  $N(J)$  of (4-6). Typical distributions of  $N(v^*, J) / N(v^*, J)_{max.}$  are given in Fig. 4-11a,b and are designated by the circled points with the scale shown on the right. Superimposed on these curves are plots of  $v^*(J)$  as a function of  $J$ . One can see from curve (11a), that the maximum population occurs for  $J=260$ , with a corresponding  $v^*=58$ , while from (11b), the maximum in  $N(v^*, J)$  has shifted down to  $J=200$  and  $v^*=68$ . For the coupled rotational model, it is necessary to obtain the ratio of the population in the lowest bound rotational state,  $\tilde{J}$ , for a given vibrational state to the total population in that vibrational state. This ratio is obtained from 4-3 and is given by

$$\frac{N(v(\tilde{J}), \tilde{J})}{N_v} = \frac{N(v(\tilde{J}), \tilde{J})}{\sum_{J=0}^{\infty} (2J+1) \exp(-\beta E(v, J))} \quad (4-7)$$

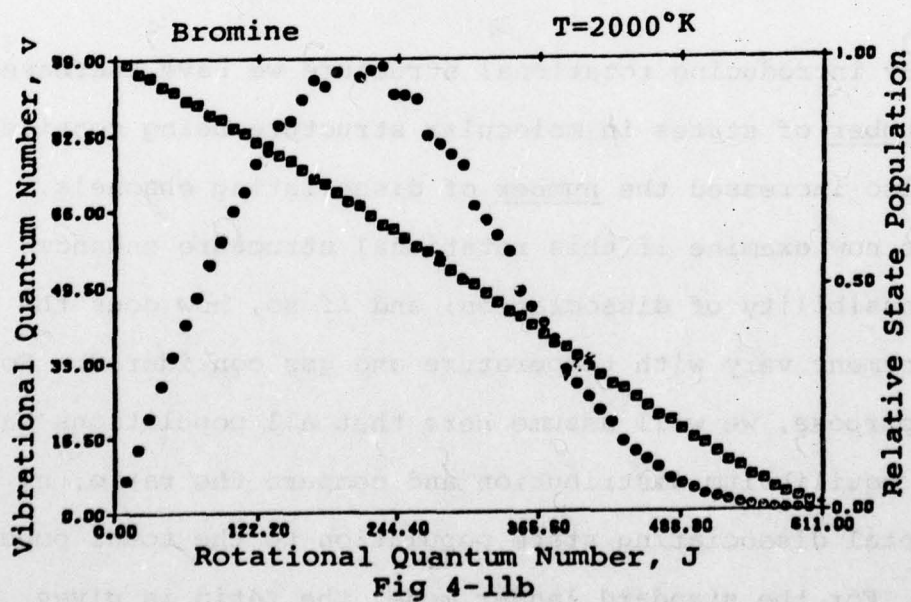
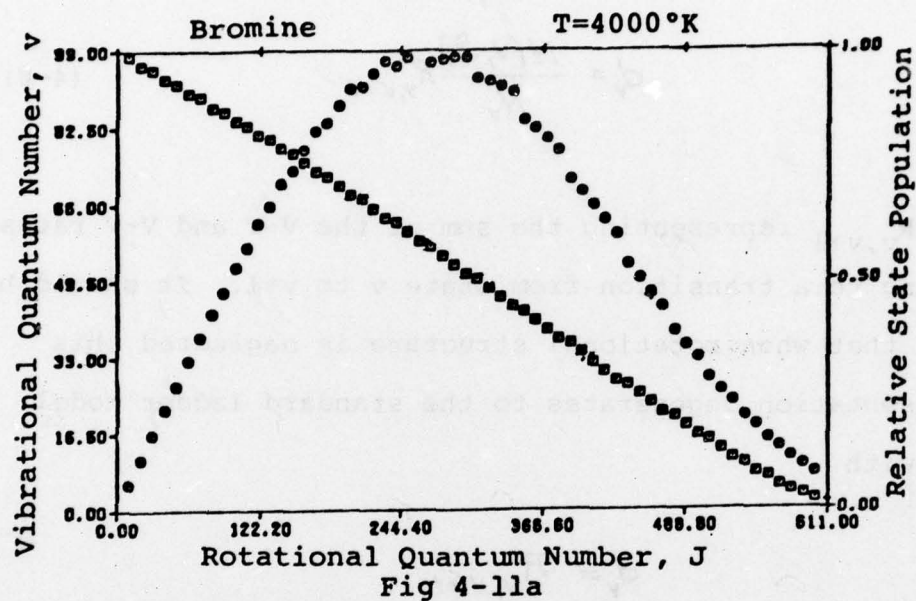


Fig 4-11 Temperature Dependence of Dissociating State Population

This factor is then incorporated into the coupled rotational model to determine the weighting of the dissociation rate  $d_v$ , given by

$$d_v = \frac{N(v, \bar{J})}{N_v} R_{v, v+1} \quad (4-8)$$

with  $R_{v, v+1}$  representing the sum of the V-T and V-V rates leading to a transition from state  $v$  to  $v+1$ . It should be noted that when rotational structure is neglected this representation degenerates to the standard ladder model form with

$$d_v = R_{v, v+1}$$

By introducing rotational structure we have increased the number of states in molecular structure being considered and also increased the number of dissociating channels. Let us now examine if this rotational structure enhances the possibility of dissociation; and if so, how does the enhancement vary with temperature and gas considered. For this purpose, we will assume here that all populations have their equilibrium distribution and compare the ratio,  $\eta$ , of the total dissociating state population to the total population. For the standard ladder model the ratio is given by

$$\eta_{\text{ladder}} = \frac{\exp(-\beta E[v^*])}{Q_{v,b}} \quad (4-9)$$

While upon including rotation, we obtain

$$\eta_{\text{rot}} = \frac{\sum_{v=0}^{v^*} (2J+1) \exp(-\beta E(v, J))}{\sum_{v=0}^{v^*} \sum_{J=0}^J (2J+1) \exp(-\beta E(v, J))} \quad (4-10)$$

In Table IV, the values of  $\eta_{\text{ladder}}$ ,  $\eta_{\text{rot}}$ , and  $\eta_{\text{rot.}}/\eta_{\text{ladder}}$  are given for  $\text{H}_2$ ,  $\text{O}_2$ ,  $\text{N}_2$ ,  $\text{CO}$ ,  $\text{Br}_2$  and  $\text{I}_2$ . (The meaning and implications of  $\eta_{\text{c}}/\eta_{\text{ladder}}$ , also listed in the table, will be considered later.) Observe that rotation not only increases the number of dissociation channels, but increases the critical state populations (i.e.,  $\eta_{\text{rot.}}/\eta_{\text{ladder}}$  is always greater than 1.). This suggests a resulting rate enhancement for dissociation. The ratio,  $\eta_{\text{rot.}}/\eta_{\text{ladder}}$ , is typically a factor of five, except for  $\text{H}_2$  where the enhancement is approximately 20. Of equal importance with the magnitude of the enhancement, is the temperature dependence. The ratio  $\eta_{\text{rot.}}/\eta_{\text{ladder}}$  decreases with increasing temperature with the power of the temperature dependence ranging from  $\phi = 1.2$  in  $\text{H}_2$  to  $\phi = 0.33$  in  $\text{I}_2$ ,  $\text{Br}_2$ , where  $\phi$  is defined by

TABLE IV  
COMPARISON OF DISSOCIATING STATES

Gas	Temperature	$\eta_{\text{ladder}}$	$\eta_{\text{rot.}}$	$\eta_{\text{rot.}}/\eta_{\text{ladder}}$	$\eta_{\text{c}}/\eta_{\text{ladder}}$
$\text{H}_2$	5000	1.45-5	2.1-4	14.6	11.7
	4000	1.09-6	2.09-5	19.1	18.5
	3500	1.68-7	3.85-6	22.6	22.8
	3000	1.38-8	3.74-7	27.5	27.6
	2500	3.95-10	1.37-8	35.1	36.2
$\text{O}_2$	10000	5.01-4	2.32-3	4.64	6.50
	5000	2.67-6	1.75-5	6.56	14.10
	3000	1.54-9	1.23-8	8.01	25.76
$\text{N}_2$	14000	5.54-5	3.27-4	5.91	9.2
	10000	2.87-6	2.02-5	7.03	13.5
	8000	1.98-7	1.53-6	7.77	17.4
$\text{CO}$	15000	3.29-5	2.19-4	6.67	9.7
	10000	6.61-7	5.55-6	8.40	15.4
	8000	3.22-8	3.00-7	9.33	19.9
$\text{Br}_2$	2000	2.15-6	9.94-6	4.62	12.6
	1300	6.67-7	3.19-6	4.78	14.1
	1200	1.67-9	9.02-9	5.38	22.1
$\text{I}_2$	2000	1.76-5	6.86-5	3.9	9.4
	1500	1.18-6	5.04-6	4.26	12.8
	1250	1.29-7	5.82-7	4.49	15.7

$$\frac{\eta_{rot}}{\eta_{ladder}} = T^{-\phi}$$

These results are in good agreement with the analysis of Pritchard (ref 72) for all gases except  $H_2$ . Pritchard used an exact potential curve for  $H_2$ , while using a Rydberg-Klein-Rees form for the other gases. The difference for  $H_2$  may reflect an inadequacy of the Morse representation. Using Pritchard's values or the Morse values for  $\delta$  and  $v^*(J)$  resulted in minor differences in the ultimate dissociation rate calculated.

The negative temperature dependence of the ratio,  $\eta_{rot.}/\eta_{ladder}$ , suggests that including rotational effects will not only increase the dissociation rate, but also lower the activation energy. Recall from Chapter I, that the observed activation energy is less than the dissociation energy. The dissociation coefficient, assuming an equilibrium vibrational distribution and gas kinetic losses out of the critical dissociating states, CDS, is given by

$$k_d = Z (\# \text{ in CDS}) / N_{tot}$$

For the standard ladder model,

$$k_d = \frac{Z \exp(-\beta E_{v*})}{Q_{vib}} \quad (4-11)$$

While for rotation,

$$k_{d, \text{rot}} = \frac{n_{\text{rot}}}{n_{\text{ladder}}} k_{d, \text{ladder}} = b_1 T^{-\phi} k_{d, \text{ladder}} \quad (4-12)$$

with  $b_1$  being a constant. Thus rotation enhances dissociation and would appear to yield "m's", as given in (1-4) and shown in Table I, less than those obtained in the standard ladder model, where  $m_{\text{rot.}} = m_{\text{ladder}} - \phi$ . While this is promising, we must postpone final judgement, since up to this point we have not allowed for the non-equilibrium effect of vibrational depletion. The influence of vibrational bias and vibrational depletion will be addressed in the next chapter.

#### An Alternate Path to Dissociation

As initially suggested by Bauer and Tsang (ref 62), revived by Pritchard (refs 70, 71, 72), and confirmed by recent trajectory calculations (ref 92), there is an alternate path for collisional dissociation. This path is an equal energy transition involving a quasi-bound vibrational rotational, V-R, level and was identified earlier as process C in Fig. 4-3. While addressing this process and its possible influence on the dissociation rate, let's classify the various V-R levels and identify the pathways to a dissociating state.

AD-A063 876

AIR FORCE AERO PROPULSION LAB WRIGHT-PATTERSON AFB OHIO  
COLLISION INDUCED DISSOCIATION OF DIATOMIC MOLECULES.(U)  
NOV 78 W F BAILEY

F/G 7/4

UNCLASSIFIED

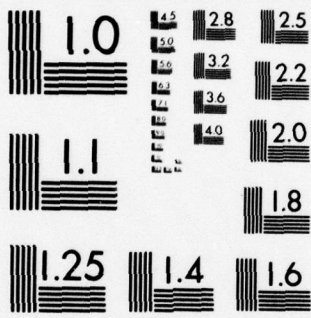
AFAPL-TR-78-105

NL

2 OF 3

AD  
A063 876





MICROCOPY RESOLUTION TEST CHART  
NATIONAL BUREAU OF STANDARDS-1963-A

Fig. 4-12 portrays a typical set of effective potentials for a diatomic molecule. Fig. 4-12a represents the ground rotational state potential and shows a transition of the A type, Fig 4-3, from a bound vibrational state to an unbound pseudo-level. This is the typical transition utilized in the majority of ladder climbing models. Fig. 4-12b illustrates the change in the effective potential due to rotational effects for various rotational quantum numbers. In this picture, the A type transition can be identified again as a collisional excitation to an unbound pseudo-level where the molecule "climbs over" the rotational barrier. In this case, however, the excitation proceeds from a quasi-bound state. In addition, the molecule can now penetrate the rotational barrier, process P, through tunneling (predissociation), but this has been established (refs 70-71) to have a low probability due to the extent of the barrier. There is yet another path to the dissociating states, identified by process C (see Figs. 4-12b and 4-3). In this process the molecule does not surmount the rotational barrier nor does it tunnel through it. Process C is an equal energy transition from a quasi-bound ( $v', J'$ ) state to an unbound ( $v, J$ ) pseudo-level of near equal energy, where  $v' < v$  and  $J' > J$ . It illustrates the mechanism whereby a molecule trapped in the quasi-bound state, undergoes a collision which removes some angular momentum and simultaneously increases its state of vibrational excitation. If this process is very efficient, it will

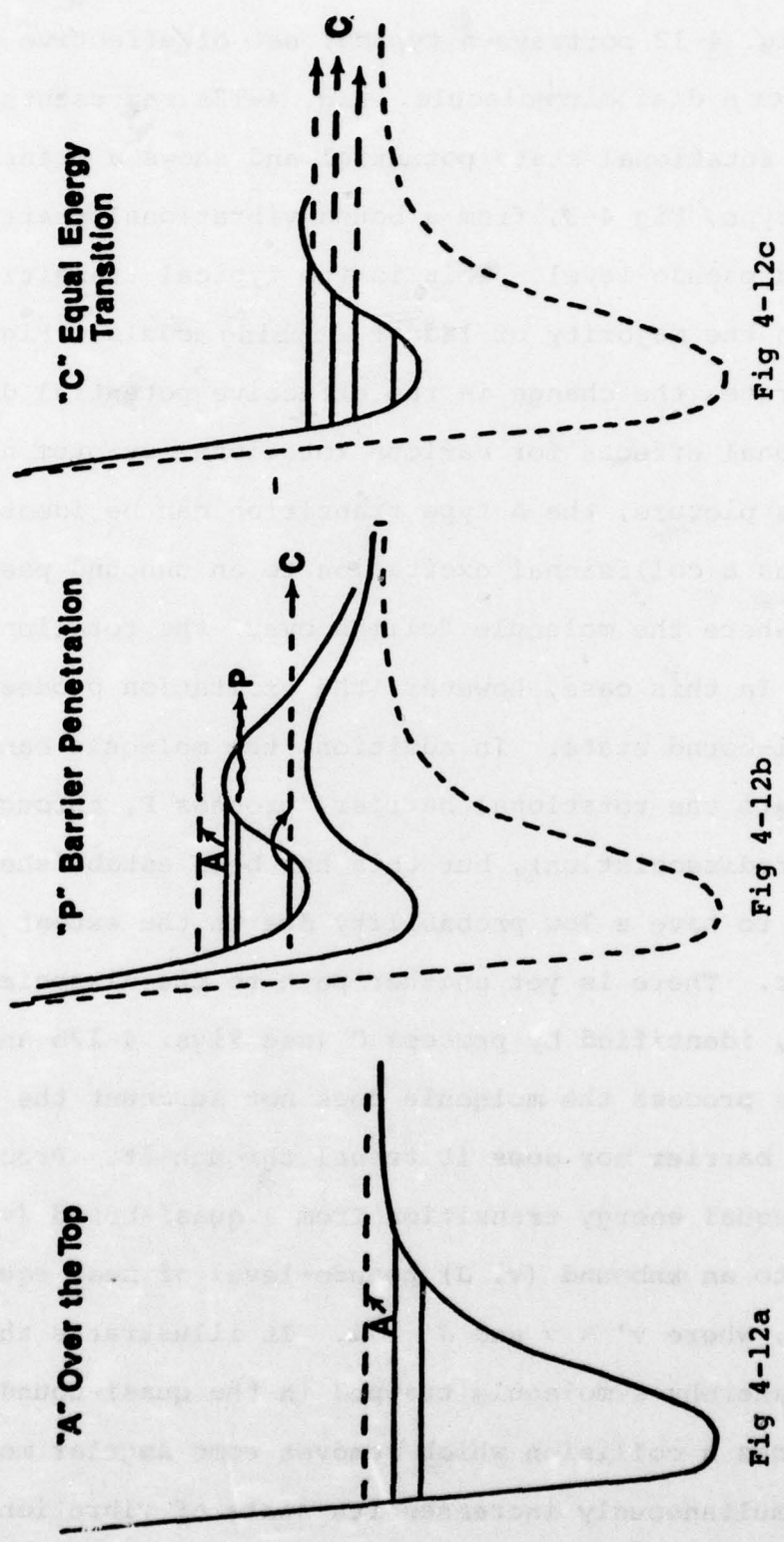


Fig 4-12 Alternate Paths for Dissociation

proceed in a cascaded fashion to successively reduce the rotational barrier height ultimately leading to the effective disappearance of the barrier as depicted in Fig.

4-12c. An upper limit to the dissociation rate when this mechanism is effective can be obtained by now redefining the critical state as the last bound vibrational rotational state. This is in contrast with our previous designation, when discussing the A type mechanism, of the critical state being the last quasi-bound vibrational rotational state. Thus equal energy transitions essentially remove the rotational barrier and lead to a new distribution of critical dissociating states, CDS.

Let's examine and contrast the distribution of CDS under conditions when mechanism A or mechanism C are in effect. Fig. 4-13a presents the A type, "over the top," picture for a quasi-bound state. The distribution of CDS's is given by equation (4-3, 4-4) and displayed in Fig. 4-13b. The distribution is depressed at large values of  $J$  due to the dominance of the rotational barrier and departs from its initial linear behavior in  $J$ . Should equal energy transitions be highly effective, we obtain the C type picture presented in Fig. 4-14. The effective potential for a given value of  $J$  is presented in Fig. 4-14a,b with the unbound pseudo-level given by a wavy line, the quasi-bound states by the dashed lines, and the bound states by solid lines. Fig. 4-14a gives the effective potential and vibrational states for an intermediate value of  $J$ , and

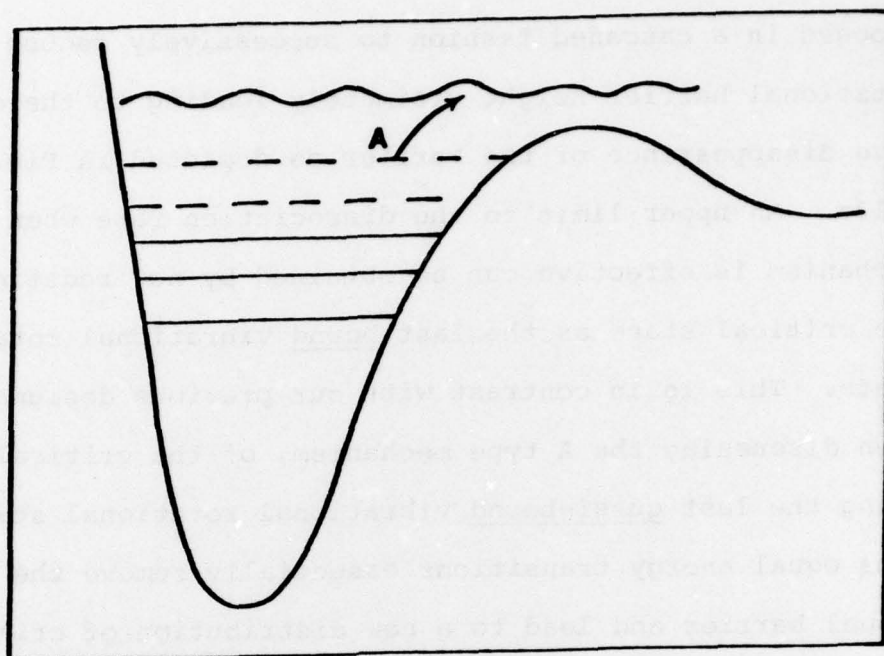


Fig 4-13a

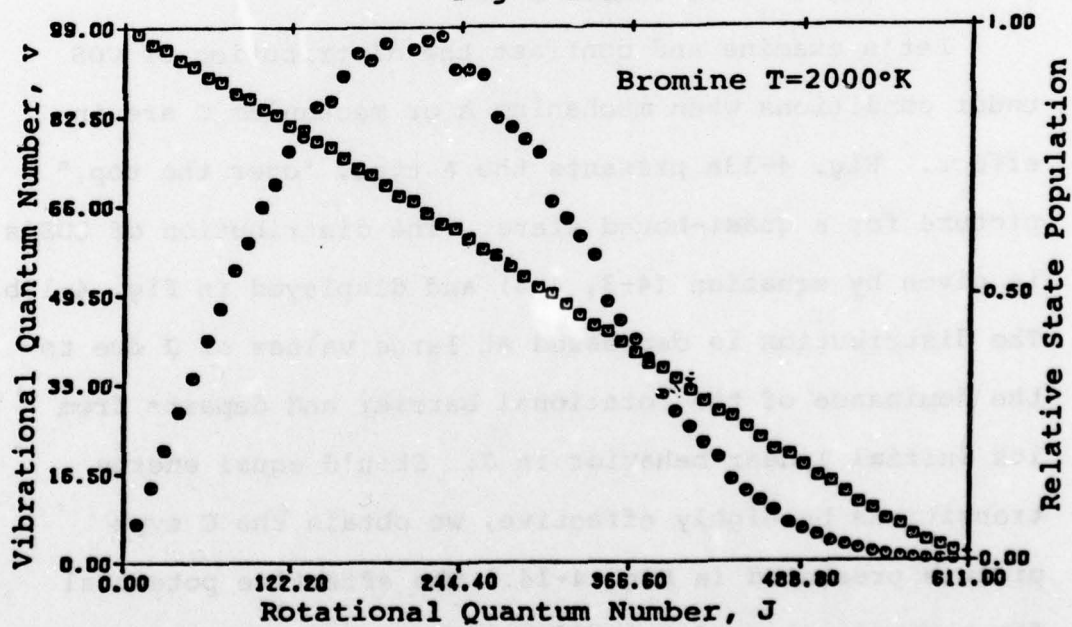


Fig 4-13b

Fig 4-13 CDS for Mechanism A, Over-the-Top

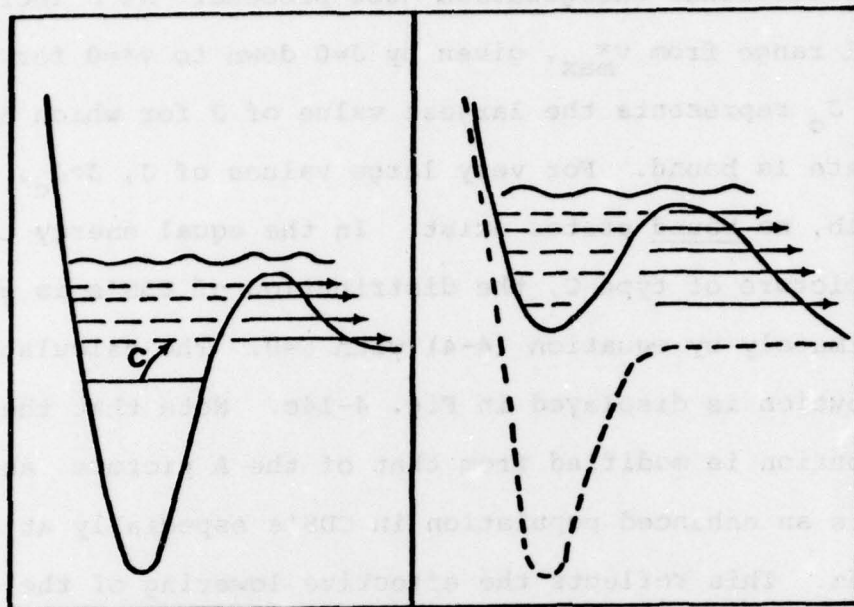


Fig 4-14a

Fig 4-14b

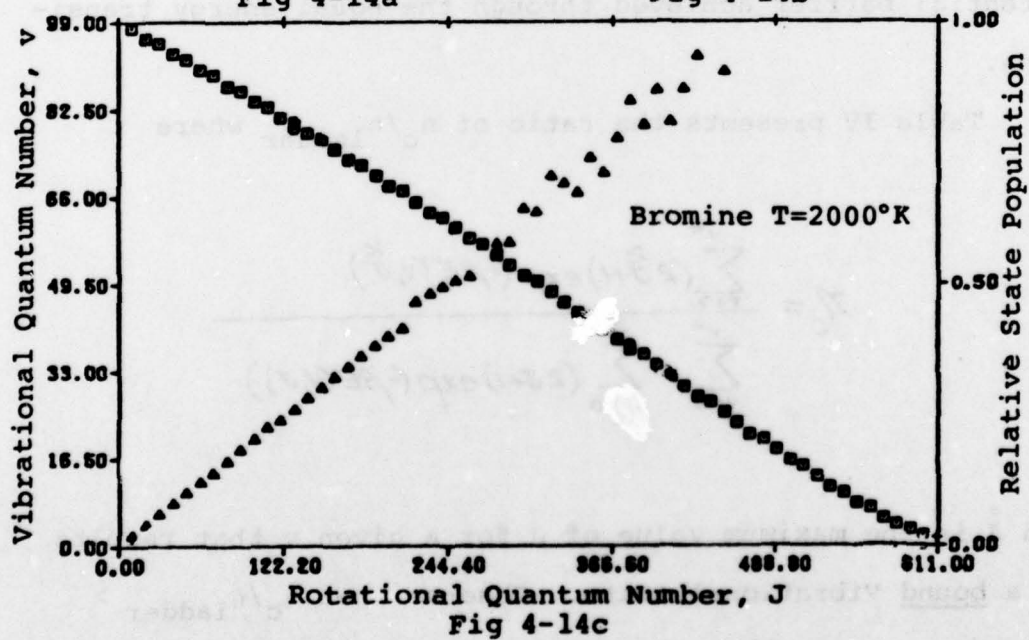


Fig 4-14c

Fig 4-14 CDS for Mechanism C, Equal Energy Transition

identifies level  $v^*$  as the critical dissociation state from which collisional energization must proceed. As  $J$  increases  $v^*$  will range from  $v_{\max}^*$ , given by  $J=0$  down to  $v^*=0$  for  $J=J_c$ .  $J_c$  represents the largest value of  $J$  for which the  $v=0$  state is bound. For very large values of  $J$ ,  $J > J_c$ , Fig. 11b, no bound states exist. In the equal energy transition picture of type C, the distribution of CDS's is given approximately by equation (4-4) with  $\delta=0$ . The calculated distribution is displayed in Fig. 4-14c. Note that the C distribution is modified from that of the A picture, and exhibits an enhanced population in CDS's especially at large  $J$  values. This reflects the effective lowering of the potential barrier achieved through the equal energy transition.

Table IV presents the ratio of  $\eta_c/\eta_{\text{ladder}}$  where

$$\eta_c = \frac{\sum_{v=0}^{v^*} (2\tilde{J}+1) \exp(-\beta E(v, \tilde{J}))}{\sum_{v=0}^{v^*} \sum_{J=0}^{\tilde{J}} (2J+1) \exp(-\beta E(v, J))}$$

and  $\tilde{J}$  is the maximum value of  $J$  for a given  $v$  that results in a bound vibrational state. Observe that  $\eta_c/\eta_{\text{ladder}} > \eta_{\text{rot.}}/\eta_{\text{ladder}}$  or that the critical state population is enhanced in the C picture over that obtained in the A picture and hence over the standard ladder model. The ratio maintains the negative temperature dependence

previously cited for the A process, and indeed even exhibits a stronger temperature dependence.

The effects of changes in the CDS distribution and its temperature dependence will be evaluated in the next chapter where detailed results including the non-equilibrium effects of vibrational depletion will be presented and contrasted for the three dissociation models

1. standard ladder
2. coupled rotation
3. uncoupled rotation

which we have developed here.

## Chapter V. Calculated Dissociation and Recombination Rates

### General

Having established the Master Equation formalism and developed the kinetic models of dissociation, we now present the results obtained for the dissociation and recombination rate coefficients. We begin with an examination of the temporal evolution of the dissociation process and the behavior of the incubation times. Following the time-dependent results, dissociation rates in diluted mixtures are presented. Next, rate enhancement in pure gases will be addressed by considering the aspects of changes in collisional efficiency due to mass variation and V-V enhancement. Finally, the calculated recombination coefficients will be presented and compared with experiment.

### Matrix of Computational Capabilities

As pointed out in Chapter III, the dissociation process, one of the simplest of all collisionally induced gas phase reactions, is nevertheless very complex. While a detailed time dependent solution of the full set of kinetic equations for each electronic, and vibrational-rotational state is possible in principle, it represents an undesirable approach due to the large number of equations involved and the lack of detailed exchange rate data for each of the states. In this study, therefore, we will parameterize the

the dissociation process over a wide range of temperatures and gases using the three simplified models of dissociation that were introduced in Chapter IV:

1. Standard Ladder Model
2. Coupled Model
3. Uncoupled Model

These models are established to permit an evaluation of the influence of rotational effects and complex collision phenomena on the dissociation process and represent different limiting cases, or approximations to the fully coupled problem. By examining the rates calculated under the various models, we may establish a model of dissociation that includes all essential elements. This model should provide reasonably accurate values for dissociation and recombination coefficients, exhibit an acceptable temperature dependence, and permit an evaluation of rate enhancement effects in pure gases.

Within the framework of the three dissociation models, the following capabilities were established and are schematically presented in Table V-1. A time-dependent capability represents the time-dependent integration of the coupled rate equations utilizing the Gear (ref 85) integration scheme for stiff systems of equations. The steady-state solutions utilize equation (3-3) for the ladder and coupled models, and a rotational average of equation (3-25) for the ladder\* and uncoupled model. The "Dilute" column refers to

---

\*No rotational average is needed for the ladder model.

TABLE V-1  
MATRIX OF COMPUTATIONAL CAPABILITIES

	Time Dependent		Quasi-Steady-State	
	Dilute	Pure	Dilute	Pure
Ladder	A	A	A	A
Coupled	A/C	A/C	A/C	A/C
Uncoupled	-	-	A/C	-

calculations of the dissociation rate for cases in which the diatomic gas is diluted in a monatomic gas such as argon. This is an interesting case to consider, not only because extensive experimental data exist for these circumstances, but because the collisional processes are especially simplified. Under these conditions the energy transfer process and collisional activation are dominated by V-T exchanges with the buffer gas, and complex exchanges can be neglected. In contrast, the "Pure" column refers to calculations in pure diatomic, (undiluted), gases. Under these circumstances, in addition to the change from the dilute case in the colliding masses for V-T exchanges, the influence of complex collisions, V-V, must be included and analyzed. The designation "A" or "C" refers to the critical dissociation states considered, "A" referring to the "over the top," ott, model, while "C" designating the pseudo-barrier penetration resulting from equal energy vibrational-rotational-translation, V-R-T, transitions. It should be noted that no detailed time-dependent solutions for the uncoupled model were performed because it would involve the solution for the full set of vibrational-rotational states, (over 300 for  $H_2$  and 50,000 for  $I_2$ ). The uncoupled model was not analyzed for the pure case, due to the linear form assumed in the development of (4-11). Complex exchanges could have been included in this development and the resulting equations linearized, but this was not considered necessary due to the agreement obtained

between the coupled and uncoupled models for the "dilute" cases.

Utilizing this matrix of calculational capabilities, we have analyzed the dissociation process in  $H_2$ ,  $O_2$ ,  $N_2$ ,  $CO$ ,  $Br_2$ ,  $I_2$  considering dilute and pure gases. Let's discuss these results by reviewing the time dependent evolution of the vibrational distribution and the dissociation rate. Within this discussion, we will demonstrate the existence of a quasi-steady-state, justifying the application of a steady-state analysis. Then the incubation times of the dissociation reaction will be examined.

#### Time Dependent Results

We wish to examine the shock heating of a diatomic gas and the resulting thermal relaxation and dissociation. This heating is modeled as an instantaneous rise in the translational and rotational temperatures occurring as the shock passes, followed by a period of vibrational excitation and relaxation. During this relaxation period, the vibrational manifold is populated by heavy particle collisions and rapidly attains a quasi-steady-state. The vibrational "relaxation" is calculated through a numerical integration of the coupled vibrational rate equations using the SSH (ref 20) exchange rates as modified by Keck and Carrier (ref 43) and fitted to the data of Millikan and White (ref 5) and of Hancock and Smith (ref 33). The purpose of the time-dependent solution is to establish the

existence of a quasi-steady-state vibrational distribution, to calculate the associated incubation time, and to be able to verify any subsequent steady-state calculations.

Before considering the details of the relaxation process in terms of the vibrational populations, let us examine for illustrative purposes the typical time profiles of the molecular and atomic densities as given in Fig. 5-1, where we have adopted this data from the calculations of Fisher (ref 86) and Bauer and Hilden (ref 87). The solid lines represent the molecular and atomic densities. Superimposed on the plot is the unidirectional flux coefficient,  $k_d$ , where:

$$k_d = \frac{\sum_{v=0}^{v^*} d_v N_v(t)}{\sum_{v=0}^{v^*} N_v(t)}$$

Note that the dissociation process can be divided into three characteristic time regimes: (1) the vibrational relaxation regime in which the molecule is "heated" through collisional energy exchanges and where insignificant dissociation occurs, (2) the quasi-steady state regime (Q.S.S.) where the state populations have obtained a quasi-steady balance between collisional activation and dissociation, and where recombination is negligible, and (3) the chemical equilibrium regime where atomic and molecular concentrations

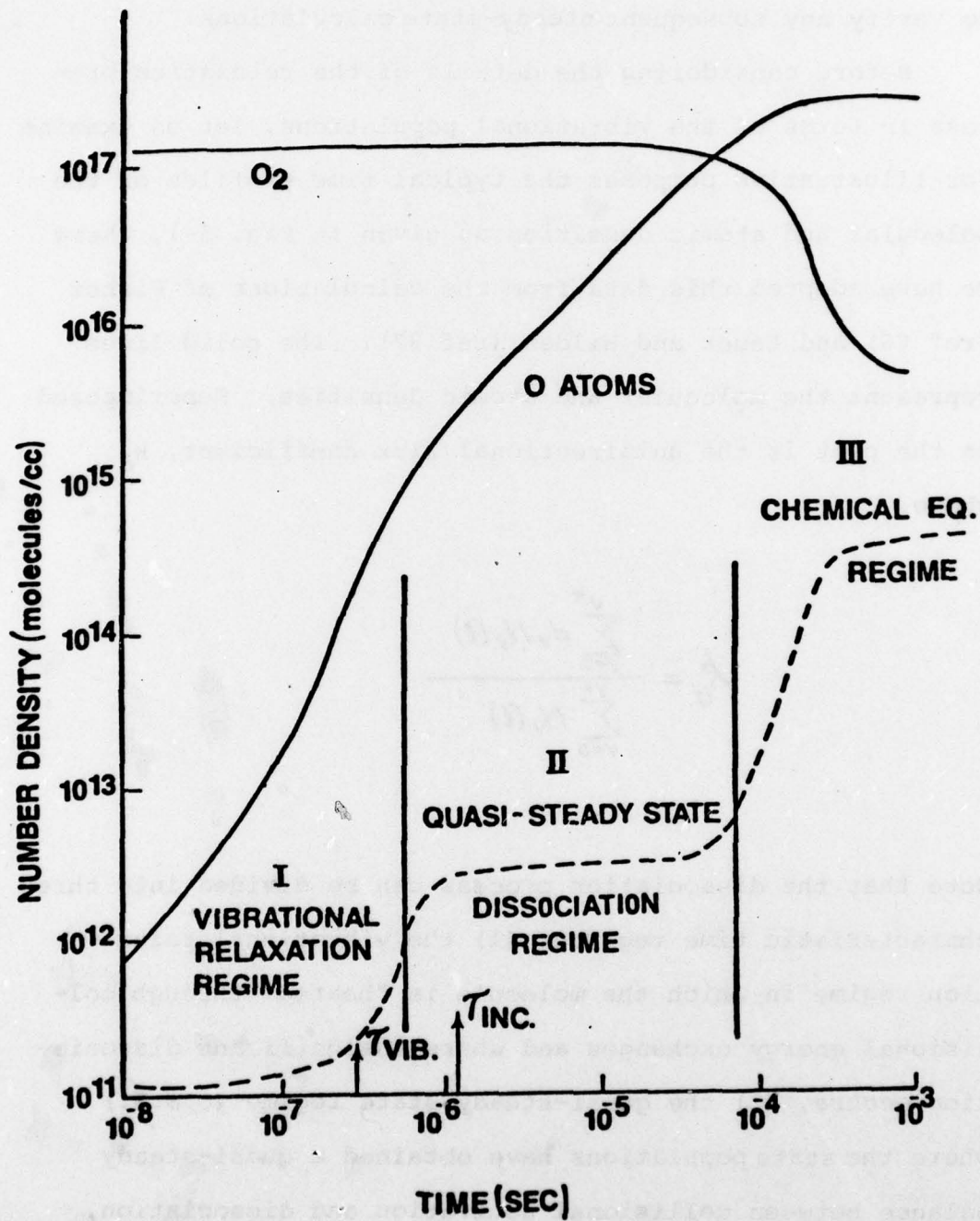


Fig 5-1 Time Profiles and Uni-Directional Flux

have achieved their equilibrium values and state populations are Boltzmann. The characteristic times associated with the first two regimes are the vibrational relaxation time and the incubation time. The vibrational relaxation time is defined by

$$\frac{dE_{\text{tot}}}{dt} = - \frac{(E_{\text{eq}} - E_{\text{tot}}(t))}{\tau_{\text{vib}}}$$

in which  $E_{\text{tot}}(t)$  is total vibrational energy and  $E_{\text{eq}}$  is the equilibrium value of this energy. The incubation time,  $\tau_{\text{inc}}$ , is defined as the onset time for Q.S.S. dissociation. Observe that the phenomenological rate equation

$$\frac{d[A_2]}{dt} = -k_d[M][A_2]$$

applies in the region from  $t = \tau_{\text{inc}}$  to  $t = 10^{-4}$  seconds and that a steady-state analysis is justified under these circumstances. Also note that the chemical equilibrium value of the dissociation flux is significantly larger than the Q.S.S. value, reflecting the influence of depletion on the Q.S.S and the increased atomic dissociation efficiency.

Let us consider Regimes I and II and examine the relaxation process and ensuing quasi-steady state. At time=0, the translational and rotational modes assume a high temperature, ( $T=4000^\circ\text{K}$ , in this example).

Subsequently, the vibrational states are populated via V-T collisions and relax toward a distribution compatible with this temperature and consistent with the dissociation losses. A quasi-steady-state is then established.\* During the period of time, indicated as starting  $\tau_{\text{incubation}}$ , quasi-steady-state dissociation takes place. The vibrational distribution maintains a self-similar form as the vibrational populations decay exponentially with the same time constant. This is the time interval over which most experimental observations are made and from which dissociation rates are inferred. During this time period, the molecular and atomic densities are far from their equilibrium concentration values and the recombination process does not have a significant effect on the vibrational distribution or atom density. As dissociation proceeds, the molecular density decreases and the atom density increases to the point where it is comparable with the molecular density. Near this point a departure from the quasi-steady-state, Q.S.S., occurs. The reasons for this departure are twofold. First, as discussed earlier, during the Q.S.S., energy losses due to dissociation modify the vibrational distribution and vibrational depletion results. This modification of the vibrational distribution is

---

\*At very high temperatures, the relaxation and dissociation coupling may be so strong that the separation of the relaxation and dissociation regimes may be invalid.

manifested in the reduction in the occupation of the high lying vibrational states below their equilibrium values and a consequent reduction in the dissociation rate. As recombination begins to become important, the net loss from the vibrational manifold decreases, ultimately reaching zero when true chemical equilibrium is established. Therefore, recombination reduces depletion and the unidirectional dissociation rate is enhanced as recombination becomes important. Hence the approach to equilibrium is accelerated by the recombination process.

The second reason for the departure from the Q.S.S. is related to the dissociation efficiency of atoms. The product atoms are very efficient collision partners with respect to the parent molecule, with O atoms being almost an order of magnitude more efficient than O<sub>2</sub> or Ar (ref 93). When significant atom concentrations are achieved, they will accelerate the approach to chemical equilibrium by increasing the dissociation flux and consequently the atomic density in a typical "chain reaction" type process. This aspect of the reaction has not been modeled in our calculations.

With the background provided by reviewing the molecular and atomic profile data of Fig. 5-1, we can now present selected results of our time dependent calculations in Figs. 5-2 and 5-3. These results reveal the details of the vibrational relaxation occurring in regime I, and quantify the concepts of Q.S.S. and vibrational depletion

# RESULTS OF TYPICAL TIME DEPENDENT CALCULATION

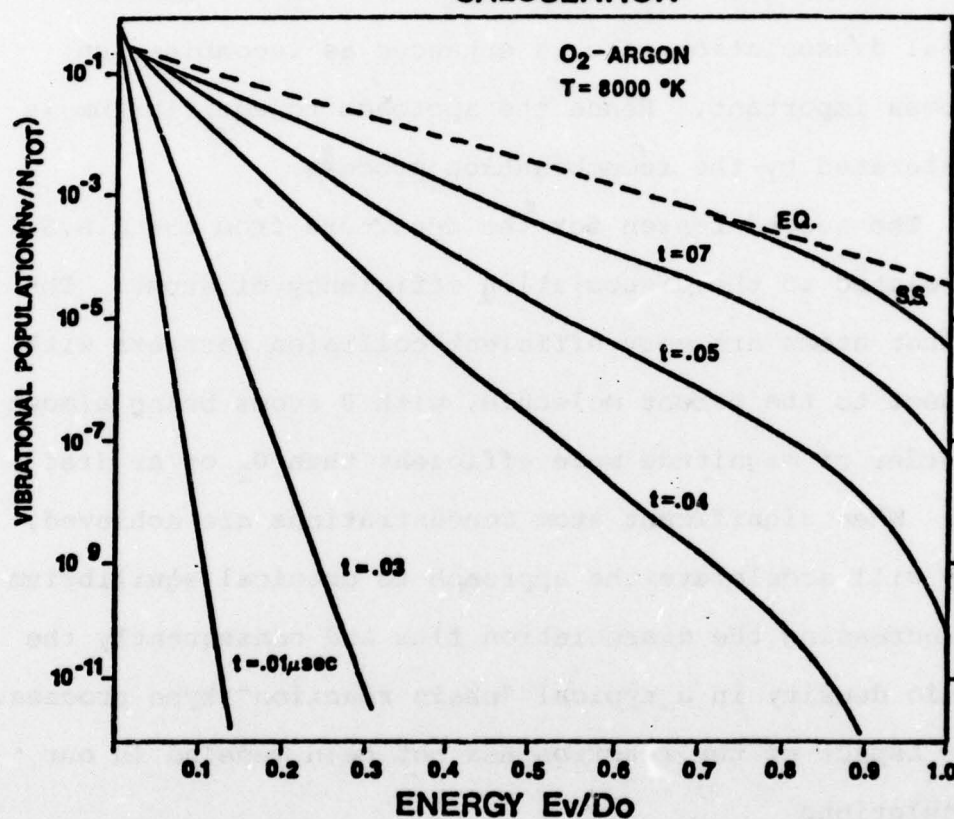


Fig. 5-2 Time Dependent Results for  $O_2$ -Ar  
 ( $[O_2] = 2.67 \times 10^{16} \text{ cm}^{-3}$ ,  $[Ar] = 2.67 \times 10^{19} \text{ cm}^{-3}$ )

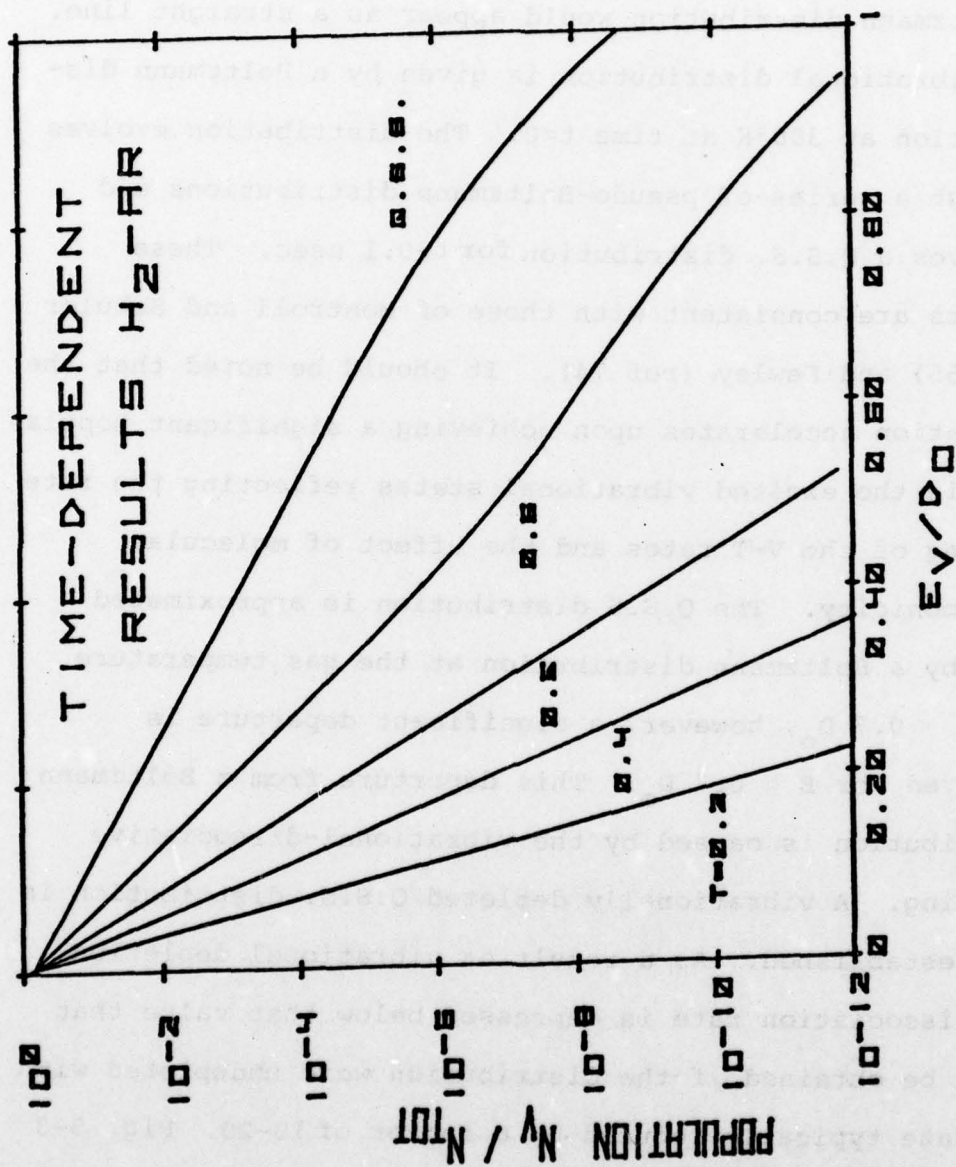


Fig 5-3 Time Dependent Results for H<sub>2</sub>-Ar  
( $T=3000^\circ\text{K}$ ,  $[\text{Ar}]=5.34 \times 10^{19} \text{ cm}^{-3}$ ,  $[\text{H}_2]=2.67 \times 10^{17} \text{ cm}^{-3}$ )

encountered in regime II. In Fig. 5-2, a semi-log plot of normalized vibrational population as a function of normalized vibrational energy is presented for selected times in the relaxation process. In this representation a Boltzmann distribution would appear as a straight line. The vibrational distribution is given by a Boltzmann distribution at 300°K at time  $t=0$ . The distribution evolves through a series of pseudo-Boltzmann distributions and achieves a Q.S.S. distribution for  $t > 0.1 \mu\text{sec}$ . These results are consistent with those of Montroll and Schuler (ref 55) and Kewley (ref 74). It should be noted that the relaxation accelerates upon achieving a significant population in the excited vibrational states reflecting the rate scaling of the V-T rates and the effect of molecular anharmonicity. The Q.S.S distribution is approximated well by a Boltzmann distribution at the gas temperature for  $E < 0.7 D_0$ , however, a significant departure is observed for  $E > 0.7 D_0$ . This departure from a Boltzmann distribution is caused by the vibrational-dissociative coupling. A vibrationally depleted Q.S.S. distribution is thus established. As a result of vibrational depletion, the dissociation rate is depressed below that value that would be obtained if the distribution were undepleted with the rate typically reduced by a factor of 10-20. Fig. 5-3 shows the results of similar calculation for  $\text{H}_2$ .

Thus from Figs. 5-2 and 5-3 we have established that the vibrational distribution rapidly attains a quasi-steady-

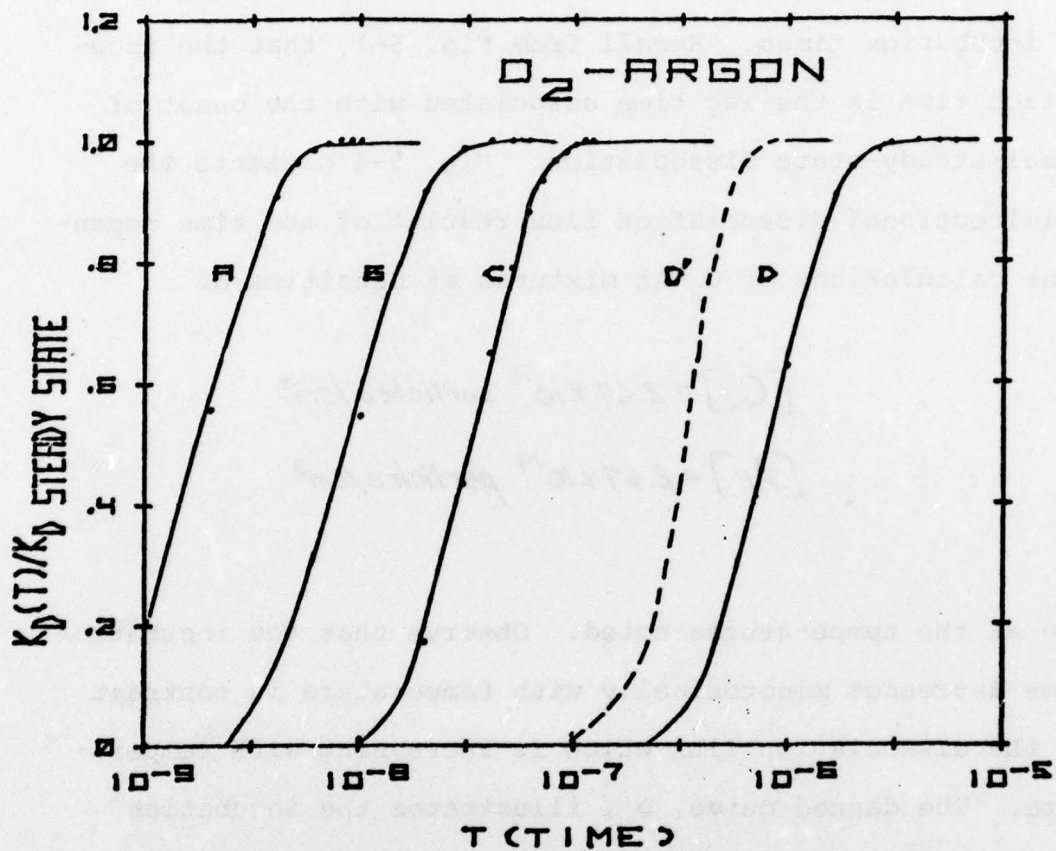
state and that a steady-state analysis is reasonable and justified. In addition, we have illustrated that the vibrational-dissociative coupling results in a vibration depletion and a significant rate reduction.

Let us now direct our attention to the calculation of incubation times. Recall from Fig. 5-1, that the incubation time is the lag time associated with the onset of quasi-steady-state dissociation. Fig. 5-4 presents the unidirectional dissociation flux results of the time dependent calculations of  $O_2$ -Ar mixtures at densities of

$$[O_2] = 2.67 \times 10^{16} \text{ particles/cm}^3$$

$$[Ar] = 2.67 \times 10^{19} \text{ particles/cm}^3$$

and at the temperatures noted. Observe that the incubation time decreases monotonically with temperature in contrast to the dissociation flux which is increasing with temperature. The dashed curve, D', illustrates the incubation profile for pure  $O_2$ , and reveals a reduction in the incubation time resulting from V-V exchanges in addition to the increased V-T exchange rates for  $O_2$ - $O_2$  collisions. Recombination has not been included in our calculation, so that the transition to Regime III will not be observed. A comparison of the calculated incubation times with the experimental data of Watt (ref 94) and Wray (ref 95) is presented in Fig. 5-5 where the results have been normalized



A=12000 °K B=8000 °K C=6000 °K  
D=3000 °K D' ( $O_2-O_2$ )=3000 °K

Fig 5-4 Time Dependence of Unidirectional  
Dissociation Flux  
(for Curve D',  $[O_2]=2.67 \times 10^{19}$ )

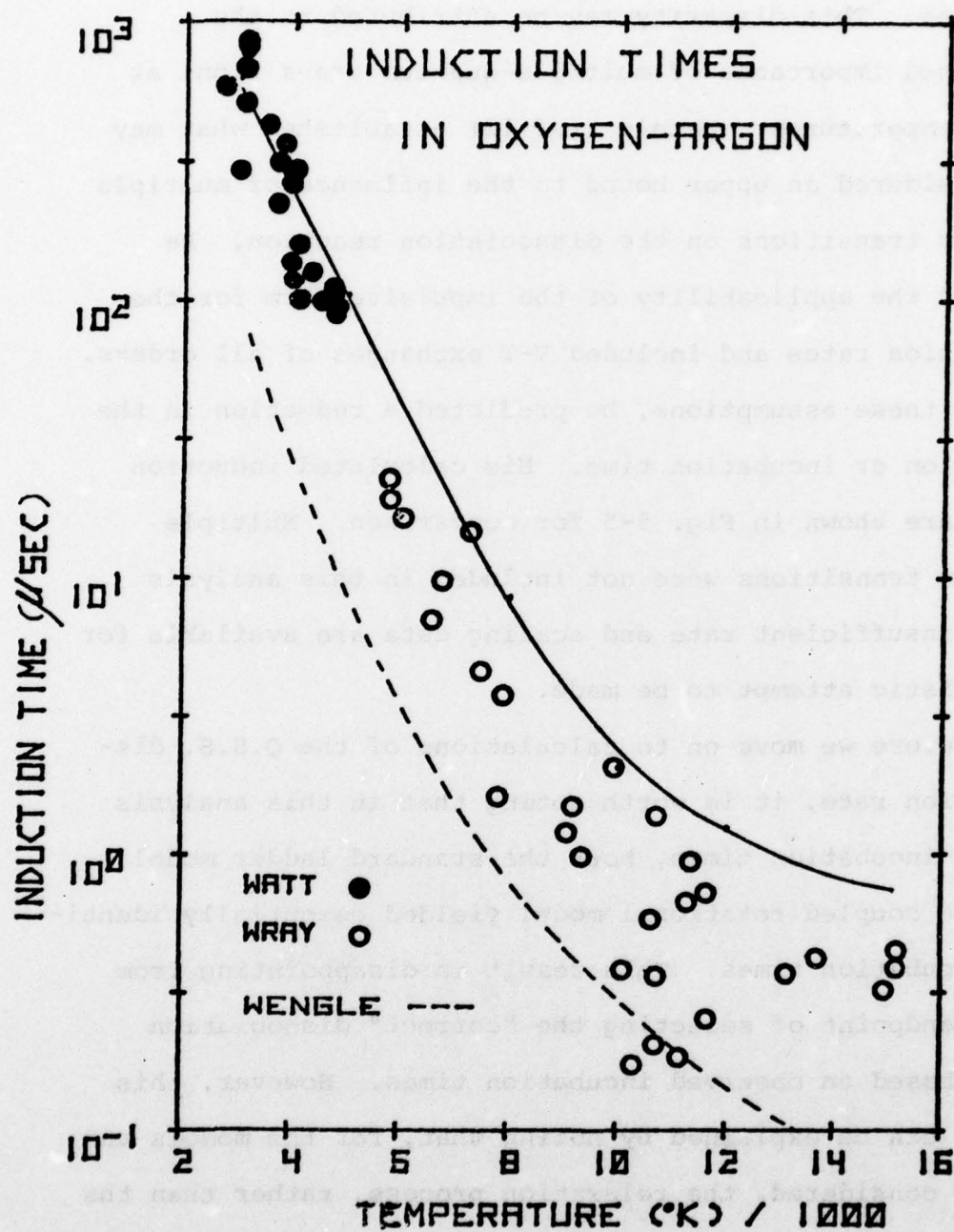


Fig 5-5 Induction Times in  $O_2$ -Ar

to an argon density of  $1.28 \times 10^{17} \text{ cm}^{-3}$ . Good agreement is obtained from 3000°K to 10,000°K; however at temperatures in excess of 10,000°K the calculated incubation times were too long. This disparity may be attributed to the increased importance of multiple-quantum transitions at high temperatures. Wengle (ref 12) established what may be considered an upper bound to the influence of multiple quantum transitions on the dissociation reaction. He assumed the applicability of the impulsive form for the transition rates and included V-T exchanges of all orders. Within these assumptions, he predicted a reduction in the induction or incubation time. His calculated induction times are shown in Fig. 5-5 for comparison. Multiple quantum transitions were not included in this analysis since insufficient rate and scaling data are available for a realistic attempt to be made.

Before we move on to calculations of the Q.S.S. dissociation rate, it is worth noting that in this analysis of the incubation times, both the standard ladder model and the coupled rotational model yielded essentially identical incubation times. This result is disappointing from the standpoint of selecting the "correct" dissociation model based on observed incubation times. However, this result can be explained by noting that, for the models and biases considered, the relaxation process, rather than the dissociation rates or their distribution, controls the incubation times. This conclusion is consistent with the

results obtained in this study, where identical V-V and V-T rates were used in both model calculations, and is also supported by Wengle's (ref 12) results.

Dissociation of Diatomics Diluted  
in an Argon Heat Bath

Most of the dissociation data from shock tube experiments has been obtained for various diatomic species highly diluted in argon. This is an extremely simple physical situation from a collisional analysis viewpoint, in that collisional exchanges are limited to V-T exchanges with the argon buffer. It therefore offers a test of any collisional theory of dissociation. In this section, we present the predicted dissociation rate coefficients for the dilute case based on the calculational matrix in Table V-1.

Time dependent solutions for the ladder model (A), and coupled model (A/C) showed agreement within 0.1% with the steady-state analysis, based on equation (3-13), for all gases and for the entire range of temperatures presented in this study. Since this agreement was within the convergence criteria established for the iterative solution, it serves as a validation of these calculations. A comparison of time dependent results with the steady-state analysis of equation (3-25) also yielded acceptable agreement with the maximum deviation being less than 2%. In addition to this cross-validation of codes, each calculation was checked for the following limiting cases.

1. No dissociation

2.  $d_v = \text{const.}$

For both of these cases, the required Boltzmann distribution was obtained.

Having documented the calculations, let us compare the dissociation coefficient calculated under the three different models,

1. standard ladder,

2. coupled, and

3. uncoupled,

to experimental data for mixtures of a diatomic gas highly diluted in argon. From this comparison, we will establish three significant points:

1. The standard ladder model is inadequate, yielding dissociation coefficients that are much too low.

2. Models including the influence of rotation predict larger dissociation coefficients than the standard model and these coefficients are in substantial agreement with experimental data.

3. Equal energy, V-R-T, transitions lead to an increase in the dissociation rates; this increase is especially marked in  $\text{Br}_2$  and  $\text{I}_2$  and yields improved agreement with experimental data.

For all gas mixtures considered here, the argon number density was  $2.67 \times 10^{19} \text{ cm}^{-3}$  while the diatomic density was  $2.67 \times 10^{16}$  or lower. Under these conditions, V-T

processes dominate the V-V processes for all temperatures and diatomic gases considered.

Hydrogen. Hydrogen has been studied extensively both experimentally and theoretically. Sufficient experimental data is available to establish the dissociation coefficient to within a factor of two. A comparison of experimental (ref 96) and theoretical values is presented in Fig. 5-6 where the logarithm of the dissociation coefficient is plotted against the gas temperature. The theory is shown in solid lines, experiment in dashed. (This convention will be utilized throughout the entire data comparison.) All calculated values fall below the experimental data, but exhibit an acceptable temperature dependence. The ladder model is a factor of 6 low. All rotational models

1. coupled, equal energy transition, CC;
2. coupled, "over the top," CA;
3. uncoupled, equal energy transition, UC; and
4. uncoupled, "over the top," UA

yield essentially identical results and are represented by the curve marked "ROT." Rotation enhances the dissociation coefficient in hydrogen by a factor of 3. This factor is much less than that anticipated from our equilibrium analysis, and reflects the fact that the vibrational transfer rates are not large enough to support the full rotation enhancement and therefore are rate controlling.

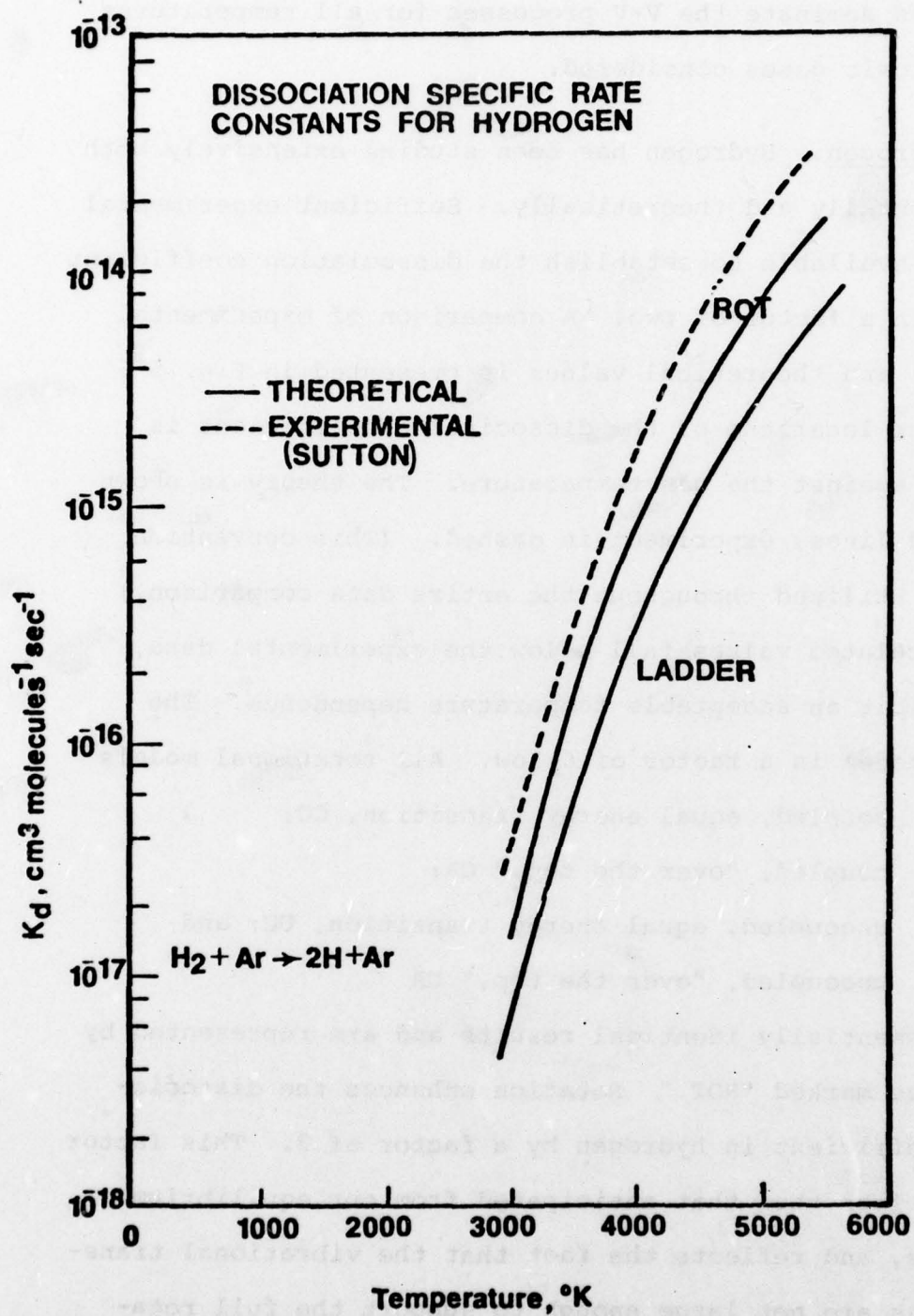


Fig 5-6 Dissociation of Hydrogen Diluted in Argon

This "bottle-necking" effect and consequent depletion has been pointed out by Pritchard (ref 57).

Oxygen and Nitrogen. The dissociation of oxygen and nitrogen has received much attention, primarily in order to elucidate the chemical behavior of air at high temperatures. The theoretical results for oxygen are compared with experiment in Figs. 5-7 and 5-8. Fig. 5-7 parallels the format and trends noted in Fig. 5-6 for hydrogen. Including rotation increases the dissociation coefficient once again. For oxygen, we are now able to observe slight differences among the rotational models. These differences will become more pronounced in  $N_2$ , CO,  $Br_2$ ,  $I_2$ , but the general ordering will remain the same. In Fig. 5-7,  $CC > CA > UC > UA$ . We will see that in general  $CC > CA$  and  $UC > UA$ . This is consistent with our equilibrium analysis of CDS and reflects the fact that equal energy transitions provide an easier path for the dissociation process. The coupled curves, CC and CA, are higher than the uncoupled, UC and UA, due to the more uniform distribution of the dissociation rates with respect to the vibrational levels in the coupled model. Stated simply, the vibrational bias in the coupled model is less than that in the uncoupled model. This lower vibrational bias reduces the vibrational depletion and leads to a larger dissociation rate. Fig. 5-8 is an Arrhenius plot over a wider temperature range, where the logarithm of the dissociation coefficient is

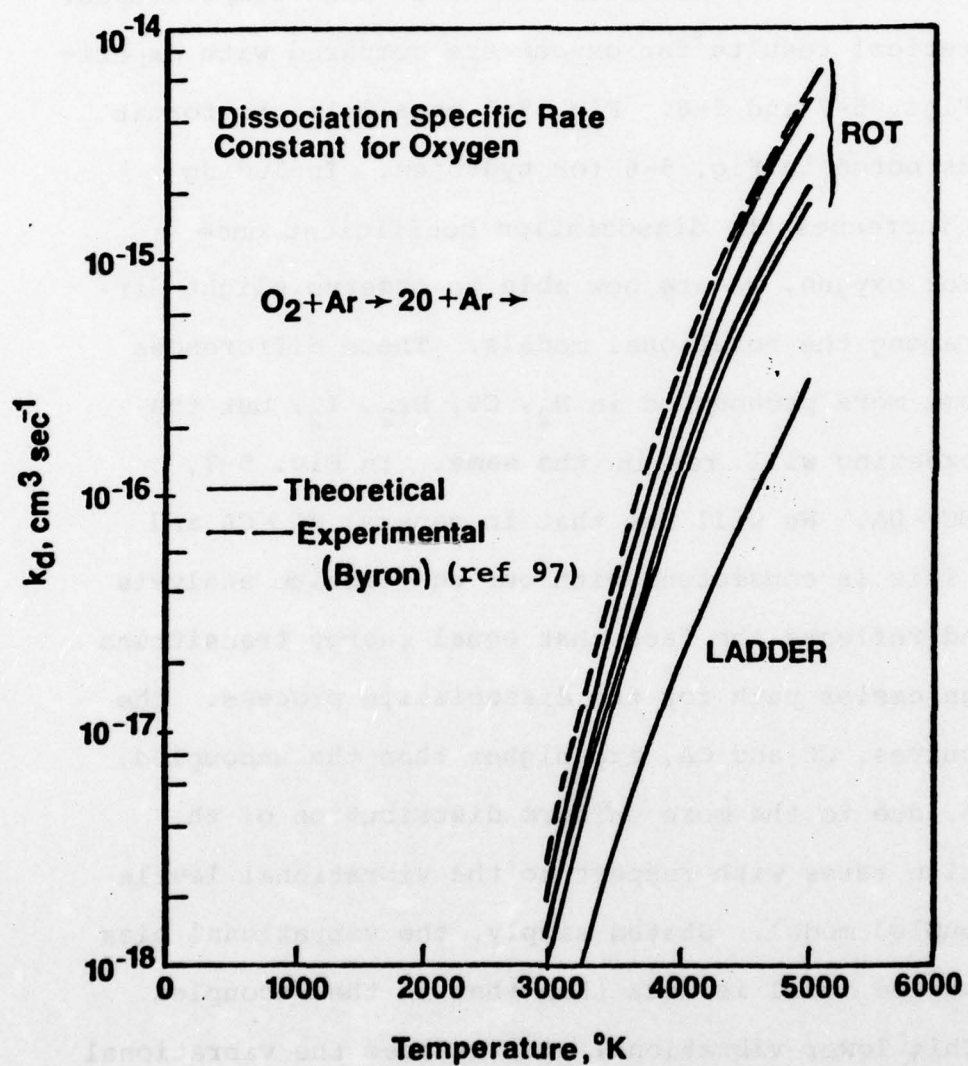


Fig 5-7 Dissociation of Oxygen Diluted in Argon

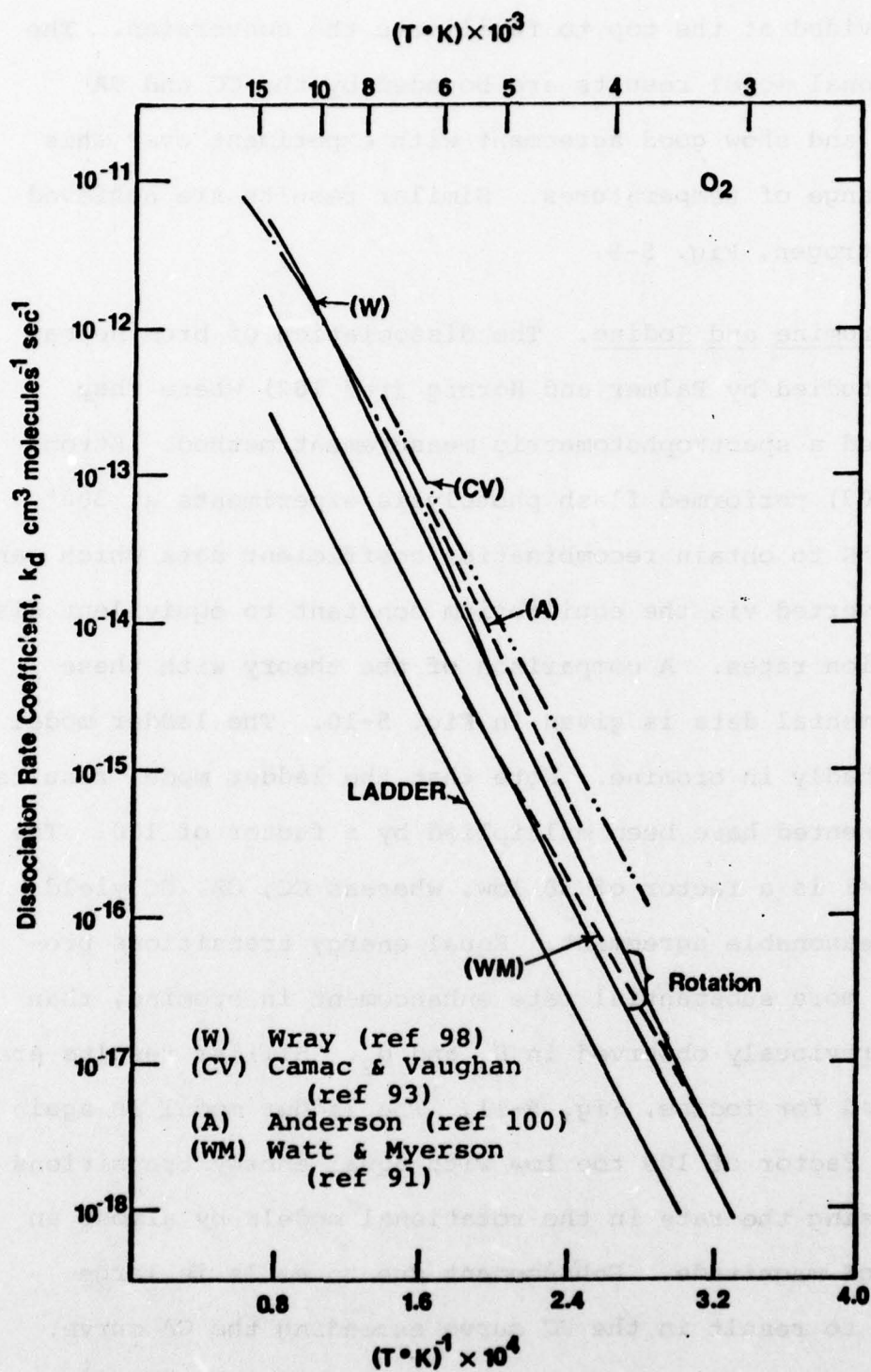


Fig 5-8 Arrhenius Plot of  $O_2$  Dissociation

plotted as a function  $T^{-1}$ . An additional temperature scale is provided at the top to facilitate the conversion. The rotational model results are bounded by the CC and UA curves and show good agreement with experiment over this wide range of temperatures. Similar results are achieved for nitrogen, Fig. 5-9.

Bromine and Iodine. The dissociation of bromine has been studied by Palmer and Hornig (ref 102) where they employed a spectrophotometric measurement method. Strong (ref 103) performed flash photolysis experiments at 300° to 430°K to obtain recombination coefficient data which can be converted via the equilibrium constant to equivalent dissociation rates. A comparison of the theory with these experimental data is given in Fig. 5-10. The ladder model fails badly in bromine. Note that the ladder model results as presented have been multiplied by a factor of 100. The UA model is a factor of 50 low, whereas CC, CA, UC yield more reasonable agreement. Equal energy transitions provide a more substantial rate enhancement in bromine, than that previously observed in  $O_2$  and  $N_2$ . Similar results are obtained for iodine, Fig. 5-11. The ladder model is again over a factor of 100 too low with equal energy transitions increasing the rate in the rotational models by almost an order of magnitude. Enhancement due to eet's is large enough to result in the UC curve exceeding the CA curve.

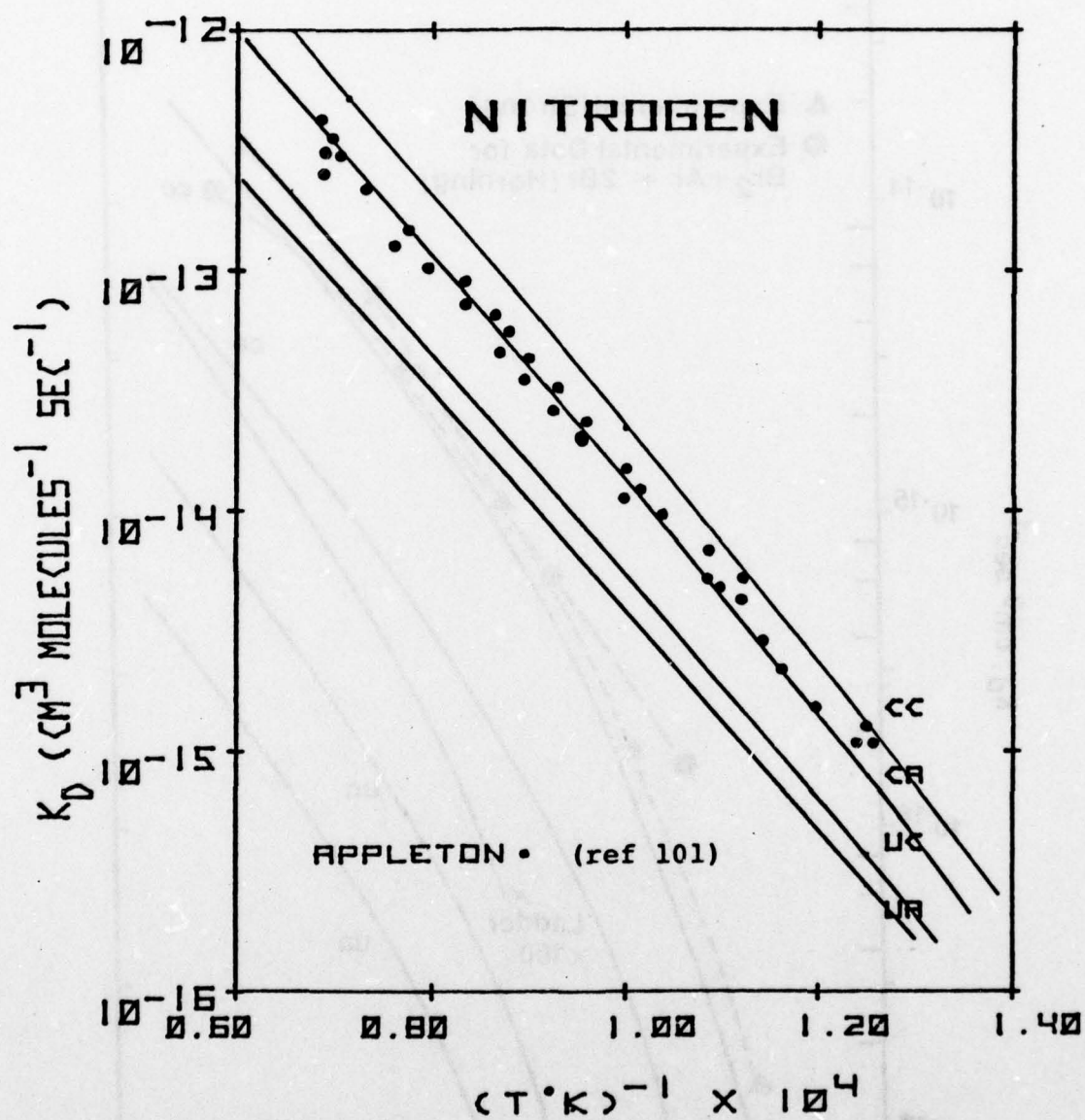


Fig 5-9 Arrhenius Plot of Nitrogen Dissociation

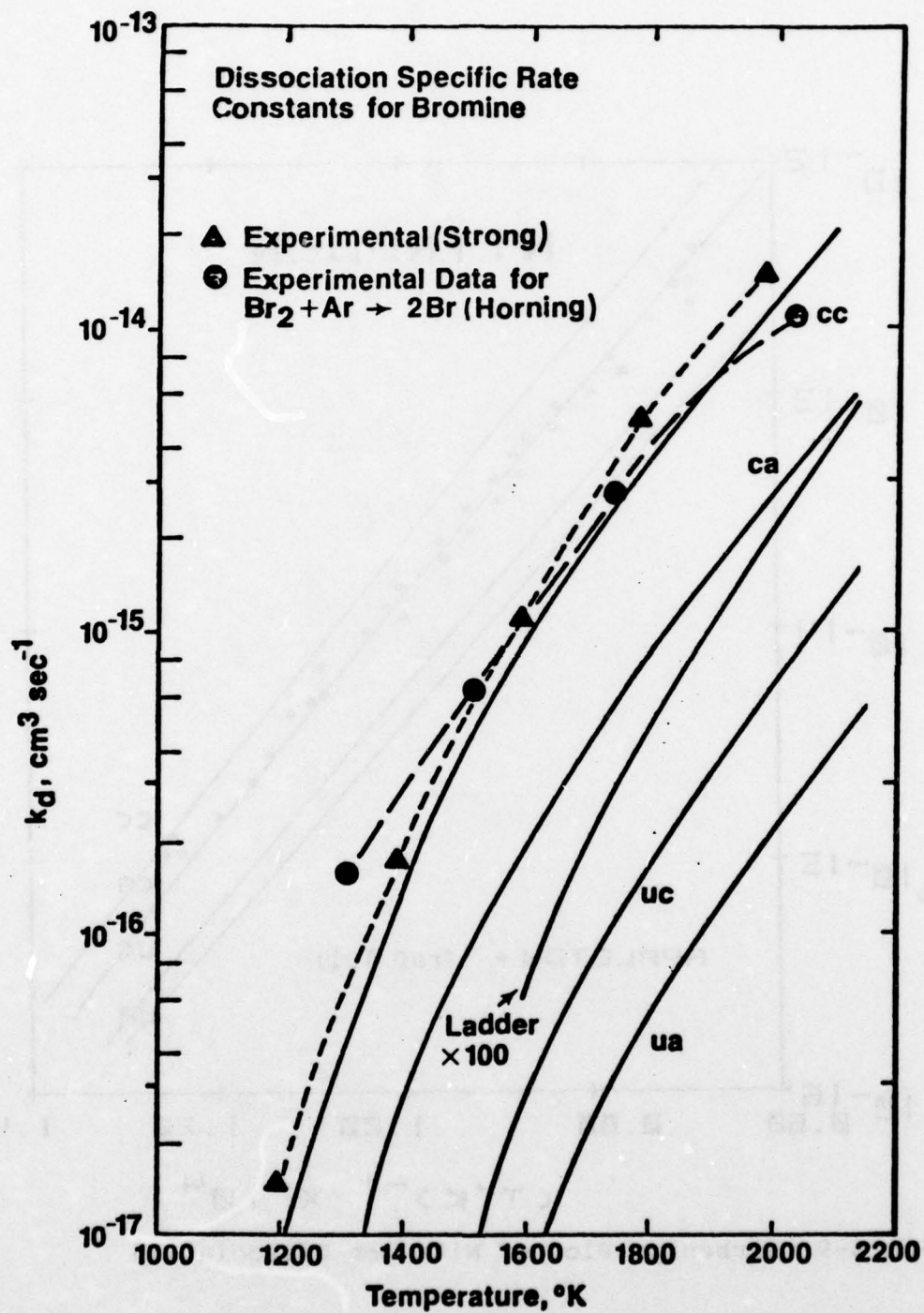


Fig 5-10 Dissociation of Bromine Diluted in Argon

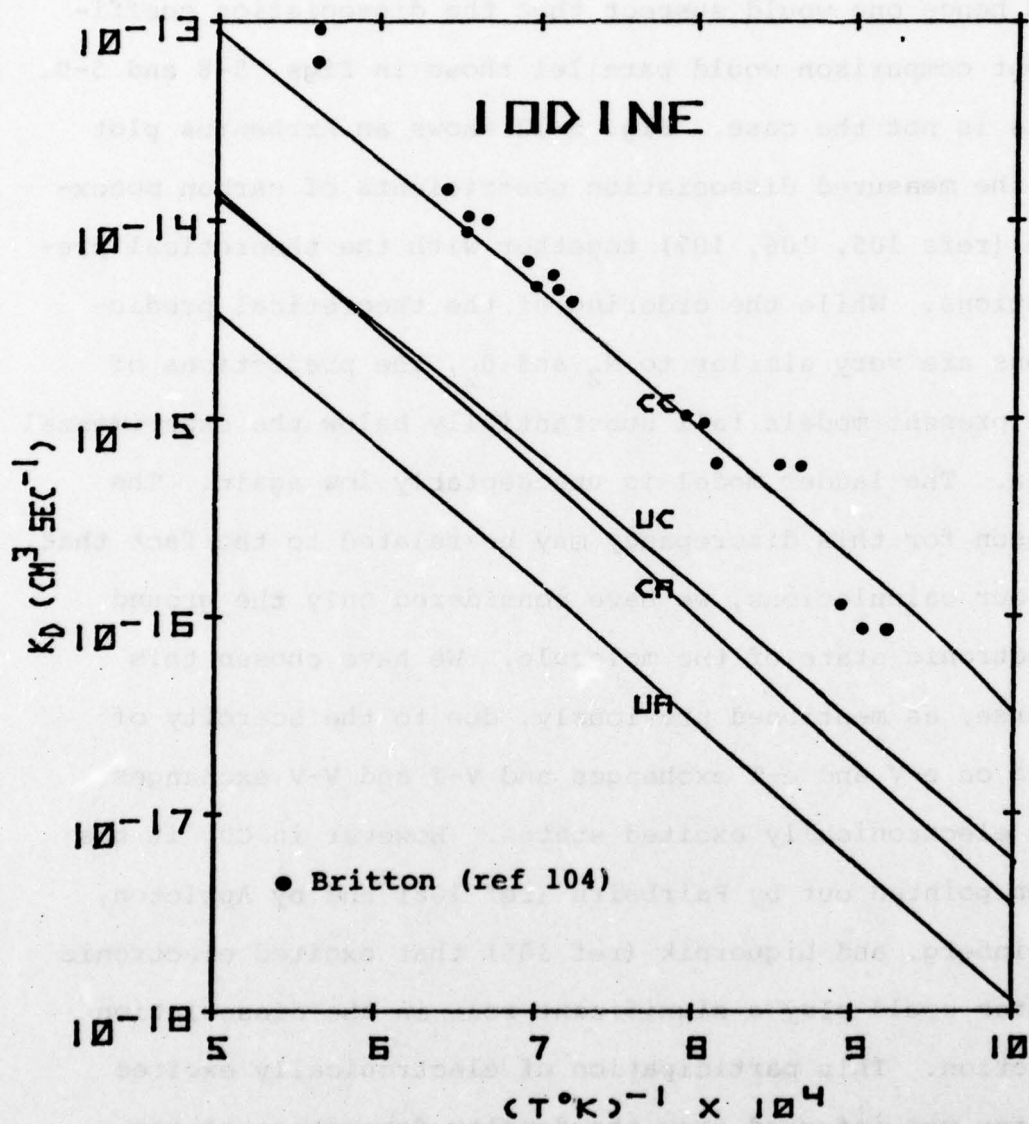


Fig 5-11 Dissociation of Iodine Diluted in Argon

This reveals that, in iodine, equal energy transitions and vibrational bias are of equal importance.

Carbon Monoxide. Carbon monoxide is very similar in mass and vibrational energy spacing to oxygen and nitrogen, and hence one would suspect that the dissociation coefficient comparison would parallel those in Figs. 5-8 and 5-9. This is not the case. Fig. 5-12 shows an Arrhenius plot of the measured dissociation coefficients of carbon monoxide (refs 105, 106, 107) together with the theoretical predictions. While the ordering of the theoretical predictions are very similar to  $N_2$  and  $O_2$ , the predictions of the present models fall substantially below the experimental data. The ladder model is unacceptably low again. The reason for this discrepancy may be related to the fact that, in our calculations, we have considered only the ground electronic state of the molecule. We have chosen this course, as mentioned previously, due to the scarcity of data on e-V and e-T exchanges and V-T and V-V exchanges for electronically excited states. However in CO, it has been pointed out by Fairbairn (ref 108) and by Appleton, Steinberg, and Liquornik (ref 105) that excited electronic states could play a significant role in the dissociation reaction. This participation of electronically excited states was inferred from the density dependence of the induction time. It is difficult to accurately estimate the magnitude of the enhancement due to electronically excited

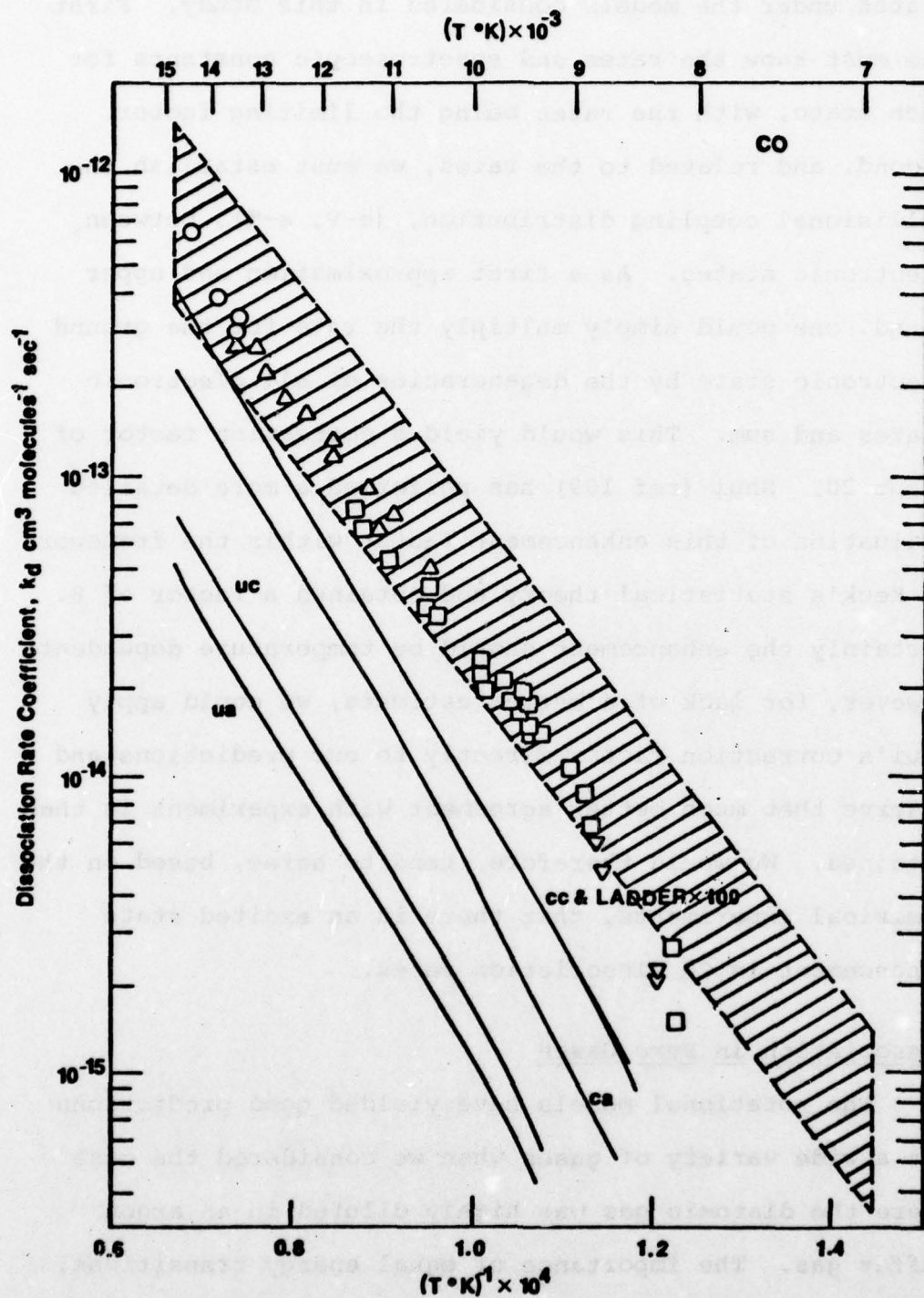


Fig 5-12 Arrhenius Plot of CO Dissociation

states under the models considered in this study. First one must know the rates and spectroscopic constants for each state, with the rates being the limiting factor. Second, and related to the rates, we must establish the collisional coupling distribution, (e-V, e-T), between electronic states. As a first approximation and upper bound, one could simply multiply the rate for the ground electronic state by the degeneracies of all electronic states and sum. This would yield a correction factor of about 20. Shui (ref 109) has performed a more detailed evaluation of this enhancement factor within the framework of Keck's statistical theory and obtained a factor of 8. Certainly the enhancement should be temperature dependent; however, for lack of a better estimate, we could apply Shui's correction factor directly to our predictions and observe that much better agreement with experiment is then obtained. We would therefore, tend to agree, based on the numerical experiments, that there is an excited state enhancement in CO dissociation rates.

#### Dissociation in Pure Gases

The rotational models have yielded good predictions for a wide variety of gases when we considered the case where the diatomic gas was highly diluted in an argon buffer gas. The importance of equal energy transitions, especially in Br<sub>2</sub>, and I<sub>2</sub>, has been pointed out as well as the role of electronically excited states in CO. We now

consider dissociation in pure gases. We will omit the ladder model in future discussions due to its failure in the dilute case.

In general, the dissociation rate in pure gases is larger than that obtained when the diatomic is highly diluted. The extent of this increase varies from gas to gas, being about a factor 1.5 for  $\text{Br}_2\text{-Br}_2$  and a factor of 10 for  $\text{O}_2\text{-O}_2$ . This rate enhancement in pure gases has been investigated within the calculational matrix of Table V-1, where the influence of vibrational-to-vibrational exchanges and changes in collisional efficiencies due to mass variation have been included. From this study, it was established that: (1) changes in the collisional efficiencies do not properly account for either the observed magnitude of the rate enhancement or its temperature dependence, and (2) V-V exchanges, however, lead to rate enhancements similar in magnitude and temperature dependence to those experimentally observed.

Hydrogen. The Arrhenius plots of the dissociation coefficient for  $\text{H}_2\text{-H}_2$  and  $\text{H}_2\text{-Ar}$ , illustrated in Fig. 5-13, show a comparison of experimental and theoretical results. The experimental results of Breshears and Bird (ref 110) differ from those of Sutton (ref 96). Sutton's data show the ratio  $k_d(\text{H}_2\text{-H}_2)/k_d(\text{H}_2\text{-Ar})$  to be almost constant and equal to 4. This is in contrast to the more recent data of Breshears, which reveal a temperature dependence to the

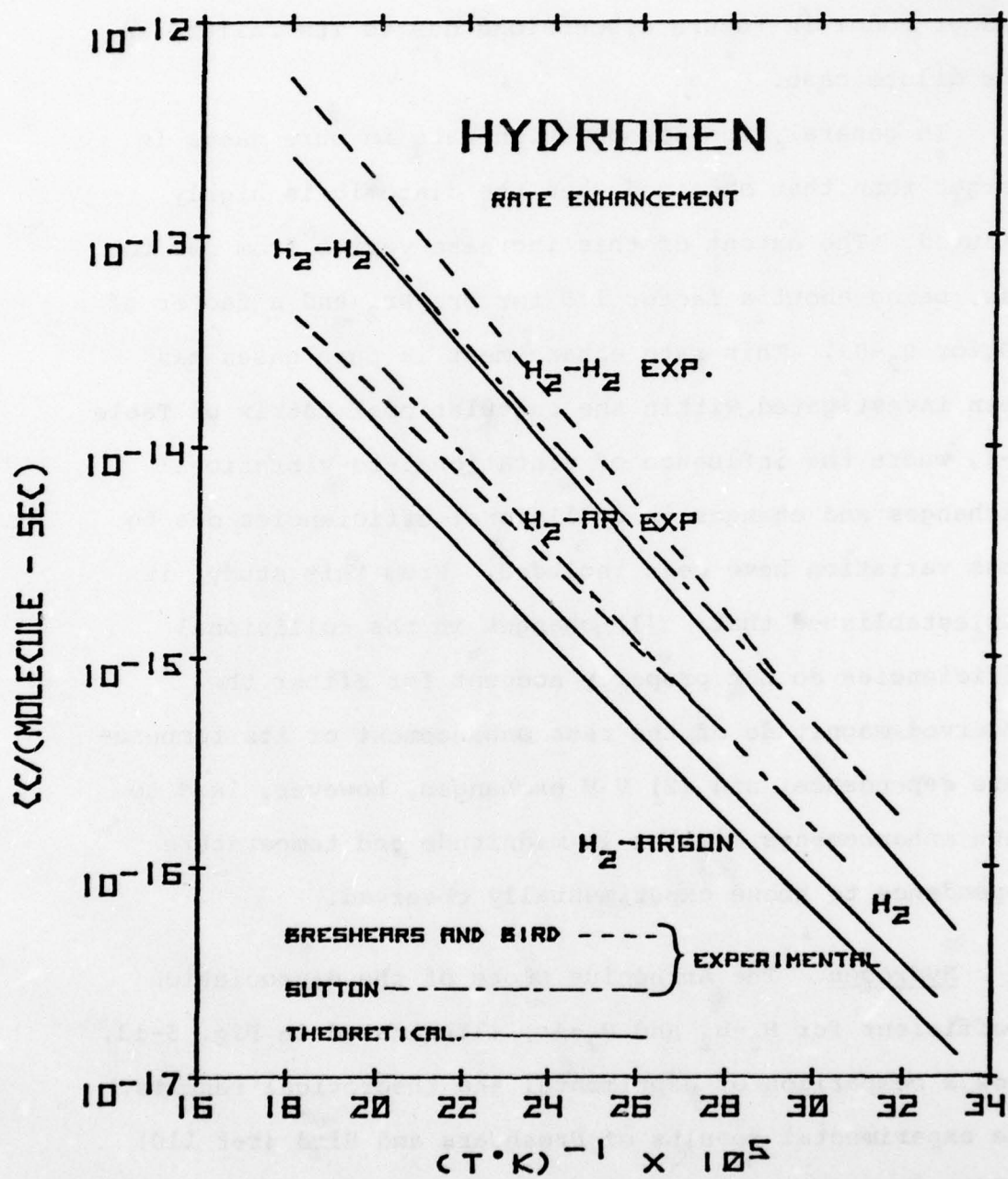


Fig 5-13 Rate Enhancement in  $H_2$

ratio varying from 3 at 3500°K to 10 at 5000°K. Three theoretical predictions are shown. The  $H_2$ -argon curve duplicates the rotational results obtained for the dilute case which were presented previously in Fig. 5-6 in a different format. The curve marked  $H_2$  illustrates the effect of changes in colliding masses, ( $H_2$ - $H_2$  vs  $H_2$ -Ar), and does not include the influence of V-V exchanges. The  $H_2$ - $H_2$  curve includes both V-V effects and mass changes, where we have utilized the theory of Rapp and Englander-Golden (ref 111) for the V-V rates.

The increase in the rate constant due to mass changes was less than the observed experimental enhancement and insensitive to variations in temperature. V-V exchanges, however, produced a more significant increase in the rate constant and introduced a temperature dependence very similar to that observed by Breshears (ref 110). The observed rate enhancement due to V-V exchanges is consistent with the calculations of Bauer and Hilden (ref 87), who used an empirical form for the dissociation rates. The magnitude of the enhancement is fairly sensitive to the magnitude of the V-V rates. Direct application of the Rapp form yielded a factor of 2.2 enhancement at 3000°K and a factor of 4.4 at 5000°K; whereas if the V-V rates were multiplied by ten, the enhancement changed to 10 and 30. Shown in the illustration are results for the Rapp rate multiplied by 3. Further theoretical and experimental work is required to establish the true magnitude and

temperature dependence of the V-V exchange rates. Summarizing, we conclude that V-V exchanges can account for the observed rate enhancement in hydrogen.

Oxygen. We now examine oxygen to see if the results obtained for  $H_2$  find general applicability. A comparison of these experimental and theoretical results is provided in Fig. 5-14. The experimental data of Byron (ref 97) shows that the ratio  $k_d(O_2-O_2)/k_d(O_2-Ar)$  is about ten and independent of temperature over the temperature range reported. The theoretical predictions yielded the following dissociation rate ratios for the values of V-V exchanges listed:

VV X f	$\frac{k_d(O_2-O_2)}{k_d(O_2-A)}$
f = 1	3.0
f = 3	3.8
f = 10	10

The curve for  $f=3$  is presented in the illustration where it should be pointed out that mass enhancement alone increased the dissociation rate by a factor of two. It is gratifying that, with minor adjustments in the V-V rates, rate enhancements in both oxygen and hydrogen are consistently accounted for. This even includes the temperature dependence of the observed enhancement.

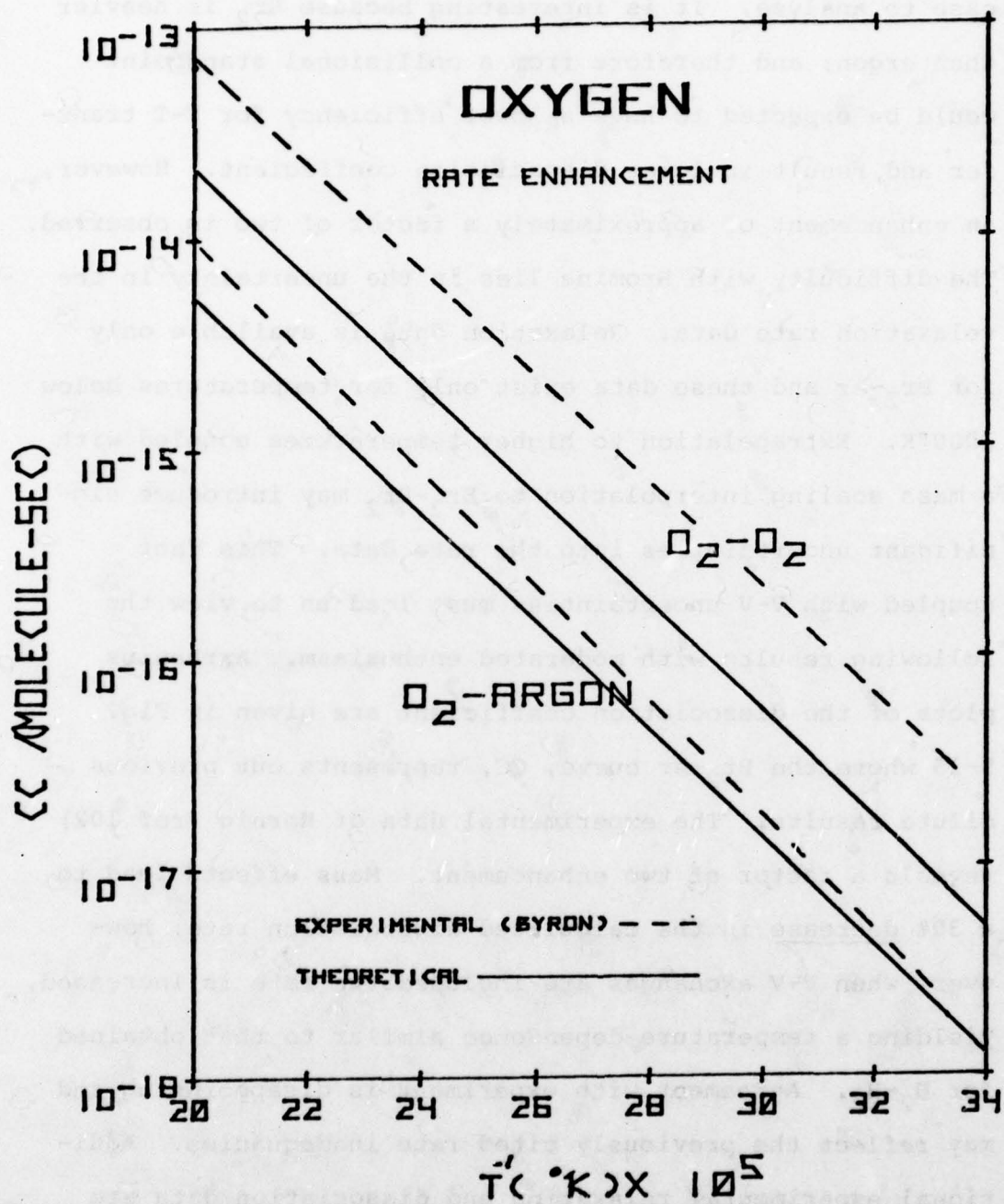


Fig 5-14 Rate Enhancement in  $O_2$

Bromine. Bromine is an interesting, but difficult case to analyze. It is interesting because  $\text{Br}_2$  is heavier than argon; and therefore from a collisional standpoint would be expected to have a lower efficiency for V-T transfer and result in lower dissociation coefficient. However, an enhancement of approximately a factor of two is observed. The difficulty with Bromine lies in the uncertainty in the relaxation rate data. Relaxation data is available only for  $\text{Br}_2$ -Ar and these data exist only for temperatures below  $1000^\circ\text{K}$ . Extrapolation to higher temperatures coupled with a mass scaling interpolation to  $\text{Br}_2$ - $\text{Br}_2$  may introduce significant uncertainties into the rate data. This fact coupled with V-V uncertainties must lead us to view the following results with moderated enthusiasm. Arrhenius plots of the dissociation coefficient are given in Fig. 5-15 where the  $\text{Br}_2$ -Ar curve, CC, represents our previous dilute results. The experimental data of Hornig (ref 102) reveals a factor of two enhancement. Mass effects lead to a 30% decrease in the calculated dissociation rate; however, when V-V exchanges are included the rate is increased, yielding a temperature dependence similar to that obtained for  $\text{H}_2$ - $\text{H}_2$ . Agreement with experiment is disappointing and may reflect the previously cited rate inadequacies. Additional experimental relaxation and dissociation data are needed to provide further knowledge about the factors controlling dissociation in  $\text{Br}_2$ .

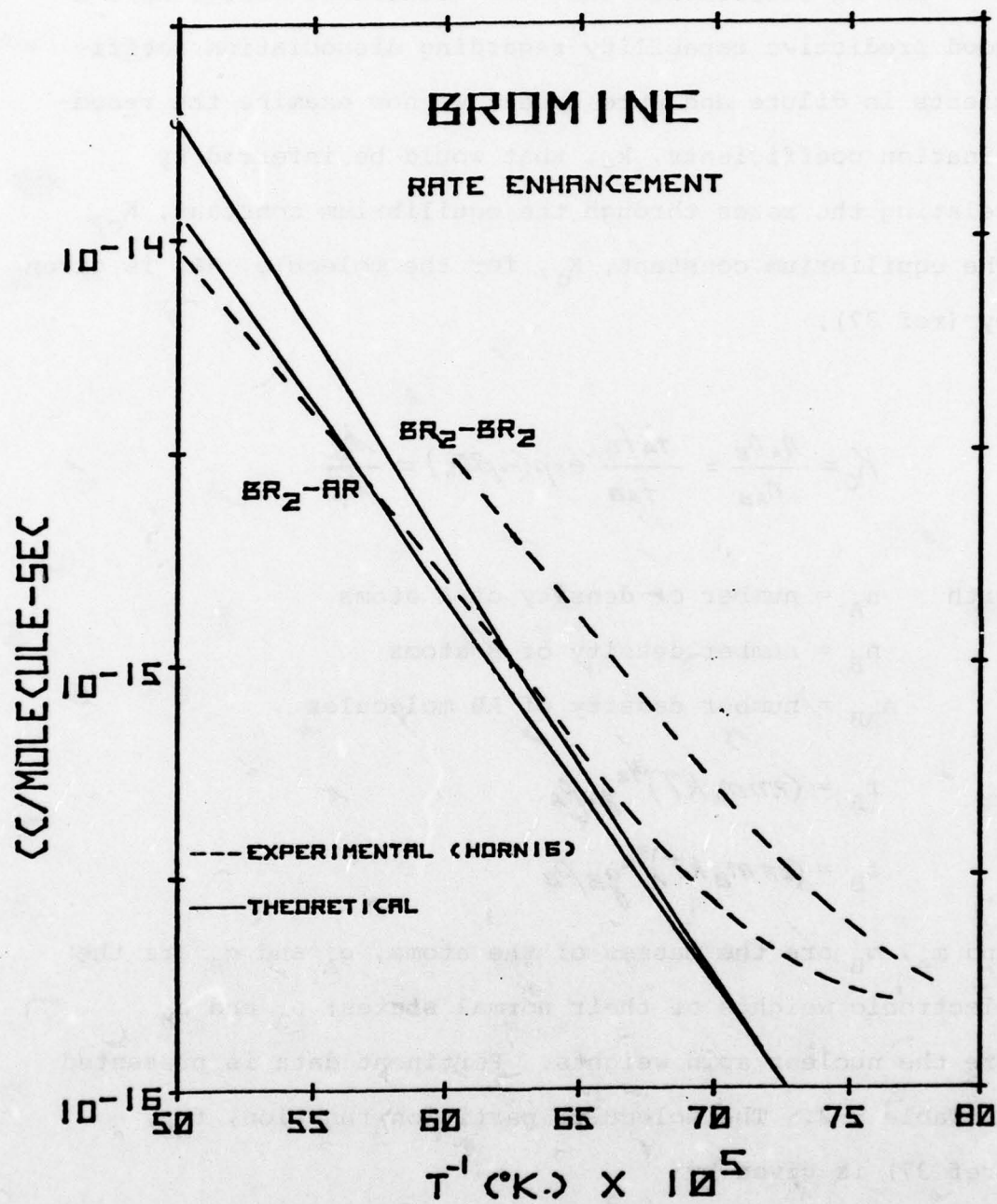


Fig 5-15 Rate Enhancement in  $\text{Br}_2$

### Recombination Coefficients

Having established that the rotational models have a good predictive capability regarding dissociation coefficients in dilute and pure gases, we now examine the recombination coefficients,  $k_r$ , that would be inferred by relating the rates through the equilibrium constant,  $K_c$ . The equilibrium constant,  $K_c$ , for the molecule, AB, is given by (ref 37),

$$K_c = \frac{n_A n_B}{n_{AB}} = \frac{f_A f_B}{f_{AB}} \exp(-\beta D_0) = \frac{k_d}{k_r}$$

with  $n_A$  = number of density of A atoms  
 $n_B$  = number density of B atoms  
 $n_{AB}$  = number density of AB molecules

$$f_A = (2\pi m_A kT)^{3/2} g_A \rho_A$$

$$f_B = (2\pi m_B kT)^{3/2} g_B \rho_B$$

and  $m_A$ ,  $m_B$  are the masses of the atoms,  $g_A$  and  $g_B$  are the electronic weights of their normal states;  $\rho_A$  and  $\rho_B$  are the nuclear spin weights. Pertinent data is presented in Table V-2. The molecular partition function,  $f_{AB}$ , (ref 37) is given by:

$$f_{AB} = \left\{ 2\pi (m_A + m_B) kT \right\}^{3/2} Q_{\text{vib-rot}} g_{AB} \left( \frac{\rho_A \rho_B}{\sigma_{AB}} \right)$$

TABLE V-2

## SPECTROSCOPIC DATA FOR THE MOLECULES

Species	Molecular State	Dissociation Products	Equilibrium Separation $r_e$ (Å)	Dissociation Energy D (eV)	Electronic Degeneracy Factor $g_{XY}/g_{XY}$	Vibrational Energy Spacing $\omega$ (cm <sup>-1</sup> )
H <sub>2</sub>	X <sup>1</sup> Σ <sub>g</sub> <sup>+</sup>	2 S + 2 S	0.742	4.477	1/4	4161
N <sub>2</sub>	X <sup>1</sup> Σ <sub>g</sub> <sup>+</sup>	4 S + 4 S	1.10	9.76	1/16	2358
O <sub>2</sub>	X <sup>3</sup> Σ <sub>g</sub> <sup>-</sup>	3 P + 3 P	1.21	5.12	1/27	1556
Br <sub>2</sub>	X <sup>1</sup> Σ <sub>g</sub> <sup>+</sup>	2 P <sub>3/2</sub> + 2 P <sub>3/2</sub>	2.28	1.97	1/16	323.2
I <sub>2</sub>	X <sup>1</sup> Σ <sub>g</sub> <sup>+</sup>	2 P <sub>3/2</sub> + 2 P <sub>3/2</sub>	2.67	1.542	1/16	215
CO	X <sup>1</sup> Σ <sub>g</sub> <sup>+</sup>	3 P + 3 P	1.128	11.1	1/81	2170
	a <sup>3</sup> Π	3 P + 3 P	1.206	5.09	2.27	1744
	a' <sup>3</sup> Σ <sub>g</sub> <sup>+</sup>	3 P + 3 P	1.352	4.24	1/27	1231

TABLE V-2--Continued

Species	Molecular State	Dissociation Products	Equilibrium Separation	Dissociation Energy	Electronic Degeneracy Factor	Vibrational Energy Spacing
C0	d $^3\Delta$	$3p + 3p$	1.370	3.58	2/27	1153
	e $^3\Sigma^-$	$3p + 3p$	1.383	3.33	1/27	1114
	i $^1\Sigma^-$	$3p + 3p$	1.416	2.96	1/81	1064
	A $^1\Pi$	$3p + 3p$	1.235	3.08	2/81	1516

with  $\sigma_{AB}$  the symmetry number. This yields, after canceling the nuclear spin weights (ref 37),

$$K_C = \frac{(2\pi m_A m_B kT)^{3/2} \sigma_{AB} g_A g_B \exp(-\beta D_0)}{(m_A + m_B)^{3/2} h^3 Q_{\text{vib-rot}} g_{AB}}$$

Since  $K_C \propto \exp(-\beta D_0)$  and  $k_d$  is approximately  $\propto \exp(-\beta D_0)$  the recombination coefficient

$$k_r = \frac{k_d}{K_C}$$

strips away the exponential factor in the dissociation coefficient and provides a detailed way of examining the activation energy or the pre-exponential temperature dependence. In looking at the recombination coefficients, we will examine the UC and UA models only, since these models behaved similarly to the CC and CA models differing mainly in magnitude and exhibiting only a slightly stronger (lower activation energy), temperature dependence. The following theoretical predictions were made for the dilute case, assuming that argon was the collision partner. This was the case in the majority of experimental investigations chosen for comparison. In addition, we continue to include only the contribution of the ground electronic state, (see Table V-2). Our major concern in all these comparisons

will be the temperature dependence, since we have noted variations in magnitude of the various models previously when we discussed the dissociation coefficients. We will observe throughout the recombination comparisons that the predicted temperature dependence is extremely good, especially when one considers the temperature range, rate scaling, and variety of gases considered.

Hydrogen. The predicted  $k_r(\text{H}_2)$ , again given by the solid line, is compared with the recombination coefficients inferred from the high temperature dissociation rate measurements (refs 112, 113, 114, 115) and the direct recombination rate measurements (refs 116, 117) in Fig. 5-16. The agreement between our prediction and the high temperature measurements of Sutton (ref 114), Myerson (ref 115), Jacobs (ref 112), and Hurle (ref 113) is good, reproducing the temperature dependence despite being about a factor of three low. At lower temperatures, the temperature dependence is too strong, and may reflect a breakdown in the assumption of rotational equilibrium, an inadequacy in the scaling of the exchange rates to low temperatures, or an increased sensitivity to the molecular potential and state designation at low temperatures. The results obtained for hydrogen showed the largest disparity of all gases considered.

Oxygen. The predicted rate coefficients for oxygen are presented in Fig. 5-17 and are compared to the high temperature dissociation data of Wray (ref 98), Camac and

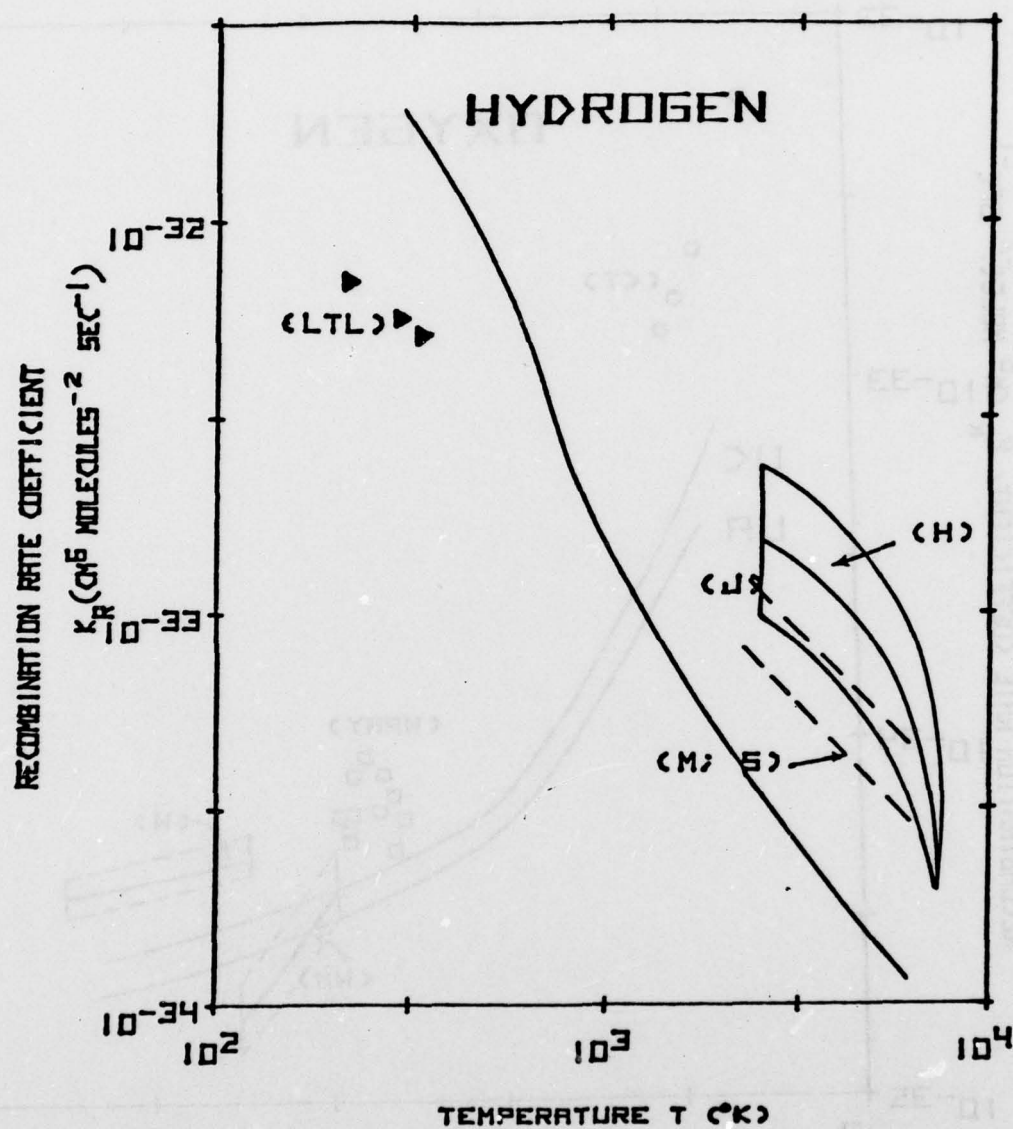


FIG 5-16  $\text{H}_2$  Recombination Coefficient

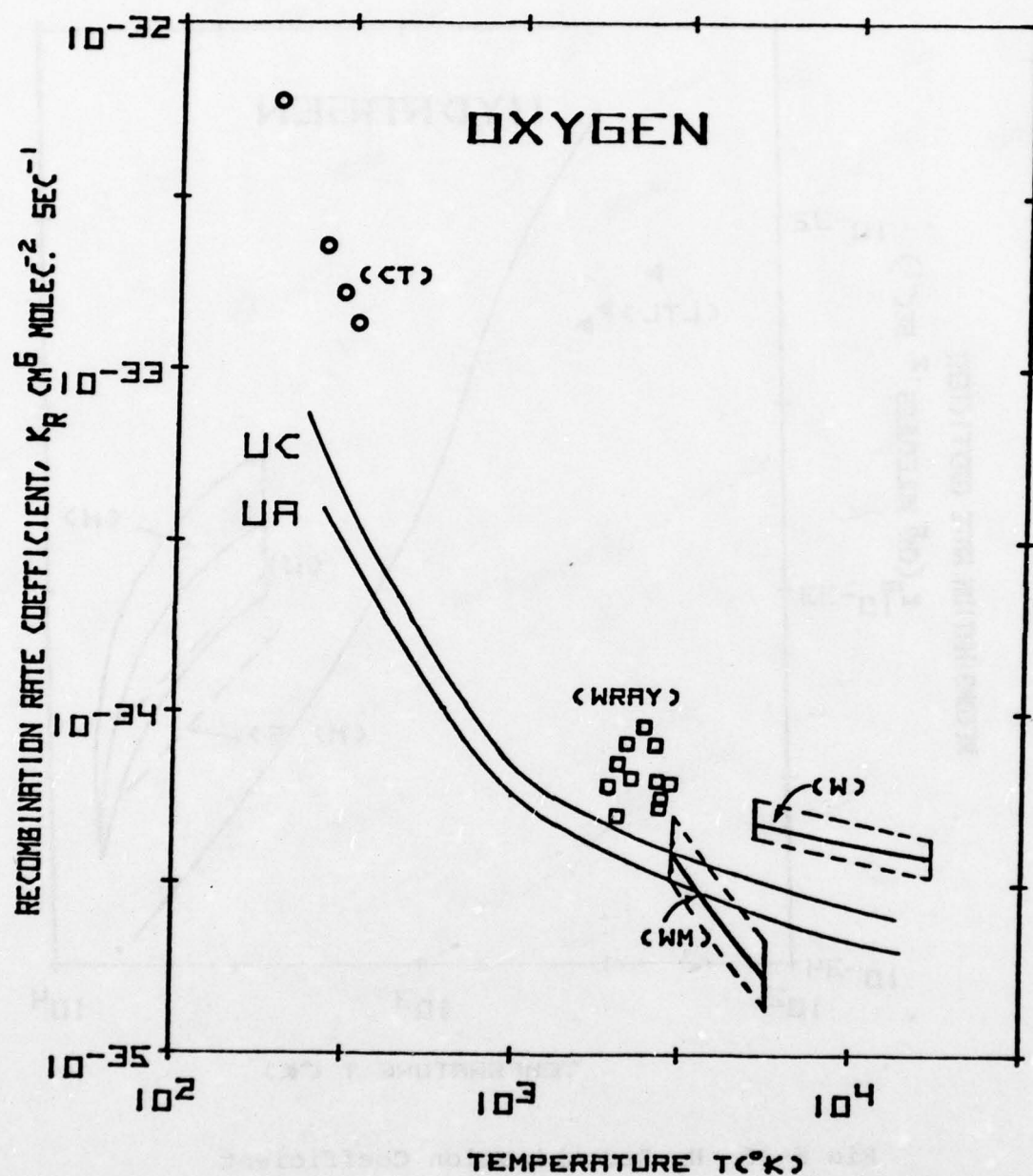


Fig 5-17  $\text{O}_2$  Recombination Coefficient

Vaughan (ref 93), and Watt and Myerson (ref 118). Note the disparity in the temperature dependence between the experimental data of Watt and Myerson and Wray and Watt. Our calculations favor the latter dependence and exhibit good agreement with that data. This agreement, obtained for both models considered, extends down to the low temperatures where it compares favorably with the direct measurements of Campbell and Thrush (ref 119). No significant difference in temperature dependence exists between the UC and UA curves.

Nitrogen. The agreement obtained in nitrogen is good and comparable to that obtained in oxygen. Fig. 5-18 illustrates this comparison with the low temperature point measurements of Campbell and Thrush (ref 120) and Clyne and Stedman (ref 121), and the high temperature data of Appleton (ref 122), Byron (ref 123) and Cary (ref 124). Observe that at low temperatures the UC curve, incorporating equal energy transitions, exhibits a stronger temperature dependence than the UA curve representing the "over the top" model, and yields substantially better agreement with experiment.

Bromine. The data comparison in bromine, Fig. 5-19, reinforces the idea that equal energy transitions, represented by UC, play a significant role in the dissociation reaction. The point data at low temperatures are due to I<sub>p</sub> and Burns (refs 125, 126, 127), while the higher

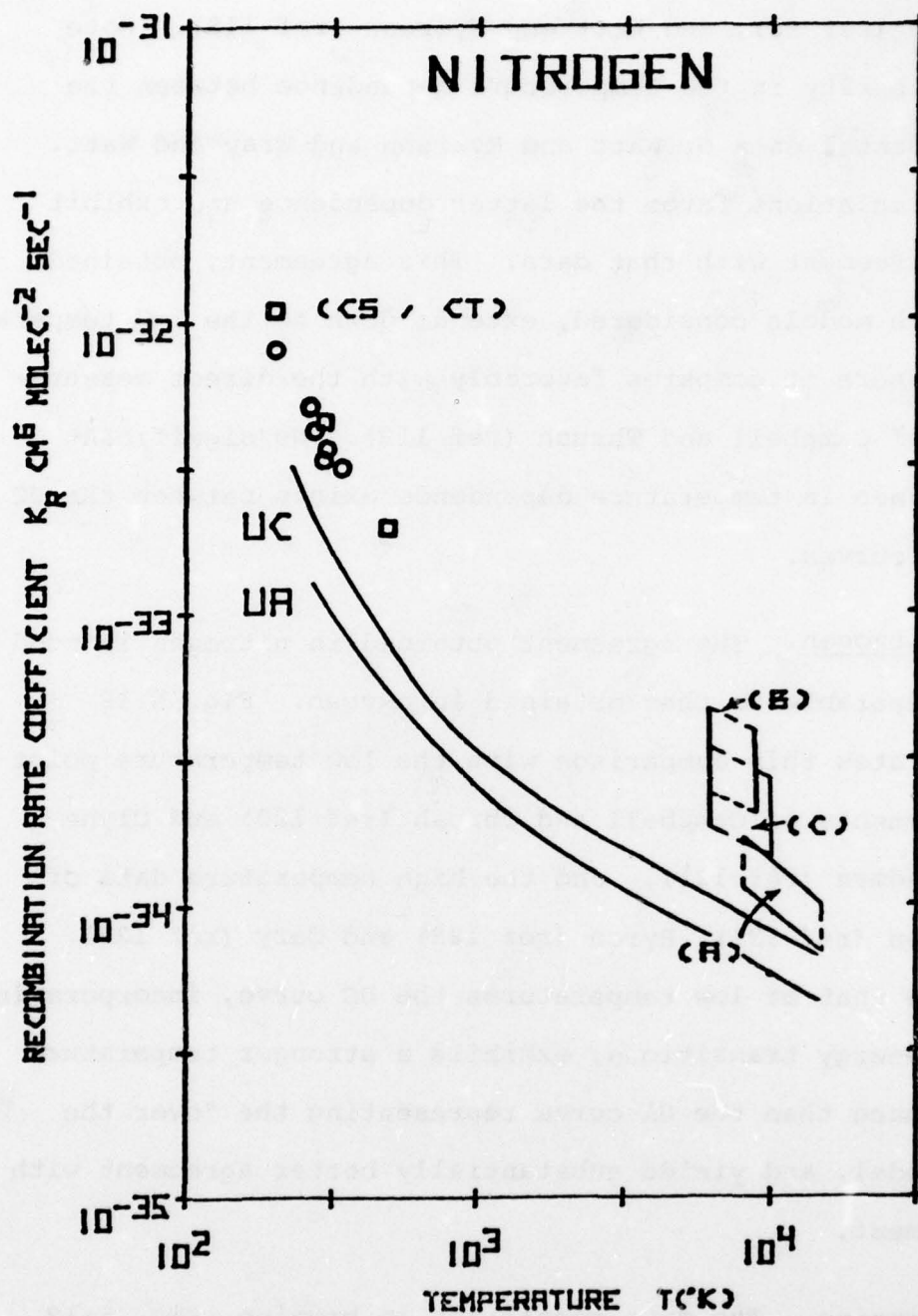


Fig 5-18  $N_2$  Recombination Coefficient

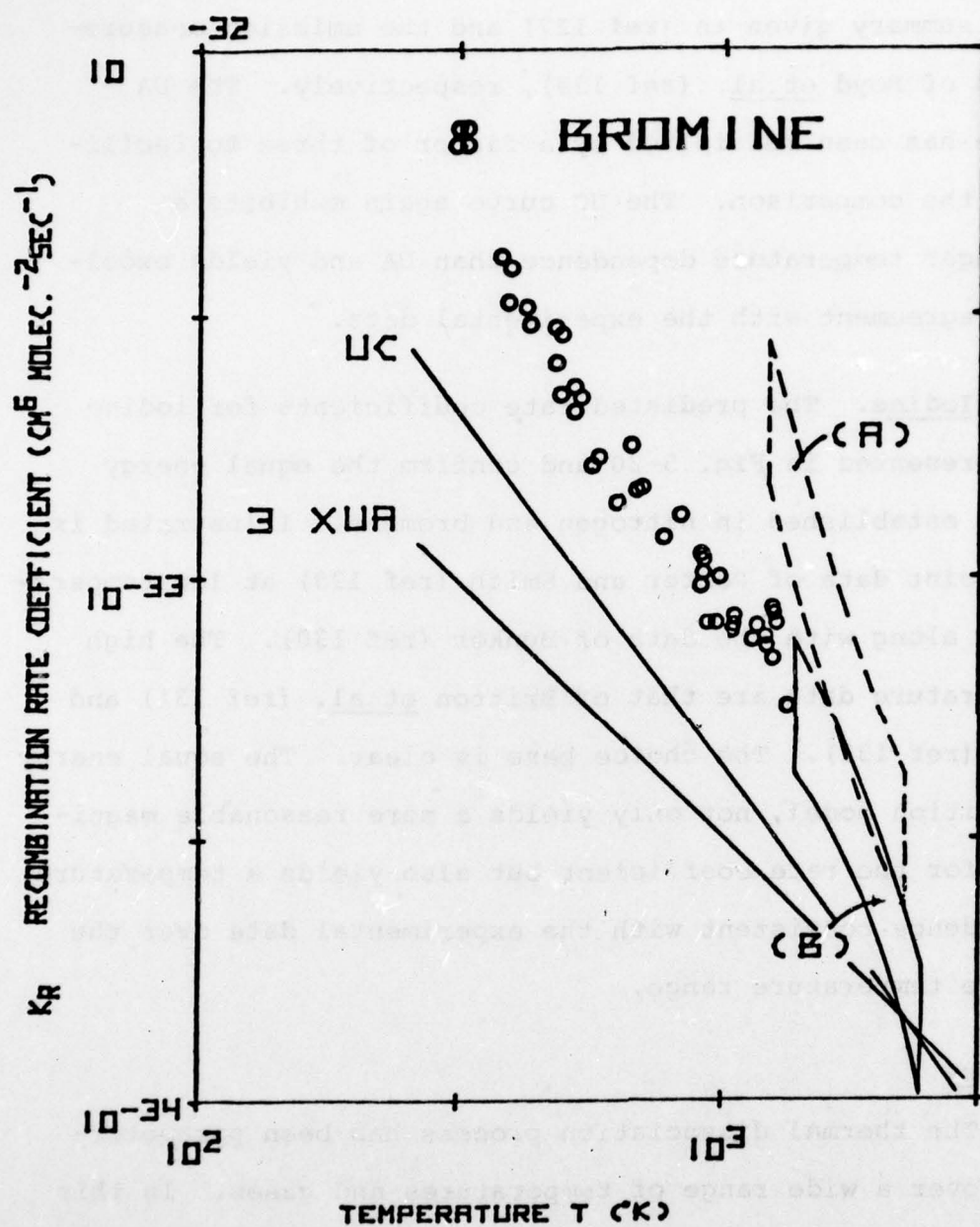


Fig 5-19  $\text{Br}_2$  Recombination Coefficient

temperature data represented as areas A and B are from the data summary given in (ref 127) and the emission measurements of Boyd et al. (ref 128), respectively. The UA curve has been multiplied by a factor of three to facilitate the comparison. The UC curve again exhibits a stronger temperature dependence than UA and yields excellent agreement with the experimental data.

Iodine. The predicted rate coefficients for iodine are presented in Fig. 5-20 and confirm the equal energy trend established in nitrogen and bromine. Illustrated is the point data of Porter and Smith (ref 129) at low temperatures along with the data of Bunker (ref 130). The high temperature data are that of Britton et al. (ref 131) and Troe (ref 132). The choice here is clear. The equal energy transition model, not only yields a more reasonable magnitude for the rate coefficient but also yields a temperature dependence consistent with the experimental data over the entire temperature range.

#### Summary

The thermal dissociation process has been parameterized over a wide range of temperatures and gases. In this particular study, we have used three simplified models.

1. Standard ladder
2. Coupled Model
3. Uncoupled Model

to evaluate the rotational contribution to dissociation.

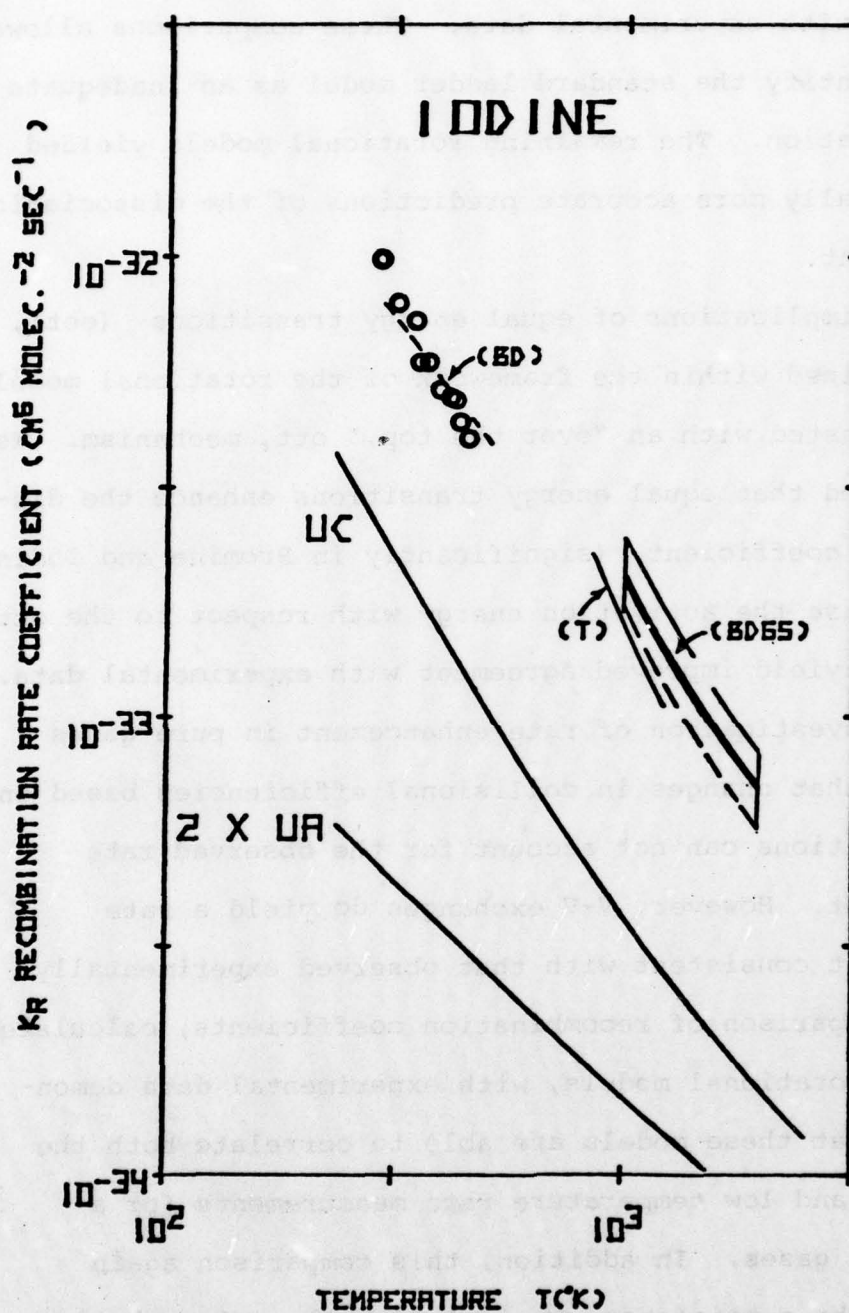


Fig 5-20  $I_2$  Recombination Coefficient

Time-dependent and steady-state solutions were obtained and compared with experimental data. These comparisons allowed us to identify the standard ladder model as an inadequate representation. The remaining rotational models yielded substantially more accurate predictions of the dissociation coefficient.

The implications of equal energy transitions (eet), were examined within the framework of the rotational models and contrasted with an "over the top," ott, mechanism. We established that equal energy transitions enhance the dissociation coefficient (significantly in Bromine and Iodine), and decrease the activation energy with respect to the ott model, to yield improved agreement with experimental data.

An investigation of rate enhancement in pure gases revealed that changes in collisional efficiencies based on mass variations can not account for the observed rate enhancement. However, V-V exchanges do yield a rate enhancement consistent with that observed experimentally.

A comparison of recombination coefficients, calculated from the rotational models, with experimental data demonstrated that these models are able to correlate both the very high and low temperature rate measurements for a variety of gases. In addition, this comparison again revealed the consistency of including the eet mechanism in the calculations.

## Chapter VI. Dissociation Under Highly Non-Equilibrium Conditions

### Introduction to Non-Equilibrium Processes

In the preceding chapters, time-dependent and steady-state solutions of the Master Equation have been utilized in an investigation of thermal dissociation and recombination. This analysis of elementary processes in excited molecules, including energy relaxation and vibrational exchange, plays an important role in studies of combustion and gas dynamics, but deals with systems that are only slightly perturbed from thermal equilibrium. In recent years, however, there have been significant advances and interest in the fields of chemical kinetics and molecular lasers where highly non-equilibrium situations are encountered. These highly non-equilibrium conditions can be achieved by electron impact excitation or radiative pumping of the vibrational manifold. Given the success of the presented collisional analyses in addressing dissociation under essentially equilibrium conditions, it is reasonable to attempt to extend these theories to treat those highly non-equilibrium conditions encountered in electric gas discharges or optically pumped systems. In this chapter, we will utilize the simple chemical reaction of dissociation to illustrate the effect of non-equilibrium on chemical processes. We will investigate the dissociation process

under highly non-equilibrium conditions and, for interesting plasma conditions, compare the dissociation caused by electron impact with the dissociation due to heavy particle collisions.

In this section of the study, we will consider only a gas mixture of carbon monoxide and argon. The analysis and conclusions, however, have general application to other molecular gases and gas mixtures.\* The CO/Ar system is an attractive one to analyze since abundant data is available on electron impact cross-sections, and the molecular transfer rates are reasonably well known. This is not a minor point, since the electron energy distribution, vibrational energy distribution, and dissociation rates are sensitive functions of these input data. In addition, the CO/Ar system is experimentally versatile; capable of being either optically pumped or excited in a gas discharge. Reliable experimental data is available for both situations, thus permitting a benchmarking of the calculations. Here we will make comparisons with the experimental distributions obtained by Rich (ref 133) who utilized direct optical pumping of CO. Under conditions of either discharge or optical pumping, efficient excitation of CO is achieved and a highly non-equilibrium state is obtained.

To address non-equilibrium dissociation, we utilize for the vibrational manifold of the molecules the Master

---

\*Selected calculations have also been performed in CO/He, O<sub>2</sub>/Ar, N<sub>2</sub>/Ar, and O<sub>2</sub>/He mixtures at various concentrations.

Equation formalism previously developed for the near equilibrium conditions; and for the electrons we use a steady-state solution of the collisional Boltzmann equation. The presentation of these detailed calculations will be prefaced by a development of the collisional Boltzmann equation, and a discussion of the relevant electron-molecule collisional processes. We will examine the molecular kinetics, the characteristics of the vibrational distribution under strongly pumped conditions, and review an analytic approximation to the vibrational distribution. This will provide us with a better insight when we subsequently present time-dependent and steady-state calculations of the vibrational distribution and dissociation coefficient. Finally, we will link the two analyses in a parametric mapping of the heavy particle and electron impact dissociation processes under non-equilibrium conditions.

### Electron Kinetics

Background. Under appropriate conditions, electron impact excitation is an efficient method of delivering energy to molecular gases. In this section, we will present results of a numerical investigation of the electron-molecule energy transfer processes and the resulting electron energy distributions obtained in electrically excited molecular gases. Emphasis is placed on conditions encountered in low pressure discharges, as well as those encountered at high pressures when using an electron beam-sustainer configuration. Both of these discharge cases

are characterized by a low degree of ionization,  $\sim 10^{-7}$ , and electron mean energies in the range of 0.5 to 2.0 ev. For these conditions, the electron energy distribution, eed, is non-Maxwellian and exhibits a structure that is consistent with the features of the electron-molecule excitation processes. Since the eed is generally non-Maxwellian, a detailed analysis of the electron kinetics involving a steady-state solution of the collisional Boltzmann equation is required to evaluate the electron impact excitation, ionization, and dissociation rates. Relatively accurate and complete data on electron-impact cross-sections for argon and CO, have been reported. These are conveniently listed in the reference compilation of Kieffer (ref 134). Using these data, the eed is calculated by numerically integrating the Boltzmann equation assuming that the distribution is spatially uniform and a steady-state exists.

Boltzmann Equation Theory. The collisional Boltzmann equation is the fundamental equation governing energy transfer in electron-molecule collisions. Several detailed and general developments have previously been given (refs 135, 136, 137, 138, 139). Here we will merely summarize those features relevant to the present analysis and provide a convenient review of the development following the previously cited references. The eed is obtained by solving the Boltzmann equation

$$\frac{\partial f}{\partial t} + \vec{v} \cdot \nabla f + \vec{a} \cdot \nabla_v f = \left( \frac{\partial f}{\partial t} \right)^c \quad (6-1)$$

where  $f = f(\vec{v}, \vec{r}, t)$  is the electron velocity distribution function,  $\vec{v}$  the velocity,  $\vec{a}$  the acceleration and  $\left( \frac{\partial f}{\partial t} \right)^c$  represents the rate of change of  $f$  due to electron collisions of all types. Note that the terms on the left-hand side of equation (6-1) represent the continuum flow in phase space of the eed, whereas the right-hand side accounts for discrete transitions in the phase space resulting from elastic and inelastic collisions.

For typical discharge conditions we will consider; the electric field, gas density, and electron density are constant in time and spatially uniform. By introducing spherical coordinates in the velocity space, the eed can be expressed as an infinite series of products

$$f(t, v, \theta) = \sum_{n=0}^{\infty} f_n(t, v) P_n(\theta) \quad (6-2)$$

where  $P_n(\theta)$  is the  $n$ th Legendre polynomial,  $\theta$  the polar angle with respect to the electric field direction, and  $f_n$  an expansion coefficient which is a function of the electron speed,  $v$ , and time,  $t$ .

In this representation the Boltzmann equation takes the following form (ref 138)

$$\frac{df}{dt} + \left( \frac{-eE}{m} \right) \left( \mu \frac{df}{dv} + \frac{[1-\mu^2]}{v} \frac{df}{d\mu} \right) = \left( \frac{df}{dt} \right)^c \quad (6-3)$$

with  $\mu = \cos \theta$ . If we next introduce the following identities (ref 140)

$$\frac{(1-\mu^2) dP_n(\mu)}{d\mu} = \frac{n(n+1)}{2n+1} (P_{n-1}(\mu) - P_{n+1}(\mu)) \quad (6-4)$$

$$\mu P_n(\mu) = \frac{n+1}{2n+1} P_{n+1}(\mu) + \frac{n}{2n+1} P_{n-1}(\mu)$$

equation (6-3) yields

$$\sum_{n=0}^{\infty} \frac{df_n}{dt} + \left( \frac{-eE}{m} \right) \left[ \left( \frac{n+1}{2n+1} \frac{df_n}{dv} - \frac{n(n+1)}{(2n+1)v} f_n \right) P_{n+1} + \left( \frac{n}{2n+1} \frac{df_n}{dv} + \frac{n(n+1)}{(2n+1)v} f_n \right) P_{n-1} \right] = \left( \frac{df}{dt} \right)^c_n \quad (6-5)$$

By equating terms with the same angular dependence, an infinite set of coupled differential equations is obtained. Under normal discharge conditions, the electron velocity distribution is nearly spherically symmetric, and retention

of only the leading terms in the expansion is justified (refs 135, 136, 137). Retaining the first three terms, we obtain (refs 136, 137, 138)

$$\frac{df_0}{dt} + \left(\frac{-eE}{m}\right) \left[ \frac{1}{3} \frac{df_1}{dt} + \frac{2}{3} \frac{f_1}{v} \right] = \left(\frac{df}{dt}\right)_0^c \quad (6-6)$$

$$\frac{df_1}{dt} + \left(\frac{-eE}{m}\right) \left[ \frac{df_0}{dv} + \frac{2}{5} \frac{df_2}{dv} + \frac{6}{5} \frac{f_2}{v} \right] = \left(\frac{df}{dt}\right)_1^c \quad (6-7)$$

$$\frac{df_2}{dt} + \left(\frac{-eE}{m}\right) \left[ \frac{2}{3} \frac{df_1}{dv} - \frac{2}{3} \frac{f_1}{v} + \frac{3}{7} \frac{df_3}{dv} + \frac{12}{7} \frac{f_3}{v} \right] = \left(\frac{df}{dt}\right)_2^c \quad (6-8)$$

In order to evaluate,  $\left(\frac{\partial f}{\partial t}\right)_n^c \equiv \left(\frac{\partial f}{\partial t}\right)_+^c + \left(\frac{\partial f}{\partial t}\right)_-^c$ , let us first

define the differential scattering cross-section for an electron with speed  $v$  scattered through an angle  $\alpha$  into a unit solid angle to be  $q(v, \alpha)$ . The collision geometry and coordinate definitions and relations are shown in Fig. 6-1. Note that  $\psi$  is the azimuthal angle in velocity space around the vector  $\vec{v}$ . The total rate of scattering out of a differential volume in velocity space at  $\vec{v}(v, \theta, \phi)$ , for process  $h$  is given by (refs 136, 138)  $\left(\frac{\partial f}{\partial t}\right)_-^c$ , where

$$\left(\frac{\partial f}{\partial t}\right)_-^c = -N_h v \int_0^{2\pi} \int_0^\pi q_h(v, \alpha) \sum_{n=0}^{\infty} f_n(t, v) P_n(\mu) \sin(\alpha) d\alpha d\psi \quad (6-9)$$

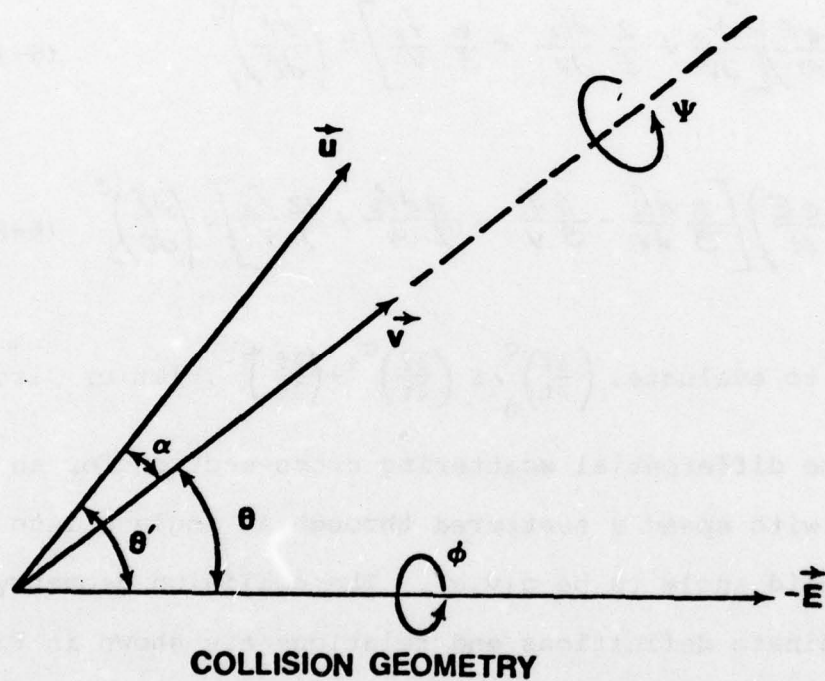


Fig 6-1 Collision Geometry

and with  $N_h$  representing the gas number density in the initial state. The effective rate is obtained by summing over all processes,  $h$ , including elastic and inelastic collision channels.

Similarly, the positive term,  $\left(\frac{\partial f}{\partial t}\right)^{C+}$ , representing the rate of scattering into the volume at  $\vec{v}$  from  $\vec{u}$  ( $u, \theta', \phi'$ ) is (refs 136, 138)

$$\left(\frac{\partial f}{\partial t}\right)^{C+} = N_h u \int_0^{2\pi} \int_0^{\pi} g_h(u, \alpha) \sum_{n=0}^{\infty} f_n(t, u) P_n(\mu') \sin \alpha d\alpha d\psi / J \quad (6-10)$$

where  $J$  is the Jacobian of the transformation and represents the ratio of that differential volume in velocity space from which the electron scatters to that volume into which the electron scatters,

$$u^2 \sin \alpha d\alpha d\psi du \quad \text{to} \quad v^2 \sin \alpha d\alpha d\psi dv$$

Consider, for illustrative purposes, a truly "elastic" collision in which there is no energy transfer; but only a change in direction. Under these circumstances

$$u = v \\ f(t, u) = f(t, v)$$

and the Jacobian is unity. Then upon integrating over  $\psi$ ,

equations (6-9) and (6-10) yield (ref 138)

$$\left(\frac{df}{dt}\right)_+^c + \left(\frac{df}{dt}\right)_-^c = - \sum_{n=0}^{\infty} N_h v Q_n^h(v) f_n(t, v) P_n(\mu) \quad (6-11)$$

where the elastic cross-section for process  $h$  and order  $n$  is given by

$$Q_n^h(v) = 2\pi \int_0^\pi g_h(v, \alpha) (1 - P_n(\cos \alpha)) \sin \alpha \, d\alpha \quad (6-12)$$

with the three lowest order elastic cross-sections given by

$$\begin{aligned} Q_0^h(v) &= 0 \\ Q_1^h(v) &= 2\pi \int_0^\pi g(v, \alpha) (1 - \cos \alpha) \sin \alpha \, d\alpha \equiv Q_r^h \\ Q_2^h(v) &= 3\pi \int_0^\pi g(v, \alpha) (1 - \cos^2 \alpha) \sin \alpha \, d\alpha \end{aligned}$$

Thus under the "elastic" assumption, such collisions yield no contribution to the zeroth order, spherically symmetric equation.  $Q_1^h(v)$  is identified as the experimentally measured momentum transfer cross-section,  $Q_r^h$ , and represents the first non-zero contribution.

Now consider inelastic collisions, such as those resulting in vibrational or electronic excitation. In this case, one must properly account for the energy loss.

From equations (6-9) and (6-10) we obtain (refs 136, 138)

$$\left(\frac{\partial f}{\partial t}\right)^{-} = -N_h v Q_h(v) f(t, v) \quad (6-13)$$

$$\left(\frac{\partial f}{\partial t}\right)^{+} = N_h u Q_h(u) f(t, u) \frac{u^2 du}{v^2 dv} \quad (6-14)$$

where

$$Q_h(v) = 2\pi \int_0^{\pi} q_h(v, \alpha) \sin \alpha \, d\alpha$$

is the cross-section for the interaction in which an electron with speed  $v$  undergoes process  $h$  upon colliding with the molecules  $N_h$ , loses energy  $\Delta_h$ , and terminates the collision with speed  $u$  in equation (6-13) with  $\frac{1}{2} m v^2 = \frac{1}{2} m u^2 + \Delta_h$ . Equation (6-14) represents the positive rate which populates the element at velocity  $\vec{v}$ . Since energy is conserved in the collision process;

$$u \, du = v \, dv$$

and the volume ratio given by the Jacobian,  $u^2 du / (v^2 dv)$  reduces to  $u/v$ . Thus for inelastic isotropic scattering, the lowest order collision terms are (refs 136, 137, 138)

$$\left(\frac{\partial f_0}{\partial t}\right)_0^c = -N_h \left[ v Q_h(v) f_0'(t, v) - u Q_h(u) f_0'(t, u) \frac{u}{v} \right] \quad (6-15)$$

$$\left(\frac{\partial f_1}{\partial t}\right)_1^c = -N_h Q_h(v) v f_1'(t, v) \quad (6-16)$$

$$\left(\frac{\partial f_2}{\partial t}\right)_2^c = -\frac{3}{2} N_h v Q_h(v) f_2'(t, v) + \frac{1}{2} N_h(u) u Q_h(u) f_2'(t, u) \frac{u}{v} \quad (6-17)$$

To obtain a form more suitable for calculation, we transform the set of equations, (6-6), (6-7), (6-8), from functions of velocity to functions of energy,  $w$ , by using the following relations;

$$v = \left(\frac{2w}{m}\right)^{1/2}$$

$$dv = \frac{dw}{(2mw)^{1/2}}$$

We then obtain (refs 136, 137, 138),

$$\left(\frac{mw}{2}\right)^{1/2} \frac{\partial f_0(t, w)}{\partial t} + \left(\frac{-eE}{3}\right) \left[ w \frac{\partial f_1(t, w)}{\partial w} + f_1(t, w) \right]$$

$$= - \sum_h \left\{ N_h \left[ w Q_h(w) f_0'(t, w) - w' Q_h(w') f_0'(t, w') \right] \right\} \quad (6-18)$$

$$\left(\frac{mw}{2}\right)^{1/2} \frac{\partial f_1(t, w)}{\partial t} + \left(\frac{-eE}{3}\right) \left[ 5w \frac{\partial f_0(t, w)}{\partial w} + 2w \frac{\partial f_2(t, w)}{\partial w} + 3f_2(t, w) \right]$$

$$= -Nw f_1(t, w) \left\{ Q_h(w) + \sum_h \frac{N_h}{N} Q_h(w) \right\} \quad (6-19)$$

$$\begin{aligned} & \left(\frac{mW}{2}\right)^{\frac{1}{2}} \frac{df_2(t, W)}{dt} + \left(\frac{-eE}{g}\right) \left[ 2W \frac{df_1(t, W)}{dW} - f_1(t, W) \right] \\ &= -N W f_2(t, W) \left\{ Q_2(W) + \sum_h \frac{N_h}{N} \left[ \frac{3}{2} Q_h(W) + \frac{1}{2} \frac{W'}{W} Q_h(W') \right] \right\}^{(6-20)} \end{aligned}$$

where  $W' = W + \Delta_h$ , and  $\Delta_h$  is again the energy loss associated with the inelastic cross-section  $Q_h$ .

Equations (6-18, 6-19, 6-20) represent the general form of the coupled differential equations used for solving the collisional Boltzmann equation. We now restrict ourselves to a two term expansion, and include (refs 135, 136, 137, 138) the effects of energy transfer in momentum transfer collisions, and superelastic collisions. Assuming a quasi-steady-state we obtain from equations (6-18, 6-19)

$$\left(\frac{E/N}{3W}\right) \frac{d(W f_1(W))}{dW} + \sum_h \frac{Q_h(W)}{N} \left[ N_h f_0(W) - N_h' f(W - \Delta_h) \right] \quad (6-21)$$

$$= \frac{2}{W} \left(\frac{m}{M}\right) \frac{d}{dW} (W^2 Q_m f_0) + \sum_h \frac{Q_h(W) W'}{N W} \left[ N_h f_0(W) - N_h' f_0(W) \right]$$

$$\left(\frac{E/N}{\partial W}\right) \frac{\partial f_0(W)}{\partial W} = - \left( Q_r(W) + \sum_h \left\{ \frac{N_h}{N} Q_h(W) + \frac{N_h'}{N} \left(\frac{W'}{W}\right) Q_h(W') \right\} \right) f_1(W) \quad (6-22)$$

where  $H'_N$  is the relevant excited state density for process  $h$ .

$Q_m$  is the sum of the momentum-transfer cross-sections for each gas weighted by mole fraction and the reciprocal of

the molecular weight, whereas  $Q_r$  is the sum of the momentum-transfer cross-sections weighted simply by mole fraction. The ratio of the electron to proton mass is given by  $m/M$ . We may write equations (6-21, 6-22) as a single equation in  $f_0$  by integrating equation (6-21) with respect to energy, substituting into equation (6-22), and integrating again to yield (ref 139):

$$f_0'(w) = C \exp \left[ -\frac{3}{(E/N)^2} \left( \frac{2m}{M} \int_0^w Q_m Q_t dw \right. \right. \\ \left. \left. + \sum_h \int_0^w \frac{Q_t}{w f_0} \int_0^{w'} \left\{ \frac{Q_h(u)u}{N} (N_h f_0(u) - N_h' f_0(u - \Delta_h)) \right\} du \right) dw \right] \quad (6-23)$$

where  $C$  is determined by the condition  $\int_0^\infty f_0(w) w^{1/2} dw = 1$

and  $Q_t = Q_r + \sum_h \left( \frac{N_h}{N} Q_h(w) + \frac{N_h' w'}{N w} Q_h(w') \right)$ . This integral form of the Boltzmann equation (ref 139) can be solved by iteration for  $f_0(w)$ , substitution into equation (6-22) yields  $f_1(w)$ .

Electron Collision Processes. Having developed the Boltzmann formalism, we recognize that the solution requires cross-section data for momentum transfer, vibrational and electronic excitation of the gases constituting the specific mixture under consideration. In this analysis we will be concerned with mixtures of carbon monoxide and argon.

Most of the required data are available from a JILA compilation by Kieffer (ref 134). These experimental data have been obtained using high energy resolution electron beam techniques coupled with a detailed analysis (ref 141) of electron transport data. The resulting data set is quite reliable and relatively complete, providing an adequate basis to quantify our results.

The momentum transfer cross-sections for argon and carbon monoxide were obtained from Kieffer (ref 134). Momentum transfer collisions tend to reduce the anisotropy in the eed resulting from the applied field and channel some of the discharge power into "elastic heating" of the gas.

Vibrational excitation is the dominant excitation process for the conditions considered in this study because the cross-sections are very large at the mean energies characteristic of laser discharges. Vibrational cross-sections and excitation rates are required for an analysis of the molecular kinetics. In carbon monoxide, vibrational excitation proceeds predominately via "shape resonances." The cross-section characterizing this excitation displays a structure related to the lifetime of the compound state,  $AB^-$ ; and the characteristic vibrational frequency. When the lifetime is short, as it is in  $H_2$ , the cross-section exhibits a broad maximum. In  $CO$ , the lifetime of the compound temporary negative ion is comparable to the vibrational period and the cross-section exhibits broadened

spikes corresponding to the energy resonances of the compound state. Erhardt (ref 142) and Schulz (ref 143) have reported electron cross-section data,  $\sigma_{0,v}$ , for vibrational excitation from the ground state,  $v=0$ , to vibrational level  $v$  for  $v=1$  to 8. This data is presented in Figs. 6-2 and 6-3. Referring to Fig. 6-2, note that near threshold the effective cross-section\* has a value of approximately  $2 \times 10^{-17} \text{ cm}^2$  which rapidly increases to a value approaching  $10^{-15} \text{ cm}^2$  at 1.7ev before decreasing by orders of magnitude in the 4ev range. Fig. 6-3 presents the individual cross-section data,  $\sigma_{0,v}$ , of Schulz for excitation from the ground state to vibrational state  $v$ . The cross-sections all exhibit the resonant spikes, and decrease in magnitude with increasing  $v$ . The magnitude and energy dependence of these cross-sections will be reflected in the calculated distribution functions, and fractional power transfer, which will be examined later.

Since we anticipate highly non-equilibrium vibrational distributions exhibiting a substantial excited state population, we have not restricted the electron-molecule vibrational excitation to excitation only from the ground vibrational state. Instead, we assume  $\sigma_{0,m} = \sigma_{v,v+m}$  for  $m=1$  to 8. Electron excitation cross-sections from excited states are not available; however, guided by the theoretical

---

\*The effective cross-section is defined as the summation of all vibrational cross-sections from the ground vibrational state.

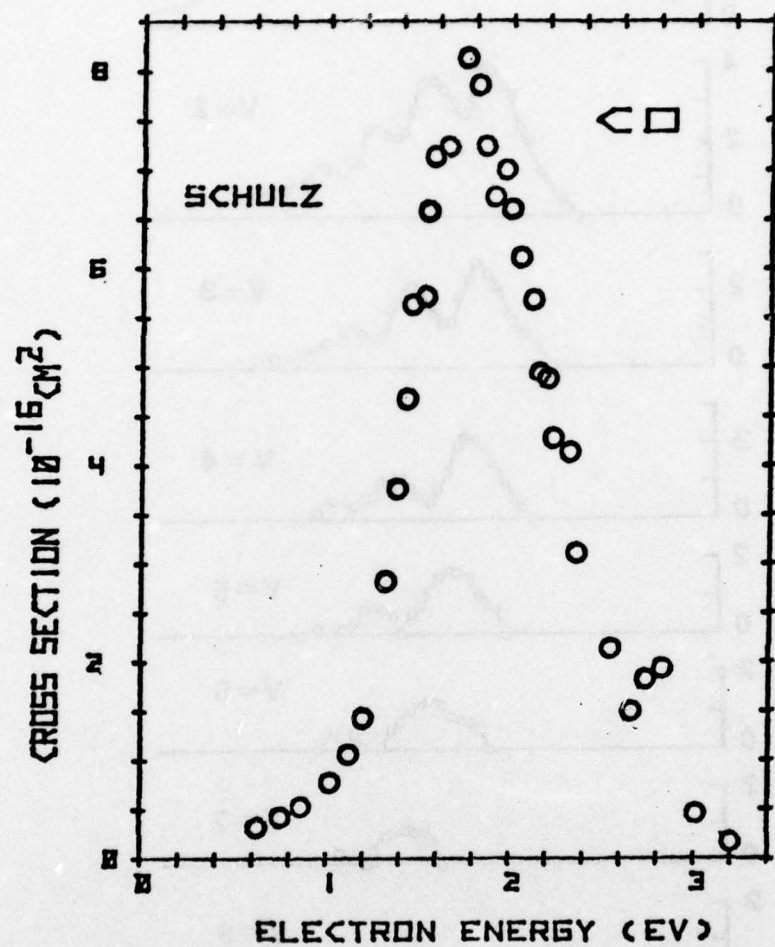


Fig 6-2 Effective Vibrational Cross Section

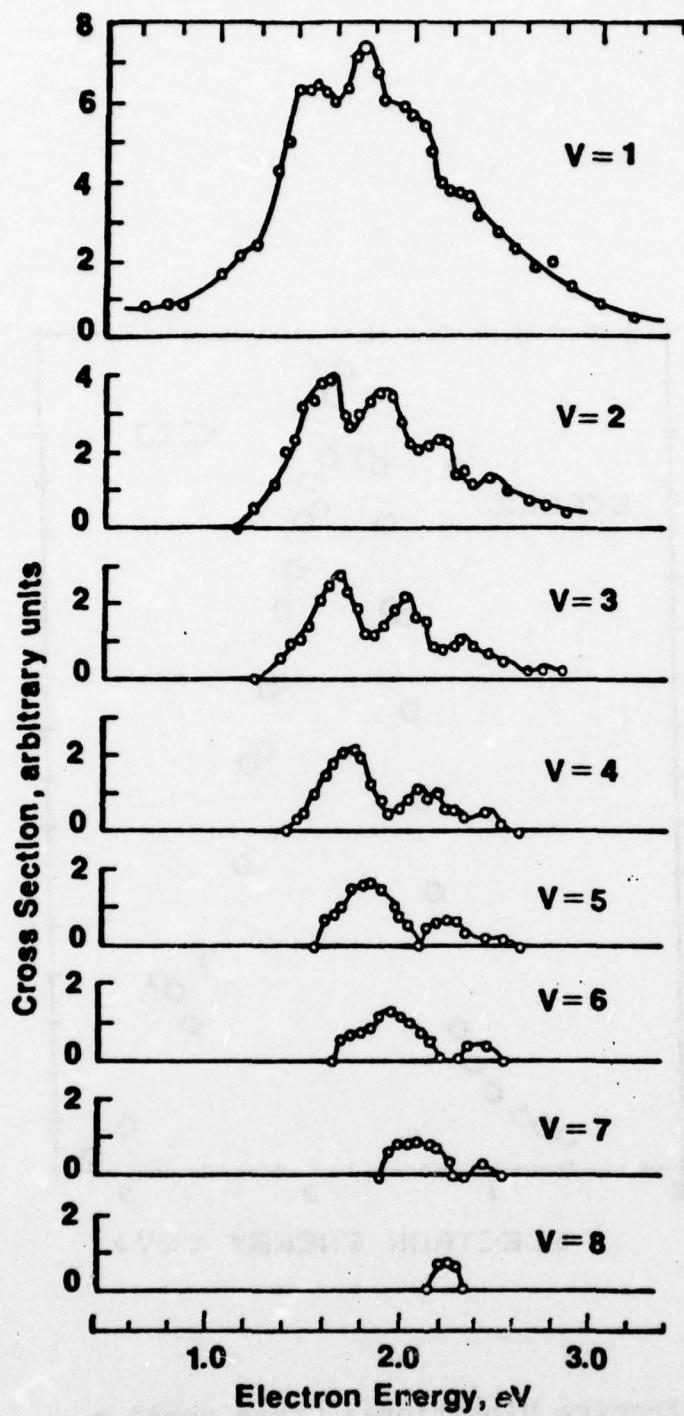


Fig 6-3 CO Vibrational Cross Sections  
(Schulz, ref 143)

calculations of Chen (ref 144) in  $N_2$  and based on the isoelectronic relationship of  $N_2$  to CO, this assumption is reasonable. Detailed calculations of these excited state cross-sections (ref 145) and experimental measurements (refs 146, 147) are the topic of current research.

Electronic excitation cross-sections for the excitation of  $a^3\Pi$ ,  $A^1\Pi$ ,  $b^3\Sigma$ ,  $C^1\Sigma$ ,  $E^1\Pi$ , and a 13.5 ev. loss (ref 148) were included, as well as the dissociative attachment, ionization and dissociative ionization cross-sections. Under conditions typical of self-sustained or e-beam sustained operation, only a small fraction of the energy is channeled into these electronic states. However, it is necessary to include these states in order to properly evaluate the rate of dissociation due to electron impact. Consistent with our reasoning concerning the highly non-equilibrium distribution of vibrational states, we have investigated the implication of assuming that the dissociative ionization, DI, cross-section from excited vibrational states is equal to that from the ground state with the threshold displaced by the vibrational energy relative to  $v=0$ . We will expand on this point later when we discuss and compare dissociation rates. The dissociative ionization cross-section measured by Rapp (ref 149) is given in Fig. 6-4. A threshold energy of 16.5 ev should be noted as well as the small magnitude in comparison with the vibrational cross-sections given previously. In addition to dissociative ionization, dissociative attachment, DA, occurs

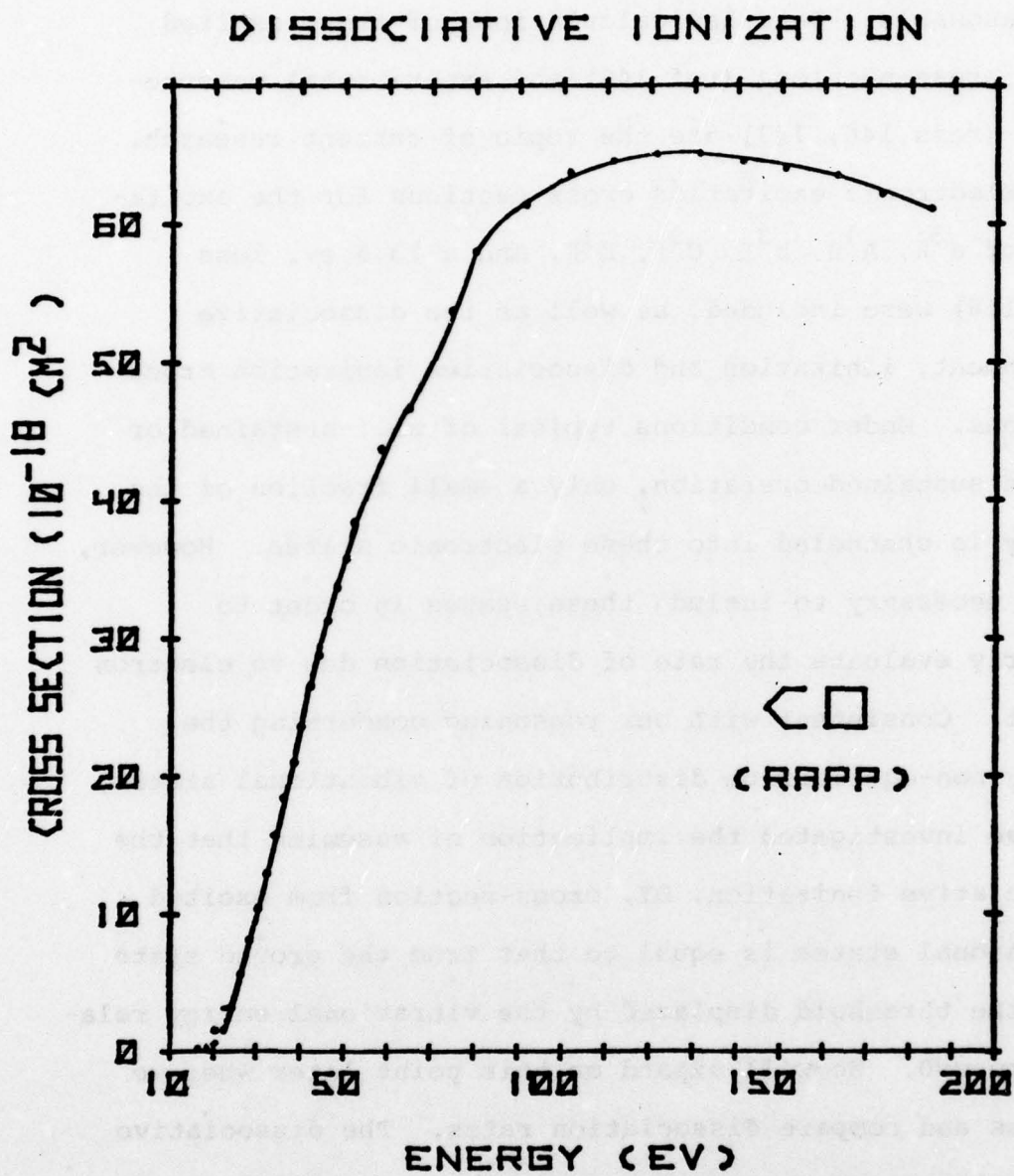


Fig 6-4 CO Dissociative Ionization Cross Section

and will be included in this analysis. Fig. 6-5 displays the cross-section for the dissociative attachment process as measured by Chantry (ref 150). This cross-section, in contrast to that of dissociative ionization, is resonant in character exhibiting a pronounced maximum of  $2 \times 10^{-19} \text{ cm}^2$  at 10ev. Also note that the threshold for this excitation is approximately 7 ev. below that of dissociative ionization. This fact coupled with the relative magnitudes of the two cross-sections results in dissociative attachment being the dominant electron impact dissociation process.

Calculated Electron Energy Distributions. Using the cross-section data and the integral form of the Boltzmann equation previously described, the electron energy distribution was calculated for a 10/90 mix of CO/Argon, (mole fraction), for a wide range of values of the ratio of the electric field strength to the total neutral gas number density,  $E/N$ . The selected values of  $E/N$  yield mean electron energies in the range of .5-3.0ev. These mean energies are typically encountered in self-sustained and e-beam sustained discharges. Fig. 6-6 is a semi-log plot of the calculated energy distribution, with the distribution density at energy  $w$  given by  $f_0(w)w^{1/2}dw$ . In this representation, a Maxwellian distribution would appear as straight line with a negative slope of  $(1/kT_e)$ , with  $T_e$  being the "electron temperature." The calculated distributions depart significantly from a Maxwellian. The

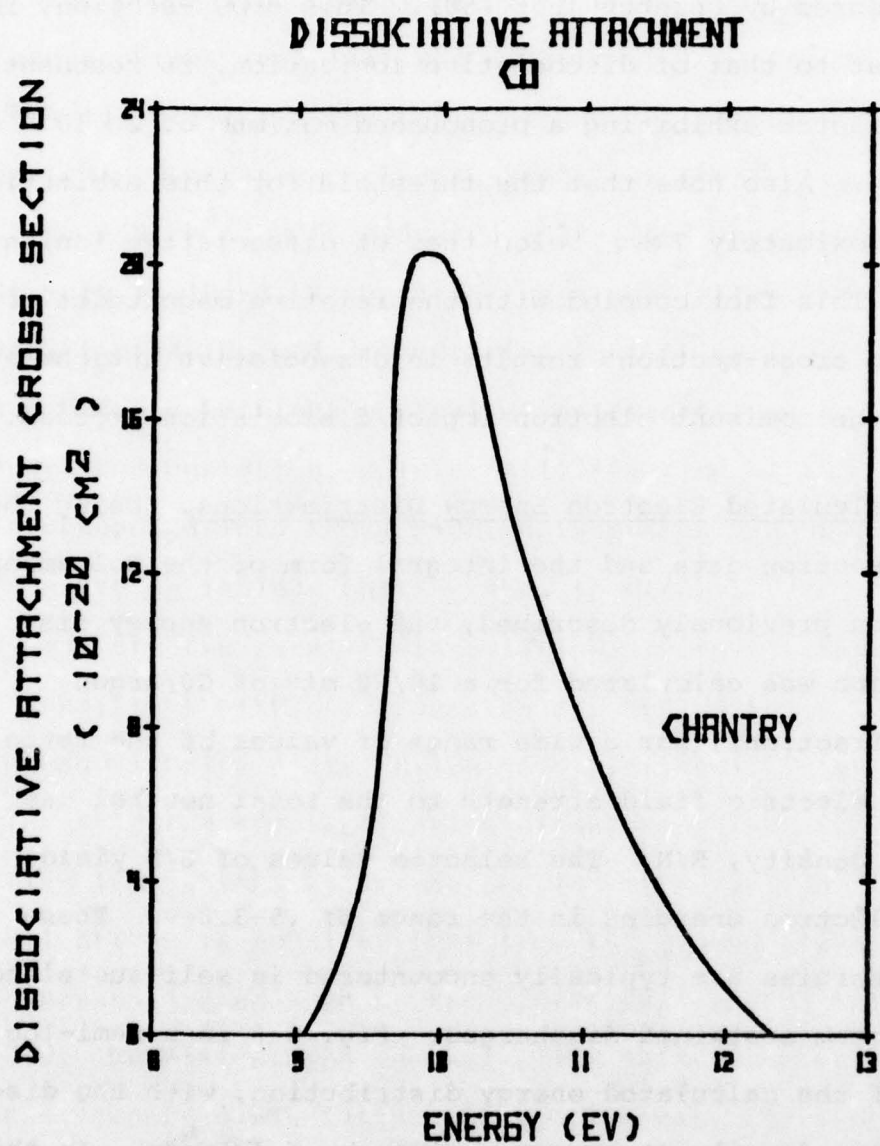


Fig 6-5 CO Dissociative Attachment Cross Section

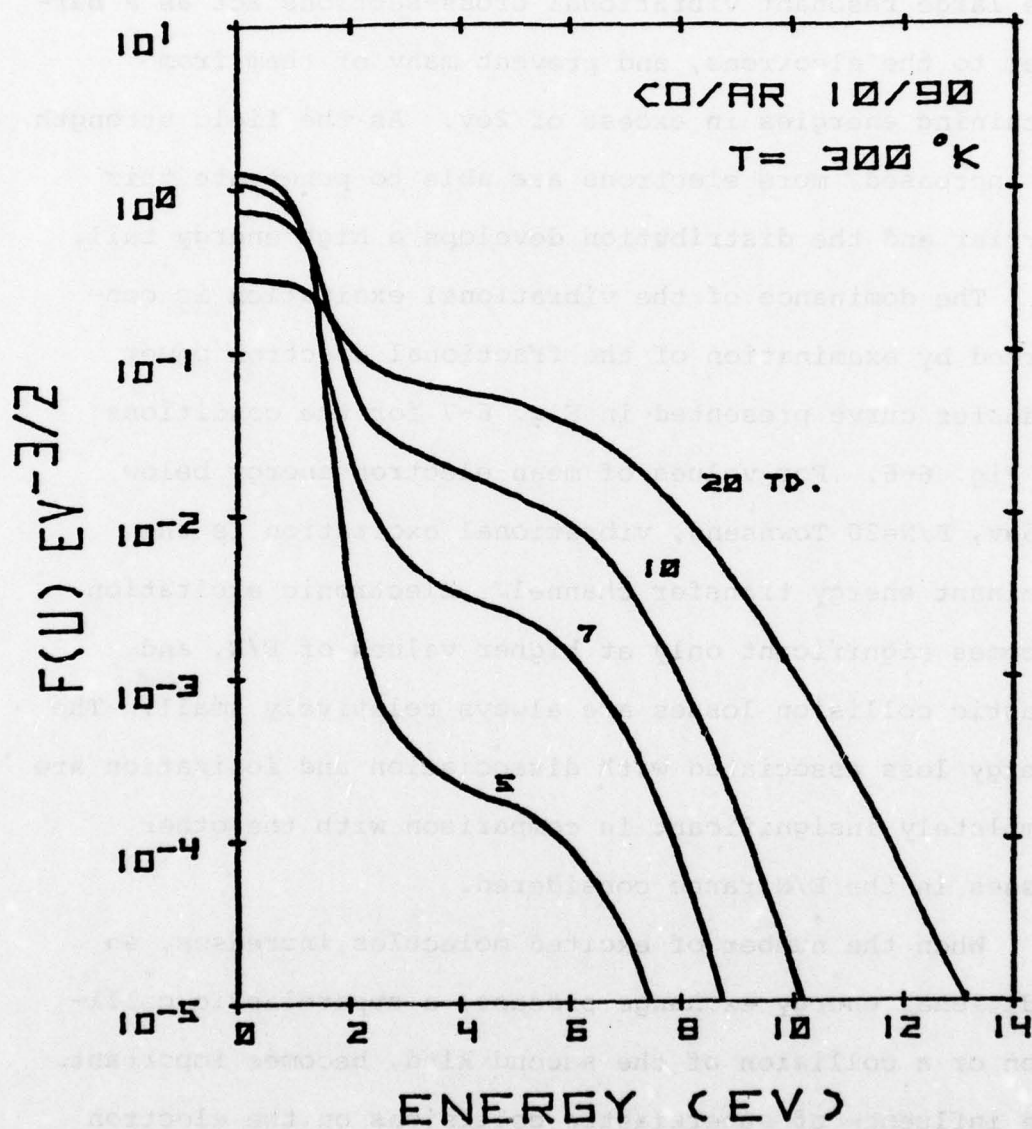


Fig 6-6 Electron Energy Distributions, eed's

distributions reflect the dominant electron-molecule collision processes, by exhibiting a rapid decrease in the energy region, 1-2ev, of significant vibrational excitation. The large resonant vibrational cross-sections act as a barrier to the electrons, and prevent many of them from obtaining energies in excess of 2ev. As the field strength is increased, more electrons are able to penetrate this barrier and the distribution develops a high energy tail.

The dominance of the vibrational excitation is confirmed by examination of the fractional electron power transfer curve presented in Fig. 6-7 for the conditions of Fig. 6-6. For values of mean electron energy below 1.5ev,  $E/N=20$  Townsend, vibrational excitation is the dominant energy transfer channel. Electronic excitation becomes significant only at higher values of  $E/N$ , and elastic collision losses are always relatively small. The energy loss associated with dissociation and ionization are completely insignificant in comparison with the other losses in the  $E/N$  range considered.

When the number of excited molecules increases, an additional energy exchange process, a superelastic collision or a collision of the second kind, becomes important. The influence of superelastic collisions on the electron energy distribution can be understood by referring to equation (6-23). The bracketed term in the summation is proportional to net inelastic excitation rate. Consider the vibrational excitation of the first vibrational level

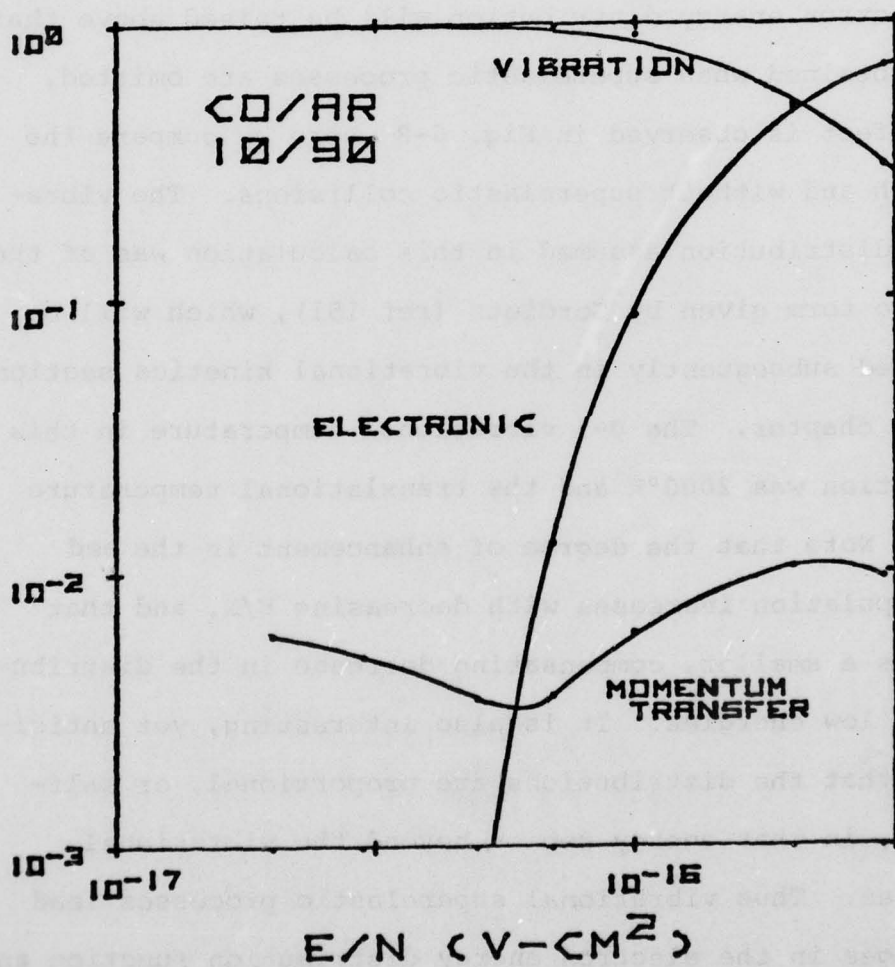


Fig 6-7 Fractional Electron Power Transferred

from the ground state and the reverse process. In this case  $N_h$  represents the number density in the state  $v=0$ , and  $N_h'$ , the number density in  $v=1$ . A significant excited state population will decrease the value of the integrand, reduce the net excitation rate, and result in a lowering of the effective vibrational barrier. As a result, the tail of the electron energy distribution will be raised above that value obtained when superelastic processes are omitted. This effect is observed in Fig. 6-8 where we compare the eed with and without superelastic collisions. The vibrational distribution assumed in this calculation was of the analytic form given by Gordiets (ref 151), which will be discussed subsequently in the vibrational kinetics section of this chapter. The 0-1 vibrational temperature in this calculation was 2000°K and the translational temperature 300°K. Note that the degree of enhancement in the eed tail population increases with decreasing  $E/N$ , and that there is a smaller, compensating decrease in the distribution at low energies. It is also interesting, yet anticipated, that the distributions are proportional, or self-similar, in that energy region beyond the vibrational exchanges. Thus vibrational superelastic processes lead to changes in the electron energy distribution function and enhance electronic excitation and dissociation rates.

Summary. We have examined the electron kinetics of a CO-Ar gas discharge within the framework of the collisional

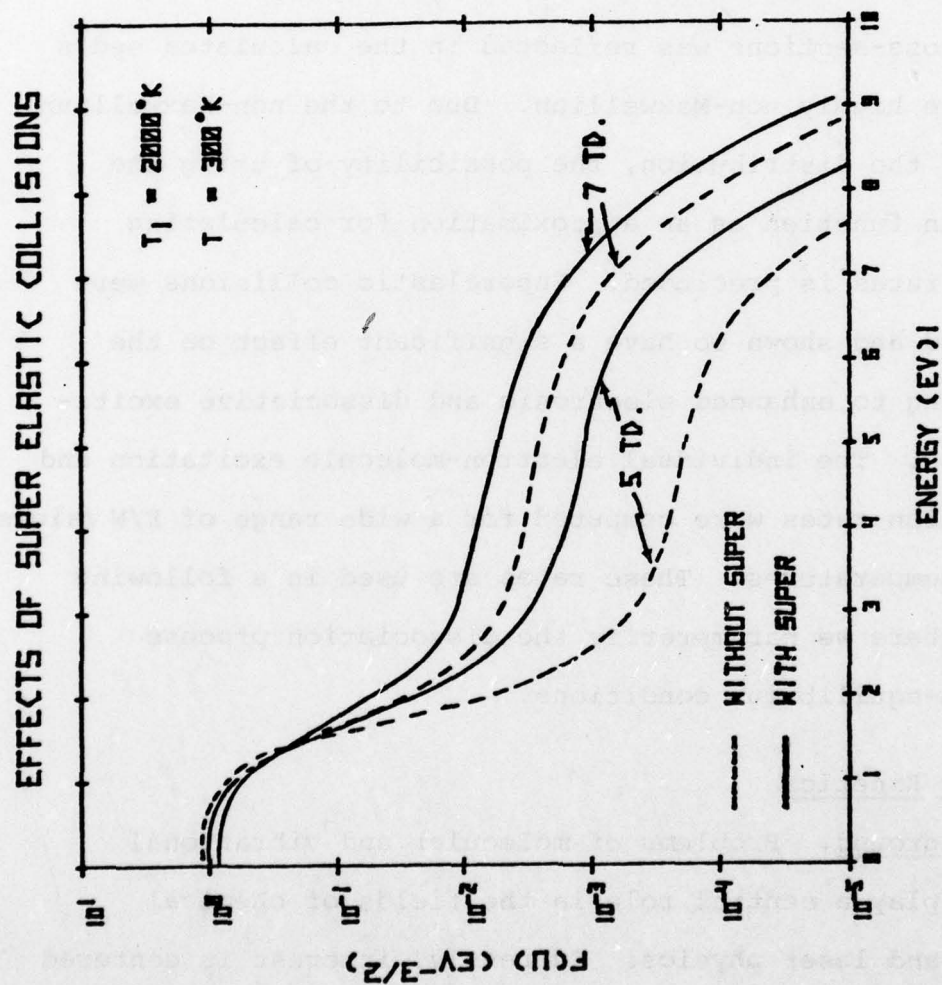


Fig 6-8 Influence of Superelastic Collisions on the eed

Boltzmann equation. For this purpose we developed the integral form of the Boltzmann equation, specifically including superelastic collisions. It was established that the electron kinetics are dominated by the large resonant vibrational cross-sections, which permit efficient molecular excitation to be achieved. The dominance of the vibrational cross-sections was reflected in the calculated eed's which were highly non-Maxwellian. Due to the non-Maxwellian nature of the distribution, the possibility of using the Maxwellian function as an approximation for calculating transfer rates is precluded. Superelastic collisions were considered and shown to have a significant effect on the eed leading to enhanced electronic and dissociative excitation rates. The individual electron-molecule excitation and dissociation rates were computed for a wide range of  $E/N$  values and gas temperatures. These rates are used in a following section where we parameterize the dissociation process under non-equilibrium conditions.

### Molecular Kinetics

Background. Problems of molecular and vibrational kinetics play a central role in the fields of chemical kinetics and laser physics. Currently, interest is centered around an analysis of energy exchange processes occurring when significant amounts of energy are introduced into a gas. All interactions be they thermal, chemical, optical, or electrical result in a redistribution of state

populations. The ultimate distribution then determines the nature of chemical and physical processes occurring in the resulting non-equilibrium state. Here we will be primarily concerned with the investigation of the non-equilibrium vibrational distributions of a molecular gas excited by an electric discharge or obtained through intense optical pumping of the vibrational states. For the moment, we will conveniently assume the existence of some "pump" term delivering energy to the vibrational manifold and proceed to characterize the molecular kinetics and the vibrational distribution. Within this section we first review the fundamental kinetic processes involved, their relative strengths and characteristic time scales. Based on a time scale argument and guided by the results of detailed numerical calculations, we will establish that there are 3 characteristic regions of the vibrational energy distribution, VED. A simplified, analytic approach to the calculation of vibrational distributions (refs 151, 152) under highly non-equilibrium conditions will then be reviewed. The dependence of the VED on input energy, V-V and V-T rate magnitude, or translational temperature will be examined using this approach. Finally, for completeness and for the additional insight they reveal, selected detailed numerical solutions of the VED, both time dependent and steady-state, will be presented. These distributions will be compared with experiment to establish the degrees of non-equilibrium that can be achieved and lead

us into our parameterization of non-equilibrium dissociation.

Characteristic Regions of the VED. Let us examine the factors that determine the populations,  $N_v$ , of the vibrational energy levels. In general these factors can be classified as follows.

1. Net rate of external excitation or de-excitation for each level (pumping),  $\dot{N}_{v_{\text{pump}}}$
2. Rates of collisional V-V energy transfer,  $\dot{N}_{v_{V-V}}$
3. Rates of collisional V-T energy transfer,  $\dot{N}_{v_{V-T}}$

We will omit consideration of radiative processes as loss mechanisms, while recognizing the limitation they impose when considering optical pumping. This is appropriate for the high pressures considered in this study. The rate equation for each vibrational level  $v$ , from equation (3-5), can now be written in the simple form:

$$\frac{dN_v}{dt} = \dot{N}_{v_{\text{pump}}} + \dot{N}_{v_{V-V}} + \dot{N}_{v_{V-T}} \quad (6-24)$$

By examining the relative strengths and time scales of the three terms in equation (6-10), we will establish that, for highly non-equilibrium conditions, the VED exhibits 3 characteristic regions.

The mechanism for vibrational excitation in electric discharge systems is electron impact collisions, which proceed via the formation of temporary compound excited states. As noted in the previous section, the rate of excitation depends not only on the eed, but also on the population of the levels. The pump term, when considering optical excitation, is also a function of the level population of the pump transition as well as the intensity of the radiation.

Subjecting a diatomic gas, initially at a temperature  $T$ , to external excitations, results in a departure of the vibrational distribution from its initial Boltzmann distribution given by:

$$N_{v_{EQ}} = N_0 \exp(-\beta[E_v - E_0]) \quad (6-25)$$

The resulting non-equilibrium distribution and the relaxation process will be governed by the Master Equation, and depend upon the various energy exchange rates, the molecular structure, and the strength of external excitation. We are interested in the quasi-equilibrium distribution of  $N_v$  under conditions of intense pumping.

Representative probabilities of the various exchange processes, given in Fig. 6-9, show that V-V collisions dominate the relaxation process for low vibrational quantum numbers. The V-V exchanges, which involve collisions between excited molecules and are a near resonant

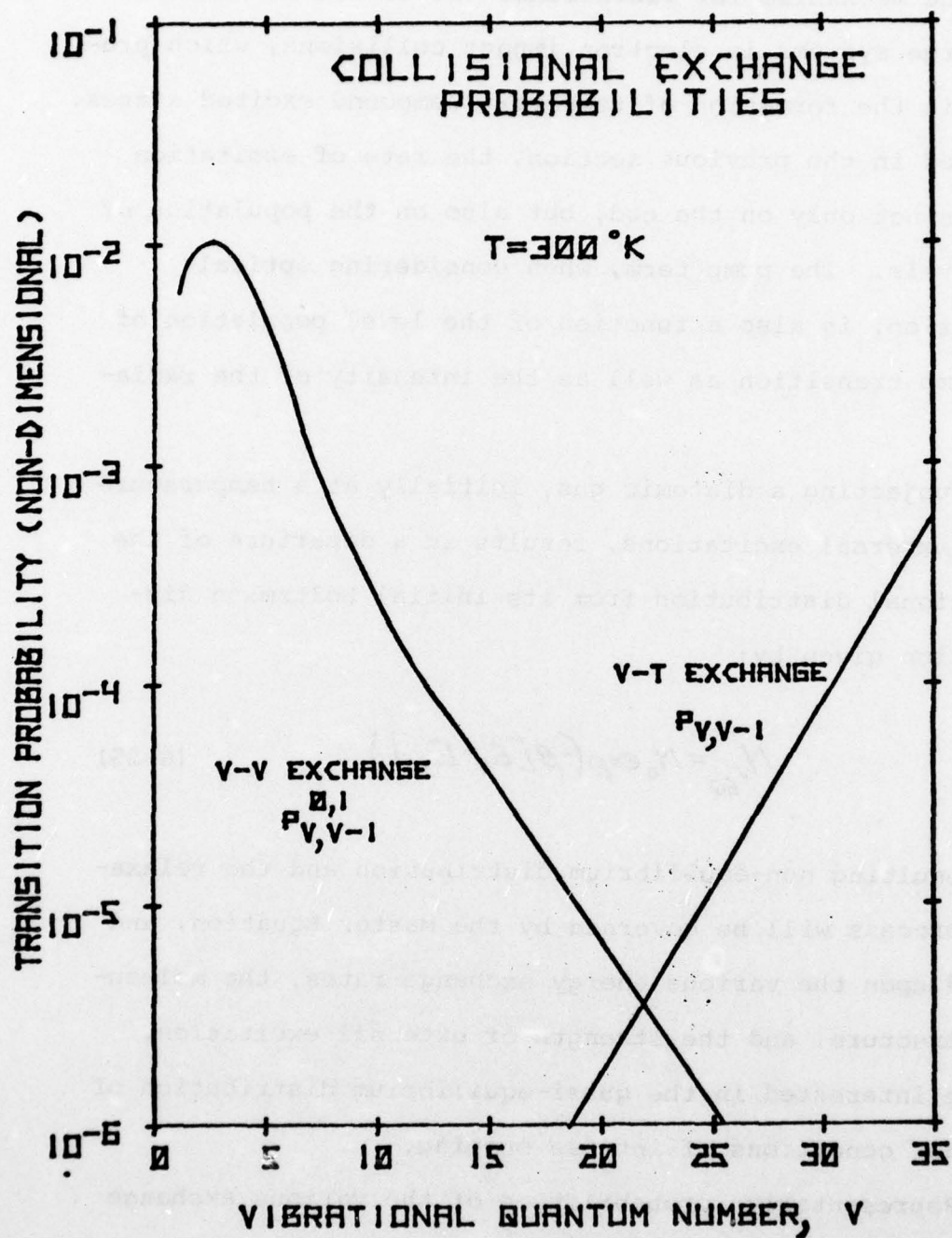


Fig 6-9 Representative Exchange Probabilities

process, result in a rapid redistribution of the externally pumped vibrational quanta prior to their ultimate deactivation by the slower V-T process. Guided by the data in Fig. 6-9 at 300°K, let us assume that, for sufficiently low vibrational quantum number, we can neglect VT exchange and assume rotational-translational equilibrium at temperature, T. Under these conditions, the vibrational distribution is given by the Treanor distribution (ref 153),

$$\begin{aligned} N_v &= N_0 \exp \{ \phi_v - \beta(E_v - E_0) \} \\ &= N_{v, \text{Eq}}(T) \exp(\phi_v) \end{aligned} \quad (6-26)$$

In order to gain insight as to the meaning of  $\phi$ , we define the population of the v-th level by the relation:

$$N_v = N_0 \exp \left( - \frac{[E_v - E_0]}{k T_v} \right)$$

For a Boltzmann distribution,

$$T_v = \text{constant} \quad v = 0, 1, \dots, v^* \quad (6-27)$$

Using this definition, we can rewrite  $\phi$  in terms of  $T_1$ , the effective 1-0 temperature,

$$\phi = \frac{(E_i - E_0)}{k T} - \frac{(E_i - E_0)}{k T_1} \quad (6-28)$$

The Treanor distribution becomes upon substitution for  $\phi$ ,

$$N_v = N_0 \exp \left\{ -\frac{v(E_i - E_0)}{k T_1} + \frac{v(E_i - E_0) - (E_v - E_0)}{k T} \right\} \quad (6-29)$$

Thus we can interpret  $\phi$  as representing the influence of an external pumping of the  $0 \rightarrow 1$  transition, resulting in the vibrational temperature  $T_1$ .

For a simple harmonic oscillator,  $E_v - E_0 = v(E_1 - E_0)$ , and consequently the Treanor distribution degenerates into a simple Boltzmann characterized by a temperature  $T_1$ . For an anharmonic oscillator, however,  $v(E_1 - E_0) > (E_v - E_0)$ . For  $T_1/T > 1$ , the second term of the exponential in equation (6-29), now leads to a distribution with an increased population relative to the Boltzmann at  $T_1$ . The dependence of the Treanor distribution on  $T$  and  $T_1$  is presented in Figs. 6-10 and 6-11. The distributions pass through a minimum and exhibit a population inversion for values of  $T_1/T > 1$ . Such significant inversions are not obtained when the Master Equation is solved in detail with V-T losses being included. The V-T losses prevent these large total inversions. Instead, the dominance of these V-T processes in the high vibrational levels results in the establishment of a Boltzmann "tail," at a temperature  $T$ , for the population of high vibrational levels. This behavior can be confirmed by noting in Equation (3-13) that if V-T terms were completely dominant the entire distribution would be

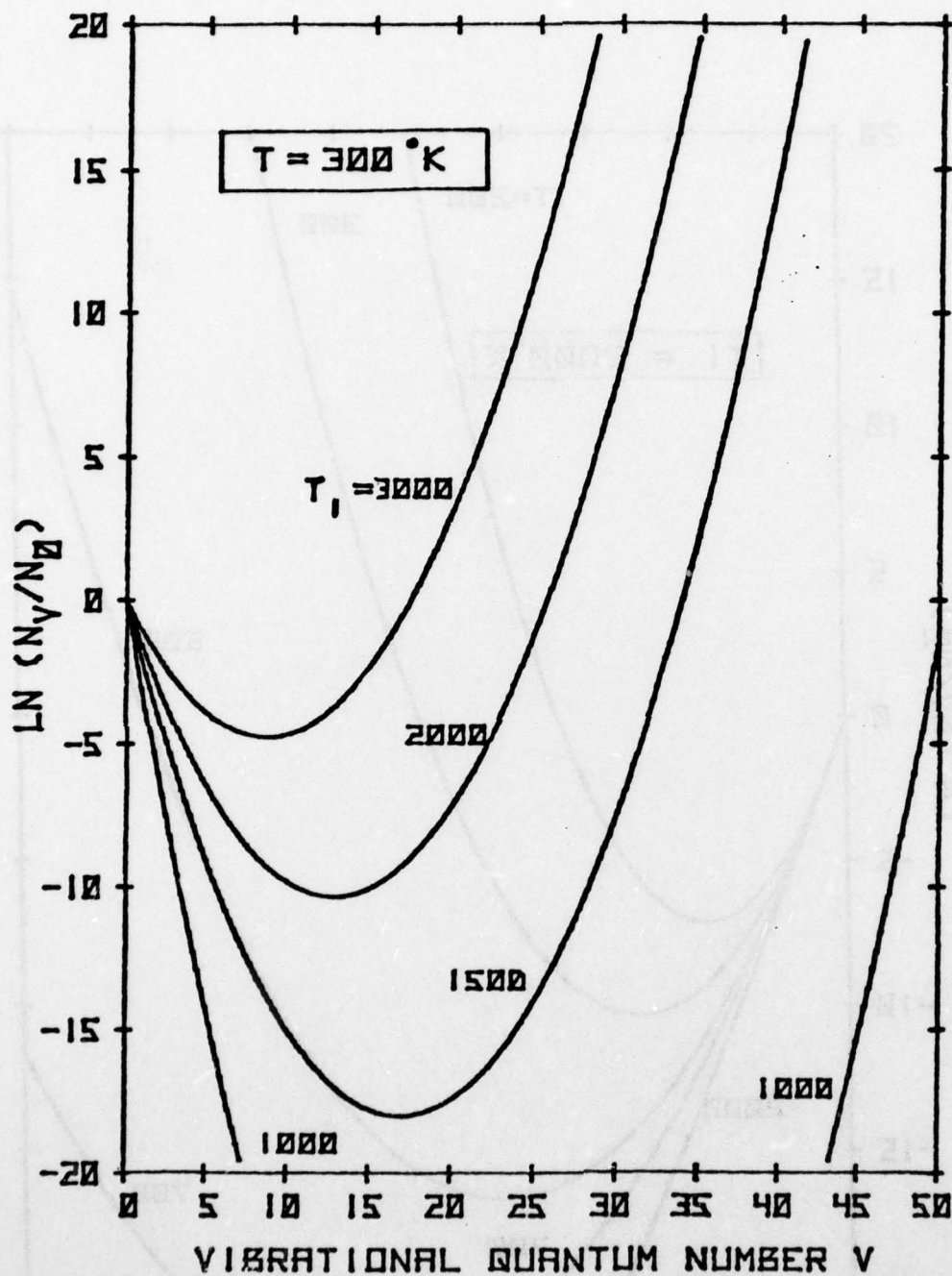


Fig 6-10 Treanor Distribution Parameterized in  $T_1$

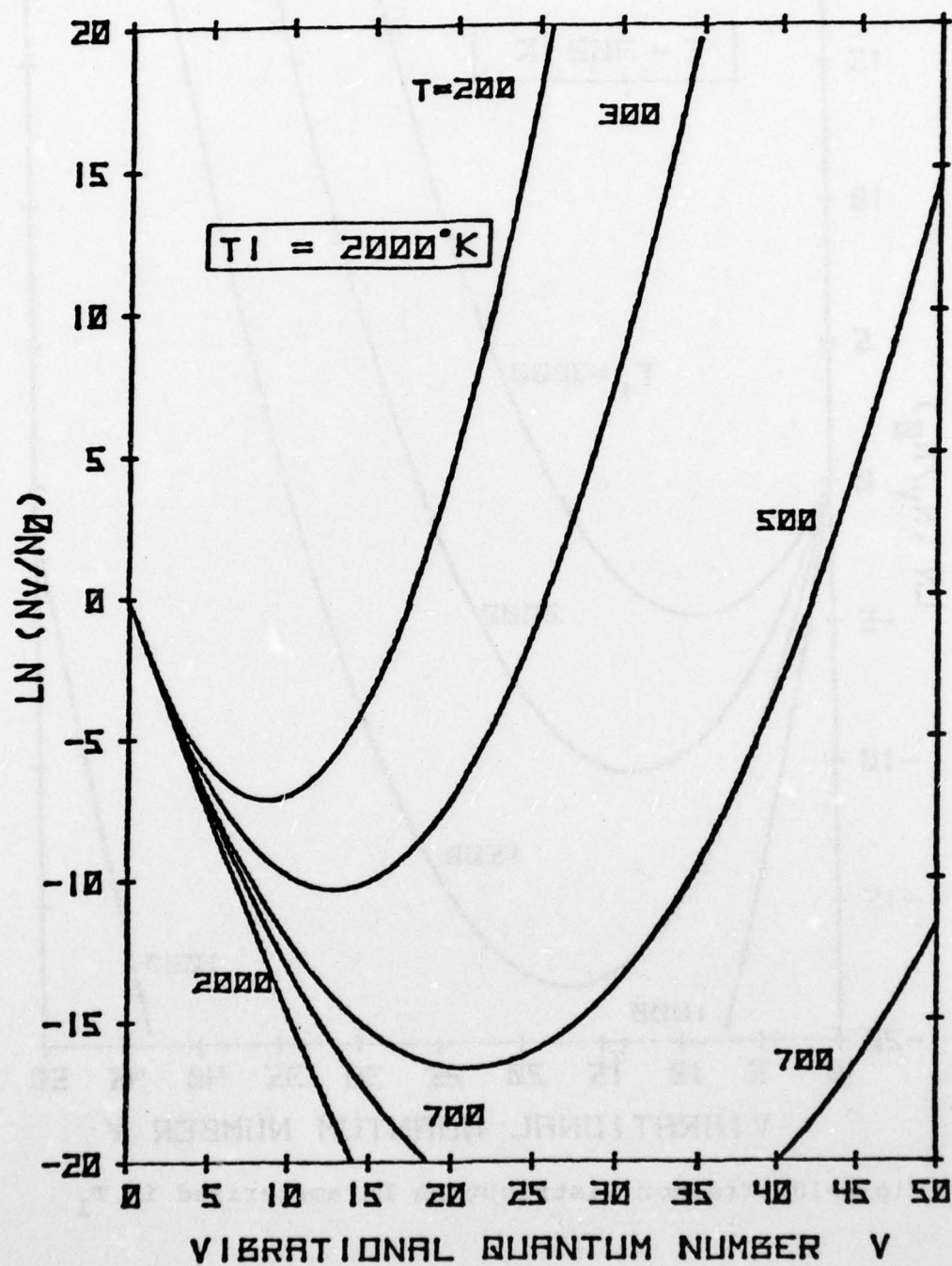


Fig 6-11 Treanor Distribution Parameterized in  $T$

described by a Boltzmann distribution at the gas temperature.

Numerical solutions of the complete Master Equation are presented in Figs. 6-12 and 6-13, where effective pumping rates,  $T_1$ , are shown. Three regions of the vibrational distribution can be identified. At low vibrational levels, where the V-T probabilities are insignificant relative to the V-V probabilities, the distribution is Treanor. Beyond the minimum of the Treanor distribution, the "resonance" or "plateau" region is established. In this region the distribution is well approximated by  $N_v = \text{constant}$ . The third region, existing at high vibrational quantum numbers, is a Boltzmann at the gas temperature, reflecting the dominance of the V-T process. The existence of the Treanor and the Boltzmann regions is consistent with our earlier discussion. We next discuss the "resonance" or "plateau" region.

The vibrational quanta, being pumped into the gas predominantly at low vibrational levels, are deactivated by local V-T collisions when the pumping is weak. However, when strong pumping is imposed, the local V-T deactivations are insufficient to balance the source and the distribution reacts to establish a quanta flow balance. This balance is achieved through the action of the rapid V-V exchanges, which due to the anharmonic nature of the energy levels, preferentially direct the excess quanta to the higher vibrational levels where they can be de-activated by the

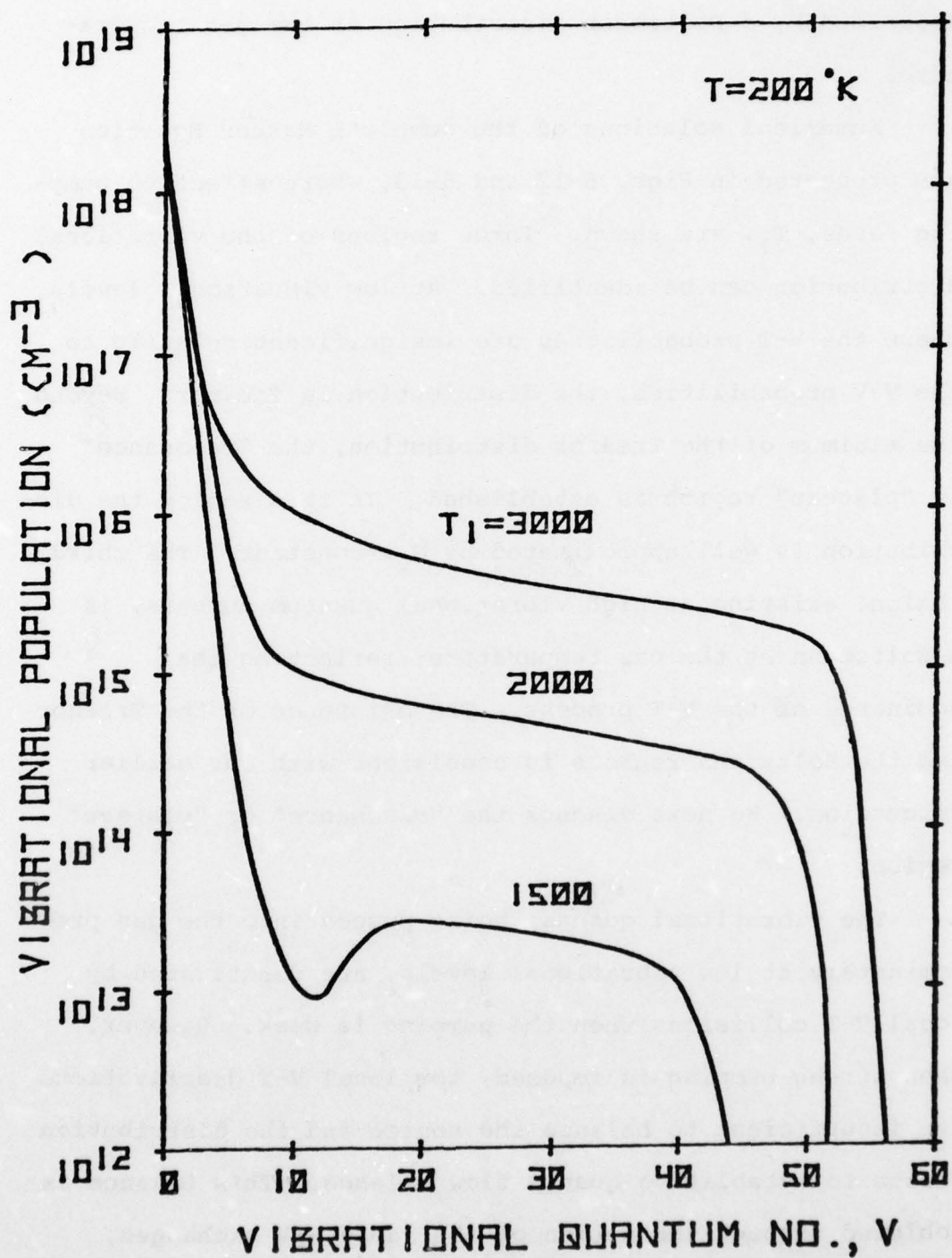


Fig 6-12 Numerical Solutions of VED Parameterized in  $T_1$

AD-A063 876

AIR FORCE AERO PROPULSION LAB WRIGHT-PATTERSON AFB OHIO  
COLLISION INDUCED DISSOCIATION OF DIATOMIC MOLECULES.(U)

F/G 7/4

UNCLASSIFIED

NOV 78 W F BAILEY  
AFAPL-TR-78-105

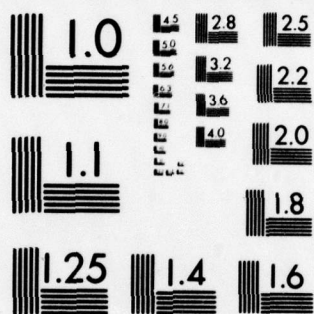
NL

3 of 3

AD  
A063 876



END  
DATE  
FILMED  
3-79  
DDC



MICROCOPY RESOLUTION TEST CHART  
NATIONAL BUREAU OF STANDARDS-1963-A

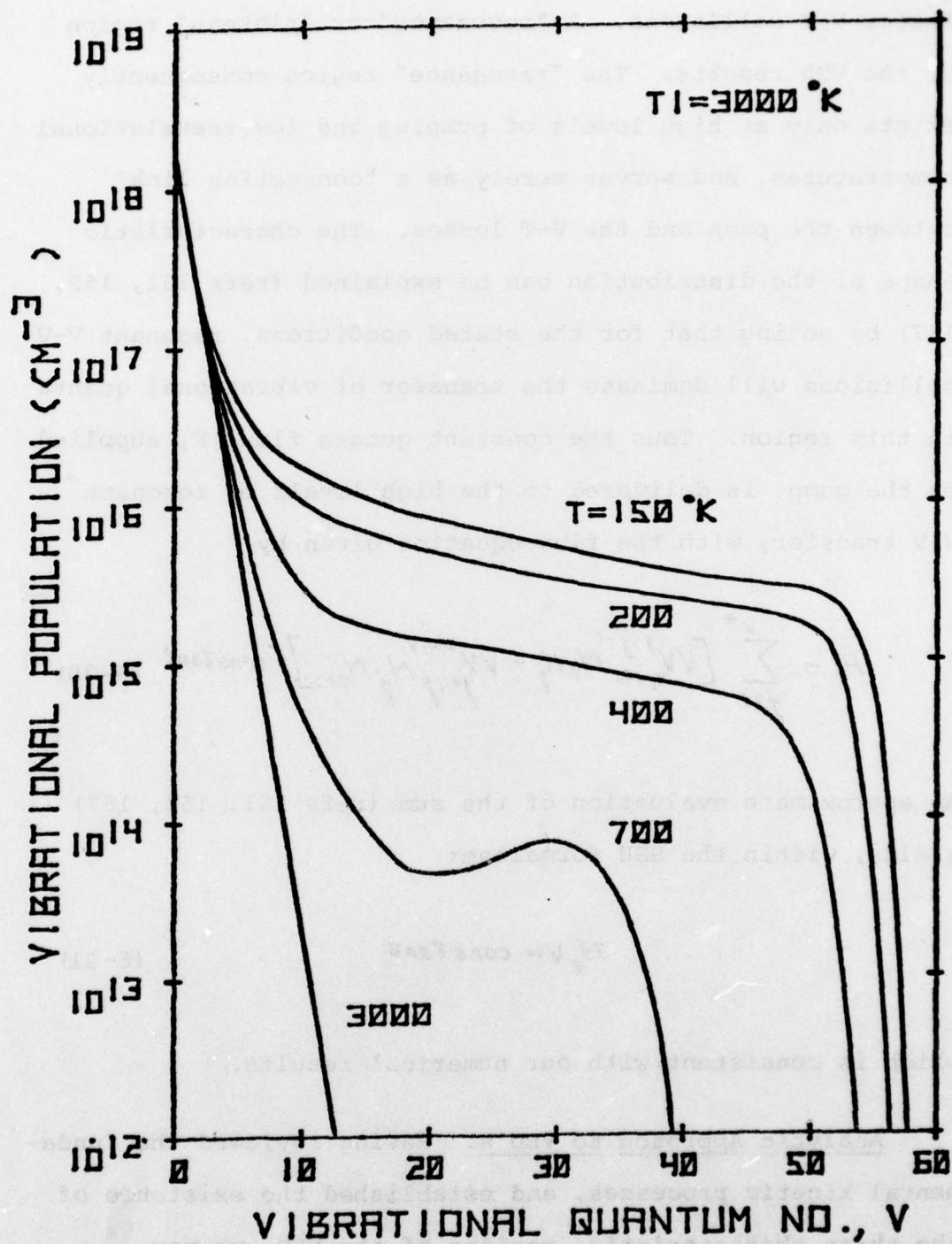


Fig 6-13 Numerical Solutions of VED Parameterized in T

faster V-T collisions. A "resonance" or "plateau" region of the VED results. The "resonance" region consequently exists only at high levels of pumping and low translational temperatures, and serves merely as a "connecting link" between the pump and the V-T losses. The characteristic shape of the distribution can be explained (refs 151, 152, 157) by noting that for the stated conditions, resonant V-V collisions will dominate the transfer of vibrational quanta in this region. Thus the constant quanta flux,  $F$ , supplied by the pump, is delivered to the high levels by resonant V-V transfer, with the flux equation given by

$$F_V = \sum_{j=1}^{V^*} [V V_{V, V+1}^{j, j-1} N_V N_j - V V_{j+1, j}^{V+1, V} N_j N_{V+1}] = \text{constant} \quad (6-30)$$

An approximate evaluation of the sum (refs 151, 152, 157) yields, within the SSH formalism:

$$N_V V = \text{constant} \quad (6-31)$$

which is consistent with our numerical results.

Analytic Approach to VED's. Having reviewed the fundamental kinetic processes, and established the existence of the three characteristic regions of the VED, we now highlight the development of an analytic expression for the vibrational distribution under strongly-pumped

conditions. The details of this development are given in a series of papers by Gordiets (refs 151, 154, 155). An independent and more general approach by Lam (ref 152) yields a similar form. Here we follow Gordiets (ref 151), and start out with the Master Equation for the vibrational populations, equation (3-5); with the notation given by

$$VV_{v+1,v}^{m,m+1} = (v+1)(m+1) \left[ Q_{10} e^{-\delta_{vv}/|v-m|} \left( \frac{a}{2} - \frac{1}{2} e^{-\delta_{vv}/|v-m|} \right) + Q_{10}^L e^{-\Delta_{vv}(m-v)^2} \right]$$

$$VT_{v+1,v} = P_{10} (v+1) e^{\delta_{vv} v}$$
(6-32)

$$E_v = \epsilon_0 v (1 - \delta(v+1))$$

$$\Delta E = \delta \epsilon_0$$

Gordiets used the diffusion approximation to obtain an analytic form for the populations of the vibrational levels. Omitting here the intermediate calculations, we reproduce his final result for  $N_v$ :

$$N_v = N_0 \exp \left\{ -v \left[ \frac{E_1}{T_1} - \frac{(v-1)\Delta E}{T} \right] \right\} \quad v < \underline{v}$$
(6-33a)

$$N_v = \frac{C}{v+1} - \frac{P_{10} e^{\delta_{vv} v}}{Q_{10} K \delta_{vv} (v+1)} \quad \underline{v} \leq v \leq \bar{v}$$
(6-33b)

with the following additional notation introduced

$$C = (Y+1) N_0 \exp \left\{ -Y^2 \frac{\Delta E}{T} - \frac{1}{2} \right\} + \frac{P_{10}}{Q_{10} K} \exp(\delta_{VT} Y) \quad (6-34)$$

$$K = \left[ 1 + \frac{\delta_{VV}^3}{12 \Delta_{VV}} \left( \frac{\pi}{\Delta_{VV}} \right)^{1/2} \frac{Q_{10}^4}{Q_{10}} \right] \frac{36 \Delta E}{\delta_{VV}^3 T} \quad (6-35)$$

The quantity  $T_1$  is again the vibrational "temperature" of the first level;  $\underline{y}$  and  $\bar{v}$  are respectively determined from the conditions for the minimum of function, equation (6-33a), and for the vanishing of the function, equation (6-33b).

where,

$$\underline{y} = \frac{E_1 T}{2 \Delta E T_1} + \frac{1}{2}$$

and

$$\exp(\delta_{VT} \bar{v}) = C \delta_{VT} Q_{10} K / P_{10}$$

Let us now examine the form of this analytic solution and correlate its predictions of the vibrational population with the three characteristic regions of the distribution previously identified. We will then examine the influence of the V-V and V-T rate magnitude, gas temperature, and pump rate on the calculated distribution.

Referring back to equation (6-29) and taking  $E_0$  as the zero energy reference observe that

$$VE_i - E_v = vE_0 \delta(v-1) = vAE(v-1) \quad (6-36)$$

Inserting this identity into equation (2-29) yields equation (6-33a). Thus the analytic distribution for  $v < \bar{v}$  is merely the Treanor representation of the distribution characterized by  $T_1$  and  $T$ . This is reasonable in light of our previous discussion. Beyond the Treanor minimum,  $v > \bar{v}$ , we note that

$$N_v(v+1) \approx \text{constant} \quad (6-37)$$

reflecting the characteristic "resonance" region of the distribution. Thus the Gordiets solution explicitly contains two of three characteristic VED regions. The Boltzmann "tail" is not a limiting form of the analytic solution; but the onset of the tail correlates well with the value of  $\bar{v}$ . Therefore, by limiting the falloff of the distribution to that of the Boltzmann at temperature  $T$ , reasonable agreement with detailed numerical solutions are achieved, Fig. 6-14.

When we consider the dissociation process, we will be specifically interested in the exact population of the Boltzmann "tail" region and can not rely on this simple analytic model. However, the formalism of equation (6-33)

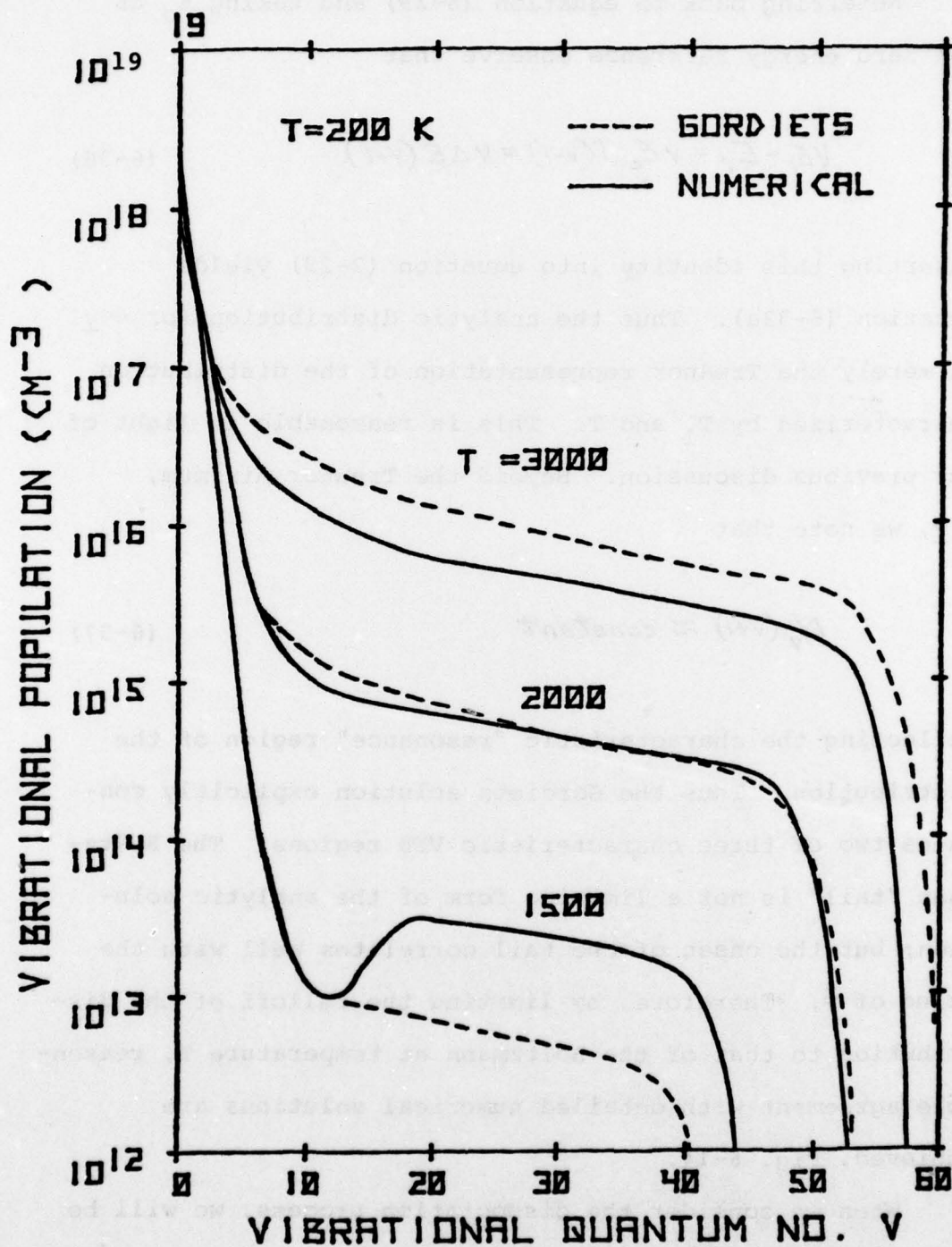


Fig 6-14 Comparison of Numerical and Analytic VED's

is very useful in showing explicitly the effects of the strength of pumping, the molecular anharmonicity, and the V-V and V-T rates. In addition, it offers a method for quantitative determination of kinetic rate information for highly excited vibrational states (refs 133, 152).

Referring to equation (6-33), let us examine the explicit effects of variations in different parameters. First, let us consider variations in the strength of pumping at a fixed temperature,  $T$ . An increase in  $T_1$  is equivalent to an increase in the net pumping. The strength of pumping determines the location of  $\underline{v}$ , the Treanor minimum, and subsequently the value of  $\bar{v}$  required to balance this source term with a V-T loss. Note that as  $T_1$  increases,  $\underline{v}$  decreases, being proportional to  $T_1^{-1}$ . This results in a significant increase in  $N_{\underline{v}}$ . Thus as  $T_1$  increases the location of the Treanor minimum,  $\underline{v}$ , moves to a lower vibrational quantum number and achieves a larger population. Since this population is given by equation (6-33b) as  $C/(v+1)$ ,  $C$  also increases. Noting that the second term in equation (6-33b) is independent of  $T_1$ , we see that  $\bar{v}$  must increase as  $T_1$  increases. This behavior is confirmed in Fig. 6-12 for the strongly pumped conditions of  $T_1=3000$ , 2000, 1500°K at  $T=200^\circ\text{K}$ .

The dependence of the VED on translational temperature,  $T$ , is slightly more complex, since  $\delta_{VT}$ ,  $\delta_{VV}$ ,  $\Delta_{VV}$ ,  $Q_{10}^L$ ,  $Q_{10}$ , and  $P_{10}$  are all functions of this parameter. Fig. 6-13 presents the detailed numerical parameterization of

the VED with respect to  $T$ . The gross behavior observed can be understood, once again, in terms of the variation of  $\underline{v}$ . In this case, note that  $\underline{v}$  is proportional to  $T$ . Therefore,  $\underline{v}$  decreases as  $T$  decreases, resulting again in an increase in  $N_{\underline{v}}$ . As before, since  $N_{\underline{v}}$  increases,  $\bar{v}$  will also tend to increase as  $T$  decreases. To establish the variation of  $\bar{v}$  with  $T$ , we must also consider the temperature dependence of the second term in equation (6-33b). For the cases considered,

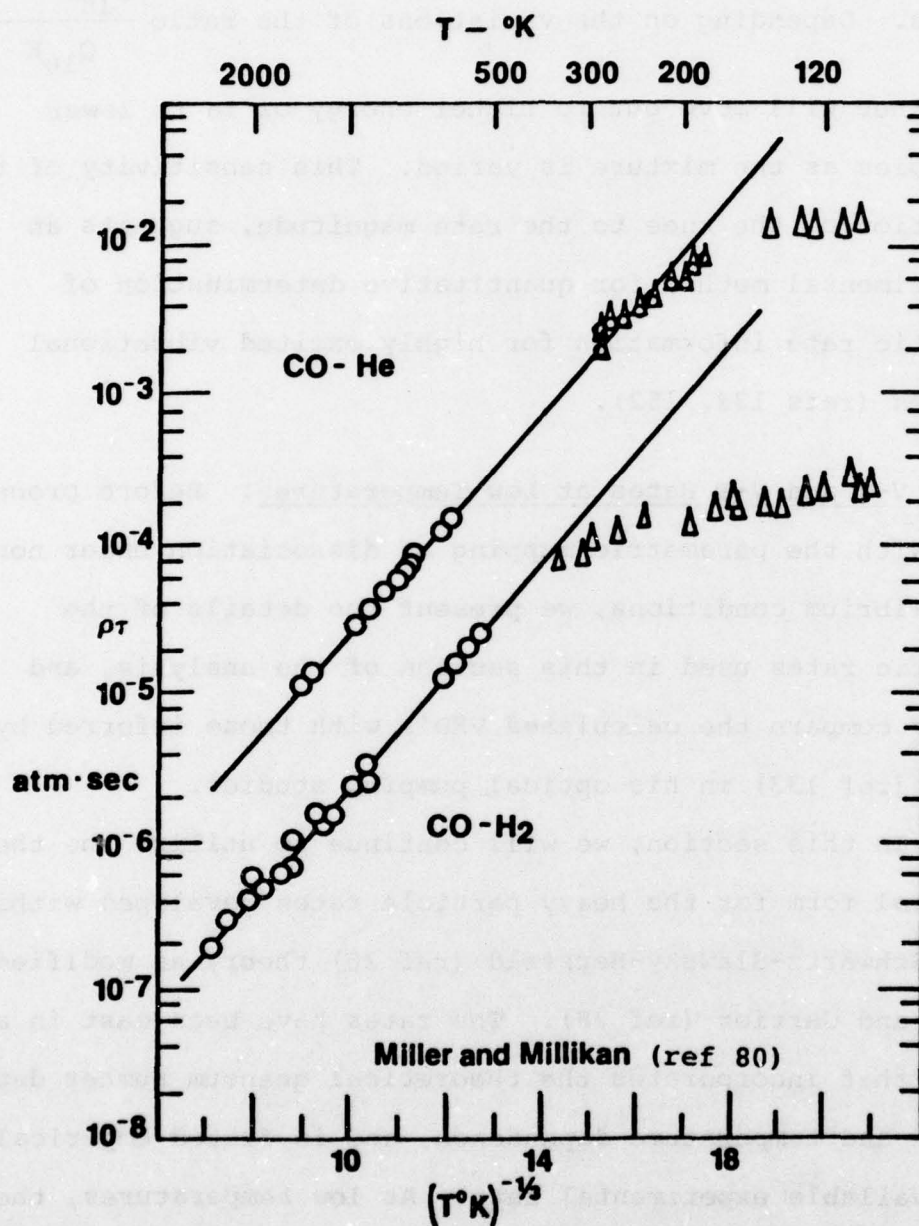
$$Q_{10} K \propto T^{-3/2}$$

and

$$\begin{aligned} P_{10} &\propto \exp(A/T^{1/3}) & T > 300 \text{ } ^\circ\text{K} \\ P_{10} &\propto T^{1/2} & T \leq 300 \text{ } ^\circ\text{K} \end{aligned}$$

(See Fig. 6-15 for examples of this temperature dependence of the V-T rates.) The temperature dependence of these terms would therefore reinforce the increase of  $\bar{v}$  as the temperature decreases. This increase in  $\bar{v}$ , however, is tempered by the  $T^{-1/2}$  dependence of  $\delta_{VT}$  given by the SSH theory. Thus the increase in  $\bar{v}$  tends to saturate at the lower temperatures.

The mixture dependence of the VED can be appreciated by noting in this case that  $P_{10}$  and  $Q_{10}$  of equation (6-33b)



### V-T DEACTIVATION of CO

Fig 6-15 V-T Deactivation of CO

now represent the averaged V-T and V-V strengths using the appropriate mole fractions of diluent and diatomic gases. Depending on the variations of the ratio  $\frac{P_{10} e^{\delta_{VT}^V}}{Q_{10}^K}$ , the knee will move out to higher energy or in to lower energies as the mixture is varied. This sensitivity of the location of the knee to the rate magnitude, suggests an experimental method for quantitative determination of kinetic rate information for highly excited vibrational states (refs 133, 152).

V-V and V-T Rates at Low Temperatures. Before proceeding with the parametric mapping of dissociation under non-equilibrium conditions, we present the details of the kinetic rates used in this section of the analysis, and later compare the calculated VED's with those inferred by Rich (ref 133) in his optical pumping studies.

In this section, we will continue to utilize the theoretical form for the heavy particle rates developed within the Schwartz-Slowsky-Herzfeld (ref 20) theory as modified by Keck and Carrier (ref 28). The rates have been cast in a form that incorporates the theoretical quantum number dependence and temperature dependence, and is fitted empirically to available experimental data. At low temperatures, the V-T rates depart from the Landau-Teller form of  $\ln(P_T)$  proportional to  $T^{-1/3}$ , as observed in Fig. 6-15. In addition, long range force contributions to the V-V rates become

significant and are included utilizing fits to the calculations of Sharma and Brau (ref 81).

The V-T rates used are based on the semi-empirical modification of the SSH theory proposed by Keck and Carrier. This modification provides for a smooth variation of rates from states with low vibrational quantum number, experiencing near-adiabatic collisions, to high vibrational states, where collisions approach the impulsive limit. This modification attempts to extend the first order perturbation theory results of the SSH theory, which are invalid for transitions occurring with high probability. The expression used for the V-T transition probabilities was given previously in equation (3-3).

The V-V rate model incorporates a sum of the contributions from a short range force (SSH) and a long range force contribution which is most effective for near resonant collisions. The present calculations incorporate a weighting factor for each contribution, which permits a matching to experimental data over the temperature range of interest. Following Rockwood (ref 89) and Rich (ref 99), the expressions used for the V-V transition probabilities for C0 are given by equation (3-4) for  $v+1 \rightarrow v$  and  $w \rightarrow w+1$ :

$$P_{v+1,v}^{w,w+1} = \left[ S_{v+1,v}^{w,w+1}(\tau) + L_{v+1,v}^{w,w+1}(\tau) \right] \exp \left\{ \frac{\beta [E_{v+1} E_v - E_{w+1} + E_w]}{2} \right\} \quad (3-4)$$

where S corresponds to the short range and L the long range contribution. The short range contribution is functionally similar to that encountered in the V-T model and is given by

$$S_{v+1,v}^{w,w+1}(T) = S^o(T) \left[ \frac{v+1}{1-\delta(v+1)} \right] \left[ \frac{w+1}{1-\delta(w+1)} \right] F_{v+1,v}^{w,w+1}(\lambda_{v+1,v}^{w,w+1}) \quad (6-38)$$

where

$$F_{v+1,v}^{w,w+1}(\lambda) = \frac{1}{2} \left( 3 - \exp \left[ -\frac{2}{3} \lambda_{v+1,v}^{w,w+1} \right] \right) \exp \left( -\frac{2}{3} \lambda_{v+1,v}^{w,w+1} \right)$$

$$\lambda_{v+1,v}^{w,w+1} = \left( \delta / \sqrt{2} \right) \left( \frac{\theta}{T} \right)^{1/2} |v-w|$$

and for C0

$$\delta = 0.00598$$

$$\theta = 4.45 \times 10^6$$

$$S^o(T) = 1.25 \times 10^{-15} T^{.96}$$

The long range contribution for C0 self-collisions, which arises for molecules with permanent dipole moments, is included following the theory of Sharma-Brau (ref 81). Their rate expressions are algebraically complex, therefore,

we have retained the functional form of the rate being proportional to the dipole matrix elements and specified the resonant character by a Gaussian function of the energy defect (ref 89). This yields

$$L_{V+1,V}^{W,W+1}(T) = L^0(T) G(V-W) Q_L(V+1) Q(W+1) \quad (6-39)$$

with

$$Q_L(V+1) = \left[ \frac{165.2}{167.2 - 2(V+1)} \right]^2 \left[ \frac{166.2 - 2(V+1)}{164.2} \right] \left[ \frac{168.2 - (V+1)}{167.2 - (V+1)} \right] (V+1)$$

$$G(J) = \exp \left[ - \frac{(2\delta E, J)^2}{1.2 \times 10^4} \left( \frac{300}{T} \right) \right]$$

$$L^0(T) = 3.8 \times 10^{-11} T^{-1/2}$$

The V-V rates are explicitly formulated to satisfy detailed balance, so that

$$V V_{V+1,V}^{W,W+1} = V V_{W+1,W}^{V,V+1} \exp \left\{ \frac{(E_{V+1} - E_V) - (E_{W+1} - E_W)}{kT} \right\} \quad (6-40)$$

The resulting fit of the combined long and short range contribution is depicted in Fig. 6-16 where it is compared with the experimental data of Hancock and Smith (ref 33), Stephenson (ref 160), Sackett (ref 159) and Powell (ref 156).

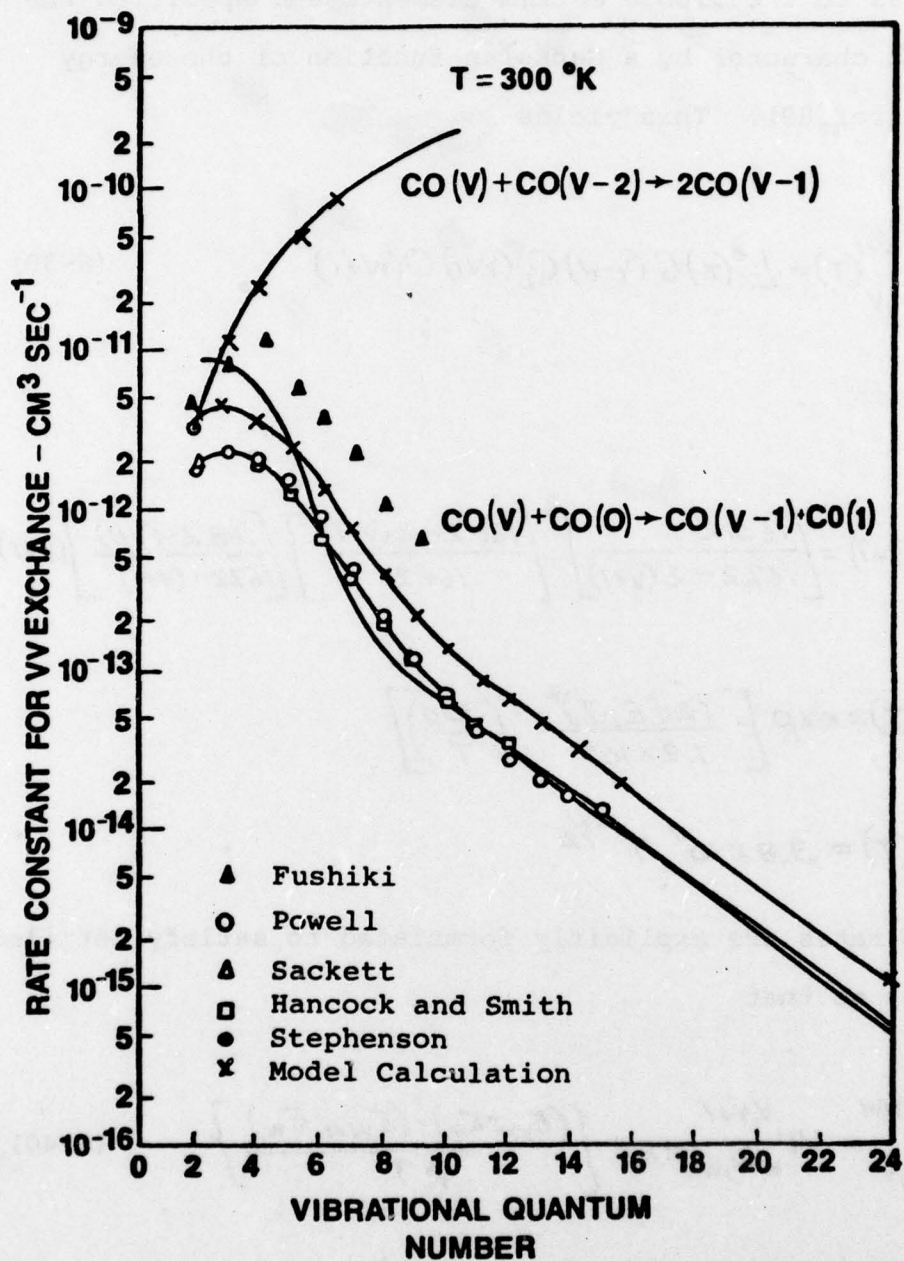


Fig 6-16 Rate Constants for CO-CO V-V Exchange

Note that this form provides a reasonable fit to the experimental data, being a factor of 2.0 higher than the data of refs (33, 160, 159) and a factor of 3 lower than the recent data of Fushiki (ref 158). The selection of this particular fit will be discussed when we next compare the predicted VED's with Rich's (ref 133) inferred populations from optical pumping experiments.

Comparison with Optically Pumped VED's. From a kinetic standpoint, optical pumping offers a simple and contaminant free method of analyzing molecular energy exchange processes. Here we utilize the experimental data of Rich to benchmark our non-equilibrium analysis. Rich (ref 133) used a flowing gas absorption cell containing CO/Ar/He, in which vibrational excitation was obtained by direct optical pumping from an electrically excited, supersonic flow, CW, carbon monoxide laser. Utilizing this technique, mean vibrational energies of 0.3 to 0.4 eV per CO molecule were obtained at a translational temperature of 300°K. Vibrational populations were inferred from infrared spectra from the first overtone, ( $\Delta v=2$ ), emission bands of CO. These populations are presented in Fig. 6-17. Note that the "resonance" region, in the zero helium mix, extends out to vibrational quantum number,  $v=40$ . Addition of helium causes the knee to move down to lower quantum number, reflecting the dominance of the helium V-T rate over that of argon or of CO. This behavior is consistent

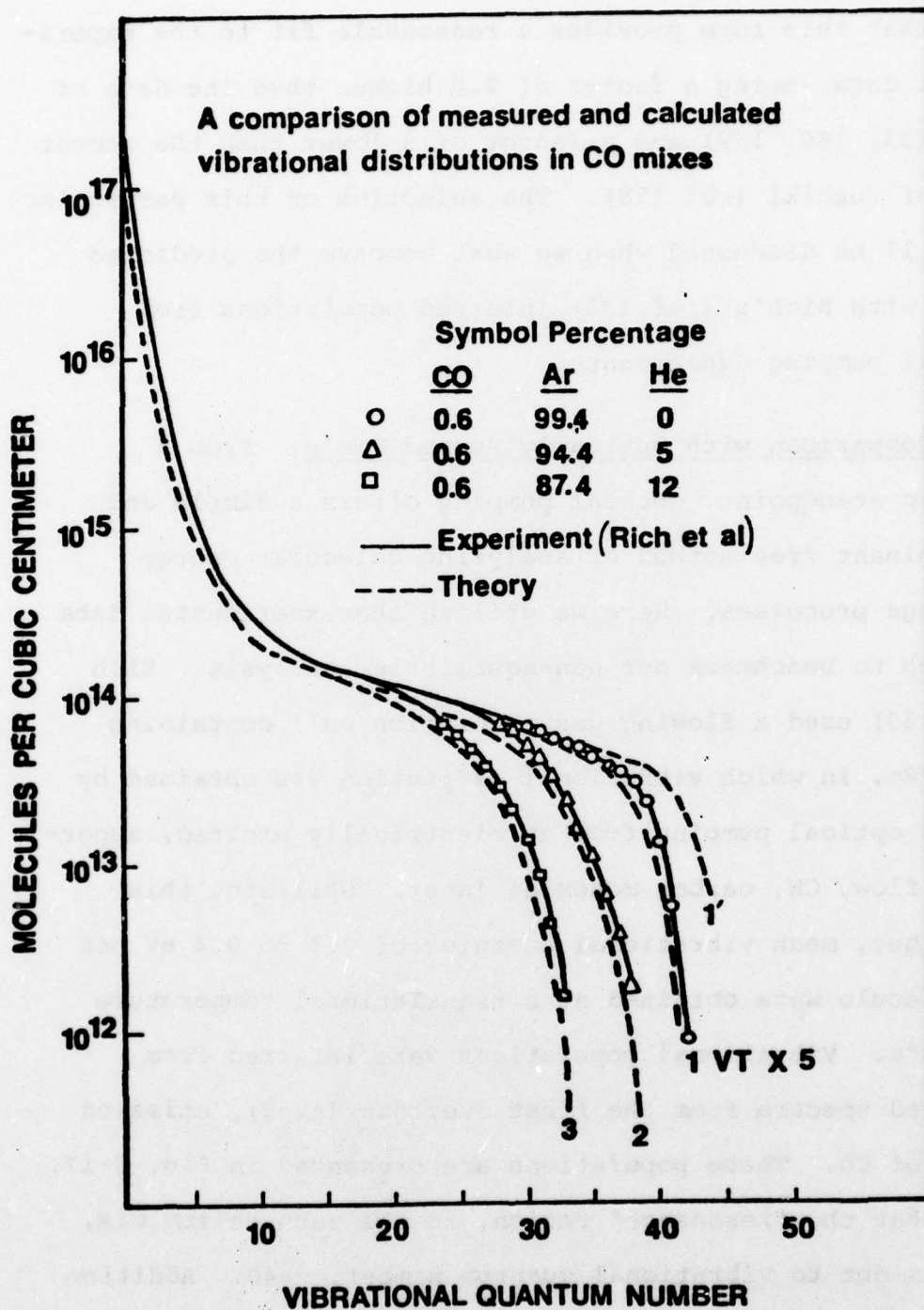


Fig 6-17 Optically Pumped VED's

with our previous discussion of Gordiets' analytic form,

since  $P_{10} e^{\delta_{VT}^V} / (Q_{10} K)$  increases with helium addition. Also observe that the remaining lower state populations are essentially unchanged.

Extracting the vibrational temperature,  $T_1$ , from Rich's data, a steady-state calculation of the VED was made for  $T_1 = 2700^\circ\text{K}$  and  $T = 300^\circ\text{K}$ , with the results given by the dashed line in Fig. 6-16. Agreement is excellent, the theoretical curve being displaced only to permit convenient comparison. Initial calculations using V-V rates a factor of 2.25 lower which would have yielded a better fit to the experimental data of ref (33) in Fig. 6-16, failed to accurately reproduce the data and resulted in the distribution for the 0.6/94.4/5 mix essentially overlapping the experimental distribution for the 0.6/87.4/12 mix. Based on numerical experiments, it was established that agreement could be obtained by either decreasing the magnitude of CO-He V-T rate or increasing the magnitude of the V-V rate, while retaining the same vibrational quantum number dependence. (Note that this adjustment confirms the dependence of the knee location on the ratio  $P_{10} e^{\delta_{VT}^V} / (Q_{10} K)$ ). We have selected the latter adjustment placing more confidence in the V-T rate measurements and noting the scatter in the measured V-V rates. Fixing the value of the V-V rates at this value in all subsequent calculations, the zero helium

mix was investigated. Low temperature data on CO-Ar V-T probabilities, in contrast to CO-He and CO-H<sub>2</sub>, do not exist; we therefore extrapolated the high temperature data using the empirical  $P_T$  fit of Millikan and White (ref 5). Using this form, curve 1' in Fig. 6-16 was obtained. By increasing the magnitude of the CO-Ar V-T rate by a factor of 5, which is consistent with the low temperature behavior of CO-He V-T exchanges, good agreement with experiment could be obtained. The result of this adjustment is given by curve 1.

#### Parameterization of Dissociation

Having discussed the electron and vibrational kinetics and benchmarked the calculational techniques and kinetic rates, we are now prepared to investigate the dissociation process under highly non-equilibrium conditions. In this parameterization we will compare the rate of dissociation resulting from heavy particle collisions to the rate of electron impact dissociation. From this analysis, we will establish two characteristics of non-equilibrium dissociation. First, non-equilibrium conditions lead to a significant rate enhancement of both types of dissociation. Second, under typical conditions encountered in self-sustained and e-beam sustained discharges, electron impact dissociation exceeds, by orders of magnitude, the heavy particle dissociation rate.

A detailed parametric analysis of the dissociation process under non-equilibrium conditions would involve a time-dependent solution of the coupled Boltzmann and Master equations for electron impact dissociation, or similarly an absorption calculation coupled to the Master Equation in order to handle the case of optical pumping. Inherent in the analysis would be an extensive parameterization with respect to  $E/N$ , electron density, gas temperature and radiation intensity. The codes developed in this study are well suited to such an approach. However, rather than embarking on such an ambitious course for an initial survey, we have chosen a simplified approach which adequately treats the dominant processes of non-equilibrium dissociation and permits an evaluation of magnitude and functional dependencies of the heavy particle and electron impact dissociation rates. In this approach, we decouple the electron and molecular kinetics. As in the equilibrium case previously addressed, we are primarily interested in the behavior of a quasi-steady-state. On the time scales of interest, both the eed and the VED achieve such a steady state. The vibrational distribution is relatively insensitive to the form of eed depending mainly on the total net vibrational excitation and gas temperature. The net excitation rate of the vibrational manifold is insensitive to the form of the vibrational distribution for conditions considered in this study. For this reason we have parameterized the heavy particle dissociation rate in either  $T_1$ ,

or pump rate, and gas temperature. The eed, however, does reflect the state and distribution of vibrational excitation, especially when electronic and dissociative collisions are examined. To account for this interaction, while retaining an uncoupled approach, we have bounded the vibrational temperature,  $T_1$ , for typical discharge conditions and incorporated Gordiets' (ref 151) analytic form of the vibrational distribution into the electron kinetics solution.

We will consider a gas mixture of CO/Ar, 10/90, as an illustrative and representative mix. The electron impact dissociation process will be parameterized in  $E/N$ ,  $T_1$ , and  $T$ . We will consider  $E/N$ 's ranging from 3 to 40 Townsend and gas temperatures ranging from 100 to 3000°K for  $T_1=2000$  and 3000°K. This space adequately covers the normal operating parameters of gas discharges. In parallel, the heavy particle dissociation process will be examined over a similar parameter space. In addition, we will examine the heavy particle dissociation process for conditions encountered in optical pumping studies. Here we will consider constant pump rates which span the optical pumping regime,  $10^3$  to  $10^7$  quanta molecule<sup>-1</sup> sec<sup>-1</sup>, for gas temperatures ranging from 100 to 2000°K.

Electron Impact Dissociation. Electron impact dissociation occurs in gas discharges and initiates a change in

the discharge chemistry, gas composition, and electron and molecular kinetics. Often these changes lead to an eventual degradation of laser discharge efficiency or a transition of the glow discharge to an arc (ref 1).

In this section, we will present data on the rate of dissociation due to electron impact collisions. These data were obtained from a numerical solution of the Boltzmann equation. We will examine the influence of dissociation from excited states and the influence of superelastic collisions. The dissociation coefficient  $k_d^e$  is related to the rate of electron impact dissociation,  $R_d$ , by

$$R_d(\text{sec}^{-1}) = n_e k_d^e = \left( \frac{n_e}{N_{\text{tot}}} \right) N_{\text{tot}} k_d^e = \tilde{k}_d^e N_{\text{tot}} \quad (6-41)$$

with  $n_e$  = electron number density ( $\text{cm}^{-3}$ )  
 $N_{\text{tot}}$  = total neutral gas number density ( $\text{cm}^{-3}$ )  
 $k_d^e$  = dissociation coefficient ( $\text{cm}^3/\text{sec}$ )

Here we will consider two different electron impact dissociation reaction channels:

- a. dissociative ionization
- b. dissociative attachment

We will first examine the rate of dissociative ionization and establish that this reaction rate can be significantly enhanced under non-equilibrium conditions. The rate of dissociative attachment will then be presented and compared

with the rate of dissociative ionization. The influence of superelastic collisions on both reaction rates will be discussed.

The dissociative ionization cross-section, presented in Fig. 6-4 was utilized for the calculation of  $k_d^e$  ( $E/N$ ,  $T, T_1$ ). The calculated coefficient of electron impact dissociative ionization,  $k_d^e$ , is presented in Fig. 6-18. In order to evaluate the influence of excited states on the reaction rate, we have assumed that the cross-section from excited vibrational states is equal to that from the ground state with the threshold being displaced by the vibrational energy relative to the  $v=0$  state. The excited state vibrational distributions were calculated using the Gordiets' (ref 151) formalism. When dissociation is assumed to occur only from the ground vibrational state, the calculated rate is low in magnitude and exhibits a strong dependence on  $E/N$ .

Dissociative ionization from excited states results in a rate enhancement of many orders of magnitude. This enhancement is due to the highly non-equilibrium distribution of both the VED and the eed. The excited state dissociation rate is dominated by the contributions from the vibrational states in the high energy end of the VED plateau. This dominance can be understood in terms of the population and the threshold for dissociative ionization of the high lying vibrational states. These states obtain a significant population for large  $T_1$  and low  $T$  as a result of anharmonic pumping and the formation of the "resonant

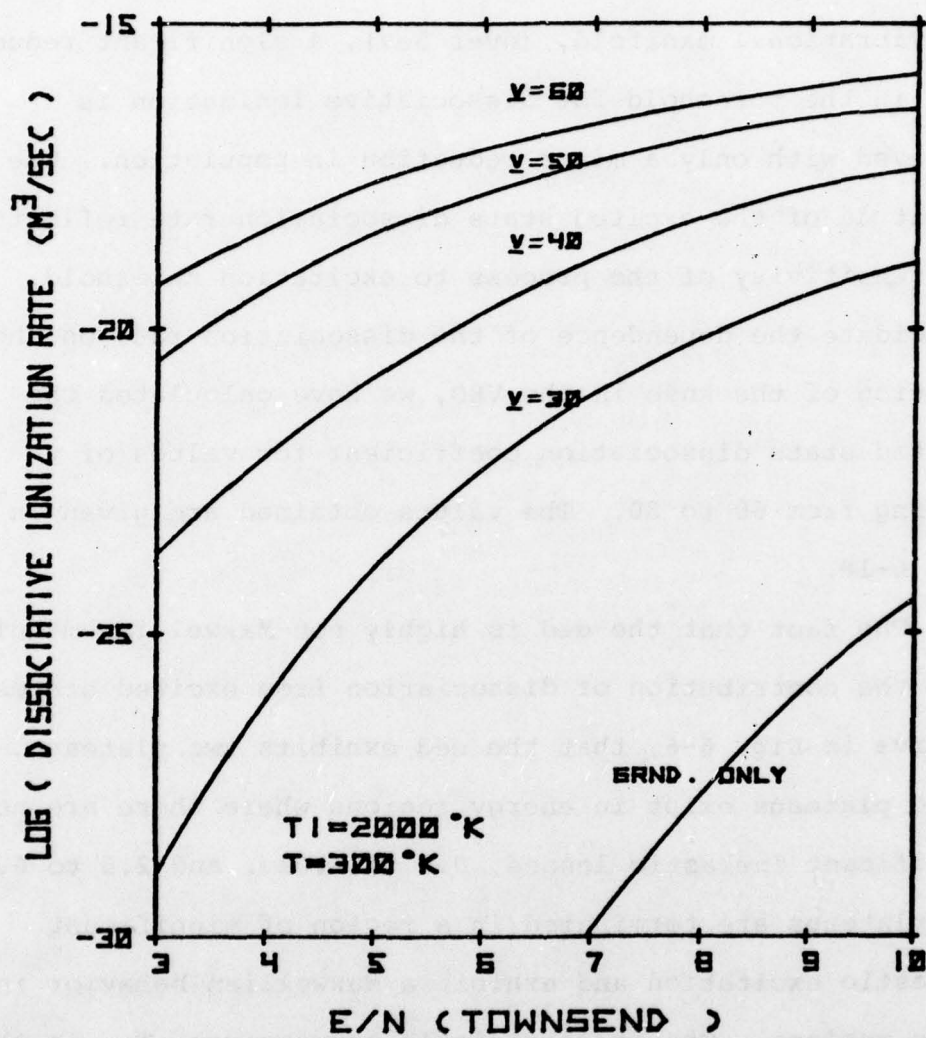


Fig 6-18 Dissociative Ionization Coefficients ( $k_d^e$ )

plateau." Recalling that  $N_v \bar{v} \approx \text{constant}$  in this region, we note that there is only a slight decrease in state population from the Treanor minimum,  $\underline{v}$ , to the knee location,  $\bar{v}$ . Since the plateau can be maintained over a wide range of the vibrational manifold, (over 5ev), a significant reduction in the threshold for dissociative ionization is achieved with only a minor reduction in population. The magnitude of the excited state dissociation rate reflects the sensitivity of the process to excitation threshold. To elucidate the dependence of the dissociation rate on the location of the knee in the  $V_{00}$ , we have calculated the excited state dissociation coefficient for values of  $\bar{v}$  ranging from 60 to 30. The values obtained are given in Fig. 6-18.

The fact that the eed is highly non-Maxwellian magnifies the contribution of dissociation from excited states. Observe in Fig. 6-6, that the eed exhibits two plateaus. These plateaus exist in energy regions where there are no significant inelastic losses, 0.0 to 1.0ev. and 2.5 to 6.0ev. The plateaus are terminated in a region of significant inelastic excitation and exhibit a Maxwellian behavior in these regions. The characteristic temperature,  $T_c$ , in these regions, where

$$f(u) = \exp(-u/(kT_c)) \quad (6-42)$$

is much less than  $T_{avg}$ , where

$$\frac{3}{2} kT_{avg} \equiv \text{mean energy} \quad (6-43)$$

This results in an enhanced sensitivity of the rates to the threshold energy of the excitation and points out the inadequacy of any Maxwellian model of the eed.

Superelastic collisions also enhance the dissociation rate, with this effect being strongest at low E/N. The influence of superelastic collisions on the dissociative attachment, DA, and dissociative ionization, DI, rates is presented in Fig. 19. The DI curve includes dissociation from excited states. The source of rate enhancement due to superelastic collisions and the self-similar form of the eed were discussed previously in reference to Fig 6-8.

Dissociation Due to Heavy Particle Collisions: Electric Discharge Conditions.\* We now examine the heavy particle dissociation rate over the discharge parameter space and compare this rate with the electron impact rate. We will find that electron impact dissociation substantially exceeds the heavy particle rate for typical discharge operating conditions.

Here we will utilize the standard ladder model for the heavy particle analysis. This is a convenient and reasonable

---

\*It is assumed throughout that we are dealing with a C.W. discharge and not a pulse discharge or afterglow.

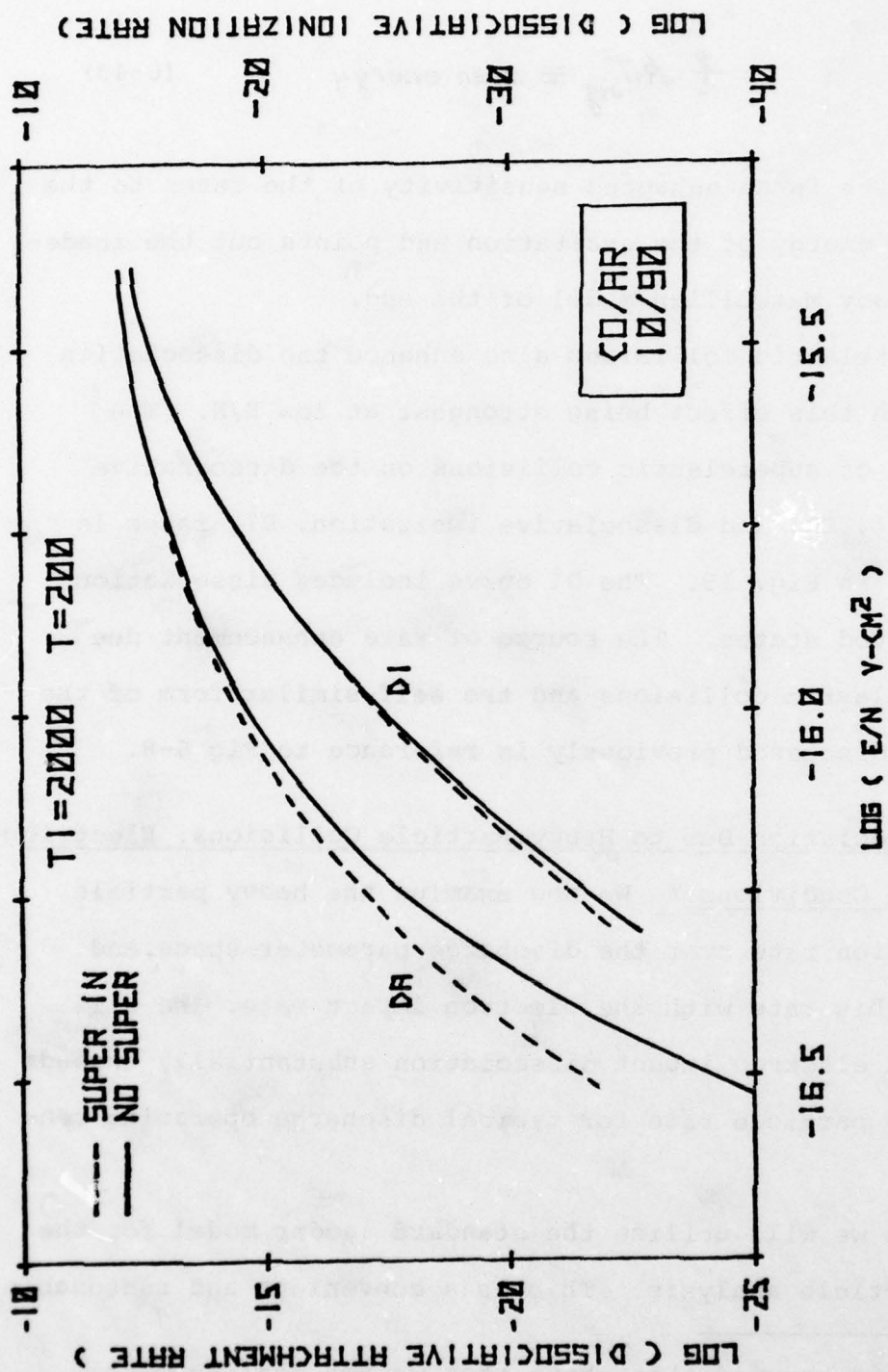


Fig 6-19 Electron Impact Dissociation Coefficients ( $k_d^e$ )

approach, since at the low temperatures considered here, the various heavy particle dissociation models approach the same limit and no rate variation of significance in this parameterization results. The heavy particle coefficients,  $k_{dH}$ , are parameterized in  $T$  and  $T_1$ . With

$$k_{dH} = \frac{\dot{N}_{co}}{N_{co} N_{tot}} \left( \frac{cm^3}{sec} \right) \quad (6-44)$$

The results of this analysis are presented in Figs. 6-20 and 6-21. Fig. 6-20 compares the electron,  $\tilde{k}_d^e$ , and heavy particle,  $k_{dH}$ , coefficients for conditions of vibrational equilibrium,  $T_1=T$ . The heavy particle rate coefficient retains its Arrhenius form, and is very low in comparison to the electron impact coefficient at the typical discharge operating temperatures below 700°K. The influence on  $k_{dH}$  of discharge induced departures of VED from equilibrium is established in Fig. 6-21. Here  $k_{dH}$  is presented as a function of  $T$  for  $T_1=2000^\circ K$  and  $3000^\circ K$ . The departure of the VED from equilibrium enhances the population in the high energy states and substantially increases the dissociation rate above its equilibrium value. Despite this increase, the heavy particle dissociation rate remains many orders of magnitude below  $\tilde{k}_d^e$  and never obtains a physically significant magnitude. The magnitude and temperature dependence of the heavy particle rate can be understood in terms of the simplified analysis of the VED previously presented.

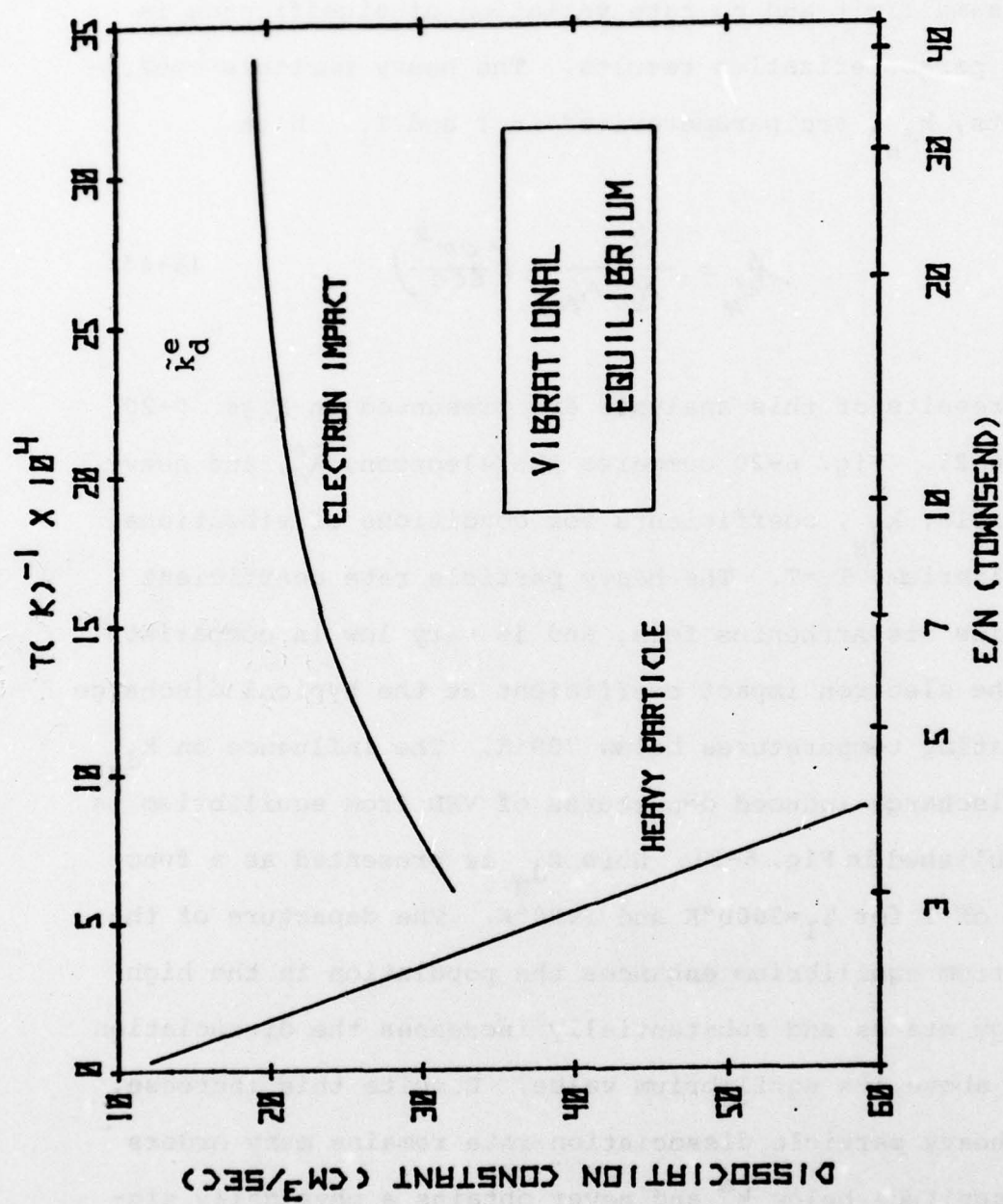


Fig 6-20 Equilibrium Comparison of Electron and Heavy Particle Dissociation

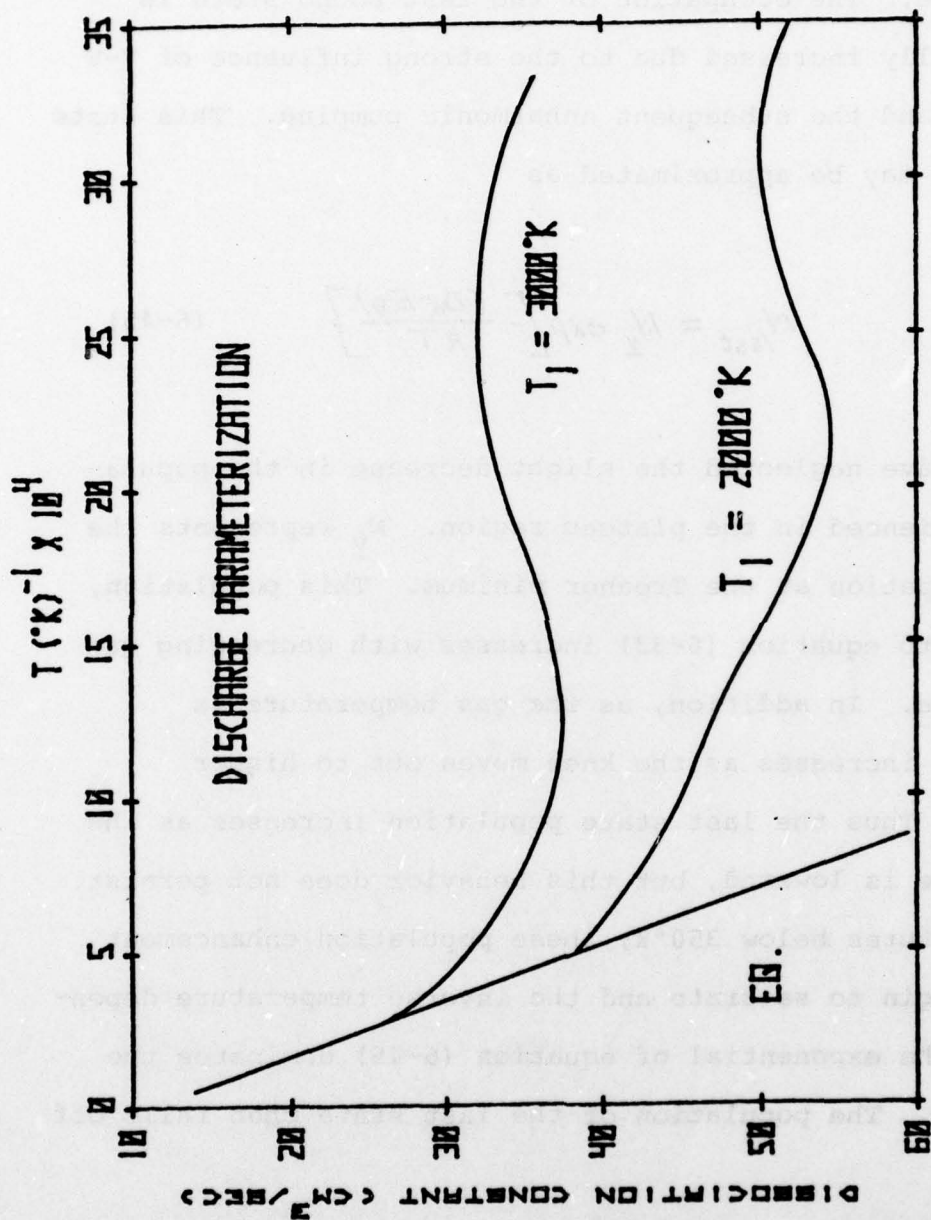


Fig 6-21 Non-Equilibrium Heavy Particle Dissociation Constant

Within the framework of the ladder model, the dissociation rate is proportional to the occupation of the last bound state. The occupation of the last bound state is substantially increased due to the strong influence of V-V exchanges and the subsequent anharmonic pumping. This state population may be approximated as

$$N_{last} = N_y \exp \left[ - \frac{(D_0 - E_v)}{kT} \right] \quad (6-45)$$

where we have neglected the slight decrease in the population experienced in the plateau region.  $N_y$  represents the state occupation at the Treanor minimum. This population, according to equation (6-33) increases with decreasing gas temperature. In addition, as the gas temperature is lowered  $E_v$  increases as the knee moves out to higher energies. Thus the last state population increases as the temperature is lowered, but this behavior does not persist. At temperatures below 350°K, these population enhancement effects begin to saturate and the inverse temperature dependence in the exponential of equation (6-45) dominates the expression. The population of the last state then falls off rapidly.

Dissociation Due to Heavy Particle Collisions: Optical Pumping. In order to complete the parameterization of the heavy particle rate, we now consider the case in which

excitation is achieved through intense optical pumping.

Optical pumping has advantages over discharge excitation:

1. A greater degree of vibrational excitation can be achieved in comparison to electric discharge excitation.
2. Gas mixture, pressure, and temperature need not be compatible with discharge operation.

These advantages force one to consider the possibility of achieving a significant heavy particle dissociation rate under conditions of intense optical pumping. In this section we parameterize the dissociation reaction under conditions of intense optical pumping with respect to gas temperature and effective,  $v=0 \rightarrow 1$ , pump rate. The temperatures considered ranged from 100 to 1000°K, while pump rates extended from those characteristic of discharge excitation to gas breakdown threshold,  $10^3$  to  $10^7$  quanta/(molecule-sec.)

Paralleling our treatment of thermal dissociation, we will first present the results of a time-dependent solution of the Master Equation, Fig. 6-22. This solution establishes the existence of a quasi-steady-state and reveals the temporal evolution of the Treanor, Plateau, and Boltzmann regions of the VED. We here consider a 10/90, CO/Ar gas mixture with pump rate  $P=10^3$  and  $T=300$  at a total number density of  $2.67 \times 10^{19} \text{ cm}^{-3}$ . The initial distribution is assumed to be the equilibrium Maxwellian distribution at the gas temperature  $T$ . The quasi-steady-state is achieved in 90  $\mu\text{sec}$  and exhibits the three characteristic regions

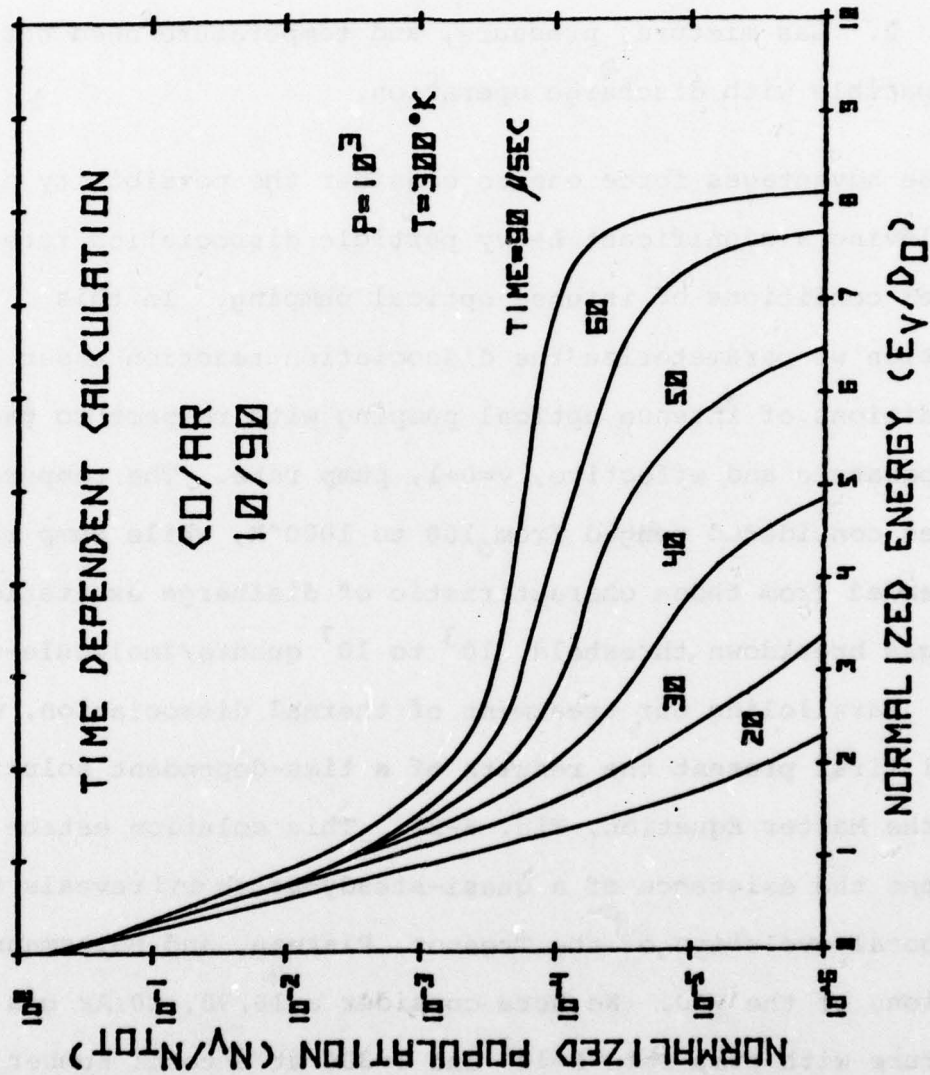


Fig 6-22 Optical Pumping, Time Dependent Calculation

discussed previously. In the early stages of the transient evolution, the relaxation is dominated by the 0→1 pumping and off resonant V-V exchanges with the first excited vibrational state. These exchanges drive the low vibrational states toward a Treanor distribution and lead to a significant increase in the population of the higher vibrational levels. This evolution proceeds until a sufficient population is achieved in these high energy states. Then vibrational exchanges become dominated by near resonant exchanges and the plateau begins to be established. The input quanta are conveyed along the plateau towards the Boltzmann deactivation zone. The zone moves toward higher energies to finally achieve a balance with the energy input rate and the quasi-steady state is established.

A similar VED evolution and attainment of a quasi-steady-state was obtained for all pump rates and gas temperatures considered. In no instance was it possible to extend the plateau region to the dissociation limit and obtain a VED without a Boltzmann "tail." As a result, the heavy particle dissociation rates obtained for conditions of intense optical pumping were extremely slow and not comparable to those obtained by electron impact excitation.

The heavy particle dissociation coefficients obtained for pump rates,  $P$ , of  $10^3$  and  $10^6$  are plotted against  $T^{-1}$  in Fig. 6-23. The dissociation coefficient decreases monotonically with temperatures, falling off more rapidly at temperatures below 400°K. This fall off is due to the

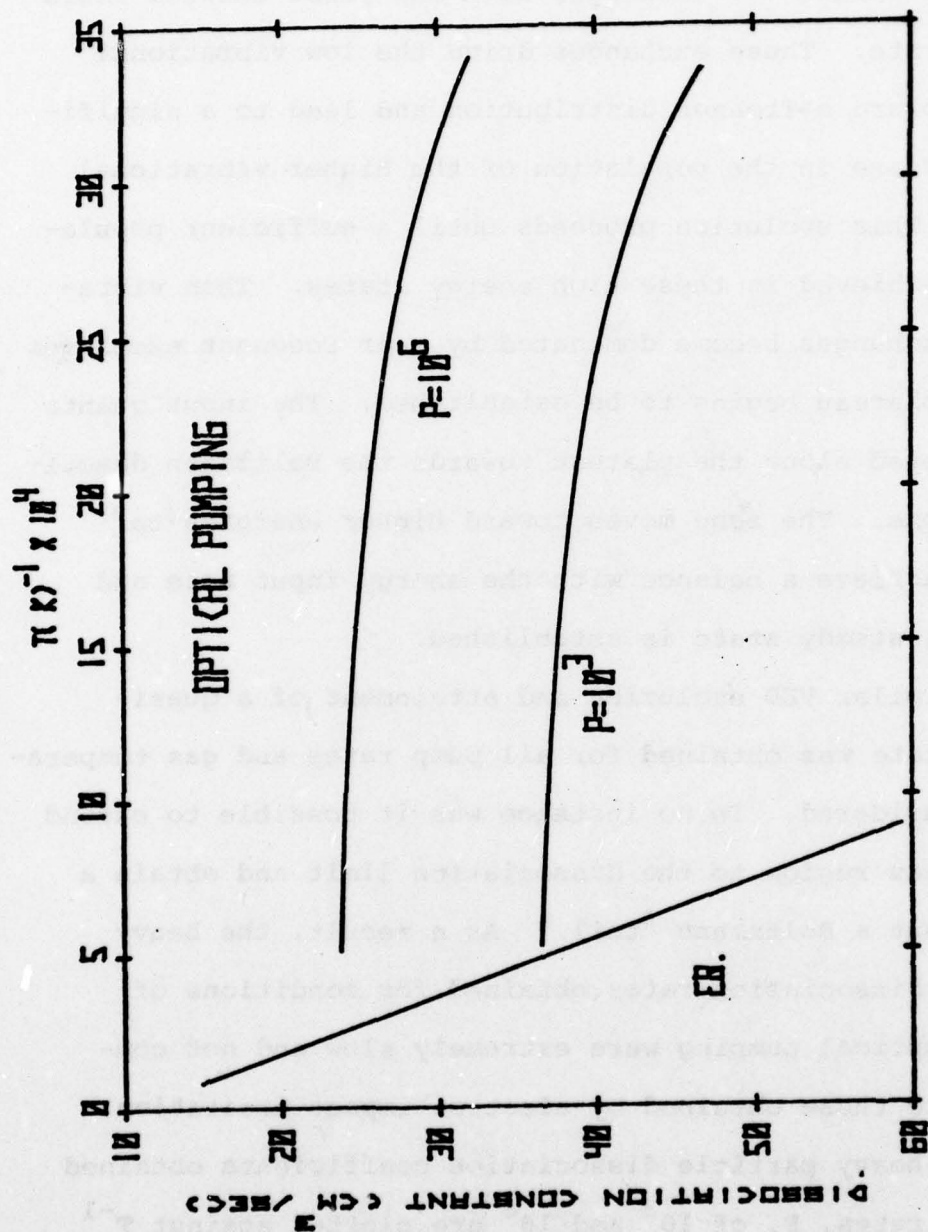


Fig 6-23 Optical Pumping, Heavy Particle Dissociation Constant

exponential temperature dependence of the final state population discussed previously with regard to the discharge parameterization and equation (6-45). The gross temperature dependence is different from that obtained in the  $T_1$  parameterization. This can be understood by noting that although  $T_1$  is proportional to a pump rate, and an increase in  $T_1$  at a fixed  $T$  corresponds to an increase in pumping,  $T_1$  being equal to a constant does not imply a constant pump rate if the gas temperature is varied. Note that by increasing the pump rate by three orders of magnitude, the dissociation rate has increased over 10 orders of magnitude. This enhancement is caused by the increase in plateau population and the extension of the "knee" to higher energies as the pumping is increased. This behavior saturates, however, as shown in Fig. 24, where the dissociation constant is plotted as a function of pump rate at a fixed temperature of 300°K.

Evaluation and Comparison of Heavy Particle Dissociation Rates. Based upon the discharge and optical pumping analyses, we conclude that, within the framework of the ladder model, it is difficult to achieve substantial heavy particle induced collisional dissociation under non-equilibrium conditions. Quantitative experimental data on non-equilibrium dissociation rates are not available, however, qualitative information has recently been obtained by Rich (ref 133) in his optical pumping studies. These

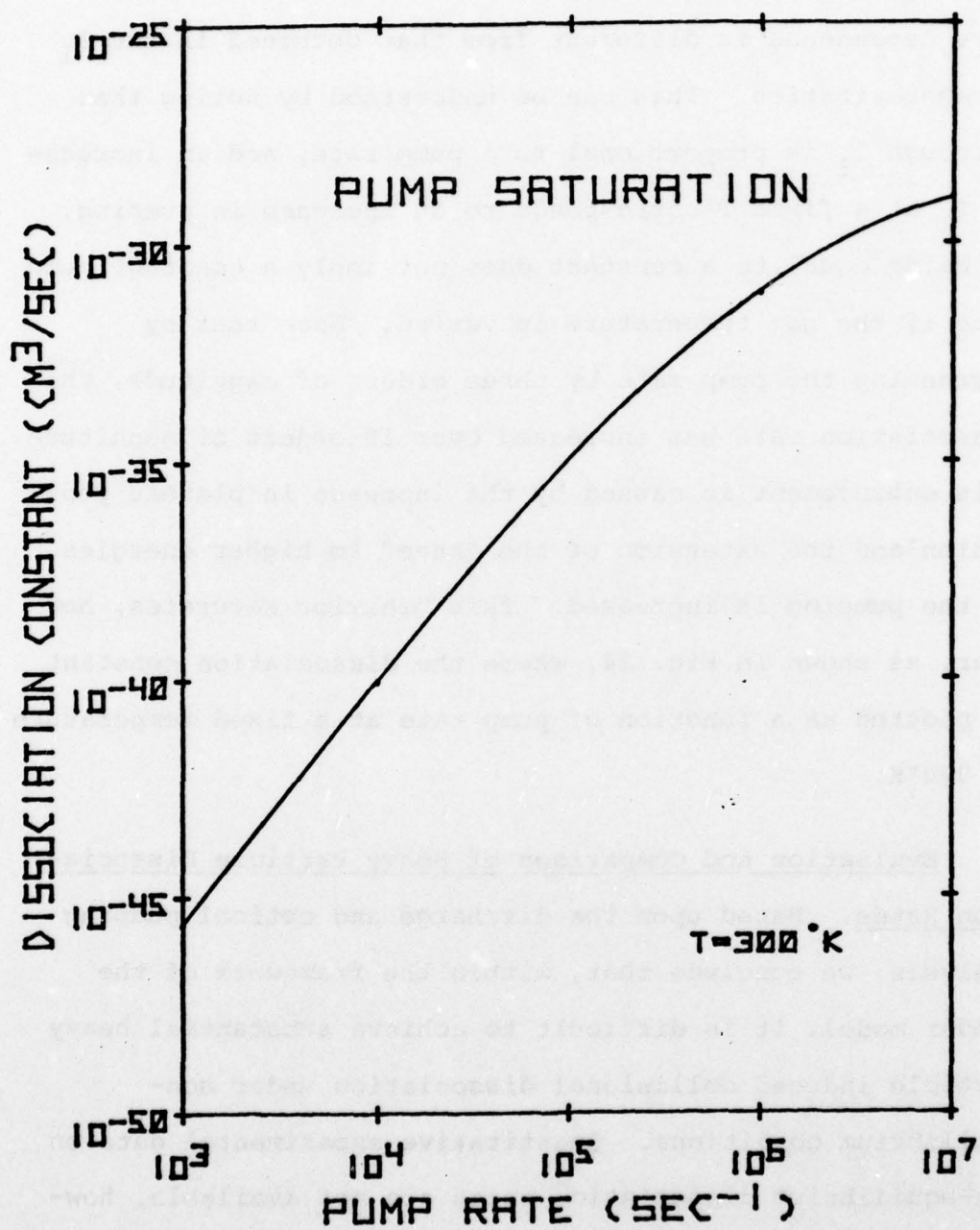


Fig 6-24 Saturation of Heavy Particle Dissociation

studies were motivated by interest in high energy CO lasers and infrared avionics programs, and were directed towards measurement of the V-T deactivation rates for high vibrational quantum levels of CO in collisions with helium and argon. During the investigation, however, significant non-equilibrium dissociation of CO was observed to occur, the inferred dissociation rate being similar in magnitude to that obtained under electric discharge conditions. This observation is inconsistent with the predictions of our non-equilibrium calculations and requires a re-evaluation of the kinetic model used in the analysis.

First, let us review Rich's observations (ref 133).

1. Carbon is deposited on cell walls during excitation.
2. At gas pressures below 6 atmospheres in CO/Ar, a visible blue emission, (Swan Bands of  $C_2$ ), is observed. The intensity increases as the total pressure decreases.
3. A comparison of the relative intensities of the  $C^{13}C^{12}$   $v=1 \rightarrow 0$  and the  $C^{12}C^{12}$   $v=1 \rightarrow 0$  band heads suggest an isotopic enrichment of "several" hundred percent.
4. Observed isotopic enrichments appear to be essentially independent of gas temperature.
5. Emission from the CO electronic bands is not observed.

Now let us re-examine our model predictions of non-equilibrium dissociation rates in light of these observations and the calculated VED's. The obvious deficiency

lies in the magnitude of the dissociation constant. For  $k_d = 10^{-43}$ , a dissociation rate of  $10^{-43} N_{co} N_{tot} = 10^{-6} \text{ cm}^{-3} \text{ sec}^{-1}$  is obtained. This rate would have to be increased about 20 orders of magnitude to yield a rate consistent with experiment.

A disparity of this order of magnitude might result from inaccuracies in the kinetic rates used in the calculation. To provide a measure of the sensitivity of the calculation to kinetic rates and molecular potential and obtain a perspective as to what variation in the VED would be required to produce such a significant variation in the dissociation rate, consider the following two cases. First, assume that the V-V and V-T models did not accurately identify the "knee" location. If the knee actually was displaced by 1 ev to a higher energy, the final state population and rate would be increased by  $e^{40} \sim 10^{17}$  at 300°K, or a factor of  $(55)^j$  for every tenth of an ev. displacement, j. As a second situation, and really a limiting form of the first case mentioned, consider the possibility of obtaining a VED in which the plateau extends to the dissociation limit. Under these circumstances, neglecting vibrational depletion due to dissociation, the rate would approximately be increased by a factor g, where

$$g = \exp \left[ \frac{(D_0 - E_v)}{kT} \right]$$

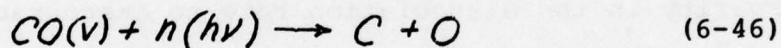
It is therefore critical, in a non-equilibrium ladder climbing analysis of dissociation, to know the magnitude and level scaling of the V-V and V-T rates. This data is currently not available. The current work of Rich (ref 133), Lam (ref 152), and Fisher (ref 161) on V-V and V-T rate measurements for high vibrational states will be extremely beneficial in this respect.

Before setting aside the delicate question of rates, let us return to the reality of experiment and examine Rich's VED data as previously presented in Fig. 6-16. In view of the reasonable agreement obtained between theory and experiment, we conclude that while the heavy particle dissociation rate is extremely sensitive to the magnitude and level scaling of the rates, the rates used in the calculation are adequate. We, therefore, do not attribute the disparity in the dissociation rate to inaccuracies in the V-V and V-T rates.

Continuing now with an examination of the experimental data, we establish that the "ladder" model itself is inconsistent with the experimentally observed dissociation reaction in C0/Ar. The Boltzmann "tail" of the VED of experimental curve onsets at less than 3/4 of the 11 eV. dissociation energy of C0. The approximate population of the last bound state would be  $10^{-50}$  of the total number density yielding a  $k_{d_H}$  of approximately  $10^{-60}$ . This magnitude, although consistent with numerical calculations, is not consistent with the experimentally observed rate. We

therefore conclude that under these conditions dissociation does not only proceed from vibrational states near the dissociation limit. A more efficient reaction channel must exist.

Alternative Processes and Reaction Mechanisms. Let's examine various alternative processes and reaction mechanisms. First, we assume from the description of the experiment, ref (133), that under the present conditions of optical pumping it is reasonable to neglect any electron impact excitation process. We can also neglect any uncertainties in knee location since the experimental distributions were inferred from the radiative properties of the molecule. We consider next the possibility of a multi-photon, photo-dissociation of vibrationally excited CO.

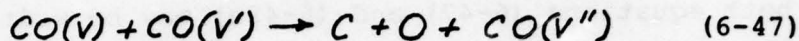


The pump intensities used in the experiment do not favor this process, especially for large  $n \sim 10$  (ref 171). For  $n \sim 3$ , states accessed would lie in the Boltzmann tail and yield a rate much lower than observed. We therefore conclude that the observed dissociation results from a heavy particle collision process. For the dissociation process to be efficient, it must access states in either the plateau or Treanor regions of the VED. We suggest two possible reaction mechanisms:

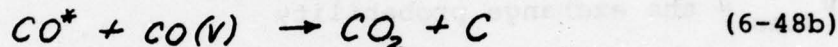
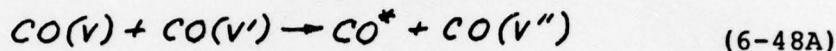
a. Multi-quantum V-V exchange

b. Vibrational-to-Electronic exchange

For mechanism (a) the dissociation reaction proceeds via,



Whereas for mechanism (b), the dissociation reaction is related to the following reaction sequence,



where  $CO^*$  is an electronically excited state of CO. Both reactions require the exchange of significant amounts of vibrational energy, with  $|v-v'| \sim 30$ . Experimental data on multiple quantum exchanges of this order does not exist. However, the recent data of Brechignac (ref 162) for two quantum exchange,  $|v-v'| = 2$ , suggest a large cross-section, up to 20% of that of the single-quantum V-V transition. Theoretical analyses of multiple quantum exchanges are also very limited and complex. These analyses do not address quanta exchanges of the order,  $(\Delta v=30)$ , considered here. However, the theory of Dillon and Stephenson (ref 163) for  $\Delta v=2$  appears to qualitatively agree with the data of Brechignac. It is therefore difficult to directly estimate the transition rates for the reactions given in

equations (6-47) and (6-48). We can, however, estimate the magnitude of the transition rate that would be required to be consistent with the observed dissociation rate. Assuming that reaction equation (6-48a) is rate controlling, both equations (6-47) and (6-48a) may be written as

$$\dot{N}_{CO} = -P_{diss} g N_V N_{V'} \quad (6-49)$$

with

$g$  = the specific collision frequency ( $\text{cm}^3/\text{sec}$ )

$P_{diss}$  = the exchange probability

$N_V$  = the vibrational state population

Rich has stated (ref 164) that the observed dissociation resulted in a variation of less than 1% in the CO density in a time of 60 sec. We can, therefore, place an upper bound on the dissociation coefficient  $k_{dH}$ , at  $10^{-21} \text{ cm}^3/\text{sec}$ . This would require a maximum value of  $P_{diss}$ , for both mechanisms, to be of the order of  $10^{-3}$ - $10^{-6}$ . In view of Brechignac's results (ref 162), we consider this probability to be obtainable and continue with analysis of dissociation via mechanisms (a) and (b).

In discussing non-equilibrium dissociation via a multi-quantum V-V exchange or a V-e transition, we will attempt to characterize dependence of each mechanism on gas temperature and  $T_1$ . In addition, we will examine the consistency

of the proposed mechanisms, a and b, with experimental observations. Finally, simple experiments and parameterizations will be suggested to establish and evaluate the relative importance of each mechanism.

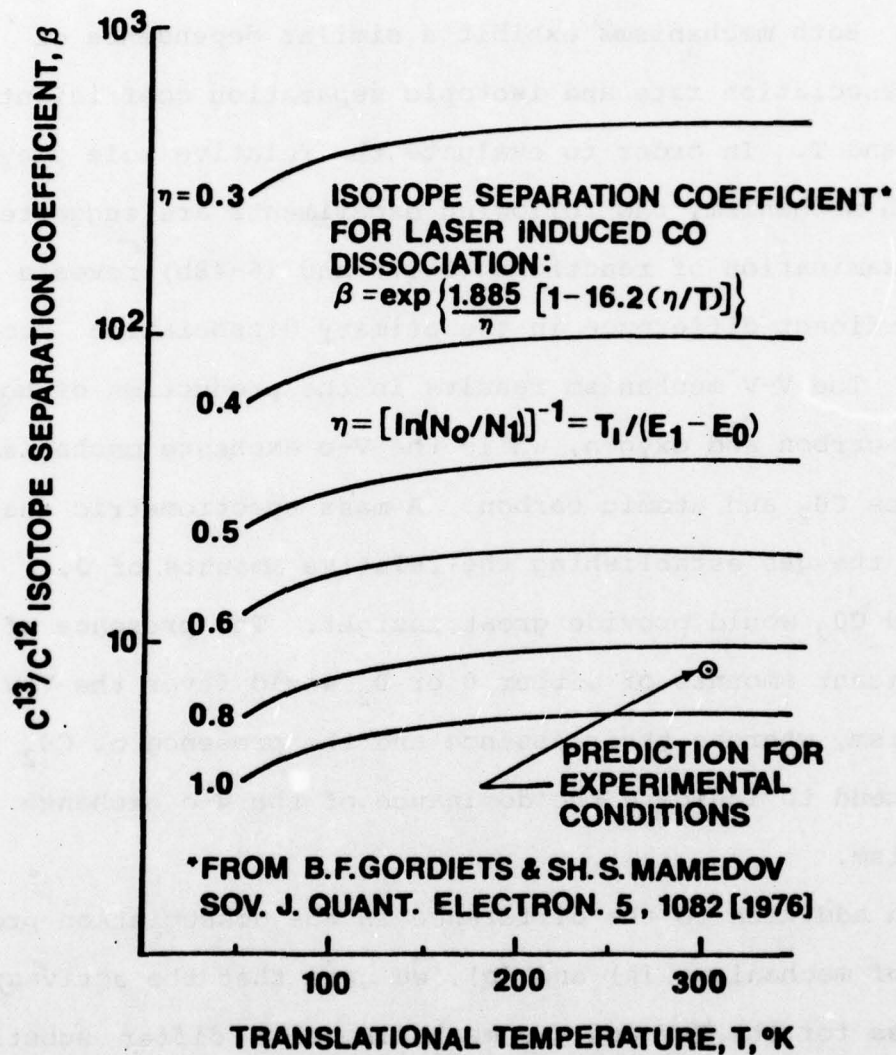
Both mechanisms involve vibrational states in either the Treanor or Plateau regions of the VED. Consequently, they will exhibit a similar dependence on  $T_1$  and  $T$ . The reaction rate, if primarily proportional to the level occupation, will increase with increasing pump rate and increase with decreasing gas temperature at a fixed pump rate. This behavior is consistent with Rich's observation of increased Swan band emission under conditions of higher pumping (ref 133). Despite the fact that the V-e exchange of mechanism (b) results in the formation of  $CO^*$ , which we hypothesize to be  $CO(a^3\Pi)$ , significant emission from the  $CO$  electronic bands would not be anticipated when this mechanism is active. This can be understood by noting that reaction (6-34b) is strongly exothermic probably proceeding at a rate near gas kinetic, (refs 165, 166) while the radiative lifetime,  $\tau_{rad}$ , of this state is of the order of  $10^{-3}$  sec (ref 166). Thus for the experimental conditions the collision time,  $\tau_c < \tau_{rad}$  and a significant  $CO^*$  population will not be obtained. This is consistent with experiment.

Rich observed an isotopic enhancement of several hundred percent in the dissociation products. This enhancement is consistent with either the V-V or V-e mechanism and can be understood in terms of the anharmonic pumping of

the isotope in this binary mixture of diatomics (refs 18, 153, 133). Using the theory of Gordiets (ref 18), Rich (ref 133) has calculated the ratio  $\beta$  of the specific dissociation rate for  $C^{13}O^{16}$  to the corresponding rate for  $C^{12}O^{16}$ . These results (ref 133) are presented in Fig. 6-25 where the separation coefficient,  $\beta$ , is plotted as a function of temperature  $T$ , for various values of  $T_1$ . The essence of the solution can be understood by noting that the calculation assumes that the VED of the isotope is dominated by resonant exchange processes with  $C^{12}O^{16}$ , the normal isotopic abundance being only 1.1%. Since the vibrational energy levels of the isotope are more closely spaced than that of  $C^{12}O^{16}$ , this resonant exchange occurs between different vibrational levels of the isotope and  $C^{12}O^{16}$ . The resonance shift is approximately two vibrational levels. Thus the isotope VED essentially reproduces that of the  $C^{12}O^{16}$  with a two level shift; i.e.

$$\frac{N_v(C^{13}O^{16})}{N_{tot}(C^{13}O^{16})} = \frac{N_{v+2}(C^{12}O^{16})}{N_{tot}(C^{12}O^{16})}$$

This yields a  $T_1$  for the isotope greater than that of  $C^{12}O^{16}$ , and results in a higher relative excited state population in the isotope VED. Note that higher values of  $\eta$  in Fig. 6-24, corresponding to lower  $T_1$ , give a larger separation coefficient, but yield a lower rate magnitude.



# **ISOTOPE SEPARATION COEFFICIENT FOR LASER INDUCED CO DISSOCIATION**

**Fig 6-25** Isotope Separation Coefficient for Laser  
 Induced CO Dissociation (ref 133)

In addition, this analysis reveals that the separation coefficient is fairly insensitive to gas temperature, in quantitative agreement with Rich's observation (ref 133).

Based on the previous discussion, both a V-V or V-e exchange mechanism are consistent with experimental observations. Both mechanisms exhibit a similar dependence of the dissociation rate and isotopic separation coefficient on  $T_1$  and  $T$ . In order to evaluate the relative role played by each mechanism, the following experiments are suggested.

Examination of reactions (6-47) and (6-48b) reveals a significant difference in the primary dissociation products. The V-V mechanism results in the production of both atomic carbon and oxygen, while the V-e exchange mechanism produces  $\text{CO}_2$  and atomic carbon. A mass spectrometric analysis of the gas establishing the relative amounts of  $\text{O}$ ,  $\text{O}_2$ , and  $\text{CO}_2$  would provide great insight. The presence of significant amounts of either  $\text{O}$  or  $\text{O}_2$  would favor the V-V mechanism, whereas their absence and the presence of  $\text{CO}_2$  would tend to indicate the dominance of the V-e exchange mechanism.

In addition to the difference in the dissociation products of mechanisms (a) and (b), we note that the activation energies for the V-V and V-e mechanism also differ substantially. For the V-V mechanism, it is required that  $E_v + E_{v'} > D_{\text{O}}$ , 11 eV.; while for the V-e mechanism  $E_v + E_{v'} > E^*$ ,  $E^*$  denoting the energy of the electronic state, 6.2 eV. for  $\text{CO}(a^3\Pi)$ . Capitalizing on this difference, a sequence of

experiments in which controlled amounts of helium are introduced into the gas mix, while the Swan band intensity is simultaneously being monitored, would establish the dependence of the dissociation rate on the location of the knee in the VED. This information could then be used in conjunction with the results of the gas mass analysis to determine the relationship of  $v$  and  $v'$  for each mechanism. If the V-V process, a, proceeds through states  $v$  and  $v'$ , with  $v' \approx v$ , then a rapid fall off in Swan band intensity would occur only when the knee drops below 5.5 ev. If the process proceeds dominantly with  $v' > v$ , then a more continuous reduction in intensity will be observed as the knee moves to lower energies.

It was previously believed that the V-e transfer process proceeded dominantly through those vibrational levels nearly resonant with the electronic state (ref 168). More recent data has revealed that this situation does not always hold (ref 169). The helium addition experiments would shed light on this aspect of the V-e transfer. If a cutoff of the dissociation reaction is observed when the knee drops below 6.2 ev., a resonant exchange would be suggested. A "softer" fall off of the dissociation rate, on the other hand, would favor an off resonant exchange.

Further work, both theoretical and experimental, is required in the area of V-e and V-V exchanges. However, based on Rich's experimental data and our analysis, both mechanisms offer the possibility of a more efficient channel

for the non-equilibrium dissociation of diatomic molecules and provide a simple method of achieving significant isotope separation factors using optical pumping.

## Chapter VII. A Review and Some Considerations for Future Study

### General Review

In the present study, we have performed a detailed and comprehensive analysis of the collisionally induced dissociation of diatomic molecules under equilibrium and non-equilibrium conditions. In this chapter we will highlight the interesting and important results. By referring again to Table II, one can establish the scope of previous works and note the contradictions that exist in these studies. This study has resolved many of these inconsistencies. We have utilized both time-dependent and steady-state analyses of the Master Equation while incorporating an experimentally consistent set of exchange rates. Within this computational framework, we have critically evaluated three different dissociation models and established the significant influence of rotation, vibrational depletion, equal energy transitions, V-V exchanges, and electronic states on the dissociation reaction. The scope of this analysis has been broad, including calculations for  $H_2$ ,  $O_2$ ,  $N_2$ ,  $CO$ ,  $Br_2$ , and  $I_2$ ; and examination of both dissociation and recombination coefficients. In our parameterization of dissociation under non-equilibrium conditions, we have considered excitation due to electron impact and optical pumping and evaluated the relative importance of electron impact and thermal dissociation.

### New Aspects of Dissociation for Near-Equilibrium Conditions

The emphasis of the near equilibrium aspect of this study has been directed toward the critical evaluation of collisional theories of the thermal dissociation of diatomic molecules. Semi-classical exchange probabilities based on a distorted wave treatment were utilized in time-dependent and steady-state solutions of the kinetic equations. The dissociation process, in pure diatomic gases and diatomic gases highly diluted in an inert gas, was parameterized over a wide range of temperatures and gases. In this parameterization, to evaluate the rotational contribution to dissociation, three kinetic models of dissociation were considered:

1. Standard Ladder
2. Coupled Model
3. Uncoupled Model

In addition, the implications of equal energy transitions were examined within the framework of the rotational models, (2) and (3), and these results contrasted with the more standard "over-the-top" mechanism.

A time-dependent solution of the Master Equation established that the VED rapidly attains a pseudo-steady-state, Figs. 5-2 and 5-3. This steady-state distribution deviates substantially from the equilibrium distribution because of vibrational-dissociative coupling. The resulting depletion of population substantially reduces the

dissociation rate from that which would be obtained if the coupling were not considered. Induction times were calculated for the various models. No significant variation in induction times was observed among the dissociation models considered. We concluded that this indicated that the induction time is primarily controlled by the relaxation or exchange rates and is relatively insensitive to the vibrational biases of the dissociation process considered here. A comparison of predicted and experimental induction times, Fig. 5-5, showed good agreement with experiment except at very high temperatures. At temperatures in excess of 10,000°K, the calculated incubation times were too long. We concluded that this deviation at high temperatures can be attributed to a more rapid relaxation due to the increased importance of multiple quantum V-T transitions in this temperature range. It is only in this temperature range, however, that collisions are sufficiently impulsive that multiple quantum transitions need be considered. When sufficient transition rate data becomes available, a realistic attempt at substantiating this hypothesis can be made.

The quasi-steady-state dissociation coefficient was calculated for the three models and compared to experimental data for mixtures of a diatomic gas highly diluted in argon. Gases considered included  $H_2$ ,  $O_2$ ,  $N_2$ , CO,  $Br_2$ , and  $I_2$ . From this comparison, we establish three significant points. First, the standard ladder model is inadequate and yields dissociation coefficients that are much too low. Second,

models including the influence of rotation predicted larger dissociation coefficients than those obtained from the standard ladder model. These coefficients exhibited substantial agreement with experiment for all gases considered. Within the rotational models, equal energy transitions were found to yield an additional increase in the dissociation rates; (the increase was especially marked in  $\text{Br}_2$  and  $\text{I}_2$ ), and decrease the activation energy in comparison to the over-the-top model. Agreement with experiment was further improved by their inclusion. This latter observation is consistent with the recent results of trajectory calculations for dissociation in  $\text{I}_2$  (ref 92).

Dissociation in pure diatomic gases was then considered in an effort to establish the cause of the observed rate enhancement. This analysis revealed that the observed rate enhancement can not be attributed to changes in collisional efficiencies based upon mass variation. However, V-V exchanges lead to rate enhancements similar in magnitude and temperature dependence to those experimentally observed.

Having established the predictive capabilities of the rotational models regarding the dissociation coefficients in dilute and pure gases, a comparison of the calculated recombination coefficients with experiment was presented. This comparison expands the temperature range over which the models can be evaluated and provides a detailed examination of the pre-exponential factor in the dissociation coefficient. Reasonable agreement with experiment was

achieved for all gases considered, demonstrating an ability to quantitatively correlate very high and low temperature rate measurements for a wide variety of gases. The equal energy transition model was found to yield not only a more reasonable magnitude for the recombination coefficient, but also a temperature dependence consistent with experimental data over the entire temperature range.

As a consequence of this aspect of the study, we reach the broad conclusion that collisionally induced thermal dissociation rates of diatomic molecules can be accurately calculated using a simple molecular model which includes both rotational structure and equal energy transitions.

#### Non-equilibrium Dissociation--Heavy Particle Vs. Electron Impact

An examination of dissociation under highly non-equilibrium conditions was utilized to illustrate the effect of non-equilibrium on a simple chemical process. A parametric mapping of heavy particle and electron impact induced dissociation was performed. For the vibrational kinetic analysis, we utilized the Master Equation formalism previously developed for the near equilibrium case. The electron impact analysis of dissociation was based on a steady-state solution of the collisional Boltzmann equation.

The electron impact analysis showed that significant dissociation occurs under normal discharge operating conditions. The magnitude of the dissociation rate exhibits a strong dependence on  $E/N$ , and is substantially enhanced due

to the influence of superelastic vibrational collisions. Within this analysis, the influence of dissociation from excited vibrational states was considered. A considerable increase in the rate of dissociation, Fig 6-18, was noted. The magnitude of this enhancement reflected the highly non-equilibrium nature of both the VED and eed under normal discharge operating conditions.

The dissociation rate due to heavy particle collisions was examined over the discharge parameter space. A time-dependent solution of the Master Equation established the existence of a quasi-steady-state for the VED under the non-equilibrium conditions considered and revealed the temporal development of the three characteristic regions of the VED. The calculation was benchmarked against the experimental data of Rich (ref 133) and showed good agreement with experimentally inferred distributions. The predicted heavy particle dissociation rate was compared with the electron impact rate. Electron impact dissociation was determined to substantially exceed the heavy particle rate for typical discharge operating conditions. In order to complete the parameterization of the heavy particle rate, excitation achieved by means of intense optical pumping was considered. Based upon this analysis, within the framework of the ladder model, we concluded that it is difficult to achieve substantial heavy particle collision induced dissociation under non-equilibrium conditions. This conclusion, however, was inconsistent with Rich's experimental

observation of substantial dissociation in CO. We, therefore, decided that a more efficient reaction channel for CO dissociation must exist. A multi-quantum V-V exchange mechanism and a V-e exchange mechanism were proposed and were shown to be consistent with available experimental data. Experiments were suggested to evaluate the effectiveness of each of the proposed exchanges.

#### Considerations for Future Study

In the course of this study we have examined the dissociation process under equilibrium and non-equilibrium conditions. As a result of these analyses, the following broad areas can be identified as warranting further theoretical and experimental investigation:

- a. Heavy particle energy transfer rates
- b. Excited state reactions

These areas are not mutually exclusive, but are generically different in the way they affect the dissociation process. The heavy particle transfer rates form the kinetic basis for a Master Equation approach. Whereas, excited state reactions dictate the critical reaction channels to be considered.

Significant strides have been made in the theoretical field of heavy particle kinetics using semi-classical or exact quantum mechanical calculations of inelastic collision processes. Much of this work is based on the availability of improved interaction potentials. The

experimental and theoretical determination of these potentials is critical if accurate predictions of energy transfer rates are to be achieved.

New experimental techniques (refs 133, 161) are complementing and capitalizing on the recent theoretical predictions; however, the following rate deficiencies still exist:

1. There is a lack of sufficient experimental data relating to the dependence of V-T, V-V, V-R-T, V-R-V-R-T, vibrational rate coefficients on the initial state quantum number.

2. Multiple quantum V-V and V-T exchanges have received little critical consideration. In view of Brechniacs' recent results and their implications, further work should be devoted to this topic.

3. Finally, vibrational to electronic, V-e, or electronic to vibrational, e-V, transfers should be given attention commensurate with the unique possibilities they offer. The possibilities of new lasers based on electronic transitions, isotope separation, and new energy storage concepts using metastable states should spur new research in this area.

The experimental observation (refs 105, 108) and our numerical confirmation of the participation of excited electronic states in CO dissociation process suggest that further efforts and new techniques be applied to establish the role of excited states in the dissociation process. Under non-equilibrium conditions, we have established that

excited vibrational and electronic states can significantly alter reaction rates, discharge chemistry, and laser efficiency. Further work is required in this area to establish excited state, vibrational and electronic, electron impact excitation and ionization cross-sections. Detailed knowledge of these cross-sections offers the opportunity to control electric discharge chemistry, optimize discharge efficiency, and temporally tailor discharge excitation.

### Bibliography

1. Bletzinger, P., D. LaBorde, W. F. Bailey, W. H. Long, P. D. Tannen, and A. Garscadden. "The Influence of Contaminants on the CO<sub>2</sub> Electric-Discharge Laser." IEEE Journal of Quantum Electronics, QE-11 (1975).
2. Breshears, W. D. and P. F. Bird. Symposium on Combustion 14th Univ. Park, D.A. (1973), p. 211; "Density Gradient Measurements of HCl Dissociation in Shock Waves." Journal of Chemical Physics, 58:5176 (1973).
3. Hanson, R. K. and D. Baganoff. "Shock Tube Study of Nitrogen Dissociation Using Pressure Measurements." AIAA Journal, 10:211 (1972).
4. Appleton, J. P., M. Steinberg, and D. J. Liquornik. "Shock Tube Study of Carbon Monoxide Dissociation Using Vacuum-Ultraviolet Absorption." Journal of Chemical Physics, 52:2205 (1970).
5. Millikan, R. C. and D. R. White. "Systematics of Vibrational Relaxation." Journal of Chemical Physics, 44:668 (1966).
6. Kiefer, J. H. and R. W. Lutz. "Vibrational Relaxation of Hydrogen." Journal of Chemical Physics, 44:668 (1966).
7. Breshears, W. P. and P. F. Bird. "Effect of Oxygen Atoms on the Vibrational Relaxation of Nitrogen." Journal of Chemical Physics, 48:4768 (1968).
8. Serry, D. J. "Vibrational Relaxation in HCl with Inert Gas Collision Partners." Journal of Chemical Physics, 58:1796 (1973).
9. Johnston, H. and J. Birkes. "Activation Energies for the Dissociation of Diatomic Molecules are Less Than the Bond Dissociation Energies." Accounts of Chemical Research, 5:327 (1972).
10. Tregay, G. W., W. G. Valence, and P. I. MacLean. "Dissociation of Diatomic Molecules I. Effect of Limited Number of Rotational States." Journal of Chemical Physics, 59:1634 (1973).

11. Dove, J. E. and D. G. Jones. "Effect of Rotation on Computed Thermal Dissociation Rate of  $H_2$ ." Chemical Physics Letters, 17:134 (1972).
12. Wengle, H. "Vibrational Relaxation and Dissociation of Diatomic Molecules." Zeitschrift Fur angewante Mathematik und Physik (SAMP), 26:377 (1975).
13. Kiefer, J. H., H. P. Joosten, and W. D. Breshears. "On the Preference for Vibrational Energy in Diatomic Dissociation." Chemical Physics Letters, 30:424 (1975).
14. Rich, J. W. "Dissociation and Energy Transfer in Diatomic Molecular Systems." Ph.D. Dissertation, Princeton University, Department of Chemistry (1964).
15. Kiefer, J. H. "Effect of V-V Transfer on the Rate of Diatomic Dissociation." Journal of Chemical Physics, 57:1938 (1972).
16. Gordiets, B. F., A. I. Osipov, and L. A. Shelipen. "Non-Equilibrium Dissociation Processes and Molecular Lasers." Soviet Physics, JETP, 34:2 (1972).
17. Belenov, E. M., et al. "Isotope Separation in Chemical Reactions Not in Thermodynamic Equilibrium." Soviet Physics Technical Physics, 20:9 (1975).
18. Gordiets, B. F. and Sh. S. Mamedov. "Isotope Separation in Chemical Reactions of Vibrationally Excited Molecules." Soviet Journal of Quantum Electronics, 5:1082 (1975).
19. Landau, L. and E. Teller. "The Theory of Sound Dispersion." S.L.A. Translation of "Zur Theorie Der Schalldispersion." Physik Zeitschrift Der Sowjetunion, 10:34 (1963).
20. Schwartz, R. N., Z. I. Slawsky, and K. F. Herzfeld. "Calculation of Vibrational Relaxation Times in Gases." Journal of Chemical Physics, 20:1591 (1952).
21. Jackson, J. M. and N. F. Mott. "Energy Exchange Between Inert Gas Atoms and A Solid Surface." Proceedings of the Royal Society (London), A137:703 (1932).
22. Herzfeld, K. F. and T. A. Litovitz. Absorption and Dispersion of Ultrasonic Waves. New York: Academic Press (1959).
23. Takayanagi, K. Advances in Atomic and Molecular Physics, Vol. 1, 1949 (1965).

24. Cottrell, T. L. and J. C. McCoubrey. Molecular Energy Transfer in Gases. London: Butterworths (1961).
25. Rapp, D. and T. Kassel. "The Theory of Vibrational Energy Transfer Between Simple Molecules in Non-reactive Collisions." Chemical Review, 69:61 (1969).
26. Nikitin, E. E. Theory of Elementary Atomic and Molecular Processes in Gases. Oxford: Clarendon Press (1974).
27. Mies, F. H. "Effects of Anharmonicity on Vibrational Energy Transfer." Journal of Chemical Physics, 40:523 (1964); Mies, F. H. "Impact Parameter Treatment of Vibrational Excitation." Journal of Chemical Physics, 41:903 (1964).
28. Keck, J. and G. Carrier. "Diffusion Theory of Non-Equilibrium Dissociation and Recombination." Journal of Chemical Physics, 43:2284 (1965).
29. Rich, J. W. and C. E. Treanor. Annual Review of Fluid Mechanics, 2:355 (1970).
30. Secrest, D. Annual Review of Physical Chemistry, 24:379 (1973).
31. Verter, M. R. and H. Rabitz. "Theoretical Evaluation of Vibrational Transition Rates and Relaxation in CO-He." Journal of Chemical Physics, 64:2939 (1976).
32. McKenzie, R. NASA Technical Report, NASA TR R-466. Vibration-Translation Energy Transfer in Vibrationally Excited Diatomic Molecules, October (1976).
33. Hancock, G. and I. W. M. Smith. "Quenching of Infrared Chemiluminescence. 1: The Rates of De-Excitation of CO(4<v<13) by He, CO, NO, N<sub>2</sub>, O<sub>2</sub>, OCS, N<sub>2</sub>O, and CO<sub>2</sub>." Applied Optics, 10:1827 (1971).
34. Callear, A. B. and I. W. M. Smith. "Fluorescence of Nitric Oxide, Part 2, Vibrational Energy Transfer between NO A<sup>2</sup>Σ<sup>+</sup>(v=3,2, and 1) and N<sub>2</sub>X<sup>1</sup>Σ<sub>g</sub><sup>+</sup>(v=0)." Transactions of the Faraday Society, 59:1735 (1963).
35. Stanley, C. R. "A Method for the Determination of Collision Induced Vibrational Transition Probabilities with Results for N<sub>2</sub>(B<sup>3</sup>Π<sub>g</sub>)-N<sub>2</sub> Collisions." Proceedings of the Royal Society, A, 241:180 (1957).
36. Steinfeld, J. I. and W. Klemperer. "Energy Transfer Processes in Monochromatically Excited Iodine Molecules." Journal of Chemical Physics, 42:3475 (1965).

37. Fowler, R. and E. A. Guggenheim. Statistical Thermodynamics. London: Cambridge University Press (1952).
38. Rice, O. K. "On the Recombination of Iodine and Bromine Atoms." Journal of Chemical Physics, 9:258 (1941).
39. Rice, O. K. "Reply to Careri's 'Note on the Rate of Recombination of Free Atoms.'" Journal of Chemical Physics, 21:750 (1953).
40. Careri, D. Nuovo Cim. 6:94 (1949); 7:155 (1950).
41. Careri, D. "Note on the Rate of Recombination of Free Atoms." Journal of Chemical Physics, 21:749 (1953).
42. Keck, J. C. "Variational Theory of Chemical Reaction Rates Applied to 3-Body Recombination." Journal of Chemical Physics, 32:1035 (1960).
43. Keck, J. C. and G. Carrier. "Diffusion Theory of Non-Equilibrium Dissociation and Recombination." Journal of Chemical Physics, 43:2284 (1965).
44. Keck, J. C. "Variational Theory of Reaction Rates." Advances in Chemical Physics, 13:851 (1967).
45. Wigner, E. "Calculation of the Rate of Elementary Association Reactions." Journal of Chemical Physics, 5:720 (1937).
46. Wigner, E. "Some Remarks on the Theory of Reaction Rates." Journal of Chemical Physics, 7:646 (1939).
47. Wigner, E. "The Transition State Method." Transactions of the Faraday Society, 34:29 (1938).
48. Nikitin, E. E. "On Deviations From the Boltzmann Distribution in the Dissociation of Diatomic Molecules." Soviet Physics, Doklady, 2:453 (1957).
49. Nikitin, E. E. "Calculation of the Rate of Thermal Decomposition of Diatomic Molecules." Proceedings of the Academy of Sciences of the USSR (Dok. Ak. Nauk), p. 197 (1958).
50. Nikitin, E. E. "Theory of Thermal Second Order Decomposition of Molecules." Journal of Chemical Physics, 31:1371 (1959).
51. Stupochenko, E. V. and A. I. Osipov. "Kinetics of Thermal Dissociation of Diatomic Molecules." Journal of Physical Chemistry, 33:36 (1959).

52. Montroll, E. W. and K. E. Shuler. "Studies in Non-Equilibrium Rates Processes. I. The Relaxation of a System of Harmonic Oscillators." Journal of Chemical Physics, 26:464 (1957).
53. Shuler, K. F. "Studies in Non-Equilibrium Rate Processes. II. The Relaxation of Vibrational Non-Equilibrium Distributions in Chemical Reactions and Shock Waves." Journal of Physical Chemistry, 65:849 (1957).
54. Bazley, N. W., et al. "Studies in Non-Equilibrium Rate Processes. III. The Vibrational Relaxation of a System of Anharmonic Oscillators." Journal of Chemical Physics, 28:700 (1958).
55. Montroll, E. W. and K. E. Shuler. "The Application of the Theory of Stochastic Processes to Chemical Kinetics." Advances in Chemical Physics, Vol. I, p. 361, ed. by I. Prigogine. New York: Interscience (1958).
56. Shuler, K. E. "Vibrational Distribution Functions in Bimolecular Dissociation Reactions." Journal of Chemical Physics, 31:1375 (1959).
57. Pritchard, H. O. "The Kinetics of Dissociation of a Diatomic Gas." Journal of Physical Chemistry, 65:504 (1961).
58. Benson, S. W. and T. Fueno. "Mechanism of Atom Recombination by Consecutive Vibrational Deactivations." Journal of Chemical Physics, 36:1597 (1962).
59. Treanor, C. E. and P. V. Marrone. "Effect of Dissociation on the Rate of Vibrational Relaxation." Physics of Fluids, 5:1022 (1962).
60. Marrone, P. V. and C. E. Treanor. "Chemical Relaxation with Preferential Dissociation from Excited Vibrational Levels." Physics of Fluids, 6:1215 (1963).
61. Herzfeld, K. F. "The Rate and Mechanism of the Thermal Dissociation of Oxygen." Seventh Symposium on Combustion, p. 27. London: Scientific Publications (1959).
62. Bauer, S. H. and S. C. Tsang. "Mechanisms for Vibrational Relaxation at High Temperatures." Physics of Fluids, 6:182 (1963).

63. Snider, N. S. On the Theory of Rates of Dissociation and Recombination of Diatomic Molecules. Ph.D. Dissertation, Princeton University, Department of Chemistry (1964).
64. Rich, J. W. Dissociation and Energy Transfer in Diatomic Molecular Systems. Ph.D. Dissertation, Princeton University, Department of Aeronautical Engineering (1965).
65. Dove, J. E. and D. G. Jones. "Numerical Calculation of Vibrational Relaxation and Dissociation for a Quantum Anharmonic Oscillator." Journal of Chemical Physics, 55:1531 (1971).
66. Dove, J. E. and D. G. Jones. "Effect of Rotation on the Computed Thermal Dissociation Rate in H<sub>2</sub>." Chemical Physics Letters, 17:134 (1972).
67. Roberts, R. E., R. B. Bernstein, and E. B. Curtiss. "Resonance Theory of Termolecular Recombination Kinetics, H+H+M→H<sub>2</sub>+M." Journal of Chemical Physics, 50:5163 (1969).
68. Johnston, H. and J. Birks. "Activation Energies for the Dissociation of Diatomic Molecules are Less Than the Bond Dissociation Energies." Accounts of Chemical Research, 5:327 (1972).
69. Kiefer, J. H. "Effect of V-V Transfer on the Rate of Diatomic Dissociation." Journal of Chemical Physics, 57:5 (1972).
70. Ashton, T., D. McElwain, and H. O. Pritchard. "The Master Equation for Dissociation of a Dilute Diatomic Gas. VIII. The Rotational Contribution to Dissociation and Recombination." Canadian Journal of Chemistry, 51:237 (1973).
71. Pritchard, H. O. "The Master Equation for Dissociation of a Dilute Diatomic Gas. X. How Rotation Causes Low Arrhenius Temperature Coefficients." Canadian Journal of Chemistry, 51:3152 (1973).
72. Pritchard, H. O. "Why Atoms Recombine More Slowly as the Temperature Goes Up." Accounts of Chemical Research, 9:99 (1976).
73. Kiefer, J. H., H. P. G. Joosten, and W. D. Breshears. "On the Preference for Vibrational Energy in Diatomic Dissociation." Chemical Physics Letters 30:424 (1975).

74. Kewley, D. J. "Numerical Study of Anharmonic Diatomic Relaxation Rates in Shock Waves and Nozzles." Journal of Physics, B, Molecular Physics, 8:15 (1975).
75. Lo Dato, W. A., D. L. S. McElwain, and H. O. Pritchard. "The Master Equation for the Dissociation of a Dilute Diatomic Gas. I. A Method of Solution." Journal of the American Chemical Society, 91:7688 (1969).
76. Davies, P. K. and I. Oppenheim. "Vibrational Relaxation in Gases--Some Constraints on the Use of the Master Equations." Journal of Chemical Physics, 56: 86 (1972).
77. Flugge, S. Practical Quantum Mechanics I, pp. 82-189. Berlin: Springer-Verlag (1971).
78. Herzberg, G. Molecular Spectra and Molecular Structure. New York: Van Nostrand Reinhold Co. (1950).
79. Millikan, R. C. and D. R. White. "Systematics of Vibrational Relaxation." Journal of Chemical Physics, 44:668 (1966).
80. Miller, D. J. and R. C. Millikan. "Vibrational Relaxation of Carbon Monoxide by Hydrogen and Helium Down to 100°K." Journal of Chemical Physics, 53:3384 (1970).
81. Sharma, R. D. and C. A. Brau. "Energy Transfer in Near Resonant Molecular Collisions due to Long Range Forces with Application to Transfer of Vibrational Energy from  $\nu^3$  Mode of CO<sub>2</sub> to N<sub>2</sub>." Journal of Chemical Physics, 50:924 (1969).
82. Fisher, E. and R. H. Kummeler. "Relaxation by Vibration-Vibration Exchange Processes. Part I. Pure Gas Case." Journal of Chemical Physics, 49:1075 (1968).
83. Benson, S. W. The Foundations of Chemical Kinetics. New York: McGraw Hill (1960).
84. Gear, C. W. Numerical Initial Value Problems in Ordinary Differential Equations. Englewood Cliffs, New Jersey: Prentice-Hall (1971).
85. Gear, C. W. "The Automatic Integration of Stiff Ordinary Differential Equations." Communications in ACM, 14:176 (1971).
86. Kummeler, R. H., E. R. Fisher, et al. "Analytical and Laboratory Studies on Upper Atmospheric Energy Transfer Processes." AFCRL-TR-73-0605, pp. 20-54 (1973).

87. Bauer, S. H., D. Hilden, and P. Jeffers. "Relative Roles of Ensemble Constraints vs Cross Sections in Hydrogen Dissociation." Journal of Chemical Physics, 80:922 (1976).
88. Kewley, D. J. "Numerical Study of Anharmonic Diatomic Relaxation Rates in Shock Tubes and Nozzles." Journal of Physics, B, Molecular Physics, 8:2565 (1975).
89. Rockwood, S. D., J. E. Brau, W. A. Proctor, and G. H. Canavan. "Time Dependent Calculations of Carbon Monoxide Laser Kinetics." IEEE Journal of Quantum Electronics, QE-9:120 (1973).
90. Pritchard, H. O. "Reacting Kinetics." Vol. I. Specialist Periodical Reports. London: The Chemical Society (1975), pp. 243-290.
91. Nikitin, E. E. Theory of Thermally Induced Gas Phase Reactions. Bloomington: Indiana University Press (1966).
92. Wong, W. H. and G. Burne. "Dynamics of Collisional Dissociation: I<sub>2</sub> in Ar and Xe." Proceedings of the Royal Society, London, A, 341:105 (1974).
93. Camac, M. and A. Vaughan. "O<sub>2</sub> Dissociation Rates in O<sub>2</sub>-Ar Mixtures." Journal of Chemical Physics, 34:460 (1961).
94. Watt, W. S. and A. L. Myerson. "Atom Formation Rates Behind Shock Waves in Oxygen." Journal of Chemical Physics, 51:1638 (1969).
95. Wray, K. L. "Shock Tube Study of the Coupling of O<sub>2</sub>-Ar Rates of Dissociation and Relaxation." Journal of Chemical Physics, 37:1254 (1962).
96. Sutton, E. A. "Measurement of the Dissociation Rates of Hydrogen and Deuterium." Cornell University, Graduate School of Aeronautical Engineering Report, Ithaca, New York. (Undated.)
97. Byron, S. R. "Measurement of the Rate of Dissociation of Oxygen." Journal of Chemical Physics, 30:1380 (1959).
98. Wray, K. L. Tenth Symposium (International) on Combustion, p. 523, The Combustion Institute (1965).
99. Rich, J. W. J. A. Lordi, R. A. Gibson, and S. W. Kang. "Supersonic Electrically Excited Laser Development." Calspan Report No. WG-5164-A-3 (1974).

100. Anderson, O. L. "Shock Tube Measurement of Oxygen Dissociation Rates in Argon." United Aircraft Corporation Research Labs, Report R-1828-1 (1961).
101. Appleton, J. P., M. Steinberg, and D. J. Liguornik. "Shock Tube Study of Nitrogen Dissociation Using Vacuum Ultraviolet Light Absorption." Journal of Chemical Physics, 48:599 (1968).
102. Palmer, H. B. and D. F. Hornig. "Rate of Dissociation of Bromine in Shock Waves." Journal of Chemical Physics, 26:98 (1957).
103. Strong, R. L., J. C. W. Chien, et al. "Studies of I Atom and Br Atom Recombination Following Flash Photolysis of I<sub>2</sub> and Br<sub>2</sub>." Journal of Chemical Physics, 26:1287 (1957).
104. Britton, D., N. Davidson, W. Gehman, and G. Schott. "Shock Waves in Chemical Kinetics: Further Studies on the Rate of Dissociation of Molecular Iodine." Journal of Chemical Physics, 25:804 (1956).
105. Appleton, J. P., M. Steinberg, and D. J. Liguornik. "Shock Tube Study of Carbon Monoxide Dissociation Using Vacuum-Ultraviolet Absorption." Journal of Chemical Physics, 52:2205 (1970).
106. Davies, W. O. "Radiative Energy Transfer on Entry into Mars and Venus." ITT Research Institute, Chicago, Illinois (Quarterly Report No. 8 to NASA), August, 1964.
107. Presley, L. L. C. Chackerian, and R. Watson. "AIAA Paper No. 66-518, 4th Aerospace Sciences Meeting, June, 1966.
108. Fairbairn, A. R. "The Dissociation of Carbon Monoxide." Proceedings of the Royal Society, A, 312:207 (1969).
109. Shui, V. H., J. P. Appleton, and J. C. Keck. "The Three-Body Recombination and Dissociation of Diatomic Molecules: A Comparison Between Theory and Experiment." Massachusetts Institute of Technology, Fluid Mechanics Laboratory, Publication No. 70-3 (1970).
110. Breshears, W. D. and P. F. Bird. International Combustion Proceedings, 14th, LA-DC-72-369 (1972).

111. Rapp, D. and P. Englander-Golden. "Resonant and Near Resonant Vibrational Energy Transfer Between Molecules in Collision." Journal of Chemical Physics, 40:3120 (1964), as presented in ref 86.
112. Jacobs, T. A., R. R. Giedt, and H. J. Cohen. "Kinetics of Hydrogen Halides in Shock Waves. II. A New Measurement of the Hydrogen Dissociation Rate." Journal of Chemical Physics, 47:54 (1967).
113. Hurle, I. R., A. Jones, and J. L. Rosenfeld. "Shock Wave Observations of Rate Constants for Atomic Hydrogen Recombination from 2500 to 7000°K." Proceedings of the Royal Society, A, 310:253 (1969).
114. Sutton, E. A. "Measurement of the Dissociation Rates of Hydrogen and Deuterium." Journal of Chemical Physics, 36:2923 (1962).
115. Myerson, A. L. and W. S. Watt. "Atom Formation Rates Behind Shock Waves in Hydrogen and the Effect of Added Oxygen." Journal of Chemical Physics, 49:425 (1968).
116. Larkin, F. S. and B. A. Thrush. Tenth Symposium on Combustion, p. 397, The Combustion Institute (1965).
117. Larkin, F. S. "Homogeneous Rate of Recombination of Hydrogen Atoms." Canadian Journal of Chemistry, 46: 1005 (1968).
118. Watt, W. S. and A. L. Myerson. "Atom Formation Rates Behind Shock Waves in Oxygen." Cornell Aeronautical Laboratory, CAL. AD-1689-A-9, February (1969).
119. Campbell, I. M. and B. A. Thrush. "The Association of Oxygen Atoms and Their Combination with Nitrogen Atoms." Proceedings of the Royal Society, A, 296: 222 (1967).
120. Campbell, I. M. and B. A. Thrush. "The Recombination of Nitrogen Atoms and the Nitrogen Afterglow." Proceedings of the Royal Society, A, 296:201 (1967).
121. Clyne, M. A. and D. Stedman. "Rate of Recombination of Nitrogen Atoms." Journal of Physical Chemistry, 71:307 (1967).
122. Appleton, J. P., M. Steinberg, and D. J. Liguornik. "Shock Tube Study of Nitrogen Dissociation Using Vacuum Ultraviolet Light Absorption." Journal of Chemical Physics, 48:599 (1968).

123. Byron, S. J. "Measurement of the Dissociation Rate of Oxygen." Journal of Chemical Physics, 44:1378 (1966).
124. Cary, B. Physics of Fluids, 8:26 (1965); K. L. Wray and S. Byron. "Shock Tube Study of the Thermal Dissociation of Nitrogen." Ibid, 9:1046 (1966); B. Cary, "Comments on 'Shock Tube Study of the Thermal Dissociation of Nitrogen.'" Ibid, 9:1047 (1966).
125. Ip, J. K. and G. Burns. "Recombination of Br atoms by Flash Photolysis, II. Br<sub>2</sub> in He, Ne, Ar, Kr, N<sub>2</sub> and O<sub>2</sub>." Journal of Chemical Physics, 51:34 (1969).
126. Ip, J. K. and G. Burns. "Recombination of Br Atoms by Flash Photolysis over a Wide Temperature Range." Discussions of the Faraday Society, 44:241 (1967).
127. Ip, J. K. and G. Burns. "Negative Temperature Coefficient of Atomic Recombination Rate Constant from Flash Photolysis and Shock Wave Data, Bromine." Journal of Chemical Physics, 51:3414 (1969).
128. Boyd, R, K, G. Burns, T. R. Lawrence, and J. Lippiatt. Journal of Chemical Physics, 49:3804 (1968).
129. Porter, G. and J. A. Smith. "The Recombination of Atoms III. Temperature Coefficients of Iodine Atom Recombination." Proceedings of the Royal Society, A, 261:28 (1961).
130. Bunker, D. L. and N. Davidson. "A Further Study of the Flash Photolysis of Iodine." Journal of the American Chemical Society, 80:5085 (1958).
131. Britton, D. L., N. Davidson, W. Gehman, and G. Schott. "Shock Waves in Chemical Kinetics: Further Studies on the Rate of Dissociation of Molecular Iodine." Journal of Chemical Physics, 25:804 (1956).
132. Troe, J. and H. G. Wagner. Zeitschrift Physik Chem, 55:326 (1967).
133. Rich, J. W., R. C. Bergman, and M. J. Williams. "Measurement of Kinetic Rates for Carbon Monoxide Laser Systems." Calspan Report No. WG-6021-A-1, November (1977).
134. Kieffer, L. J. "A Compilation of Electron Collision Cross Section Data for Modeling Gas Discharge Lasers." J.I.L.A. Information Center Report 13, September (1973).

135. Dreicer, H. "Electron Velocity Distributions in a Partially Ionized Gas." Physical Review, 117:343 (1960).
136. Holstein, T. "Energy Distribution of Electrons in High Frequency Gas Discharges." Physical Review, 70:367 (1946).
137. MacDonald, A.D. Microwave Breakdown in Gases. New York: John Wiley & Sons, Inc. (1966).
138. Pistoiresi, D. J. and D. Nelson. "Supersonic CO Laser Code." Boeing Aerospace Company, AFWL-TR-75-256 (1977).
139. Sherman B. "The Difference-Differential Equation of Electron Energy Distribution in a Gas." Journal of Math. Analysis and Applications, 1:342 (1960).
140. Abramowitz, M. and I. A. Stegun. Handbook of Mathematical Functions. National Bureau of Standards, AMS 55 (1964).
141. Hake, R. D. and A. V. Phelps. Physical Review, 1958: 70 (1967).
142. Erhardt, H. and K. Willmann. Zeit. Phys., 204:462 (1967).
143. Schulz, G. "Vibrational Excitation of N<sub>2</sub>, CO, and H<sub>2</sub> by Electron Impact on Atoms and Molecules." NRDS, NBS-50 (October 1973).
144. Chen, J. C. Y. "Theory of Subexcitation Electron Scattering by Molecules II, Excitation and Deexcitation of Molecular Vibration." Journal of Chemical Physics, 40:3513 (1964).
145. Poe, R. "Calculation of Electron Impact Cross Sections in CO." Air Force Aero Propulsion Lab., Contract Status Report (1978).
146. De Joseph. Private Communication.
147. Boness, M. J. W. 30th Gaseous Electronics Conference, Workshop on Electron-Excited State Collisions, Palo Alto, California (October 1977).
148. Land, J. E. "Cross Sections and Transport Coefficients for Electrons in Carbon Monoxide, CO." Supp. to J.I.L.A. Pub. No. 1660, Memo 2 (1977).

149. Englander-Golden, P. and D. Rapp. "Total Cross Section for Ionization of Atoms and Molecules by Electron Impact." LMSC 6-74-64-12, Lockheed Missiles and Space Company (1965).
150. Chantry, P. J. "Dissociative Attachment in CO and NO." Physical Review, 172:125 (1968).
151. Gordiets, B. F. and Sh. S. Mamedov. "Vibrational Distribution Functions and Relaxation Rate in Anharmonic Molecules under Strongly Pumped Conditions." Trans., Zur. Prik. Mek. i Tech. Fiz. No. 3, p. 13 (1974).
152. Lam, S. H. "An Analytic Theory of Vibrational Relaxation for Anharmonic Molecules under Strongly Pumped Conditions." Journal of Chemical Physics, 67:2577 (1977).
153. Treanor, C. E., J. W. Rich, and R. G. Rehm. "Vibrational Relaxation of Anharmonic Oscillators with Exchange Dominated Collisions." Journal of Chemical Physics, 48:1789 (1968).
154. Gordiets, B. F., A. I. Osipov, and V. Panchenko. "Dissociation of Anharmonic Molecules by Means of High Power Infrared Emission." UDC 621.378.33, Trans. Zur. Prik. Mek. Tek. Fiz., 4:3 (1974).
155. Gordiets, B. F., Sh. S. Mamedov, and L. A. Shelepin. "Vibrational Kinetics of Anharmonic Oscillators Under Essentially Non-Equilibrium Conditions." Soviet Physics, J.E.T.P., 40:4 (1975).
156. Powell, H. T. "Vibrational Relaxation of CO Using a Pulsed Discharge." Final Report United Aircraft Research Laboratory, M911546-6 (1973).
157. Caledonia, G. E. and R. E. Center. "Vibrational Distribution Functions in Anharmonic Oscillators." AVCO Research Report 364 (1971).
158. Fusiki, Y. and S. Tsuchiya. "Vibration-to-Vibration Energy Transfer in CO in the States of  $v=2-9$ ." Japanese Journal of Applied Physics, 13:1043 (1974).
159. Sackett, P. B., A. Hordvik, and H. Schlossberg. "Measurements of the V-V Energy Transfer Rate from CO ( $V=2$ ) Using Tunable Parametric Oscillator Excitation." Applied Physics Letters, 22:367 (April 1973).

160. Stephenson, J. C. "Vibrational Excitation and Relaxation of the  $\text{CO}(v=1)$  and  $\text{CO}(v=2)$  States." National Bureau of Standards Memo (1972).
161. Fisher, E. R., H. Rabitz, and S. Lam. "CO-He V-T Rates at High Quantum Numbers." Paper, 5th Conference on Chemical and Molecular Lasers, St. Louis, Mo. (1977).
162. Brechignac, P. "Mise en evidence de transitions de transfert V-V a deux quanta dans les niveaux fortement excites de l'oxyde de carbone," Le J. de Phys. Lett., 38:L-145 (1977).
163. Dillon, T. A. and J. C. Stephenson. "Multiquantum Vibrational Energy Exchange." Physical Review, A, 6:1460 (1972).
164. Rich, J. W. Private Communication.
165. Gaydon, A. G. Dissociation Energies and Spectra of Diatomic Molecules. New York: John Wiley & Sons, Inc., (1947), p. 178.
166. Taylor, G. W. and D. W. Setser. "Quenching Rate Constants for  $\text{CO}(a^3\Pi: v'=0,1,2)$ ." Journal of Chemical Physics, 58:4840 (1973).
167. Krupenie, P. H. "The Band Spectrum of Carbon Monoxide." National Bureau of Standards, NSRDS-NBS-5 (1966).
168. Leone, S. R. "Vibration to Electronic Energy Transfer for Electronic Transition Lasers." Tech. Report ARPA, Order No. 2849, University of Southern California (30 November 1976).
169. Hertel, I. V., H. Hoffman, and K. J. Rost. "Electronic to Vibrational Energy Transfer in the Differential Scattering of  $\text{Na}^*$  by  $\text{N}_2$  Molecules." Physical Review Letters, 36:86 (1976).
170. Rapp, D. and T. Kassel. "The Theory of Vibrational Energy Transfer Between Simple Molecules in Non-Reactive Collisions." Chemical Review, 69:61 (1969).
171. Mooradian, A., T. Jaeger, and P. Stokseth. Turnable Lasers and Applications. Berlin: Springer-Verlag, 163 (1976).

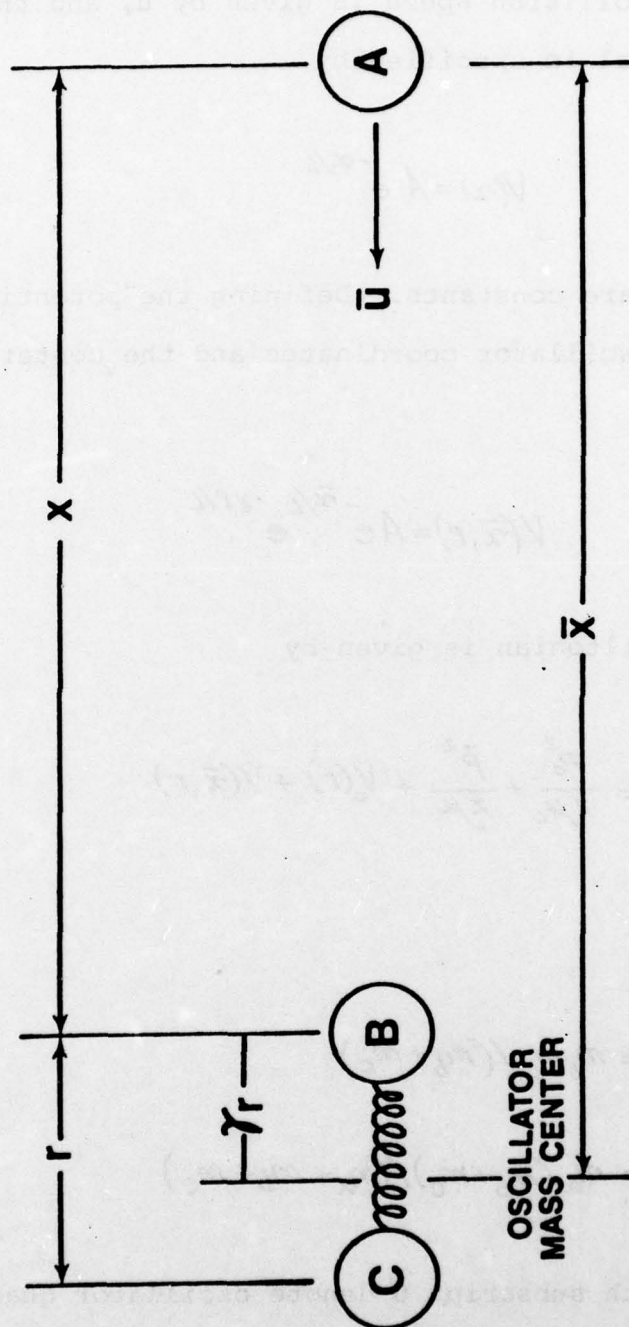
### Appendix A. The Influence of Anharmonicity on Vibrational Energy Transfer

In this appendix, we briefly review the semi-classical theory of vibrational energy transfer, V-T, and use this theory as a framework to discuss the influence of anharmonicity on the transition rates. This discussion is based on the recent work of McKenzie (ref 32) and the earlier papers of Mies (ref 27). From this discussion and subsequent examination of calculated matrix elements, we will conclude that when anharmonic effects are considered, two factors must be incorporated into the transition element analysis:

- a. Morse matrix elements
- b. Assymmetric correction factor

When both factors are properly evaluated, the scaling of transition elements is found to deviate only slightly from that of a simple harmonic oscillator.

Let us now consider the simple problem of determining the probable state of an oscillator, initially in a specified state, after it has been perturbed by undergoing a collision with a structureless atom (ref 32). Here we will utilize the simple collision geometry given in Fig. A-1 where a structureless particle of mass,  $m_a$ , impacts a diatomic molecule with nuclear masses,  $m_b$ , and  $m_c$ . The impacted oscillator nucleus,  $m_b$ , is located a distance  $\gamma r$  from the molecular mass center, where  $\gamma = m_c / (m_b + m_c)$ . We



## Collinear Collision Geometry

Fig A-1 Collinear Collision Geometry

adopt a three body center of mass reference frame in which the relative collision speed is given by  $\bar{u}$ , and the interaction potential is specified by

$$V(x) = A e^{-x/L} \quad (A-1)$$

where L and A are constants. Defining the potential in terms of the oscillator coordinates and the center of mass, we obtain

$$V(\bar{x}, r) = A e^{-\bar{x}/L} e^{yr/L} \quad (A-2)$$

The system Hamiltonian is given by

$$\mathcal{H} = \frac{P_0^2}{2\mu_0} + \frac{\bar{P}^2}{2\mu} + V_0(r) + V(\bar{x}, r) \quad (A-3)$$

with

$$\mu_0 = m_b m_c / (m_b + m_c) \quad (A-4)$$

$$\mu = m_a (m_b + m_c) / (m_a + m_b + m_c) \quad (A-5)$$

The symbols with subscript 0 denote oscillator quantities while the other symbols refer to the incident particle variables. Let us write the total wave function as

$$\Psi(\bar{x}, r, t) = \phi(\bar{x}, t) \psi(r, t) \quad (\text{A-6})$$

and treat the incident particle classically. Then the equations of motion for the incident particle yield (ref 32)

$$\mu \frac{d^2 \bar{x}}{dt^2} = \frac{A}{L} e^{-\bar{x}/L} \langle e^{yr/L} \rangle \quad (\text{A-7})$$

with

$$\langle e^{yr/L} \rangle = \int_{-\infty}^{\infty} \psi^*(r, t) e^{yr/L} \psi(r, t) \quad (\text{A-8})$$

Note that the potential constant, A, only influences the distance of closest approach, and may therefore be removed by the transformation

$$A \rightarrow \frac{\bar{E}}{V_{kk}} e^{-\bar{x}_0/L} \quad (\text{A-9})$$

where  $\bar{E} = \frac{1}{2} \mu \bar{u}^2$  is the semi-classical relative collision energy before the interaction, and

$$V_{kk} = \int_{-\infty}^{\infty} \psi_k^*(r) e^{yr/L} \psi_k(r) dr \quad (\text{A-10})$$

is the time-independent diagonal matrix element, and  $\psi_k(r)$  the initial oscillator stationary-state eigenfunction.

Defining a new interaction coordinate as  $\bar{z} = \bar{x} - x_0$ , and substituting into equation (A-7) yields (ref 32)

$$\mu \frac{d^2 \bar{z}}{dt^2} = \frac{\bar{E}}{L} e^{-\bar{z}/L} R(t) \quad (A-11)$$

where  $R(t) \equiv \langle e^{\gamma r/L} \rangle / V_{kk}$ . If the oscillator is assumed to be fixed in its initial eigenstate, then  $R(t) \approx 1$  for all time (ref 32). This assumption reduces the classical equation of motion to the equation for a constant energy trajectory:

$$\mu \frac{d^2 \bar{z}}{dt^2} = \frac{\bar{E}}{L} e^{-\bar{z}/L} \quad (A-12)$$

This equation can be integrated analytically (ref 170) to obtain the interaction potential

$$V(t, r) = \frac{\bar{E}}{V_{kk}} e^{-z(t)/L} e^{\gamma r/L} \quad (A-13)$$

in terms of time, by using the result

$$e^{-\bar{z}(t)/L} = \text{sech}^2\left(\frac{\bar{u} t}{2L}\right) \quad (A-14)$$

The oscillator motion is treated by expanding its wave function  $\psi(r,t)$  in terms of the stationary-state oscillator eigenfunctions  $\psi_n(r)$ , thus

$$\psi(r,t) = \sum_n c_n(t) e^{-i\omega_n t} \psi_n(r) \quad (\text{A-15})$$

with  $\omega_n = E_n/\hbar$  and  $E_n$  the eigenenergy of state  $n$ . The wave function,  $\psi(r,t)$  describes the oscillator response during a collision and is the solution of the time dependent Schrödinger equation.

$$i\hbar \frac{d\psi(r,t)}{dt} = \left[ -\frac{\hbar^2}{2\mu_0} \frac{d^2}{dr^2} + V_0(r) + V(t,r) \right] \psi(r,t) \quad (\text{A-16})$$

where  $V_0(r)$  is the molecular potential. The solution of equation (A-16) is reduced to a set of coupled, linear differential equations for the expansion coefficients,  $C_n$ .

By defining

$$V_{nj} = \int_{-\infty}^{\infty} \psi_n^*(r) e^{ir/\hbar} \psi_j(r) dr \quad (\text{A-17})$$

and introducing equation (A-14), the coefficients are determined to vary in time as

$$i\hbar \frac{dc_n(t)}{dt} = \frac{\bar{E}}{V_{kk}} e^{-\bar{z}(t)/L} \sum_j c_j(t) e^{i(\omega_n - \omega_j)t} V_{nj} \quad (\text{A-18})$$

The probability that an oscillator, initially in state k, will exist in state n after the interaction is

$$P_{k \rightarrow n}(E) = |c_n(\infty)|^2 \quad (\text{A-19})$$

If only the initial and final states are coupled, equation (A-18) can be written in the integral form (ref 32):

$$|c_n(\infty)|^2 = \left| \frac{\bar{E}}{\hbar} \frac{V_{nk}}{V_{kk}} \int_{-\infty}^{\infty} \text{sech}^2\left(\frac{\bar{u}t}{2L}\right) \exp\left[\frac{i}{\hbar} \int_0^t \Gamma_{nk}(t') dt'\right] dt \right|^2 \quad (\text{A-20})$$

where

$$\Gamma_{nk}(t') = \hbar(\omega_n - \omega_k) + (V_{nn} - V_{kk})E/V_{kk} \text{sech}^2\left(\frac{\bar{u}t'}{2L}\right) \quad (\text{A-21})$$

Mies (ref 27) has integrated equation (A-20) and obtained

$$P_{k \rightarrow n}(E) = \left| \frac{V_{nk}}{V_{kk}} \frac{2\pi g u L \mu}{\sinh(\pi g)} M(1+ig, 2, i2\lambda) \right|^2 \quad (\text{A-22})$$

where

$$g = \frac{L(\omega_h - \omega_k)}{\bar{u}}, \quad \lambda = \frac{\mu L \bar{u}}{\hbar} \left( \frac{V_{nn} - V_{kk}}{V_{kk}} \right) \quad (\text{A-23})$$

and  $M(1+ig, 2, i2\lambda)$  is the confluent hypergeometric series with complex arguments.

Following Mies (ref 27), we redefine this probability as

$$P_{k \rightarrow n}(E) = P_{k \rightarrow n}^0(E) \cdot A(E, \lambda) \quad (\text{A-24})$$

where

$$A(E, \lambda) \equiv V_{kk}^{-2} / M(1+ig, 2, i2\lambda)^2$$

Then  $A(E, \lambda)$  can be identified as an anharmonic correction factor to the "symmetric" transition probability,  $P_{k \rightarrow n}^0$ , where the symmetric transition probability is obtained by assuming  $V_{kk} = V_{nn}$ . Values of  $A(E, \lambda)$  for 0→1 transition have been tabulated by Mies (ref 27) for  $O_2$ ,  $N_2$ ,  $Br_2$ , and CO. Values of  $A(E, \lambda)$  range from  $10^{-1}$  to  $10^{-2}$ . Thus a general effect of removing the symmetric approximation and

including oscillator anharmonicities is to decrease the transition probability.

Mies (ref 27) also calculated the anharmonic factor,  $A(E,\lambda)$  for a limited range  $v=0 \rightarrow 4$  of initial and final oscillator states. He established that for single quantum transitions,  $A(E,\lambda)$  decreases as the vibrational quantum number of the initial state increases. To investigate this scaling in more detail, we have expanded the range of states investigated to  $v=0 \rightarrow 40$  for the CO-Ar system. The results of this analysis are presented in Fig. A-2, where we plot the normalized transitioned elements  $\langle V_{IF} \rangle^2$ , for  $F=I+1$ , where

$$\langle V_{IF} \rangle^2 \equiv \frac{|V_{IF}|^2}{|V_{10}|^2}$$

for two cases:

- a. Morse Oscillator
- b. Simple Harmonic Oscillator

For the SHO case, we have retained only the first two terms in the expansion of equation (A-2). This yields the frequently assumed form for the interaction potential being linear in  $r$ . The Morse elements were evaluated according to equation (A-17) using the formalism and numerical techniques developed by McKenzie (ref 32).

Note that the Morse elements scale much more rapidly with vibrational quantum number than the linear behavior obtained for the SHO case. However, when the Mies

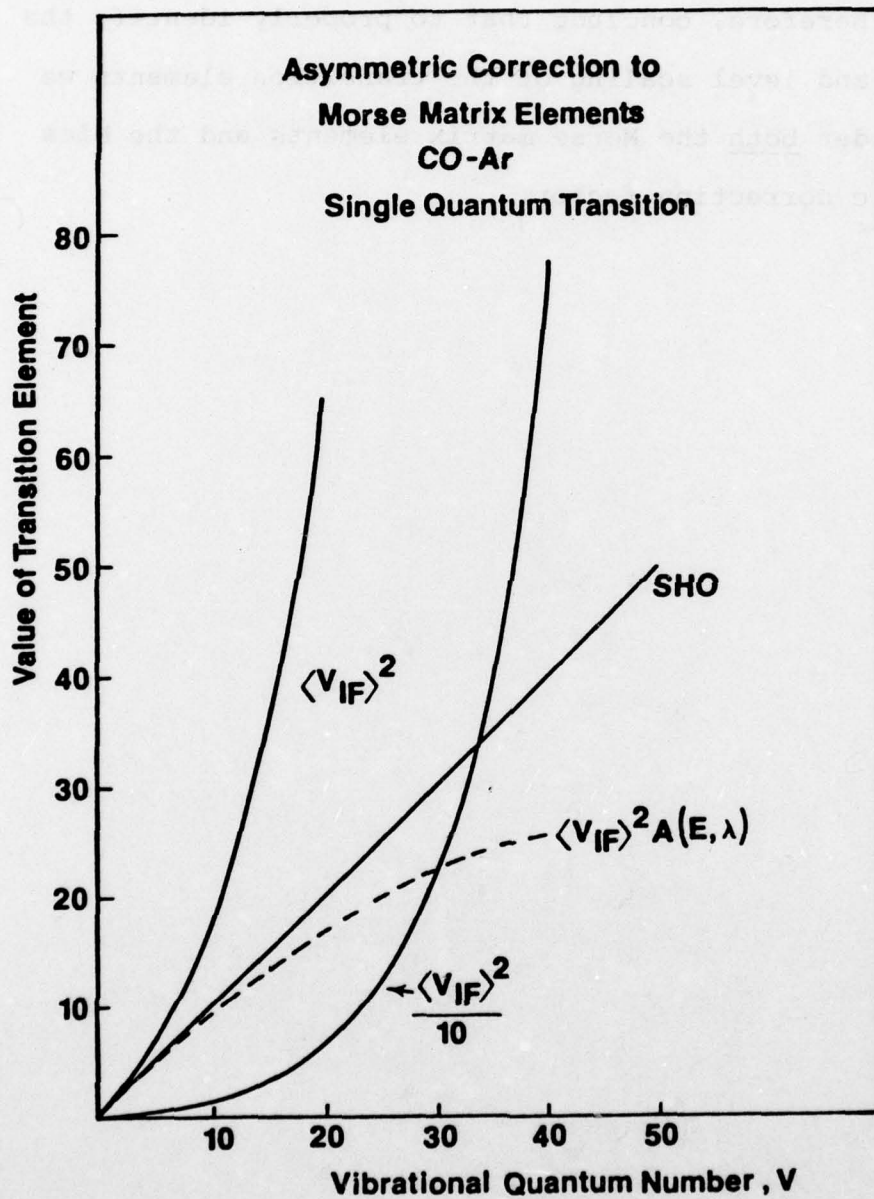
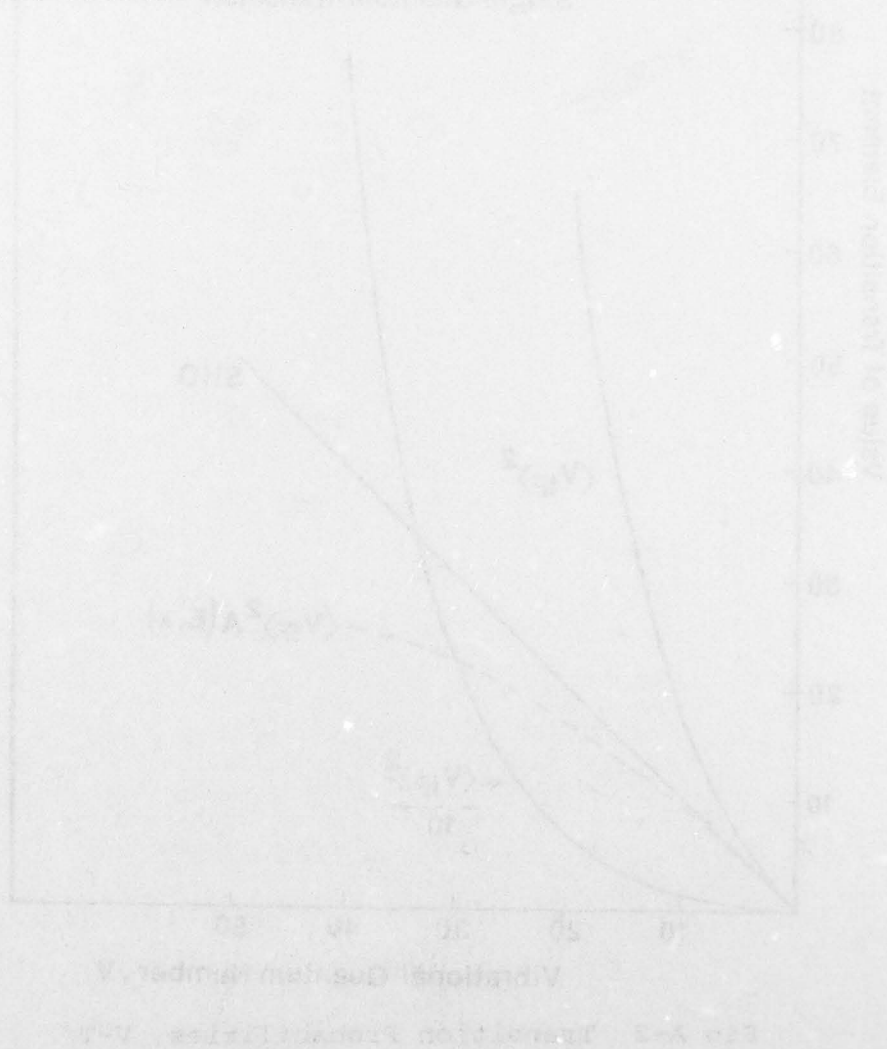


Fig A-2 Transition Probabilities, V-T

assymmetrical correction is applied, dashed curve, we observe that the effective transition elements scale less rapidly than those of the SHO.

We, therefore, conclude that to properly identify the magnitude and level scaling of the transition elements we must consider both the Morse matrix elements and the Mies assymmetric correction factor.



## Appendix B. Number of Bound Vibrational States

In any collisional theory of energy transfer and dissociation, it is necessary to enumerate all the discrete vibrational or vibrational-rotational states to be considered. There exists some inconsistency in the specification of these states. Various approaches to their specification will be discussed here.

The simplest molecular model is that of a simple harmonic oscillator with energy level spacing given by  $h\nu_e$ . The number of bound vibrational states for this model is simply  $(D_0/(h\nu_e))$

In a more refined approach, one would attempt to select a model which at least accounts for the molecular anharmonicity. The Morse potential, Fig. 4-1, is a widely used potential curve for an anharmonic oscillator. Morse proposed that

$$V = D_e \left( 1 - e^{-\alpha(r-r_e)} \right)^2 \quad (\text{B-1})$$

with  $D_e$  and  $\alpha$  being constants, (see Chapter IV), related to the dissociation energy and vibrational frequency,  $\nu_e$ , of the ground state. Within this representation, the vibrational energy levels are given by (ref 78)

$$E_v = (v + 1/2) h \nu_e - (h \nu_e)^2 / (4 D_e) (v + 1/2)^2 \quad (\text{B-2})$$

Solving for the last bound vibrational state  $v^*$ , by setting  $E_{v^*} = D_e$  we obtain with  $y = (v + 1/2)$

$$D_e = y^* h \nu_e - (h \nu_e)^2 / (4 D_e) y^{*2}$$

$$y^* = \frac{-h \nu_e \pm \sqrt{\frac{h^2 \nu_e^2 - 4 h \nu_e^2 D_e}{4 D_e}}}{2 h^2 \nu_e^2 / (4 D_e)} = 2 D_e / (h \nu_e) \quad (\text{B-3})$$

Thus in a Morse formalism, the number of bound vibrational states is twice that obtained using the truncated SHO formalism (ref 78). We have adopted the Morse formalism in this analysis because it accurately reproduces the observed spectroscopic dependence of the vibrational energy structure and is amenable to a direct incorporation of rotational effects (ref 77).

In general, anharmonicity may be accounted for by expressing the vibrational energy levels in terms of a power series in  $y$ :

$$E_y = h \nu_e y - h \nu_e x_e y^2 + h \nu_e y_e y^3 + \dots \quad (\text{B-4})$$

the value of the coefficients of the expansion are given by Herzberg (ref 78). If this formalism is adopted, rather than the Morse, and the expansion truncated at the quadratic term,  $y^*$  is given by the smaller of the two roots of:

$$D_e = h\nu_e y^* - h\nu_e x_e y^{*2}$$

Thus

$$y^* = \frac{h\nu_e - \sqrt{h^2\nu_e^2 - 4h\nu_e x_e D_e}}{2h\nu_e x_e}$$

and

$$y^* x_e = 1/2 - \sqrt{1/4 - (x_e D_e)/(h\nu_e)} \quad (B-5)$$

Thus in this formalism  $y^* < y^*_{\text{Morse}}$ . As an example, consider oxygen. Using the data of Herzberg we obtain  $y^*_{\text{Morse}} = 53$  and  $y^* = 35$ .

Preliminary investigations of the sensitivity of the dissociation rate to state specification have yielded the following general conclusions for the case of thermal dissociation.

a. The temperature dependence of the dissociation rate is relatively insensitive to the formalism selected.

b. The magnitude of the dissociation rate is smaller when additional vibrational states are assumed bound. This variation, however, was not significant enough to alter the general agreement and conclusions obtained with the Morse formalism.

In non-equilibrium studies, the dissociation results are much more sensitive to the assumed number of bound states. This is just another aspect of the rate sensitivity analysis that was discussed in Chapter VI. By using the power series expansion with a sixth order fit, no significant variation from the Morse value in calculated bound states was obtained in CO. However, if oxygen or nitrogen are considered, the variations are significant. For example, using the truncated series approach one would conclude that in oxygen significant heavy particle dissociation, via the ladder model, can occur. This question of last bound state designation and rate scaling requires additional experimental and theoretical attention.